HEPARIN AND PEG-BASED HYDROGELS TO MODULATE AND INTERROGATE DYNAMIC CELL BEHAVIOR

A Dissertation
Presented to
The Academic Faculty

by

Torri Elise Rinker

In Partial Fulfillment
of the Requirements for the Degree
Biomedical Engineering in the
School of Engineering

Georgia Institute of Technology
Emory University
December 2016

HEPARIN AND PEG-BASED HYDROGELS TO MODULATE AND INTERROGATE DYNAMIC CELL BEHAVIOR

Approved by:

Dr. Johnna Temenoff, Advisor
Department of Biomedical Engineering
Georgia Institute of Technology

Dr. Thomas Barker
Department of Biomedical Engineering
University of Virginia

Dr. Hang Lu
School of Chemical and Biomolecular Engineering
Georgia Institute of Technology

Dr. Luke Brewster
Department of Surgery
Emory University

Dr. Todd McDevitt
Department of Bioengineering and Therapeutic Sciences
Gladstone Institute of Cardiovascular Disease

Date Approved: September 19, 2016

None but those who have experienced them
can conceive of the enticements of science.
-Mary Shelley, *Frankenstein*

To Mom, Dad, Greg, Kevin, Ashley, and Jill,
who continuously assured me that I could do this.

ACKNOWLEDGEMENTS

I would like to start by generally acknowledging that the process of earning a PhD cannot be completed in isolation, and I would like to say a thanks to the hundreds of people at Georgia Tech, Emory, and in the Atlanta community and beyond who contributed to my ability to complete the work described in this dissertation. For those individuals that had an integral role in the completion of this work, a personal acknowledgment follows.

First, I would like to acknowledge my adviser, Johnna Temenoff, who made this work possible. Johnna has pushed me from day one to reach my maximum potential, and has provided unwavering support through biweekly conversations about my project, even if those conversations had to happen via skype or on the phone. She has encouraged me to think more deeply about the materials we use in lab as well as the applications towards which we use them. In addition, she has fostered a lab environment that is friendly, caring, fun, and unconditionally helpful. She has seriously considered my ideas about science and the workplace, and has kindly offered me tissues and support when the occasional problem arose in my personal life. Johnna helped enable my growth as a scientific researcher and human being during my time at Georgia Tech.

Next, I'd like to acknowledge my thesis committee. These four individuals offered substantial scientific guidance over the years and contributed both to the work in this thesis as well as my development as a researcher. First, I spoke with Todd McDevitt before I even came to Tech, and his creative ideas moved me then and continue to inspire me now. I enjoyed taking several classes with Todd, and appreciated his demand that students don't just ask "how", but ask "why" and "what for". On my committee, he has

always asked challenging questions, coached me in my scientific language, and offered excellent suggestions for future directions. Next, I spent the first two years of my PhD working on a project in collaboration with Hang Lu, and enjoyed regular meetings with her and Johnna. Hang's excitement about new findings was contagious and helped motivate me to keep digging deeper in the project. Her technical expertise on microfluidic devices is unbeatable, and I've always appreciated her willingness to talk to me on a personal level. Third, I'd like to thank Tom Barker, whose lab we worked closely with during my first four years at Tech. Tom's knowledge in matrix proteins has continuously challenged my ideas and hypotheses in my project, and has often led to many days spent pondering the implications of his words. I also really appreciated hanging out with Tom at the Matrix Biology conference, where I was invited to tour the Rock and Roll Hall of Fame with him and his lab. He also paid for an Uber to take us all to the airport when I had planned on taking the train, a kind gesture that I won't forget. Finally, I'd like to thank Luke Brewster, who has taken time away from his surgery schedule to participate in my committee. His clinical expertise has provided a helpful perspective, and his positive, happy demeanor has always acted as a calming force for me during meetings and presentations.

I'd be overlooking significant contributors to my scientific career if I didn't mention my mentors and professors at Oregon State University, including Michelle, Joe, and Skip. Michelle was my honors thesis adviser, and through the process of writing my thesis and taking her social justice class, I can truly say she changed my life and led me to understand how the systems of privilege and oppression can enter every nook and cranny of our lives, including the scientific field. Joe and Skip were excellent scientists,

teachers, and life mentors, whom I turned to for advice during grad school, and I thank them for their support. In addition, my mentors in previous lab internships, including Heather, Marina, Ken, and Scott were significant contributors to my training as a researcher, and I thank them for their patience and guidance.

Next, I'd like to thank my labmates, who acted as mentors and friends throughout this process. I've always compared the bond of the Temenoff lab members to that of family members – we help and support each other unconditionally, we bicker and laugh, and we remain in each other's lives long after graduation. When I joined the lab, Peter, Jeremy, Taymour, and Song were the senior students. Peter was in the process of writing his dissertation and defending when I joined, but he still took the time to talk to me and offer advice about how to deal with grad school. In a particularly emotional moment when I was upset over my first cell culture contamination, Peter closed the office door and spent an hour calming me down and helping me move forward. Jeremy was wonderfully easy-going and always ready to laugh and have a good time in lab. One day, while were impatiently waiting for Song and Tobias to finish lab work, Jeremy, Jen, and I constructed paper curtains for the office, which remain intact almost 4 years later. Jeremy also provided a lot of scientific guidance as I started working with GAG-based materials, and continues to be available to answer my questions even now. Taymour and I worked on a project together for a year, and I'd like to thank him for his mentorship and willingness to answer all my questions, both scientific and technical. I know we got on each other's nerves at time, but I really appreciate the patience he showed me and scientific knowledge he imparted on me during our year together. Song was an excellent role model in regards to dedication, hard work, and perseverance. She also knew a lot

about all of the projects going on in lab, as she had dabbled in a little bit of everything. We had a really fun time exploring Boston together (thanks again, Song and Masa, for inviting me and my rice crackers into your hotel room when everything else was booked) and I've always appreciated her insights about love, life, and science.

Jen (HAI you better be reading this) and I overlapped for four years of our graduate school experience and became an awesome team for solving problems around the lab. We could always count on one another to see a part of the problem that the other did not and figured things out together (often thanks to the reference wall). Jen could answer my questions around lab and was a great person to bounce ideas off when brainstorming new projects. I managed to convince her to give up her parking pass, and she and I enjoyed a ~1.2 mile walk commute together almost every evening for three years. On these walks, we talked about everything – science, our past, our future, what was going on in our lives, the dogs we passed – and supported and encouraged each other through even the darkest of times. She has been particularly encouraging while I've been writing my dissertation, for which I've appreciated probably more than she knows. Melissa and I joined the lab together, and besides relying on each other for help with lab techniques and homework, we became very close friends. I loved our long conversations, our shopping trips, our art nights, and dinners. Her introspective personality was calming and her strength admirable, and I'm glad we've stayed friends even after her move to California.

Tobias joined our lab as a post-doc during my second year, and of all my labmates, I am certainly most indebted to him for the scientific knowledge I gained while in grad school. With a chemistry background, Tobias was able to answer questions about

our materials and troubleshoot problems with ease. I spent several months observing and helping him troubleshoot microparticle formulations, and those few months of learning turned out to be some of the most valuable time I had while at Tech. Even after having been out of the lab for several years and living in Germany, Tobias still answers the questions I send him via email. But beyond science, Tobias was truly a very dear friend. We could talk deeply about many different topics, whether it was science, religion, or philosophy, and his unique perspective and commitment to his beliefs was refreshing. Plus, he always gave us laughs in lab with his use of the English language (SPOOOOONNNGGE). I cannot thank Tobias enough for the scientific guidance he provided me while I was in grad school, and I hope our friendship continues for many years to come.

Liane joined the lab as I was entering my third year, and her motivation and strong work ethic were immediately apparent. She was always an excellent person to mentor and it has been truly awesome to watch her grow as a scientist and researcher over the years, to the point where now I can ask her questions and seek her advice. But more importantly, we became close friends over the years, and our fun times outside of labs playing games, riding bikes, playing volleyball, or just talking have meant a lot to me. She was there for me during a particularly difficult time in my personal life, and her support and friendship kept me going during those months.

Jennifer worked as a lab manager for two of my years in grad school, and she was incredibly patient and helpful during my ordering and equipment panics. She was always a fun, positive person to have around lab and I wish her luck as she now embarks upon grad school. Elda has been in lab for my last two years of grad school, and her positivity

and commitment to the lab have been admirable. I'm excited for her to have the chance to mentor new students and to see her future scientific work. Finally, Gilad only joined our lab recently, but his calming presence on the day of my defense was helpful and his willingness to learn has been appreciated thus far, and I look forward to hearing of his successes in the years to come.

I've mentored several undergrads and high school students during my time at Tech, and I'd like to thank Brianna for her hard work, dedication, and humor during the year I mentored her. Max worked on a particularly challenging project during his time in lab, and I'd like to thank him for never giving up. Brandon has worked with me for several years now, and has made substantial contributions to my project. He is a fantastic researcher, an incredibly intelligent student, and has a sense of humor that has kept us all on our toes. He's been a fun person to have in lab the last few years, and I'd like to thank him for his hard work.

While I did not get to know them as well, I'd like to thank Karthik, Anne, Ali, Yifeng, Yang, and Chris for their assistance in lab. Several other labs have also been incredibly helpful both in regards to equipment use and scientific expertise, so I'd like to thank the McDevitt lab (especially Marian, Josh, Melissa, Jenna, Tracy, and Marissa), the Barker lab (especially Dwight and Vicky), the Bellamkonda lab (especially Dr. Pai and Tarun), the Kemp and Lu labs (especially Ariel), the Platt lab (especially Phil and Akia), the Lam lab (especially Reggie) and the Thomas lab (especially Alex and Nate). In addition, I'd like to thank those individuals in charge of core facilities, including Aqua, Andrew, and Lamar. I'd especially like to acknowledge Andrew for his continuous support and guidance in my microscopy work. Finally, I'd like to thank members of the

BME, IBB, and EBB teams for their support while I've been at Tech, including DeWayne, Colly, Shannon, Meg, Michelle, Floyd, Eric, and Gabe.

Last but certainly not least, I would like to thank my friends and family for their support and encouragement both during my graduate school experience and in the time leading up to it. During grad school, I made some great friends, including Marian, Melissa, Josh, Alex, Liane, Ariel, Pete, Reggie, Denise, Shereka, and Seth. We had a lot of fun over the years going out, having dinner, traveling, and talking about life. Marian and I had projects that overlapped enough to allow fruitful conversations about science and future experiments, which I really appreciated. Josh was also a great person to turn to for science and homework help. Marian, Josh, and I went on several trips that I'll always remember, and from the fights for the firm pillows to artistic selfies to Josh eating Indian food that was so spicy he had to splash himself in the face with cold water, we had some good times that relieved a lot of the stress of grad school. Ariel, Reggie and Pete also came on trips with us wine tasting and to Harry Potter World, two magical places that definitely took our minds of grad school. I'd like to acknowledge all of them for their friendship, support, and encouragement over these years.

I'd like to acknowledge my partner Greg, who more than anyone saw me through the ups and downs of grad school on a daily basis. On the days that experiments went really poorly, he's walk home with me and listen to me vent, telling me it would be OK tomorrow. On the days when everything fell into place and results were crystal clear, he'd hug me and open a bottle of wine. He never let me say I couldn't do it and always told me how smart I was. He was the person who made me laugh when I needed it the most and let me cry when I couldn't do anything else. He enriched my life with books,

music, and trips to state parks around Atlanta. I'd like to thank him for his unfailing support, patience, and encouragement through this process.

Finally, I'd like to thank my family. The Gamewells, especially Jenny and Steve, embraced me as part of their family over the years and have always accepted me into their houses in Gainesville for much-needed breaks from city life. They consistently asked how school was going and gave me space both to vent and celebrate. Jill and I have emailed regularly throughout my time at grad school, and I love hearing about her adventures kayaking and with her dogs. She has always been incredibly positive and encouraging while I've been in grad school and I've really appreciated it. Kevin and Ashley moved to Atlanta during my fourth year of grad school, which was a pleasant surprise and brought a little bit more of the PNW to Atlanta. They often invited me over for dinner and helped show me aspects of Atlanta that I hadn't seen before. They let me hang out with their dog Knives, whose furry face made me smile no matter how badly I was feeling. Finally, I can say with absolute certainty I wouldn't be where I am today if not for my parents, who loved and protected me as I grew up, providing opportunities to grow and encouraging me every step of the way. My dad is an engineer, and he could always help me with my math homework, whether it was simple addition or advanced calculus. He helped me build things for projects in school and introduced me to people at the national lab he works. He patiently taught me, even in my difficult teenage years, and has always been there when I needed him. My mom worked in a biotech lab, and I always joke that I am a perfect combination of my parents: biotech + engineer = bioengineer. Beyond science expertise, my mom ensured that I had all the books I could ever want to read (which was not an easy task, I read A LOT), signed me up for art

classes, and shuttled me around to sports games and camps. She talked me through the tough stuff in life – the first bad grade, the first break-up – and celebrated the good stuff – graduations, successful relationships. She's told me my whole life that I am beautiful and that I am smart, instilling in me a confidence that I know is a major contributor to the successes I've enjoyed. My parents provided me the tools I needed to be the person I am today, and for that, I thank them.

TABLE OF CONTENTS

	Page
ACKNOWLEDGEMENTS	v
LIST OF TABLES	xviii
LIST OF FIGURES	xix
LIST OF ABBREVIATIONS	xxii
LIST OF SYMBOLS	xxvi
SUMMARY	xxvii
CHAPTER	
1 INTRODUCTION	1
1.1 Motivation	1
1.2 Research Objectives	3
1.3 Significance and Scientific Contribution	10
2 BACKGROUND AND LITERATURE REVIEW	13
2.1 Mesenchymal Stem Cells in the Bone Marrow Microenvironment	13
2.1.1 Mesenchymal Stem Cells	13
2.1.2 MSCs in the Bone Marrow Microenvironment	15
2.1.3 Diabetes and its Effects on the Bone Marrow Microenvironment	16
2.1.4 MSCs, Adipocytes, and Osteoblasts in the Bone Marrow Microenvironment	17
2.1.5 Co-Culture of Osteoblasts, Adipocytes, and MSCs	19
2.2 Endochondral Ossification	21
2.2.1 Endochondral Ossification in the Growth Plate	21
2.2.2 Growth Plate Injuries and Repair Strategies	24

2.2.3 Articular Cartilage and Chondrogenesis 26

2.2.4 Cartilage Injury and Repair 27

2.3 *In Vitro* Cell Culture Systems 29

2.3.1 Hydrogels for *In Vitro* Cell Culture 29

2.3.1 Integrating Complexity into Hydrogel-Based Culture Platform 31

2.3.3 *In Vitro* Disease Model Systems for the Bone Marrow Microenvironment 32

2.3.4 Modulating Chondrogenesis *In Vitro* 35

2.4 Glycosaminoglycans and Protein Sequestration 38

2.4.1 Function of Heparan Sulfate and Heparin 38

2.4.2 Heparan Sulfate and Other GAGs in Chondrogenesis 40

2.4.3 Glycosaminoglycan-Based Biomaterials for Cartilage Repair 41

2.4.4 Heparin-Based Biomaterials 42

2.4.5 Biomaterial-Mediated Protein Sequestration 46

2.5 Microparticles 48

2.5.1 PEG-Based Microparticles in Tissue Engineering 49

2.5.2 GAG-Based Microparticles in Tissue Engineering 50

2.5.3 Core-Shell Microparticles 51

2.5.4 Microparticles in Cell Spheroids 54

2.6 Systems Biology Approaches to Tissue Engineering 57

3 INTERACTIONS BETWEEN MESENCHYMAL STEM CELLS, ADIPOCYTES AND OSTEOBLASTS IN A 3D TRICULTURE MODEL OF HYPERGYLCEMIC CONDITIONS IN THE BONE MARROW MICROENVIRONMENT 59

3.1 Introduction 59

3.2 Materials and Methods 63

3.3 Results 71

3.4 Discussion 79

3.5 Conclusion 87

4 HEPARIN MPS TO MODULATE CELL DIFFERENTIATION IN AN *IN VITRO* MODEL SYSTEM OF ENDOCHONDRAL OSSIFICATION 89

4.1 Introduction 89

4.2 Materials and Methods 92

4.3 Results 98

4.4 Discussion 108

4.5 Conclusion 116

5 CORE-SHELL MICROPARTICLES FOR PROTEIN SEQUESTRATION AND CONTROLLED RELEASE OF A PROTEIN-LADEN CORE 118

5.1 Introduction 118

5.2 Materials and Methods 121

5.3 Results 129

5.4 Discussion 136

5.5 Conclusion 145

6 DEGRADABLE HEPARIN-PEG-BASED MPS FOR PROTEIN SEQUESTRATION AND RELEASE 147

6.1 Introduction 147

6.2 Materials and Methods 149

6.3 Results 152

6.4 Discussion 159

6.5 Conclusion 165

7 CONCLUSION AND RECOMMENDATIONS 167

7.1 Summary 167

7.2 Conclusion 170

7.3 Future Directions 179

APPENDIX A: SURFEN INTERACTIONS WITH SOLUBLE HEPARIN AND HEPARIN MPS 190

APPENDIX B: THE EFFECT OF HEPARIN CELL COATINGS ON ATDC5 SPHEROID DIFFERENTIATION 199

APPENDIX C: SPATIAL CONTROL OVER HEPARIN MPS IN ATDC5 SPHEROIDS 207

APPENDIX D: HEPARIN MPS TO MODULATE OSTEOGENIC DIFFERENTIATION IN MC3T3 CELLS 212

APPENDIX E: SUPPLMENTARY FIGURES 216

APPENDIX F: ADDITIONAL INFORMATION 227

REFERENCES 230

LIST OF TABLES

Page

Table 3.1: National Library of Medicine accession number and primer sequences for target genes in qPCR in hyperglycemia co-culture study 68

Table 4.1: National Library of Medicine accession number and primer sequences for target genes in qPCR in ATDC5 cells and heparin MP study 96

Table 6.1: Amounts of heparin, PEG and DTT for each heparin-PEG MP formulation 150

Table 6.2: DTT concentration and degradation rate for varying heparin contents in heparin-PEG-based MPs 154

Table D.1: National Library of Medicine accession number and primer sequences for target genes in qPCR in MC3T3 Study 213

Table E.1: National Library of Medicine accession number and primer sequences for target genes in qPCR in ATDC5 monolayer study 222

LIST OF FIGURES

Page

Figure 3.1: Experimental set-up for the hyperglycemia co-culture study 65

Figure 3.2: Lipid deposition and multivariate gene expression analysis of adipocytes in all co-culture condition and glucose levels 72

Figure 3.3: Viability assessment for adipocytes in all co-culture condition and glucose levels 73

Figure 3.4: ALP activity and multivariate gene expression analysis of osteoblasts in all co-culture condition and glucose levels 75

Figure 3.5: Viability assessment for osteoblasts in all co-culture condition and glucose levels 76

Figure 3.6: Multivariate gene expression analysis of MSCs in all co-culture condition and glucose levels 78

Figure 3.7: Clonogenecity and viability assessment for MSCs in all co-culture condition and glucose levels 79

Figure 4.1: Characterization of heparin and PEG-based MPs for ATDC5 cell studies 99

Figure 4.2: Incorporation of heparin and PEG-based MPs into ATDC5 spheroids 100

Figure 4.3: Experimental set-up for ATDC5 spheroid study with heparin and PEG MPs; H&E staining for spheroids in all culture conditions at all timepoints 101

Figure 4.4: LIVE/DEAD staining for heparin and PEG MP ATDC5 spheroid groups at day 18 102

Figure 4.5: Chondrocytic gene expression for heparin and PEG MP ATDC5 spheroid groups at high and low MP ratio for *collagen II*, *aggrecan*, and *collagen X* 103

Figure 4.6: Collagen II IHC for heparin and PEG MP ATDC5 spheroid groups at low and high MP ratio at days 12 and 18 104

Figure 4.7: Safranin-O staining for heparin and PEG MP ATDC5 spheroid groups at low and high MP ratio at days 12 and 18 105

Figure 4.8: Gene expression, GAG deposition, and matrix mineralization analysis of ATDC5 cells in transwell with heparin and PEG MPs 106

Figure 4.9: DNA analysis of ATDC5 cells in transwell with heparin and PEG MPs 107

Figure 4.10: Analysis of heparin and PEG MPs protein sequestration 108

Figure 5.1: PEG-based MPs with tunable size and degradation profiles 129

Figure 5.2: Fabrication of heparin-PEG core-shell MPs 130

Figure 5.3: Correlation of heparin content in core-shell MP to MP size and mass of heparin MPs in the precursor PEG solution. 132

Figure 5.4: Degradation of PEG-based shell and release of heparin MP core from core-shell MPs 133

Figure 5.5: Pre-fabrication loaded degradable core-shell MPs modulate loaded heparin MP delivery to cells 134

Figure 5.6: Core-shell MPs temporally modulate protein sequestration 135

Figure 5.7: Post-fabrication loaded degradable core-shell MPs allow delivery of loaded heparin MPs to cells 136

Figure 6.1: Cross-linking scheme for polymeric network in heparin-PEG-based MP fabrication 153

Figure 6.2: Alcian blue staining and surfen assay show that heparin-PEG MPs can be fabricated with varying amounts of heparin 154

Figure 6.3: Degradation of PEG-based MPs and 10, 20, 30, and 40% heparin MPs 155

Figure 6.4: Degradation of 10% heparin MPs at 0.1, 1 or 3 mg MPs/mL initial concentration 156

Figure 6.5: Heparin-PEG MP loading of histone 156

Figure 6.6: Heparin-PEG MP loading and release of histone 157

Figure 6.7: Total release of protein from varying masses of 10% Heparin and PEG-based MPs incubated with ATDC5 cells 158

Figure 6.8: Degradation of PEG-based MPs in ATDC5 spheroids 159

Figure 7.1: Fabrication, degradation, and re-lamination of hydrogel co-culture system 181

Figure A.1: Fluorescence intensity of surfen-heparin solution increases with mass of heparin 193

Figure A.2: Confocal microscopy images of surfen-blocked heparin MPs 194

Figure A.3: Surfen-blocked heparin MPs run on SDS-PAGE 195

Figure B.1: Soluble heparin and heparin coatings in ATDC5 spheroids 202

Figure B.2: Viability of ATDC5 spheroids with heparin coating 202

Figure B.3: H&E staining of ATDC5 spheroids with heparin coating 203

Figure B.4: Safranin-O staining of ATDC5 spheroids with heparin coating 204

Figure B.5: Gene expression for *collagen II*, *aggrecan*, and *collagen X* of ATDC5 spheroids with heparin coating 205

Figure C.1: Spatially organized ATDC5 cell spheroids at day 1 and day 6 210

Figure D.1: Heparin MPs and MC3T3 cell transwell study 215

Figure E.1: PCA for adipocytes in hyperglycemia study and weight plots for PLS-DA models 216

Figure E.2: Representative images for MSCs, adipocytes, and osteoblasts LIVE/DEAD staining for the hyperglycemia study 217

Figure E.3: PCA for osteoblasts in hyperglycemia study and weight plots for PLS-DA models 218

Figure E.4: Global PCA for MSCs in hyperglycemia study 219

Figure E.5: Culture configuration PCA for MSCs in hyperglycemia study 220

Figure E.6: MSC weight plots for PLS-DA models 221

Figure E.7: Gene expression of *collagen II*, *aggrecan*, *Ihh*, and *collagen X* for ATDC5 cells in monolayer culture for 22 days. 222

Figure E.8: Gene expression of *collagen II*, *aggrecan*, *Ihh*, and *collagen X* for ATDC5 cells in spheroid culture for 18 days. 223

Figure E.9: Pre-fabrication load core-shell MP bioactivity assay two 224

Figure E.10: Heparin shedding from 100% heparin MPs 226

LIST OF ABBREVIATIONS

2D	Two-dimensional
3D	Three-Dimensional
ADIPOQ	Adiponectin
ALP	Alkaline Phosphatase
ATF2	Activating transcription factor 2
BMD	Bone mineral density
BMP	Bone Morphogenetic Protein
BSA	Bovine serum albumin
CD	Cluster of differentiation (alternatively cluster of determinants)
CEBPB	CCAAT/enhancer-binding protein beta
CFU-F	Colony forming unit-fibroblasts
CML	Chronic myeloid leukemia
CS	Chondroitin Sulfate
CSA	Cross-sectional area
DA	Diacrylate
Deg	Degradable
DMEM	Dulbecco's Modified Eagle Medium
DMSO	Dimethyl sulfoxide
DPP	Decapentaplegic
DTT	Dithiothreitol
EB	Embryoid body
ECM	Extracellular matrix
EDC	1-Ethyl-3-(3-dimethylaminopropyl)carbodiimide

ESCs	Embryonic stem cells
EXT1	Exostosin glycosyltransferase 1
FBS	Fetal bovine serum
FGF	Fibroblast growth factor
FGFR	fibroblast growth factor receptor
FOX01	Forkhead box protein O1
GAGs	Glycosaminoglycans
GDF	growth differentiation factors
H&E	Hematoxylin and Eosin
HA	Hyaluronic acid
Hep	Heparin
HLA-DR	Human leukocyte antigen - antigen D Related
HOBt	Hydroxybenzotriazole
HS	Heparan Sulfate
HSC	Hematopoietic Stem Cell
HUVECs	Human umbilical vein endothelial cells
IGF	Insulin-like growth factor
IHC	Immunohistochemistry
IHH	Indian Hedgehog
JUN	C-JUN
LEP	Leptin
LV	Latent variable
MAm	Methacrylamide
MAT	Marrow adipose tissue
MMP	Matrix metalloproteinase

MPs	Microparticles
MSCs	Mesenchymal stem cells
NFKB1	Nuclear factor kappa B
NHS	N-Hydroxysuccinimide
OCN	Osteocalcin
OCT	Optimal cutting temperature compound
OPF	Oligo(poly(ethylene glycol) fumarate)
OPG	Osteoprotegrin
PBS	Phosphate buffer saline
PC	Principal component
PCA	Principal Component Analysis
PDGF	Platelet-derived growth factor
PDMS	Polydimethylsiloxane
PEG	Poly(ethylene-glycol)
PG	Proteoglycan
PLA	Poly(lactic acid)
PLGA	Poly(lactic-co-glycolic acid)
PLL	Poly-L-Lysine
PLS-DA	Partial Least Squares Discriminate Analysis
PLSR	Partial least-squares regression
PPARγ	Peroxisome proliferator activated receptor gamma
PTHrP	parathyroid hormone-related protein
qPCR	Quantitative polymerase chain reaction
ROI	Region of Interest
ROS	Reactive oxygen species

RSP18	40S ribosomal protein S18
RUNX2	Runt-related transcription factor 2
SDF-1α	Stromal cell-derived factor-α
SDS	Sodium dodecyl sulfate
SDS-PAGE	Sodium dodecyl sulfate polyacrylamide gel electrophoresis
Sumf1	Sulfatase-Modifying Factor 1
SVA	Succinimidyl valerate
TGFβ	Transforming growth factor beta
TNFα	Tumor necrosis factor-α
TP	Timepoint
VEGF	Vascular endothelial growth factor
wt%	Weight percent
αMEM	Minimal Essential Medium-Alpha

LIST OF SYMBOLS

N_o	Staring amplicon number
E	Mean efficiencies
Ct	Cycle threshold
N_t	Amplicon number at the cycle threshold
R^2X	Coefficient of determination for model of ***X***
R^2Y	Coefficient of determination for model of ***Y***
Q^2	Model predictive quality

SUMMARY

Hydrogel-based biomaterials are often used for biomolecule delivery or encapsulation of cells for tissue engineering and regenerative medicine applications. However, utilizing hydrogels in dynamic cell systems can be challenging, as hydrogels must be engineered to account for changes in cellular behavior. For example, the hydrogel cell culture platforms and analyses techniques employed to investigate cell response to disease conditions should account for the variations in cellular communication resulting from changes in the external stimuli inherent to the disease. In addition, the hydrogels used to modulate cellular differentiation, either through protein delivery or direct interactions with cells, should account for the evolving cell phenotype. Thus, in this work, hydrogel-based technologies were developed and utilized to interrogate and modulate dynamic cellular behavior.

A PEG-based platform was designed and utilized to interrogate MSCs, adipocytes, and osteoblasts under hyperglycemic conditions via multivariate analyses, as these three cell types are implicated in abnormal deposition of marrow adipose tissue and bone in diabetes and osteoporosis. Then, as heparin is known to bind many growth factors involved in cellular differentiation processes, heparin-based MPs were used to temporally modulate endochondral ossification of ATDC5 cells, possibly through heparin-mediated protein sequestration. To further modulate the timing of protein sequestration, heparin-PEG core-shell MPs were designed to enable sequestration and temporally controlled redelivery of protein. Finally, hydrolytically degradable heparin-PEG-based MPs were engineered with tunable heparin content and degradation rate, to

enable temporally controlled protein release. Overall, this work demonstrates the ability of PEG and heparin-based hydrogels to investigate and regulate cellular processes that evolve in time.

CHAPTER 1

INTRODUCTION

1.1 Motivation

Hydrogel-based biomaterials are often employed in regenerative medicine due to their high water content, biocompatibility, amenability to chemical modification, and potential to evolve with time [1–3]. For example, three-dimensional (3D) hydrogel *in vitro* cell culture systems have provided extensive knowledge about cell behavior that would have be difficult to obtain *in vivo* due to the inability to assess subtle, cell-level changes to chemical and physical stimuli in animal models [4–8]. In addition, hydrogel-based delivery systems have enabled entrapment and controlled release of various biomolecules by employing protein-attractive and biodegradable materials [9–12]. However, a major obstacle in the utilization of biomaterials can be ensuring that they are engineered to permit analysis or modulation of dynamic cellular processes such as those observed in disease states and during differentiation, in which cell behaviors fluctuates in both space and time in response to various stimuli.

As tools to enable 3D cell culture, hydrogel-based platforms have facilitated capturing important aspects of the *in vivo* microenvironment during *in vitro* studies [2,8]. For example, cellular communication is a dynamic process that is critical to normal cell function, and by using co-culture to permit cellular communication *in vitro*, better understandings of *in vivo* cell behavior have emerged [13–15]. In addition, interactions between cells and the ECM in which they reside are implicated in modulating dynamic cellular processes like differentiation, and by integrating ECM molecules, such as integrin-binding peptide sequences or glycosaminoglycans, into hydrogel culture

systems, a deeper knowledge of how these materials might affect cells *in vivo* or how they could be used as tools for tissue regeneration might be gained [9,16].

Thus, the research presented in this thesis strives to develop hydrogel-based materials to enable interrogation and modulation of dynamic cellular processes. First, investigation of the complex interactions between multiple cell types under pathological conditions could provide further insight into disease progression and potential treatment. For example, it has been hypothesized that dysregulation of mesenchymal stem cell (MSC) commitment to adipogenic and osteogenic lineages could be the cause of increased marrow fat and elevated cases of osteoporosis in patients with diabetes mellitus [17–21]. As MSC lineage commitment is partially controlled by signals from mature adipocytes and osteoblasts, it is possible that dysregulation occurs due to altered cellular cross-talk in hyperglycemic conditions [22], but further studies are required to confirm this hypothesis. Therefore, development of *in vitro* biomaterials platforms that enable advanced analyses of cell co-culture could aid in understanding the complicated interactions between MSCs, adipocytes, and osteoblasts and could be applied to the study of other dynamic cellular behavior. However, challenges in designing materials that allow cell type-specific analyses, including post-culture functional assays, still must be overcome.

Second, utilization of ECM-mimicking materials could enhance control over the dynamic process of cellular differentiation, a common goal in tissue repair and regeneration [3]. For example, endochondral ossification involves the conversion of proliferating chondrocytes into bone through a process tightly regulated by signaling molecules [23], and modulation of this process could lead to improved therapies for

growth plate or articular cartilage injuries [24]. GAGs are known to bind many of the growth factors involved in endochondral ossification and other differentiation processes, including IHH, FGFs, TGFβs, BMPs, and IGFs [25,26], and this protein-binding ability could enable temporal modulation of cellular differentiation. While GAGs have been used to deliver biomolecules in a variety of tissue-engineering applications [26], their ability to act as the sole modulator of differentiation by the mechanism of protein binding has not been fully explored. In addition, the goal of designing materials to temporally control GAG-mediated protein sequestration and release has not yet been fully realized.

1.2 Research Objectives

Thus, the goal of this work was to develop hydrogel-based technologies to analyze and modulate dynamic cell processes. This was achieved by pursuing two parallel focus areas: 1) development of a PEG-based hydrogel co-culture platform to permit analysis of cellular cross-talk in pathological conditions and 2) implementation and development of heparin-based MPs to temporally modulate protein presentation in cellular differentiation processes. The biomaterials employed in these studies include heparin, which has a high affinity for growth factors involved in differentiation and developmental processes [25], and PEG, which has low affinity for proteins and permits protein diffusion when cross-linked into hydrogels [27–29].

To achieve the goals in the first focus area, a PEG-based hydrogel system was developed to evaluate the effects of cellular cross-talk in osteoblasts, adipocytes, and MSCs in co-culture under hyperglycemic conditions. Each cell type was cultured in separate PEG hydrogel blocks in a laminated co-culture system, allowing cell type-specific retrieval for analysis after culture. In addition, the MSC block was enzymatically

degradable, permitting clonogenicity studies after co-culture. Finally, multivariate analyses were applied to better understand which variables contributed to observed cell phenotypes. Overall, these studies were performed as a proof-of-concept experiment to demonstrate the utility in hydrogel-based co-culture systems for understanding how cells respond to dynamic cellular cross-talk in a disease model.

In the second focus area, the ability of heparin to modulate cellular differentiation was assessed by incorporating heparin-based MPs into ATDC5 cell aggregates (a model cell line for endochondral ossification) and culturing monolayer ATDC5 cells in transwell culture with heparin MPs. To understand the mechanism behind heparin MP-mediated changes in differentiation, PEG MP controls were evaluated alongside heparin MPs and protein sequestration in cell-conditioned media was studied. In addition, core-shell heparin-PEG MPs were designed as a tool to temporally modulate soluble factors. By encapsulating heparin MPs in a degradable PEG-based shell that permitted protein diffusion, protein could be sequestered by the heparin MP and isolated from the surrounding environment prior to degradation of the PEG-based shell. Finally, degradable heparin-PEG-based MPs were developed to better control protein sequestration and release.

The overarching rationale for this project is that development and utilization of hydrogel-based technologies can enable interrogation and modulation of cell behavior in dynamic systems. The **overarching hypothesis** of this work is that PEG-based hydrogels can be engineered to permit culture conditions and analysis techniques that account for cellular cross-talk, and heparin-based hydrogels can be employed to temporally modulate

cellular differentiation and protein presentation. These hypotheses will be addressed in the following three specific aims:

Hypothesis I: Mesenchymal stem cells, adipocytes, and osteoblasts will respond to hyperglycemic conditions in a manner that is dependent on their neighboring cell type.

Specific Aim I: Utilize a PEG-based platform to co-culture MSCs, osteoblasts, and adipocytes and evaluate gene expression, viability, and clonogenicity (MSCs only) in normal and high glucose conditions using multivariate analyses.

In vitro model systems of the bone marrow microenvironment have the potential to reduce complexity while still maintaining relevant components of the *in vivo* microenvironment [30,31]. Recently, photolithography and cell patterning techniques have enabled development of highly specified co-culture hydrogel systems, allowing cell and biomolecule patterning for a variety of applications [29]. In addition, the ability to maintain separation between cell populations while still permitting cellular communication in PEG-based hydrogels has been demonstrated [32,33]. Thus, PEG-based hydrogels were used to investigate the potential role of MSCs in the dysregulation of adipocyte and osteoblast behavior observed in diabetic patients [30,34]. A deeper understanding of how MSCs cause and are affected by abnormal levels of marrow fat and bone mineral density could lead to new therapeutic approaches for osteoporosis in diabetic patients [22], and could lead to therapies that specifically target the stem cell niche [31,35].

In these studies, MSCs, adipocytes, and osteoblasts were cultured in mono-, co-, and tri-culture in laminated PEG hydrogel blocks in normal or high glucose conditions for 7 days, with timepoints at day 1 and 7. Each block was retrieved and analyzed for cell

viability and gene expression markers for osteogenesis, pro-bone formation, adipogenesis, pro-adipocyte function, energy metabolism, and glucose-responsiveness. The MSC block was designed to be enzymatically degradable by integrating an MMP-sensitive sequence (GGGLGPAGGK) into the PEG network, and live MSCs were retrieved after collagenase-mediated degradation of the hydrogel. MSCs were then plated at clonal density to assess clonogenicity. Finally, multivariate analyses were employed to better understand how measured gene expression variables interacted to produce observed cell outcomes.

Hypothesis II: Heparin MPs can temporally modulate endochondral ossification through sequestration of soluble factors in a dose-dependent manner.

Specific Aim II: Evaluate the extent and timing of endochondral ossification in ATDC5 cells with high and low doses of heparin MPs, in comparison to a low protein-binding PEG MP control.

A variety of techniques have been employed to modulate endochondral ossification and chondrogenesis, including culturing cells in aggregate or pellet culture to better mimic the 3D microenvironment [36], co-culture of MSCs and chondrocytes, and delivery of growth factors such as TGFβ and FGFs [37]. However, achieving a stable chondrocytic phenotype is still a challenge, and dedifferentiation in chondrocytes and hypertrophic differentiation in MSCs often occurs [37]. Heparin, a highly sulfated GAG, is known to bind a variety of growth factors involved in endochondral ossification [25]. Recently, the ability of heparin-based hydrogels to sequester cell-secreted growth factors and modulate cellular behavior has been demonstrated in models of angiogenesis, chondrogenesis, and osteogenesis [38–41]. Thus, by culturing heparin MPs with cells

undergoing endochondral ossification, it may be possible to use heparin to capture cell-secreted growth factors and harness their pro-differentiation potential, thus controlling cell access to these growth factors and subsequent differentiation.

In this work, similarly sized heparin and PEG-based MPs were integrated into ATDC5 cell spheroids. Spheroids were cultured for 18 days and chondrocytic gene expression and matrix molecule deposition was assessed at days 1, 6, 12, and 18. To better understand if observed changes in cellular differentiation were due to the ability of heparin MPs to increase or decrease local concentrations of growth factors, monolayer ATDC5 cells were cultured in transwell with heparin and PEG MPs for 12 days. Chondrocytic gene expression was measured at days 6 and 12, GAG and mineral deposition was measured at day 12, and DNA content was measured at day 12. Finally, to evaluate the mechanism of action of heparin MP-mediated changes in cellular differentiation, protein sequestration in conditioned media and SDS-PAGE studies of proteins bound to heparin and PEG MPs were conducted.

Hypothesis III: Heparin-based MPs can temporally control protein sequestration and release.

Hypothesis IIIA: Core-shell MPs with a hydrolytically degradable PEG-based shell and heparin core can temporally control BMP-2 protein presentation to modulate C2C12 cell behavior.

Specific Aim IIIA: Develop and characterize heparin-PEG core-shell MPs and evaluate their ability to sequester and release BMP-2-laden heparin core to elicit a response in C2C12 cells.

Cell differentiation and tissue development processes require tight temporal control over growth factor presentation [3]. Traditionally, controlled delivery vehicles have been used to sustain the release of therapeutic proteins [10,42], but more precise temporal control over protein presentation is often required for tissue regeneration [3]. It has recently been suggested that biomaterials be used to modulate cell access to cell-secreted growth factors, which would harness the potency of endogenous protein and eliminate the need for exogenous protein delivery [3]. For instance, protein-sequestering biomaterials could be used to either amplify the signals of desirable proteins [40,43–45] or eliminate those of undesirable proteins [46]. Combining these two techniques, it could be possible to sequester and isolate a protein that is undesirable at one point in time, then re-present that protein when its function is desirable at a later point in time [3]. As core-shell MPs have been used both to sequester and isolate protein [47–50] as well as release it [51,52], it may be possible to utilize core-shell MPs to sequester and isolate cell-secreted proteins until degradation of the shell, at which point the sequestered protein would be released back into the microenvironment.

In this work, heparin-PEG core-shell MPs were fabricated using a re-emulsification technique to encapsulate pre-formed heparin MPs within a hydrolytically degradable PEG-based shell. Quantification methods indicated that core-shell MPs had tunable and predictable amounts of encapsulated heparin, and degradation studies indicated the ability of the shell to degrade and release the heparin core. Two loading methods were used to load BMP-2 onto core-shell MPs. In “pre-fabrication loading” the heparin core was loaded prior to formation of core-shell MPs, a technique that could be used for exogenous protein delivery from these core-shell MPs. In “post-fabrication

loading" the core-shell MPs were loaded after formation of core-shell MPs, a technique that could permit sequestration and eventual re-presentation of cell-secreted protein. Loading and release studies and a C2C12 BMP-2 bioactivity assay were conducted to evaluate the ability of core-shell MPs to temporally modulate release of a protein-laden heparin core.

Hypothesis IIIB: Increasing the heparin content in hydrolytically degradable heparin-PEG-based MPs will enhance protein loading and decrease protein release rate.

Specific Aim IIIB: Develop and characterize hydrolytically degradable heparin-PEG-based MPs with varying amounts of heparin and evaluate loading and release of histone, a model protein.

As heparin is a potent binder of proteins, it is often integrated into hydrogel delivery systems to enhance protein loading and prevent premature protein denaturation [53–56]. Recently, heparin MP delivery vehicles have been designed for release of therapeutic growth factors [57–59]. However, these heparin-based MPs have either been non-degradable or had degradation profiles that were difficult to control due to cross-linking techniques. For tissue engineering applications that require precisely timed delivery of protein, a heparin-based MP with tunable degradation profile is required. In addition, a heparin-based MP with tunable amounts of heparin would allow more control over protein loading and release, as well as protein sequestration after delivery *in vivo.* Thus, in these studies, heparin-PEG-based MPs were developed and characterized. Dithiothreitol (DTT) was integrated into the MP network to accelerate hydrolytic degradation [60]. 0, 10, 20, 30, and 40 wt% heparin MPs were fabricated and evaluated for heparin content, degradation rate, and histone protein loading and release.

1.3 Significance and Scientific Contribution[1]

The work described in this thesis develops and utilizes biomaterials to both investigate and control complex and dynamic cell systems. For example, the abnormal conditions in disease states can cause changes in cell-cell crosstalk that have major implications on a tissue and organ scale, and a better understanding of this altered cross-talk could leave to new disease interventions. In addition, controlling cell phenotype as it evolves in time during cellular differentiation could provide novel methods by which to control tissue development for injury and repair purposes. Thus, in this work dynamic cellular processes were interrogated by enabling cellular communication within a cell culture platform in hyperglycemic conditions and were modulated by integrating ECM molecules throughout a dense cell aggregate. Through these methods, proof-of-concept experiments demonstrated the necessity of designing *in vitro* culture platforms to permit cellular cross-talk and the utility of integrating heparin into cell aggregates to temporally modulate cell differentiation. In addition, heparin-based materials were designed to better engage with the cellular microenvironment by temporally controlling protein presentation. Overall, these studies highlight hydrogel-based technologies to enable better understanding and control of cellular processes in normal and disease states.

To demonstrate how hydrogel platforms can enable culture conditions and analyses techniques to investigate cellular cross-talk, PEG-based hydrogels were used to

---

[1] Portion of this section were adapted from T.E. Rinker, T.M. Hammoudi, M.L. Kemp, H. Lu, J.S. Temenoff, Interactions between mesenchymal stem cells, adipocytes, and osteoblasts in a 3D tri-culture model of hyperglycemic conditions in the bone marrow microenvironment., Integr. Biol. 6 (2014) 324–37. and from T.E Rinker, B.D. Philbrick, and J.S. Temenoff, Core-Shell Microparticles for Protein Sequestration and Controlled Release of a Protein-Laden Core, in revision.

co-culture MSCs, adipocytes, and osteoblasts under hyperglycemic conditions. The culture of each cell type in separate hydrogel blocks enabled individualized analyses of each cell type while still permitting cellular communication during culture. Additionally, the integration of an enzymatically-degradable peptide sequence within the PEG-based network of the MSC block allowed retrieval of viable MSCs for further culture and clonogenicity analysis. Finally, multivariate analyses techniques were employed to help identify combinations of gene expression markers that governed measured cell outcomes. Rather than analyze the gene expression of each protein individually, such a technique enables visualization of relationships between markers that can eventually be used to predict cell phenotype. The results of this work indicated that the primary source of variance in the system was a result of neighboring cell type, validating the use of hydrogels for co-culture systems to study disease. Thus, this hydrogel-based co-culture platform has unique capabilities that will enable future studies to elucidate how complex interactions between various cellular components are affected in pathological conditions.

To show the utility in incorporating ECM molecules into cell culture platforms to modulate cellular differentiation, heparin MPs were incorporated into ATDC5 cell aggregates. Unlike most biomaterial-based strategies, which depend upon protein delivery to elicit a cellular response, these studies rely solely on a heparin biomaterial to manipulate cellular differentiation. Such biomaterials-mediated sequestration strategies could reduce cost by eliminating the need for adding exogenous protein and may increase signaling efficiency, as cell-secreted growth factors are often more potent than recombinant protein [3]. In addition, unlike strategies that employ biomaterials that sequester one specific protein, heparin can sequester a multitude of proteins, enabling

heparin to continue to interact with a differentiating cell population as protein release evolves.

Still, current methods for endogenous protein sequestration only allow immediate amplification or elimination of protein signals. Thus, core-shell heparin-PEG MPs were developed to temporally modulate protein presentation. The multifunctional core-shell heparin-PEG MPs presented here can evolve with time by sequestering proteins through a PEG-based shell onto a protein-protective heparin core, temporarily isolating bound proteins from the cellular microenvironment, and re-delivering these proteins only after degradation of the PEG-based shell. Thus, these core-shell MPs are a novel tool to harness and isolate proteins produced in the cellular environment and then control when these proteins are re-introduced for the most effective tissue regeneration and repair.

Overall, this work shows the potential for biomaterial-based strategies to interrogate and modulate dynamic cell systems, both those that involve changes in cell-cell crosstalk and those that involve changes in cell state. First, a PEG-based cell-culture platform that enabled culture of multiple cell types followed by individual cell-type analysis was combined with PCA to highlight the cell changes observed in response to neighboring cell type and hyperglycemic conditions. Then, heparin MPs were used to temporally modulate differentiation in an *in vitro* model of endochondral ossification, likely through protein sequestration. Finally, core-shell heparin-PEG-based MPs and hydrolytically degradable heparin-PEG MPs were developed to allow further, user-defined control over temporally modulating protein sequestration and release. As a whole, this work provides insight into dynamic cellular processes and develops tools by which to further investigate or regulate these systems.

CHAPTER 2

BACKGROUND AND LITERATURE REVIEW

2.1 Mesenchymal Stem Cells in the Bone Marrow Microenvironment

2.1.1 Mesenchymal Stem Cells

Over the past several decades, the term "Mesenchymal Stem Cell (MSC)" has been used to describe two different populations of cells. The first population consists of postnatal, self-renewing, multipotent stem cells that give rise to skeletal tissue and are also referred to as skeletal stem cells [61]. This population has been rigorously tested through *in vivo* transplantation to generate replicas of bone containing host-derived hematopoietic marrow tissue and is known to regulate the hematopoietic microenvironment [61]. The second population is more heterogeneous and has been called several names that all fit the same acronym: multipotent stromal cells, mesenchymal stromal cells, and medicinal signaling cells [61]. These cells can be derived from every connective tissue and are defined by *in vitro* culture and metrics, including *in vitro* assays used independently of more stringent, *in vivo* assays and assessment of surface markers only after *in vitro* culture and expansion [61,62]. The inability to specifically and consistently refer to these two populations is one of the reasons that MSCs remain one of the most confusing and frustrating entities in stem cell biology [61,63]. In this review, we define MSCs as the cells described in the first population above.

Further confusion surrounding MSCs has arisen due to the isolation methods used for bone-marrow derived MSCs. Bone marrow cell suspensions contain both hematopoietic and non-hematopoietic stroma. Non-hematopoietic stroma, or stromal

cells, adhere to plastic, allowing separation of hematopoietic cells and stromal cells *in vitro* [61]. These stromal cells, called bone marrow stromal cells (BMSCs), include MSCs but must be further sorted to separate MSCs from other BMSCs [61]. In some studies, this distinction has not been made, which has led to additional confusion in regards to MSC function, identity, and potential applications [30,61].

The focus of this review is bone marrow derived MSCs, which are found perivascular and on the endosteum, and give rise to adipocytes and osteoblasts, as well as support hematopoietic stem cells [62,64]. *In vitro*, MSCs are adherent, clonal cells isolated from bone marrow cell suspensions [30,62]. MSCs are defined by a set of surface markers (positive for CD105, CD73, and CD90; negative for CD45, CD34, CD14, CD11b, CD79a, CD19, and HLA-DR) and their ability to differentiation into osteoblasts, adipocytes, chondroblasts, fibroblasts, and hematopoiesis-supporting stroma [62,64]. While assessment of surface markers and differentiation potential has proven a somewhat effective way to identify MSCs, little to no evidence exists that these surface markers are present on MSCs *in vivo*, and many are also present on pericytes [65].

Various applications have been proposed for MSCs, including tissue regeneration, immunomodulation, and release of trophic factors [64,66]. These pursuits have been met with varying success, as controversy about how best to expand MSCs, what is a "true" population of MSCs, and if it is truly MSCs responsible for immunomodulation and trophic factor secretion still exists [62]. In addition, little is understood about the anatomical location of MSCs and their role in tissue homeostasis [63,64]. For example, MSCs are known to reside in several different *in vivo* niches, and the phenotypical similarities between cells in each niche as well as their potential to self-replenish and

migrate remain poorly understood [30]. Finally, more work is required to understand surface marker differences between MSCs and their progeny prior to *in vitro* expansion [65]. Overall, more work must be done to trace the lineage of MSCs, better define the MSC population, and develop *in vitro* and *in vivo* assays to elucidate MSC function [30,62].

2.1.2 Mesenchymal Stem Cells in the Bone Marrow Microenvironment

Stem cell niches refer to the specific microenvironment that controls stem cell self-renewal, differentiation, and quiescence [67,68]. Relevant cues in the niche include soluble factors (growth factors, cytokines, etc.) derived from other niche cells, cell-cell interactions, cell-ECM interactions, oxygen level, level of reactive oxygen species, and tissue structure [31]. Within the bone marrow microenvironment, skeletal and hematopoietic progenitor cells exist alongside their progeny and other differentiated cells, such as sinusoidal endothelial cells, sympathetic nerve fibers, osteoblasts, osteoclasts, macrophages, and regulatory T cells [30,62,68,69]. Identification of other stem cells in the bone marrow microenvironment is still an area of active research, and will not be discussed here [62]. Mesenchymal stem cells are found in several locations within the bone marrow, including on the endosteum and perivascular, near the sinusoidal endothelium [68,69]. In the bone marrow microenvironment, MSCs have several functions, including regulating HSCs through a variety of soluble factors and giving rise to osteoblasts and adipocytes [68,69]. Still, much more needs to be uncovered about the *in vivo* cellular and molecular interactions of MSCs within the bone marrow niche [70].

The stem cell niche has attracted a lot of attention in the recent years, as it could be manipulated as a means to control stem cell behavior [30,35,67]. For example, it has been suggested that the niche be targeted to combat diseases like cancer and diabetes [67,69]. To gain a deeper understanding of 1) regulators of the stem cell niche and 2) how to change the niche in order to modulate stem cell behavior, development of *in vitro* model systems have been explored [30,67]. Often, these systems include multiple cell types and are three-dimensional, but incorporation of every aspect of the *in vivo* niche is not possible [31]. However, useful information that can be further explored *in vivo* can still be gained from these *in vitro* systems.

2.1.3 Diabetes and its Effects on the Bone Marrow Microenvironment

Diabetes mellitus types I and II affected 135 million people in 1990, and are predicted to affect 300 million by 2025 [71]. Categorized as a metabolic disease, diabetes is caused by lack of insulin production (primarily type I) and/or lack of insulin sensitivity (primarily type II) [72]. Insulin irregularities result in an inability to regulate blood glucose levels, which leads to a variety of complications, including chronic hyperglycemia [72]. Hyperglycemic conditions can cause debilitating dysfunction and failure of various organs, including eyes, kidneys, nerves, heart, and blood vessels [19]. In the bone marrow, hyperglycemia can result in sinusoid abnormalities and HSC dysregulation, as well as increased fat infiltration [69]. Additionally, hyperglycemic conditions result in excessive reactive oxygen species (ROS) due to glucose autooxidation, ROS overproduction by the mitochondria, non-enzymatic glycation, and the polyol pathway [73]. ROS can negatively affect cells through DNA, protein, and lipid damage, and increased oxidative stress can also lead to inflammation [73].

While diabetes alone is associated with morbidity and mortality, patients with diabetes are also at increased risk for diseases like osteopenia and osteoporosis, as well for bone fracture [19–21,74]. About 50% of patients with type I diabetes have bone loss, and 20% of patients ages 20-56 have osteoporosis [21]. Osteoporosis is defined by reduced bone mass and bone microarchitectural abnormalities, which results in reduced bone strength and increased fracture risk [72]. Clinically, osteoporosis is diagnosed by bone mineral density (BMD) measurements that are more than 2.5 standard deviations lower than the sex-matched young adult mean [72,75]. While decreased BMD has been observed in patients with type I diabetes, normal to above average bone masses have been observed in patients with type II diabetes [76]. However, both type I and II diabetes patients show higher fracture risk, indicating that other factors besides bone mass, such as abnormal bone microarchitecture, may be implicated in type II diabetes fractures [76,77]. In diabetes as well as other diseases such as osteoporosis and anorexia nervosa, BMD and marrow adipose tissue (MAT) are inversely related [17,18]. Increased MAT is observed in patients with diabetes type I and it is possible that MAT composition is different in patients with diabetes type II [76]. Still, this inverse relationship between BMD and MAT is not fully understood, and a deeper understanding of communication between cell types that make up these tissues could elucidate the biological processes that lead to abnormal levels of each tissue type.

2.1.4 MSCs, Adipocytes, and Osteoblasts in the Bone Marrow Microenvironment

Within the bone marrow microenvironment, adipocytes and osteoblasts are both derived from MSCs and contribute to mature bone and MAT [22]. While bone has a clear function in adult physiology, the precise function of MAT is still unknown [18]. Some

speculate that MAT acts as an energy source for bone remodeling, an energy-intensive process, while other evidence has pointed toward MAT as actively modulating the hematopoietic stem cell (HSC)/MSC niche and osteogenesis through soluble factor signaling [18,22,74,78]. Interestingly, MSC lineage commitment to either progeny seems to be at the expense of the other [17,22,78]. For instance, the master regulator of adipogenesis, peroxisome proliferator activated receptor gamma (PPARγ), is known to suppress osteogenesis, while the master regulators for osteogenesis, WNT and Runt-related transcription factor 2 (RUNX2), are known to suppress adipogenesis [18,22]. As MSC lineage commitment is a result of signals from other cell types in the niche, including mature adipocytes and osteoblasts, as well as systemic signals, fate decisions are likely altered in disease states [22]. Additionally, mature adipocytes and osteoblast secrete signals that could affect each other. For example, adipocytes secrete leptin, which is believed to decrease bone mass [79–81], and adiponectin, believed to have an effect on proliferation and differentiation of osteoblasts [82]. Osteoblasts secrete osteocalcin, which aids in bone matrix mineralization [79], and osteoprotegrin, which suppresses osteoclastogenesis [72,82]. Thus, altered numbers of either cell type could result in increases or decreases in release of signaling molecules that cause and perpetuate abnormal levels of MAT or BMD.

As discussed, the inverse relationship between MAT and BMD could be a result of altered MSC differentiation in diabetic disease states. While the reasons for decreased BMD are unclear, it is speculated that higher levels of glucose could have direct, toxic impact on osteoblasts or negatively alter the ROS environment [21,74]. As increased marrow fat is observed in hyperglycemic conditions, it is possible that MSCs are

triggered to commit to the adipogenic lineage at the expensive of osteoblasts, thus shifting the bone remodeling process too far toward osteoclast-mediated resorption [21,22]. In addition, all three cell types have been found to respond adversely to hyperglycemic conditions [21]. MSCs show increased apoptosis and senescence and decreased colony-forming capacity and osteogenic potential in hyperglycemic conditions [83–86].When cultured in high glucose, adipocytes have decreased insulin sensitivity, dysregulated triglyceride storage, increased production of ROS and pro-inflammatory cytokines, and decreased adiponectin secretion [87–89]. Lastly, osteoblasts demonstrate reduced proliferative capacity, mineralization capabilities, collagen I synthesis, and expression of differentiation markers in hyperglycemic conditions [90–93]. Still, how hyperglycemia alters the cellular crosstalk between osteoblasts, adipocytes, and MSCs remains unclear.

2.1.5 Co-Culture of Osteoblasts, Adipocytes, and MSCs[2]

To better understand interactions between different cell populations, two- and three-dimensional (2D and 3D, respectively) co-culture systems have been employed *in vitro* [94,95]. Traditionally, 2D cell culture has been employed due to ease of use, convenience, and high cell viability [96]. Still, results from 2D culture must be interpreted with caution, 2D culture does not replicate many the important 3D components of the *in vivo* cellular microenvironment, including cell-cell and cell-matrix

[2] Portions of this section were adapted from Rinker T.E**.** and Temenoff J.S. "Micro- and Nanotechnology Engineering Strategies for Tissue Interface Regeneration and Repair." Tissue and Organ Regeneration: Advances in Micro and Nanotechnology, 105-156, 2014.

contacts. 2D co-culture systems were used in several studies to investigate interactions between MSCs, osteoblasts, and adipocytes. In general, MSCs have shown enhanced osteogenesis when co-cultured with osteoblasts in either direct contact or transwell culture [97–101]. In one study, murine MSCs were cultured with osteoblast-like (MC3T3) or osteocyte-like (MLO-Y4) cells, and both ALP production and calcium deposition were higher in MSCs cultured with osteocytes, though osteoblast cells caused higher levels of MSC proliferation [101]. In another transwell study with murine MSCs (C3H10T1/2 cell line) and murine calvaria-derived bone cells (MC3T3 cell line), few differences were observed, though a slight increase in MSC ALP production was observed when the ratio of osteoblasts was decreased [100]. Conversely, a separate study with human MSCs in transwell co-culture with human osteoblasts showed upregulation of osteogenic markers [99]. One particularly interesting study showed that in indirect contact, osteoblasts stimulated osteogenic differentiation of MSCs, but in direct contact, inhibited osteogenic differentiation. Authors determined that in direct contact, the cadherin pathway suppressed the WNT pathway, which otherwise would have induced osteogenesis in MSCs [98]. Another co-culture experiment with murine osteoblasts and MSCs confirmed that the enhanced osteogenesis observed in MSCs was due to the WNT pathway [97]. Overall, osteoblasts appear enhance MSC osteogenesis or to have a negligible effect on MSC behavior.

In co-cultures between osteoblasts and adipocytes, osteogenesis is generally severely decreased in the presence of adipocytes [102–104]. In a study with osteoblastic MC3T3 cells and 3T3-L1 pre-adipocytes, the adipocyte-secreted free fatty acids inhibited osteoblasts proliferation, induced apoptosis, and reduced osteogenic markers (ALP

activity, RUNX2, ollagen I, and osteocalcin expression, and matrix mineralization) [104]. Similarly, a study with human adipocytes and human osteoblasts in transwell culture showed decreased osteogenic and increased adipogenic markers in osteoblasts, suggesting that transdifferentiation of osteoblasts into adipocytes may have occurred [103]. In line with the studies described above, primary human adipocytes caused decreased primary human osteoblast proliferation in transwell co-culture [102]. Few studies with MSC and adipocyte cultures have been conducted, and thus little is known about how these two cell populations affect each other. Overall, these studies indicate that MSCs, adipocytes, and osteoblasts clearly affect each other, probably both through soluble factor signaling and direct contact. More studies, possibly those that include a 3D culture platform and more comprehensive outcome measures, will need to be performed to fully elucidate how these effects might translate to *in vivo* observations within the bone marrow microenvironment.

2.2 Endochondral Ossification

2.2.1 Endochondral Ossification and the Growth Plate

Endochondral ossification occurs in the process of bone development, during which mesenchymal cells condense to form a cartilage anlagen and either permanently differentiate into articular chondrocytes or take on a transient chondrogenic phenotype before proceeding through endochondral ossification [105]. Endochondral ossification begins when mesenchymal cells condense via adhesion factors and then begin to differentiate into chondrocytes, enlarging the cartilage anlagen [23,106]. The primary ossification center forms when a portion of these chondrocytes stop proliferating and

undergo hypertrophy, resulting in mineralization and vascularization of the tissue near what will become the diaphysis of the bone [23,106]. While this occurs, chondrocytes continue to proliferate and the cartilage grows [23,106]. These proliferative chondrocytes assume a flattened shape and stack on top of one another to form columns, oriented in the direction of developing bone [23,106]. Then, secondary ossification sites are formed at each end (epiphysis) of the bone [23,106]. The remaining cartilaginous tissue trapped between the two ossification centers is called the growth plate [23,106]. Chondrocytes in the growth plate continue to proliferate and undergo hypertrophy in a process tightly controlled by both local and systemic signals, allowing bone elongation until closure of the growth plate during puberty [23,106].

Maintenance of these spatially and temporally distinct developmental stages depends on both systemic hormones and cellular communication between mesenchymal cells, chondroprogenitor cells, chondrocytes, and other cells in and around the growth plate [23,107]. The mechanisms behind how these growth factors travel long-range through the growth plate ECM and form concentration gradients are not entirely understood, but current evidence points towards GAGs as having a significant role [108]. Both chondroitin sulfate (CS) and heparan sulfate (HS) are thought to be involved in developing morphogen gradients and promoting receptor-ligand binding within the growth plate [106,107] (see Section 2.4.2 for more details). Additional studies should aim to use histological approaches to track protein and GAG movement and localization in organ culture or animal studies to further elucidate the role of GAGs in regulating growth factor-cell interactions.

At the first stage of endochondral ossification, SOX9 is required for the commitment of mesenchymal cells into chondrocytes, and growth hormone stimulates these resting zone (pre-proliferative) chondrocytes to secrete IGF-1, which enhances chondrocyte proliferation [106,109]. Several factors regulate proliferative chondrocytes. First, a negative feedback loop is created between Indian Hedgehog (IHH) and parathyroid hormone-related protein (PTHrP) to modulate the transition of proliferative chondrocytes into hypertrophic chondrocytes [23,106,109,110]. PTHrP is secreted by chondrocytes at the epiphysis of long bones, and prevents proliferative chondrocytes from undergoing hypertrophy [23,106,109,110]. However, when chondrocytes are out of range of PTHrP, they enter a pre-hypertrophic stage and begin to secrete IHH [23,106,109,110]. IHH acts to increase the rate of chondrocyte proliferation, delays hypertrophy, and through unknown mechanisms, stimulates the PTHrP secretion from chondrocytes at the end of long bones [23,106,109,110]. Another signaling molecule implicated in enhancing chondrocyte proliferation is BMP. BMP-2, 3, 4, 6, and 7 are expressed in the perichondrium, BMP-7 in proliferative chondrocytes, and BMP-2 and 6 in hypertrophic chondrocytes [23,110]. Overall, BMPs are known to promote chondrocyte proliferation and also induce IHH expression [23,106,109,110]. FGFs are also important in growth plate regulation, and several receptors, including fibroblast growth factor receptor (FGFR) 2, FGFR3, and FGFR1 are expressed in mesenchymal condensations, proliferative chondrocytes, and hypertrophic chondrocytes, respectively [23]. FGF-1, 2, 15, 18, and 19 are all expressed in the growth plate and act through FGFR3 to repress proliferation and inhibit IHH production [23,106]. GAGs, most likely heparan sulfate, are necessary for these interactions [106]. During proliferation,

chondrocytes actively lay down ECM molecules like collagen II and aggrecan, and to a lesser extent biglycan and glypican [106,109]. Expression and secretion of these molecules are also controlled by the growth factors mentioned above [106].

Finally, RUNX2 and WNT induce chondrocyte hypertrophy [23,106,110]. Hypertrophic chondrocytes are critical in bone development, as they provide a scaffold for subsequent bone formation [110]. These chondrocytes have increased levels of intracellular calcium and secrete collagen X as well as matrix vesicles that contain calcium phosphate, hydroxyapatite, and matrix metalloproteinases (MMPs) [109]. One of these secreted MMPs, MMP13, can degrade the collagen II matrix previously laid down by proliferative chondrocytes [106]. Hypertrophic chondrocytes also secrete vascular endothelial growth factor (VEGF), which, along with the hypoxic conditions in the growth plate, attracts blood vessels to the matrix [23,106,109,110]. Finally, hypertrophic chondrocytes near the ossification front undergo apoptosis, which is regulated by intracellular calcium levels, retinoic acids, and vitamin D [106,109]. Then, osteoclasts, osteoblasts, and bone marrow cells invade the newly ossified tissue [106]. Overall, endochondral ossification and maintenance of the growth plate are very tightly controlled processes, and disruption of even one of these signaling pathways can have severe consequences in long bone development.

2.2.2 Growth Plate Injuries and Repair Strategies

Injuries to the growth plate cartilage occur in 20% of childhood bone fractures and can result in bony bridge formation that hinders normal growth, resulting in limb length disparities, bone angulation deformities, and in severe cases, growth arrest

[111,112]. Current treatments involve correcting angular deformations and limb length discrepancies, and in some cases, removal of the bony bridge [112,113]. In an effort to prevent reformation of the bony bridge, filler substances such as transplanted fat, muscle, polymeric silicone, bone wax, and bone cement are injected into the defect [112]. These strategies are only partially successful and do not allow the tissue to return to its normal structure or function [112]. Currently, no biological therapies are clinically available, and development of a therapy that could promote regeneration and repair of the growth plate would be greatly beneficial [112,113].

Recent *in vivo* studies have highlighted the utility of using tissue engineering approaches to repair growth plate defects. In most approaches, a therapeutic cell type, either MSCs or chondrocytes, are seeded onto scaffolds made of collagen, chitosan, hyaluronic acid, agarose, or gelatin and then implanted into growth plate defects [111,113–118]. For example, chondrocytes within a collagen gel were implanted into a physeal defect in rabbits, which prevented early ossification and growth plate closure, and reduced angular deformity and limb length discrepancy [114]. In studies with miniature pigs, growth plate defects filled with MSCs within a collagen/chitosan gel did not show bone bridge formation, and affected limbs with MSC implants grew more than control limbs [118].

In contrast to these positive results, implantation of a gelatin sponge seeded with MSCs into a growth plate injury in an ovine model caused formation of fibrous tissue and similar functional outcomes as control groups [113]. One particularly interesting study could point to reasons why variability is observed in MSC-based growth plate therapies. MSCs were either undifferentiated or pre-differentiated down a chondrocytic lineage,

then seeded onto an agarose gel and implanted into a growth plate defect in rats. While bone bridge formation was observed in all cases, limb length discrepancy was only observed in the group with undifferentiated MSCs [116]. This study highlights the necessity of ensuring high-quality MSCs for growth-plate cell therapies. Finally, one study attempted to deliver an IGF-loaded poly(lactic-co-glycolic acid) (PLGA) scaffold rather than a cell-seeded scaffold in a rabbit model, in an effort to stimulate endogenous cells in the growth plate. This technique was partially successful, as a thin layer of disorganized cartilage remained in groups with IGF-loaded scaffolds, compared to bony infiltration observed in all other groups [111]. Overall, tissue engineering strategies for growth plate injuries are promising, but more work needs to be done to evaluate proper cell types and scaffold materials. For example, due to their tendency to undergo endochondral ossification *in vitro* and *in vivo* [37], MSCs may be an ideal candidate cell type for growth plate regeneration, and as these studies indicate, control of this differentiation process through proper growth factor presentation as well as material interactions could improve outcomes.

2.2.3 Articular Cartilage and Chondrogenesis

Articular cartilage is a hyaline cartilage found on the articulating surface of bones in joints, where it acts to provide a smooth, articulating surface and allows resistance of compressive forces [119]. Hypocellular in nature, cartilage consists primarily of collagen II, the proteoglycan aggrecan, and water [119,120]. Articular cartilage has a zonal arrangement in which cell and collagen fiber organization differ [119,120]. The superficial zone is in contact with the synovial fluid and consists of flattened chondrocytes and parallel collagen fibrils [119]. Moving toward the bone, the

intermediate or transitional zone consists of rounded chondrocytes and less organized collagen fibers [119]. Finally, in the deep/basal zone, the last layer prior to calcified tissue and the tidemark, rounded chondrocytes are oriented in vertical columns perpendicular to the articular surface [119]. Chondrocytes have long half-lives in normal, non-diseased states and act to balance matrix synthesis with matrix breakdown [119]. However, if this balance is disturbed by disease or injury, it can be very detrimental to the tissue and quite challenging to reestablish [119].

The formation and maintenance of adult articular cartilage remains poorly understood, but it is believed that as joints begin to form in the cartilage anlagen ("interzone" regions), both pre-existing chondrocytes and migrating progenitor cells make up the cell populations that become articular cartilage as cavitation and morphogenesis proceed [121,122]. Many of the same growth factors involved in endochondral ossification, including BMPs, growth differentiation factors (GDFs), TGFβ, and IHH, are thought to be involved in the development and maintenance of articular cartilage [121]; however, the mechanism by which these growth factors function in articular cartilage remain unknown. Though chondrocytes of the articular cartilage are more stable than growth plate chondrocytes, articular chondrocyte dedifferentiation can occur with age and during disease, suggesting that maintenance of articular cartilage requires strict control over environmental factors throughout life [121,123].

2.2.4 Cartilage Injury and Repair

Injuries to articular cartilage, resulting from degenerative joint diseases or traumatic injury [124], can result in pain, loss of mobility, and disability [37,125]. In

2005, arthritis, one of the degenerative joint diseases aforementioned, affected 70 million US adults, and the economic burden of arthritis in the US was estimated to be $60 billion in 2000, and estimated to increase to $100 billion by 2020 [126]. The severity of cartilage injuries can vary depending upon the type of trauma and the zones affected [119]. However, common to most injuries is the increased concentration of proteolytic enzymes and cytokines, leading to tissue degradation [119]. As previously mentioned, high rates of collagen turnover in disease states or injuries can result in chondrocytes unable to replace lost collagen, resulting in loss of a well-organized matrix, mechanical failure, matrix degeneration, and arthritis [119]. In addition, if a large portion of cartilage is lost, severe degradation of the remaining matrix can occur [119]. If the injury penetrates the tidemark, a temporary fibrocartilage matrix may be secreted to fill the defect, but this matrix does not have the same mechanical properties as cartilage and is often lost over time, resulting in areas of exposed bone [119]. Overall, due to its low capacity for healing, articular cartilage injuries have poor clinical outcomes [119,120].

Several treatments are used for articular cartilage therapies, including non-reparative strategies like debridement, chondral shaving, and lavage; reparative methods such as arthroplasty and microfracture; and finally regenerative methods such as joint replacements, cartilage autografts and allografts, and autologous chondrocyte transplantation [126,127]. Some of these regenerative methods have proved promising. For example, in autologous chondrocyte transfer, cartilage from a non-load bearing region is used to obtain autologous chondrocytes for re-implantation in the defect [37,125]. While this procedure is partially successful in many cases, it is associated with several problems, including growth of fibrous tissue, creation of additional injury site

when obtaining autologous chondrocytes, low cell yield of the cartilage biopsy, dedifferentiation of autologous chondrocytes in monolayer expansion, reduced chondrogenic potential of chondrocytes from aged patients or patients with osteoarthritis, and large inter-donor variability in the performance of autologous chondrocytes [125,128].

To mitigate these challenges, MSCs have been explored as an alternate cell source for cartilage repair, but inducing MSC chondrogenesis and maintaining a stable chondrogenic phenotype has thus far proved challenging, limiting their therapeutic potential [125]. When MSCs undergo chondrogenic differentiation *in vivo*, the chondrocytic phenotype is transient, as cells appear to be programmed for endochondral ossification, and thus eventually undergo hypertrophy and mineralization [37]. A variety of techniques have improved outcomes, including delivery of growth factors such as TGFβs, BMPs, FGFs, IGFs and PTHrP [37,129,130] as well as co-culture with articular chondrocytes [128,131–135]. Still, investigation of new techniques to promote and maintain the MSC chondrocytic phenotype is an active field of study.

2.3 *In Vitro* Cell Culture Systems

2.3.1 Hydrogels for *In Vitro* Cell Culture[3]

Recently, it has been realized that the culture of cells in 2D limits the inclusion of parameters known to be important in the 3D *in vivo* environment, where cells have an ECM meshwork on which to communicate [2,4,96,136–139]. These parameters include

[3]Portions of this section were adapted from Rinker T.E**.** and Temenoff J.S. "Micro- and Nanotechnology Engineering Strategies for Tissue Interface Regeneration and Repair." Tissue and Organ Regeneration: Advances in Micro and Nanotechnology, 105-156, 2014.

mechanical cues, communication between cells and matrix, and communication between adjacent cells [4]. To integrate these parameter into *in vitro* cell culture systems, hydrogels are often used, as they are versatile, porous 3D constructs consisting primarily of water, providing a low barrier to soluble factor diffusion between cells [2,140,141]. In addition, hydrogels tend to be biocompatible and nonimmunogenic, and able to mimic the physical properties of tissues [29,142]. Synthetic and natural polymers can be used to form gels, either of which can be modified to achieve desired bioactivity [2,140,141]. Examples of natural materials include collagen, fibrin, hyaluronic acid, Matrigel, alginate, agarose, and GAG based scaffolds [29,143]. While natural materials can be useful, given their potential to provide cells with signals commonly found in the ECM, they tend to be heterogeneous and can have ill-defined properties [29].

Synthetic materials often cannot interact with cells prior to modification, providing researchers with a blank template to chemically modify [29]. Examples of synthetic materials include PEG, poly(2-hydrosy ethyl methacrylate), poly(acrylamide), and poly(N-isopropyl acrylamide), which do not naturally promote cell attachment, but can be modified with a variety of ECM protein sequences (i.e. RGD from fibronectin, YIGSR from laminin, or GFOGER from collagen) that encourage cell adhesion [29,143,144]. PEG is especially useful as it is FDA approved and tends to be protein, and thus cell, repulsive, allowing patterning of cells through specific placement of biomolecules [29,143,144]. Thus, established and emerging techniques to modify both natural and synthetic materials have allowed 3D hydrogel culture systems to better mimic the *in vivo* cellular microenvironment, and promise to enable more accurate analyses of dynamic cell behavior.

2.3.2 Integrating Complexity into Hydrogel-Based Culture Platforms

3D cell culture platforms are most often engineered to achieve one of two goals: 1) develop a template to form a functional tissue or 2) create a platform for disease models [29,145,146]. Both of these applications require precise control over spatial localization of biomolecules, geometries, and mechanical properties [29]. Several techniques are used to pattern hydrogels for tissue engineering applications. Traditional techniques, such as solvent casting/particle leaching, freeze drying, and gas foaming allow for porous scaffolds with controllable mechanical properties, but are not able to provide the spatial patterns often desired for cell culture systems [29,143]. Recently, bioprinting has been used to deposit cells and prepolymer hydrogel solutions in specific spatial locations in a layer-by-layer approach [29]. While this technique is automated and can be used to develop relatively large layers of cells/polymer solutions, it is limited in its polymer and cell compatibility [29].

Photolithography, the use of light or photons to transfer the shape of a mask onto a light-sensitive surface, has been used to successfully pattern a variety of cell types, including hepatocytes, fibroblasts, C2C12 cells, endothelial cells, cardiac stem cells, HT1080 cells, embryonic stem cells, neurons, MSCs, osteoblasts, and adipocytes [29,32,33]. This technique can be applied in several different manners. In the simplest method, a photomask is developed and UV light is used to crosslink a photo-sensitive polymer solution that is not covered by the mask [29,33,147,148]. This method has been used to pattern RGD peptide sequences into PEG-DA hydrogels, achieving specific localization of human dermal fibroblasts [148]. In addition, a co-culture hydrogel with

spatially patterned tendon fibroblasts and MSCs was developed through use of photolithography and microfluidics [33].

Lithography techniques can also be carried out with lasers, in which multi-photon laser scanning techniques can be used to generate free-radicals at precise spatial locations, thus enabling reactions between the functional groups of a scaffold and biomolecules only at desired locations [146]. For example, multi-photon laser scanning was used to pattern RGD-peptides into vessel features, promoting human umbilical vein endothelial cells (HUVECs) and mesenchymal progenitor cells to organize around tubular networks in PEG-DA hydrogels [146]. In another study, two-photon laser scanning was used to pattern RGD into PEG-DA hydrogels to guide cell migration, as human dermal fibroblasts only migrated to areas of the hydrogel functionalized with RGD [149]. Finally, multi-photon lithography has also been used to develop selective patterning of a collagenase-sensitive peptide in PEG-DA hydrogels, which in the future could allow for cell-mediated gel degradation in specific, user-defined locations [150]. Thus, a variety of techniques are available to integrate complexity into 3D hydrogel cell culture systems. This complexity, which enables scaffolds to evolve with time through use of temporally controlled degradation or patterning of biomolecules, can guide dynamic cell behavior using strategies that mimic functions of the native ECM. Further assessment of ECM-cell interactions should be used to guide the design of future cell scaffolds.

2.3.3 *In Vitro* Disease Model Systems for the Bone Marrow Microenvironment

In vitro models of disease can often enable deeper understanding of disease progression and potential therapies than can be gained *in vivo* [5,151]. While *in vitro*

model systems cannot account for systemic effects of disease or the drugs that treat them, they do allow for specific questions to be asked and assessed in an isolated system with reduced complexity as compared to the *in vivo* environment [5,151]. In addition, *in vitro* model systems allow for the use of human cells, which is helpful for cases in which animal and human cells behave differently and can reduce the likelihood of failure in clinical trials [5,151]. Finally, *in vitro* models allow for high-throughput assessment of various disease conditions and drugs [5,151]. Recently, it has been realized that relevant cellular communication as well as three-dimensional microenvironments are important factors for many disease models, and co-culture of two or more cell types as well as utilizing 3D scaffolds and hydrogels are frequently employed in disease models [5,151].

As discussed in Section 2.1, the bone marrow microenvironment is home to multiple cell types, including at least two stem cell populations, the mesenchymal stem cell and the hematopoietic stem cells, as well as mature endothelial cells, adipocytes, osteoblasts, and other hematopoietic progeny [31]. While the bone marrow microenvironment has been studied *in vivo*, *in vitro* models of the bone marrow microenvironment could be a powerful tool to study hematological diseases, MSC behavior in various conditions, and the relative contribution of different cell types in the niche to stem cell maintenance and behavior [31,152]. Historically, models of the bone marrow microenvironment have strived to better understand HSC behavior [31,152]. Conventionally, a stromal feeder cell layer has been used to maintain HSCs *in vitro*, but these experiments have often been conducted on 2D surfaces that do not mimic the 3D microenvironment [31].

In response, 3D models of the bone marrow microenvironment have been generated. In one example, 3D spheroids of MSCs and osteoblasts were used to study the migration, lodgment, and proliferation of HSCs [153]. It was observed that HSCs were more likely to home and remain inside spheroids with MSCs and osteoblasts as opposed to just MSCs alone [153], a result that would not have been possible to observe in a 2D system. In another system, bone marrow stromal cells were cultured on 3D ceramic scaffolds with hematopoietic cells under perfusion, and higher rates of bone formation were observed as compared to 2D cultures [154]. Another study showed that MSCs, which can reside in the perivascular niche, had enhanced osteogenesis and inhibited adipogenesis when cultured with HUVECS as opposed to fibroblasts [155]. These *in vitro* models of the bone marrow microenvironment indicate that cellular communication, as well as a 3D environment, are important for cell function and lay foundations for future disease models and *in vitro* drug testing.

Several *in vitro* model systems of the bone marrow microenvironment have demonstrated investigation of disease conditions and testing of therapeutics. One system modeled the ability of "third party", or undamaged, MSCs to aid in hematopoietic cell transplantation after the damaging of resident stroma by toxic conditioning regimes (conducted to prepare tissues for transplantation) [156]. Third party MScs were able to enhance growth of the damaged stroma, a potential new strategy to improve hematopoietic cell transplant [156]. Another system modeled chronic myeloid leukemia (CML) by culturing osteogenesis-induced MSCs and bone marrow mononuclear cells from patients with CML on decelluralized bone [157]. Overall, results indicated that the 3D system was more likely than a similar 2D system to recapitulate the progression of

leukemia, and will allow more studies to be conducted in the future [157]. Finally, an artificial bone marrow microenvironment was developed by implanting a polydimethylsiloxane (PDMS) device coated with collagen I and bone-inducing powder in a mouse to create functional bone and bone marrow *in vivo* [158]. Then, the device was retrieved, connected to a microfluidic device, and co-cultured with HSCs under perfusion, which enabled maintenance of a larger population of long-term HSCs than traditional stroma-feeder layer culture [158]. Finally, the system responded to radiation and a radiation countermeasure drug in a similar fashion to *in vivo* marrow, validating the platform for further disease and drug testing [158]. Overall, these studies highlight the ability to better understand the bone marrow microenvironment through *in vitro* models, and suggest that utilization of *in vitro* models will enable deeper understanding of bone marrow disease and treatments.

2.3.4 Modulating Chondrogenesis *In Vitro*

In vitro models of chondrogenesis are often used to investigate the influence of various materials, soluble factors, and other cell types on chondroprogenitor cells and chondrocytes. In this section, the *in vitro* culture of bone marrow-derived MSCs will be considered. Chondrogenic differentiation of MSCs is generally carried out in 3D, either in dense cell aggregates or within a scaffold, which are often hydrogel-based [37]. A variety of materials have been used for hydrogel-based scaffolds for chondrogenic differentiation of MSCs, including CS, heparin, hyaluronic acid (HA), alginate, agarose, collagen, fibrin, polypeptides, chitosan, cellulose, PLGA, and poly(lactic acid) (PLA), and PEG [38,39,159–162]. As CS and heparin will be discussed further in Section 2.4.3, they will not be included here. A variety of material properties can influence

differentiation, including hydrogel cross-linking density. For example, increased cross-linking density in HA-based hydrogels resulted in decreased cartilage matrix deposition and increased hypertrophy in encapsulated MSCs [163,164]. Similarly, enhanced MSC chondrocytic differentiation was observed with increased permeability of poly(ε-caprolactone) scaffolds [165]. While the exact mechanism is unknown, it is speculated that increased scaffold permeability enhanced nutrient (and likely growth factor supplement) diffusion to MSCs, and may also be conducive to formation of cellular condensations [163–165].

Another important hydrogel property is the ability of cells to adhere to the gel, usually achieved by integrating biochemical moieties into the hydrogel that facilitate integrin binding. However, the distribution (or relative spacing) of these binding sites can influence MSC differentiation. For example, as the density of the fibronectin-derived peptide sequence RGD was increased in alginate hydrogels, MSC chondrogenesis was increasingly inhibited, possibly due to restrictions in integrin clustering [166]. However, this does not indicate that cell adhesion to hydrogels is not important for chondrogenesis, as a study with agarose hydrogels and polypeptide hydrogels showed significantly higher MSC chondrogenesis in the polypeptide hydrogels, likely due to cell adhesion [167]. Similarly, in a study with adipose derived stem cells, enhanced chondrogenesis was observed on collagen type II as compared to collagen type I gels, likely due to integrin-mediated signaling pathways allowing cells to take on a rounded shape [168]. Finally, protein-binding properties of hydrogels can modulate growth factor concentration in a manner that enhances or restricts differentiation. While a more extensive overview is provided in Section 2.4.5, one example is the ability for sulfated alginate hydrogels to

enhance MSC chondrogenesis as compared to alginate hydrogels due to increased TGFβ-1 binding [169]. Overall, the properties of the materials used to culture MSCs can influence chondrogenic potential.

In most cases, chondrogenesis is induced with soluble factors, which can be delivered individually, in combination, or over time [170]. Growth factors delivered include TFGβs 1,2, and 3; BMPs 2,4,6,7,9, 13, and 14; FGF-2; and IGF-1 [161,170], most of which are involved to some extent in endochondral ossification *in vivo* (see Section 2.2.1) [23]. While the impact of these growth factors varies greatly from experiment to experiment and is dependent on culture conditions, TGFβs appear to be the most chondro-inducive, while FGF-2 is often observed to enhance chondrocyte proliferation rate [170]. BMPs and IGFs are occasionally added in combination with TGFβs, but effects vary drastically, likely due to cell source and culture conditions [161,170]. Because growth factor concentrations change during chondrogenic differentiation *in vivo*, temporally controlled delivery of growth factors has been suggested as a means to better control differentiation [37], and has been met with some success [129,170]. While delivery of growth factors to induce chondrogenesis shows promise, optimal combinations and delivery timelines remained to be determined.

Recently, co-culture of MSCs with chondrocytes has been explored as an alternate mechanism to direct chondrogenic differentiation. Several studies have investigated the influence of chondrocyte-conditioned medium on MSCs [131,171], but found that direct co-culture between MSCs and chondrocytes produced much stronger increases in chondrocytic markers and decreases in hypertrophic markers [131], suggesting that cellular communication is required for improved MSC chondrogenesis in the co-culture

context. To this point, co-culture studies that have been conducted in transwell systems [128,132] and on scaffolds and hydrogels [133–135] have shown the potential of co-culture to induce MSC chondrogenic differentiation. In addition, co-culture pellet systems have been investigated as a means to both induce MSC chondrogenesis and prevent MSC hypertrophy and chondrocyte de-differentiation. In several studies, it has been shown that MSC in pellet co-culture with chondrocytes at ratios ranging from 50:50 to 95:5, respectively, have shown enhanced chondrogenesis and a reduction in hypertrophic markers as compared to monoculture controls [128,134,172,173]. These studies suggest that the communication between chondrocytes and MSCs allows maintenance of the chondrocytic phenotype. Overall, chondrogenesis is strongly dependent on both scaffolds and soluble factor delivery. However, techniques that utilize scaffolds and soluble factors in a manner that accounts for the dynamic temporal changes that occur during differentiation have yet to be fully realized.

2.4 Glycosaminoglycans and Protein Sequestration

2.4.1 Function of Heparan Sulfate and Heparin

Heparan sulfate (HS) and heparin are GAGs of similar structure that are implicated in regulating both developmental processes and adult tissue homeostasis through their strong affinity to proteins [174,175]. The diverse function of HS and heparin can be attributed to their structure. HS and heparin are polysaccharide chains of repeating disaccharide units (uronic acid residue and a glucosamine residue) that can be modified by the addition of sulfate groups [26,174,176]. Overall, heparin has a much higher degree of sulfation, more negative charge, and is less structurally diverse than heparan sulfate [177]. Another difference between HS and heparin is the common uronic

acid residue found in their disaccharide repeat units. While an N- and 6-O-sulfated or N-acetylated D-glucosamine residue is common for both, 2-O-sulfated L-iduronic acid and D-glucuronic acid are the common uronic acid residue for heparin and heparan sulfate, respectively [26]. The specific sulfation pattern and the overall strong negative charge of HS and heparin GAGs are thought to be two of the primary factors that allow protein interactions [175]. In the body, HS is attached to membrane-bound (syndecans, glypicans, betaglycans) or ECM associated (perlecan, agrin, collagen XVIII) core proteins to form HS proteoglycans (HSPGs) [174,175]. On the cell membrane, HS acts to facilitate ligand-receptor binding and in the ECM, participates in the development of morphogen gradients and is thought to protect growth factors from degradation [174,175,177,178]. Alternatively, heparin is found primarily in connective-tissue type mast cells, attached to the core protein serglycin in intracellular storage granules [26,175]. When released from the cell, heparin acts as an anticoagulant in the coagulation cascade either directly or indirectly by enhancing antithrombin-thrombin binding [177,179].

HS has been found to bind over four hundred proteins, including growth factors, enzymes, cytokines, and ECM molecules, and is implicated in diverse processes such as ECM assembly, cell signaling, and developmental processes [180]. Growth factors are of particular interest in tissue engineering applications, and HS facilitates signaling and gradient formation for a plethora of growth factors [178]. For example, heparan sulfate is known to act as a co-receptor between FGF-2 and its cell surface receptor and effectively reduces the concentration of FGF-2 required to initiate signaling and prolongs the signaling response [174]. It has also been suggested that heparan sulfate modulates the

range that IHH can travel *in vivo*, and may act as a low affinity binding agent to present the protein at the cell surface [178]. Heparan sulfate is believed to function similarly with BMP-2, as studies with decapentaplegic (DPP), the *drosophila* homolog for BMP-2, found that genetic modifications reducing heparan sulfate concentrations resulted in decreased ability for DPP to travel long distances [181]. Finally, evidence from studies with Wg, the WNT homolog in *drosophila*, indicate that heparan sulfate likely acts to protect Wg and enables it to travel longer distances, and also may act as a co-receptor at the cell surface [182]. Overall, these studies point toward modulating growth factor concentration and presentation to the cell surface as a major role for heparan sulfate.

2.4.2 Heparan Sulfate and Other Glycosaminoglycans in Chondrogenesis

To study how HS and HSPGs influence endochondral ossification (as well as many other developmental processes), typically genes or enzymes essential to HS production or sulfation are knocked-out or knocked-down in murine animal models and resulting phenotype is evaluated [183]. In one such study, the HSPG perlecan was knocked-out and reduced chondrogenic differentiation and matrix deposition was observed [184], possibly indicating a requirement for matrix-associated HS in driving differentiation. In contrast, another study indicated that higher than normal levels of sulfated GAGs reduced differentiation. In this study, knock-out of Sulfatase-Modifying Factor 1 *(Sumf1;* master regulator of proteoglycan desulfation) prevented GAG desufation. Overall, it appeared that higher than normal levels of GAG sulfation prevented differentiation from proceeding, likely due to increased FGF signaling [185]. Similar evidence of HS involvement in controlling spatial localization of growth factors has been found in several studies in which exostosin glycosyltransferase 1 (EXT1), an

enzyme responsible for polymerization of the HS chain, was knocked-down, resulting in reduced levels of HS. In one study, this increased the distance over which IHH could have an effect, possibly indicating that the normal function for HS is to sequester IHH and restrict its distribution and long range transport throughout the tissue [186]. Similarly, when EXT1 was knocked down in chondrocytes, ectopic cartilage formation was observed around the growth plate, likely due to increased proliferation of chondrocytes in abnormal spatial locations due to the loss of the ability of HS to control and restrict BMP-2 movement through the ECM [187]. Many similar studies have been conducted, and while these studies are only beginning to elucidate the true roles of HS and HSPGs in chondrogenesis, they all indicate that HS is necessary for tissue development, likely due to its ability to modulate growth factor signaling and matrix distribution.

2.4.3 Glycosaminoglycan-Based Biomaterials for Cartilage Repair

GAGs such as CS, dermatan sulfate, HA, and heparin have been integrated into scaffolds to enhance chondrocytic differentiation of chondrocytes and mesenchymal stem cells [38,39,159,160]. The focus of this section will be on CS and heparin, two highly sulfated GAGs that are likely to be involved in protein sequestration in a chondrocytic environment. Cartilage tissue scaffolds are often composed of a base material, such as collagen II, chitosan, or synthetic polymers, into which GAGs are incorporated [38,160,188–191]. Chondroitin sulfate is a commonly used GAG in cartilage repair scaffolds, and generally enhances the chondrocytic phenotype of cells encapsulated in or seeded on the scaffold [160,189–192]. Heparin is used less frequently, but has been

incorporated into dextran-based hydrogels and shown to enhance chondrocyte differentiation as compared to dextran controls [38].

GAGs are incorporated into scaffolds for several reasons, including to better mimic the natural cartilage ECM, enhance cell adhesive properties, control mechanical properties through increased water retention, and modulate protein presentation to cells [38,160,189–194]. As TGFβ-1 or 3 is often used as a supplement in chondrocytic cell culture, it is possible that GAGs in the scaffold sequester and prolong its activity, further enhancing chondrocytic differentiation [38,194]. Evidence of this was found in a study in which heparin or desulfated heparin was coated onto MSC aggregates, and it was shown that chondrogenesis was enhanced in the desulfated heparin group as compared to the fully-sulfated group or non-coated group. In these studies, it is possible that supplemented TGFβ-1 was attracted to both heparin and desulfated heparin, but that desulfated heparin resulted in increased detachment of TGFβ-1, as the coating was less charged, which was then better able to interact with cells [195]. Overall, GAGs have been used to enhance chondrogenesis with moderate success, likely due to modulation of protein sequestration and presentation to cells. Interestingly, similar to their natural function *in vivo*, these GAGs are able to bind a plethora of proteins involved in differentiation over time, enabling them to act upon multiple differentiation stages. However, in-depth analyses of how GAGs themselves modulate cellular differentiation due to protein binding have yet to be conducted.

2.4.4 Heparin-Based Biomaterials

Given their high affinity for a plethora of growth factors and proteins (often with dissociation constants ranging from 10^{-6}-10^{-9} M), heparin and heparan sulfate have been

used for a variety of tissue engineering applications [9]. Because interactions with heparin and heparan sulfate are specific but not covalent, they allow for protection and sustained release of growth factors, mimicking the role of ECM components *in vivo* [9]. Overall, heparin and heparan sulfate are biocompatible, relatively non-toxic, and inexpensive [196], incentivizing their use *in vivo*. As such, heparin and heparan sulfate have been delivered to modulate endogenous protein, used in cell culture systems to modulate protein localization, and used in delivery vehicles to enhance protein affinity.

Heparan sulfate has been mixed into hydrogel-based delivery systems and implanted into injury models to evaluate healing without delivery of exogenous growth factors. In one example, heparan sulfate was mixed with carboxymethylcellulose/glycerol to form a gel and implanted into a critical sized bone defect in a rat femur [197]. After two weeks, significantly improved bone formation was observed in the low dose heparan sulfate group, as compared to no and high heparan sulfate groups [197]. While the mechanism of action is unknown, it was hypothesized that the ability of heparan sulfate to interact with endogenous proteins was responsible for the enhanced differentiation [197]. In addition, the diminished effectiveness at high dosage may have been due to increased binding of growth factors, therefore decreasing growth factor availability to cells. In another example, heparan sulfate was mixed with fibrin glue and implanted into a critical sized cranial defect in a rat model [198]. After 3 months, enhanced defect closure was observed in the group with heparan sulfate, as opposed to control groups [198]. These two studies indicate the ability of heparan sulfate modulate the local cellular microenvironment, likely through growth factor binding.

Heparin has also been cross-linked into hydrogels for cell encapsulation and controlled growth factor delivery. Heparin can be physically encapsulated (through entanglement or electrostatic interactions) or covalently cross-linked into hydrogel matrices [9]. Heparin has been incorporated into PEG, HA, peptide-based, poly(N-isopropylacrylamide-co-acrylic acid), poly(vinyl alcohol), poly(L-lactide-co-ε-caprolactone), dextran, alginate, and chitosan based hydrogels [38,53,54,196,199–203]. Heparin-based hydrogels for cell encapsulation have often been used toward the goal of inducing osteogenic or chondrogenic differentiation. In one example, methacrylated heparin was cross-linked with PEG-dimethacrylate for encapsulation of MSCs, and was shown to enhance osteogenesis, possibly through enhanced presentation of fibronectin and BMP-2 [45]. In another example, encapsulation of cardiac progenitors in a heparin-hyaluronic acid hydrogel enhanced cell differentiation [41]. Assessment of growth factors trapped within the hydrogel indicated that heparin-mediated sequestration of endogenous factors was likely a contributing factor to improved cell behavior [41]. Similar results were observed when MSCs encapsulated in PEG-DA/oligo(poly(ethylene glycol) fumarate) (OPF) and heparin methacrylamide (MAm) hydrogels were co-cultured with osteoblasts [40]. Enhanced MSC osteogenesis was observed as heparin content in the gels was increased, possibly due to the ability of heparin to trap osteoblast-secreted factors that promoted MSC differentiation [40]. Another study indicated that heparin-thiol PEG-DA hydrogels were able to trap endogenous TGFβ-1, enabling re-differentiation of de-differentiated chondrocytes [39]. Finally, enhanced chondrogenesis was observed in chondrocytes encapsulated in dextran-tyramine/heparin-tyramine gels cross-linked with horseradish peroxidase, likely due to either improved fibronectin or growth factor

presentation to cells [38]. These studies suggest that heparin-based hydrogels can modulate both endogenous and exogenous protein presentation to cells for enhanced differentiation.

Heparin has been used to enhance protein loading and stability in many controlled delivery vehicles [3,11,42,196]. Often, heparin is covalently modified and cross-linked into hydrogels to control delivery of proteins such as FGFs, BMPs, VEGFs, TGF-βs, and other positively charged proteins to enhance osteogenesis, chondrogenesis and wound healing [53,54,56,204]. In general, reduced burst released and lower overall release is observed in hydrogels that contain heparin due to increased attraction of proteins to the hydrogel system [56,200,203,205]. In one case, this resulted in an inability to enhance *in vivo* bone formation with BMP-2 delivery from a heparin-based hydrogel, likely due to reduced early protein release [205]. However, sustained release of BMP-2 from a heparin-poly(L-lactide-co-ε-caprolactone) scaffold improved mineralization at the ligament-bone interface [201], indicating that heparin and BMP-2 dosage must be tightly controlled to achieve desired differentiation. In addition, starPEG-heparin hydrogels have been formed by reacting activated heparin carboxyl groups with amine-functionalized PEG using EDC/NHS chemistry, and used to deliver TGFβ-1 for enhanced myofibroblast differentiation and FGF-2 and VEGF for improved HUVEC viability [56,204]. Thus, incorporation of heparin into controlled delivery vehicles can modulate the rate of protein release, and can be tuned to enhance cell behavior. Overall, these studies indicate the ability of heparin to modulate protein sequestration and release when integrated into biomaterial scaffolds for tissue engineering regeneration and repair. Still, the contribution of heparin materials to endogenous protein sequestration and release has remained poorly

understood, and more mechanistic studies should be conducted to better understand the potential of heparin-based materials to interact with native proteins.

2.4.5 Biomaterial-Mediated Protein Sequestration

While biomaterials have been primarily used as cell scaffolds and otherwise inert delivery vehicles, it has recently been suggested that biomaterials themselves be used to manipulate the cellular microenvironment [3]. This technique could potentially be very effective, as it proposes to harness potent, cell-derived protein to either reduce or amplify cell-signaling. Overall, this technique promises to reduce cost and lessen the requirements for FDA approval [3], and has just begun to be explored in tissue engineering applications.

Due to their intrinsic ability to interact with protein *in vivo,* natural materials such as heparin, chondroitin sulfate, and peptide sequences have been used to modulate endogenously produced proteins. One common application for material-based growth factor sequestration is cartilage tissue engineering, where scaffolds containing chondroitin sulfate and heparin are often used partially as a means to sequester both exogenous TGFβ added to the media and endogenously produced proteins [38,189,190,192,194]. A recent study proved the utility of this technique. In this study, a heparin-based scaffold laden with chondrocytes was investigated after *in vitro* culture and *in vivo* subcutaneous injection to evaluate levels of TGFβ-1. In both cases, the amount of TGFβ-1 increased over time, suggesting that the materials were able to effectively sequester and concentrate at least exogenously added TGFβ-1, and possibly cell-secreted TGFβ-1 as well [39]. In a similar fashion, hyaluronic acid-heparin based hydrogels were used to present TFG-β1 to encapsulated cardiac progenitor cells, and it was found that

enhanced levels of angiogenic cytokines were sequestered by heparin-containing gels, which likely contributed to observed increases in cell function and survival [41]. In a slightly different tone, heparin was used to culture MSCs and prime them toward an osteogenic lineage, possibly by sequestering osteogenic growth factors secreted by neighboring osteoblasts [40]. Finally, it was shown that self-assembling peptide fibers with a TGF-β binding sequence resulted in enhanced cartilage repair when implanted into a full thickness cartilage defect in a rabbit animal model, likely due to the ability of the scaffold to sequester endogenous TGF-β [44].

While the examples above primarily point to examples in which growth factor function was amplified, other materials have been used to sequester and reduce protein effectiveness. A VEGF-binding peptide sequences integrated into PEG MPs reduced proliferation of human umbilical vein endothelial cell (HUVEC), likely due to sequestration of VEGF away from the cells [43]. In another study, a PEG-based hydrogel was modified with a tumor necrosis factor-α (TNFα)-binding peptide sequence in an attempt to protect encapsulated cells from the pro-inflammatory environment often encountered after hydrogel implantation. Cells encapsulated in TNFα-antagonizing hydrogels were unaffected by high TNFα concentrations in *in vitro* experiments [46], pointing toward the utility in engineering hydrogels to selectively decrease the concentration of undesirable proteins. In a study examining kidney development *in vitro*, normal growth of kidney rudiments from E11.5 mice was increasingly inhibited as heparin concentrations were increased [206], suggesting that heparin sequestered essential proteins away from the cells in the developing tissue.

Several techniques to antagonize proteins *in vivo* have also been carried out in craniosynostosis models. Craniosynostosis involves the premature closure of cranial sutures, and while surgical intervention can be employed to successfully separate the fused bones, re-fusion, or resynostosis, often occurs [207,208]. To prevent this, collagen gels with antibodies against proteins implicated in the bone fusion process, including anti-TGFβ-2 and anti-FGF-2, have been delivered to the site of the suture [209,210]. This therapy is only partially successful due to the limited half-life of these antibodies [209,210], but similar approaches with more robust protein-sequestration technique may be beneficial for craniosynostosis and resynostosis in the future. While still a relatively new concept, these studies highlight the plethora of opportunities available for biomaterial-mediated endogenous protein sequestration, to both eliminate and prolong protein presentation in the cellular microenvironment.

2.5 Microparticles

Microparticles (also called microspheres) are used frequently for drug and protein delivery [211]. Compared to larger delivery vehicles, MPs are particular advantageous because they are injectable and have a high surface area to volume ratio, allowing enhanced cargo release [211]. In general, high encapsulation efficiency and sustained release of bioactive molecules are the goals for MP delivery vehicles [211]. While many MP formulations have an unavoidable burst release of encapsulated cargo, the goal of most MP technologies is sustained release [211]. Often, MPs are engineered to be degradable to enhance release of the loaded cargo, but release is not always directly correlated to degradation [211]. While many different materials have been used to fabricate MPs, this review will focus on PEG and GAG based MPs.

2.5.1 Poly(ethylene-glycol) -Based Microparticles in Tissue Engineering

PEG is an attractive material for protein delivery because it is hydrophilic, relatively inert (i.e. it does not bind many proteins), and easy to chemically modify [28]. Traditionally, it has been integrated into hydrophobic PLA or PLGA MPs to enhance protein loading and release [212–216]. PEG has both been used in combination with PLGA, PLA, and alginate or alone to enhance MP release of hydrophobic drugs such as paclitaxel [214], genistein [217], and dexamethasome [218], and proteins such as VEGFA [219], lysozyme [213], horseradish peroxidase [218]. More recently, PEG has been chemically modified with peptide sequences to impart protein-binding capabilities, facilitate cell adhesion, or to enhance degradation. For example, 4-arm PEG norbornene was functionalized with a VEGF peptide binding sequence to enhance VEGF sequestration onto the MPs [43]. In another study, RGD (arginine-glycine-aspartic acid, an amino acid sequence from the fibronectin protein that promotes cell adhesion) was incorporated into 8-arm PEG-vinylsulfone/PEG-amine MPs to promote MSC adhesion in aggregate culture [220]. Finally, a MMP-sensitive sequence was integrated into a PEG-diacrylate (DA) hydrogels to enhance cell-mediated degradation. These MPs showed a faster release rate of hydrophilic and hydrophobic model drugs, as well as a model protein, with increased collagenase concentration [218].

Hydrolytically degradable PEG-DA MPs have also been fabricated by taking advantage of the increased susceptibility to hydrolysis of the acrylate ester bond when covalently bound to DTT [60]. 4-arm PEG-DA MPs exhibited accelerated rates of degradation as levels of DTT were increased [221]. Overall, these studies show the

diversity of PEG-based MPs that have been used for protein loading and release and in other tissue engineering applications.

2.5.2 Glycosaminoglycan-Based Microparticles in Tissue Engineering

In contrast to PEG, GAG based materials have the potential to bind a plethora of positively charged proteins. Heparin is often used in microparticles to both prolong the duration of growth factor release and protect growth factors from degradation, thus prolonging bioactivity [53,54]. Specifically, heparin-based hydrogels have been used to deliver FGF, BMP-2, hepatocyte growth factor, VEGF, and other proteins to enhance cellular behavior [53–56]. Heparin has been integrated into a variety of MP systems and is often coated onto a MP template via layer-by-layer techniques. For example, heparin-poly-L-arginine microcapsules were fabricated using a layer-by-layer approach on calcium carbonate microspheres and used to deliver TGF-β to fibroblasts, inducing their transdifferentiation into myofibroblasts [222]. Heparin coatings have been applied to both alginate and HA MPs and loaded with BMP-2 to enhance bone formation *in vivo* [223] and MSC chondrogenesis *in vitro* [224,225].

Pure heparin MPs have also been fabricated and used for growth factor delivery. In one study, low MW heparin was mixed with protamine to form MPs for FGF-2 delivery, leading to neovascularization and fibrous tissue formation when injected subcutaneously into mice [57]. In another study, methacrylamide-functionalized heparin MPs were fabricated via free radical polymerization methods and used to deliver BMP-2 to C2C12 cells, showing comparable ALP activity to that obtained by soluble BMP-2 delivery [59]. In a similar set of studies, 1-10% of a thiolated heparin and several heparin derivatives with altered sulfation patterns were incorporated into 4-arm PEG-DA MPs,

and BMP-2 bioactivity was preserved in heparin and the derivative with the next highest level of sulfation, as compared to derivatives with lower sulfation [58].

CS MPs have also been fabricated, with the goal of enhancing biocompatibility [226] or increasing loading and release capabilities [227]. Often, complex coacervation or chemical cross-linking of CS and another polymer, such as gelatin, chitosan, or collagen, is used to form CS-containing microparticles. This technique has been used to make MPs for release of ovalbumin, albumin, catalase, and an anti-cancer drug, 5-fluorouracil [226,228–230]. CS and dermatan sulfate have also been incorporated into PLGA MPs to enhance protein stability and to better control loading and release [227,231]. Finally pure CS MPs have also been employed for tissue engineering applications. Methacrylated chondroitin sulfate MPs were formed and able to be incorporated into embryonic stem cell aggregates without affecting viability [232], and produced slight upregulation of chondrocytic markers when incorporated into MSC aggregates [233]. Overall, GAG-based MPs are beneficial for preservation of protein bioactivity, enhancing release profiles of both hydrophilic drugs and proteins, and for enhancing MP biocompatibility. Due to their size and shape, MPs have the capability to interact with cells directly in the cellular microenvironment through material-protein-cell interactions, and possibly direct cell-material interactions. These interactions should be harnessed to guide and study cell behavior in future studies.

2.5.3 Core-Shell Microparticles

When using microparticles for drug and biomolecule delivery, major obstacles include minimizing burst release and controlling release kinetics of bioactive cargo [52,234–237]. In response to these challenges, core-shell microparticles have been

fabricated, towards the goal of prolonging release of a drug or biomolecule encapsulated in an inner core by manipulating the degradation prolife of an outer shell [51,52,236]. In general, core-shell MPs are generated via a double emulsion process or by pre-fabricating the inner core and coating or re-emulsifying the inner core with the shell polymer solution, either in a large batch process or using a microfluidic device [236,238–242]. Batch emulsification fabrication methods (high-shear processes like precipitation, spray-drying, and phase separation) have the benefit of requiring little specialized equipment but can have low throughput and generate heterogeneous MPs; microfluidic devices require extensive expertise and specialized equipment but generate uniform MPs with high throughput [52,240,243,244]. Depending on requirements of the MP systems and resources available, core-shell MPs can be fabricated in a variety of ways.

Core-shell MP delivery systems have been traditionally employed for small molecule or drug delivery [234,238,240,243], but their utility in delivery of biomolecules to cell-based systems has just begun to be explored. As noted by several research groups, core-shell MPs have the potential to enable temporal control over the release of one or more growth factors to cells, possibly on different time-lines, which could be beneficial for cell differentiation processes where temporal control over protein delivery is critical [237,245]. For example, VEGF was encapsulated in alginate MPs and then coated with chitosan and polycaprolactone, which resulted in a lower burst release and longer release duration [52]. Core-shell MPs also have potential to enhance protein stability. In one example, FGF was mixed with heparin and trapped in a calcium carbonate core MP, then coated with dextran sulfate and poly-l-arginine. Similar proliferation of mouse fibroblasts

was observed when subjected to free FGF or FGF-loaded core-shell MPs, indicating that entrapment in the MPs preserved protein bioactivity [246].

Finally, dual-release of proteins and drugs has been achieved by encapsulating one protein or drug into the core, and another into the shell. As the core and shell material can have different chemical properties, this can allow for efficient encapsulation of drugs and proteins with different properties. One example of this is core-shell PLGA-alginate MPs, fabricated to achieve dual-release of VEGF and platelet-derived growth factor (PDGF) to HUVECs, and cells sprouted and produced capillary-like structures in response to biomolecule delivery [247]. Similar core-shell MPs were used to encapsulate BMP-2 and dexamethasone, and BM-MSCs encapsulated in the shell layer were seen to undergo enhanced osteogenesis as compared to controls [245]. These studies indicate that core-shell MPs can be used to successfully deliver proteins and other biomolecules and have potential to improve protein stability and better control loading and release dynamics.

In addition to drug and biomolecule delivery, MPs have also been used to sequester various biological agents for diagnostic tests, removal from human plasma, and biosensors [47–50]. Core-shell MPs are of particular interest in these processes, as the materials used for the core and the shell can impart distinctly different properties onto the MP system. For example, in several studies that have aimed to sequester biomarkers from bodily fluids, the outer shell is engineered to exclude large proteins, especially albumin, but to allow passage of smaller proteins. Then, the inner core is designed to trap smaller proteins once they have entered the MP matrix, effectively allowing for the capture of

low-concentration biomarkers from a given fluid [48–50]. The design principles used to engineering these MPs could be applied to multifunctional core-shell MPs in the future.

2.5.4 Microparticles in Cell Spheroids

Recently, dense cell aggregates (also called spheroids or pellets) have been used as an alternative to monolayer cell culture, as cell aggregates are thought to better mimic the *in vivo* cellular microenvironment [248–251]. The higher cell-cell and cell-matrix contacts created in aggregate culture may be contributing factors to the enhanced cell survival, function, and differentiation observed in cells in aggregate culture [248,249,252]. For example, it has been well-established that chondrogenic differentiation of MSCs and spontaneous differentiation of embryonic stem cells (ESCs) is enhanced in aggregate culture [249,253]. Furthermore, unlike larger cell-seeded scaffolds, cell aggregates can be injected into sites of tissue injury, possibly promoting regeneration and repair [254]. However, aggregate culture can be problematic due to diffusion limitations for nutrients and oxygen [248,252,255,256]. In addition, in cases where delivery of exogenous growth factors is required, cells on the exterior of the aggregate will be exposed to that factor at a much higher level than cells on the interior, creating possibly undesirable spatial variance throughout the aggregate [255]. Finally, for injectable cell aggregate therapies, maintaining control of cell behavior within the aggregate after injection could be advantageous. To overcome these limitations, MPs have been incorporated into aggregates, both toward the goal of reducing diffusion limitations and to delivery soluble factors homogenously throughout the cell aggregate for better controlled cell behavior.

A variety of materials have been used to make MPs for incorporation into cell aggregates, including PLGA [251,253,255,257–259], PLA [251], chitosan [251,260], gelatin [248,252,259–261], Sephadex (dextran) [262], polystyrene [250], heparin [263], agarose [259], alginate [254], and PEG [220]. For some of the initial studies that developed MP-containing cell aggregates, adherent cells and MPs were cultured in non-adherent dishes or bioreactors, which promoted cell adhesion to the MP surface, and eventual formation of aggregates [251,262]. However, the size of these aggregates and the number of incorporated MPs was difficult to control, and current methods mix MPs and cell prior to deposition into low-binding well plates or agarose wells.

Several general concepts and conclusions have resulted from the numerous MP-cell aggregate studies conducted. First, it has been observed that aggregate formation is dependent on the size and number of MPs used. Too many MPs or MPs that are large can disrupt the cell-cell contacts required for aggregate formation [252]. Incorporation of MPs into aggregates can affect cell behavior, even if growth factors are not delivered. For example, gelatin MPs have been observed to enhance chondrogenesis in MSC aggregates [252], which may possibly be due to (or cause) the increased stiffness observed in MSC aggregates containing gelatin MPs observed in a separate study [248]. Relatedly, MPs of similar size but composed of different materials can affect cells differently [259]. Additionally, when loaded with an equal amount of growth factor per MP mass, larger numbers of smaller MPs have more of an effect than smaller numbers of larger MPs [253,261], indicating that release kinetics or MP distribution throughout the matrix is important to consider in aggregate culture. Finally, magnetic MPs can be used to

assemble spheroids into larger structures, allowing for potential spatial patterning of discrete cellular units in future experiments [250].

Microparticles have often been incorporated into cell aggregates to enhance cell differentiation. As MSC aggregate culture is a common technique to induce chondrogenic differentiation, several studies have investigated the incorporation of MPs in MSC aggregates. Chitosan-gelatin, gelatin, PLGA, and chondroitin sulfate-based MPs have all been used to deliver TGFβ-1 within MSC aggregates. In general, enhanced chondrogenesis (as evidenced by collagen II and GAG deposition, among other markers) was observed in groups with MPs that delivered TGFβ-1 [256,260,261,264]. Alginate and 8-arm PEG-based MPs have also been functionalized with the cell-adhesive sequence RGD and incorporated into MSC spheroids, resulting in enhanced chondrogenesis without delivery of a biomolecule [220,254]. ESCs are also more likely to undergo differentiation in 3D, which has led to incorporation of MPs within embryoid bodies (EBs). Retinoic acid delivery from PLGA MPs has been shown to be more effective than soluble delivery, and results in cystic EB formation [253,255]. In addition, BMP-4 delivery from heparin-gelatin MPs spatially oriented in one part of an EB showed localized Brachyury-T induction [263]. Several other examples of differentiation include gelatin MPs for osteogenic MSC differentiation [252], PLGA MPs for enhanced adipogenesis in the pre-adipocyte 3T3 L1 cell line [257], and nerve growth factor-loaded PLGA MPs for enhanced neuronal activity [258]. As a whole, these studies illustrate the utility of incorporating MPs in dense cell aggregates to control cellular differentiation and behavior. Of specific interest, the ability of protein-binding microparticles (such as those composed of GAGs) to sequester and release proteins within the cellular aggregate

microenvironment could be very beneficial to further harness the differentiation potential of progenitor cells for tissue regeneration and repair applications.

2.6 Systems Biology Approaches to Tissue Engineering

As biological assay techniques become more high-throughput and generate large arrays of data, univariate analysis techniques are unable to fully elucidate interactions, correlations, and multi-factor responses between measured variables [265–268]. In addition, analyses of biological systems are most powerful if multiple cell responses are investigated across several timepoints and conditions [266,268,269]. Thus, multivariate analysis techniques have recently been implemented to gain a more comprehensive understanding of cell phenotype by analyzing variables as a whole, rather than investigating one variable at a time [265,267,268]. Several different computational techniques are frequently used, including clustering (hierarchical and k-means), decision trees, Bayesian networks, principal component analysis (PCA) and partial least-squares regression (PLSR) [267,268,270]. Each of these techniques allows researchers to better visualize interactions between the variables measured in a particular system, and of particular interest in this review are PCA and PLSR.

PCA is a technique that allows visualization of data clustering by reducing the dimensionality of a dataset to 2-4 dimensions, graphed on axes called principal components (PCs), which are able to capture the majority of the variance in the dataset [266,268,270]. PLSR is an extension of PCA, where an added assumption is made that a cell outcome measure (called “Y”; i.e. apoptosis, differentiation, migration) is dependent on a combination of measurable variables (called “X”; i.e. cell signaling, surface markers, protein phosphorylation) [266,267]. A linear regression solution is then calculated to

show how cell outcome is a function of measureable variables (Y=f(X)) [265–267]. This technique can elucidate the most important combinations of measured variables that lead to an observed outcome, which allows this modeling technique to be predictive in addition to explanatory [265–267].

PCA and PLSR have been applied to a variety of tissue engineering applications. In one study, PLSR was used to analyze hepatic cytotoxicity in response to stimulation by various drugs through measurement of phosphoproteins. This analysis narrowed the original 17 phosphoproteins down to 4 that caused the largest effect on cytotoxicity [271]. Several studies have investigated specific cell-type responses to TNF-α, and PLSR analysis has indicated that these responses are dependent on cell-type and the time after drug administration [272,273]. Another study showed that both surface markers and signaling molecules can be used to predict T-cell age by using PLSR analysis [274]. These techniques have also been used to evaluate stem cell behavior. In one study, PLSR was used to establish a relationship between embryonic stem cell gene expression profiles and biomechanical properties as cells were directed to ectoderm or mesoderm lineages [275]. In another study, PLSR was used to understand how kinase pathways govern MSC differentiation, and behavior could be predicted based on several phosphoproteins [276]. Finally, PCA and PLS-Discriminate Analysis (PLS-DA, a modified version of PLSR using a dummy variable to stand in for a cell response) elucidated distinct expression dynamics for osteogenic, adipogenic, chondrogenic, and myogenic transcriptional regulators when MSCs were co-cultured with adipocytes and osteoblasts [32]. Overall, these studies indicate that PCA and PLSR are excellent tools to evaluate and develop predictive models for dynamic, complex cellular systems.

CHAPTER 3

INTERACTIONS BETWEEN MESENCHYMAL STEM CELLS, ADIPOCYTES, AND OSTEOBLASTS IN A 3D TRI-CULTURE MODEL OF HYPERGLYCEMIC CONDITIONS IN THE BONE MARROW MICROENVIRONMENT[4]

3.1 Introduction

Diabetes is associated with insulin deficiency (Type I) or resistance (Type II) and consequential dysregulation in adipose tissue and energy metabolism [74]. Notably, both type I and II diabetes are associated with increased risk of osteoporosis, a skeletal disorder characterized by low bone mass and microarchitectural deterioration of bone [277]. Among other cell types, adipocytes and osteoblasts are dysregulated during the progression of diabetes and resulting secondary osteoporosis [34]. As both cell types are differentiated from mesenchymal stem cells (MSCs) and are components of the bone marrow microenvironment [34,74,278], it is possible that the progression of these diseases involves altered MSC behavior [34].

The stem cell microenvironment, where stem cells derive signals from the extracellular matrix (ECM), cellular contacts, and both short and long range soluble factors, has been seen to change in disease states and has recently gained interest as a potential new target for disease therapies [279,280]. Within the bone marrow

[4] Portion of this section were adapted from T.E. Rinker, T.M. Hammoudi, M.L. Kemp, H. Lu, J.S. Temenoff, Interactions between mesenchymal stem cells, adipocytes, and osteoblasts in a 3D tri-culture model of hyperglycemic conditions in the bone marrow microenvironment., Integr. Biol. 6 (2014) 324–37.

compartment, MSCs are directed to differentiate to osteoblasts or adipocytes, a process that is tightly regulated, partially by cellular communication between MSCs and the osteoblasts and adipocytes in the immediate microenvironment [34]. Irregular MSC behavior has been observed in abnormal environments, such as the tumor microenvironment, where MSCs home and potentially participate in tumor pathogenesis [281]. Similarly, in an *in vitro* model of Gaucher disease, MSCs were seen to have reduced proliferative capacity and may contribute to increased bone resorption [282]. As it has been hypothesized that alterations in the MSC microenvironment both contribute to and result from interactions with bone and adipose tissues [34], understanding how environmental changes inherent to diabetes impact these interactions may provide insight into the role MSCs play in the progression of diabetes and concomitant osteoporosis.

Clinically, diabetes is often associated with hyperglycemic conditions due to the body's inability to properly regulate the amounts of glucose in the blood [278]. Studies have shown that elevated glucose levels have negative effects on MSCs, adipocytes and osteoblasts, all of which are cell types that influence the MSC microenvironment. Data suggest that at high glucose levels, MSCs undergo increased apoptosis and senescence as well as lose colony forming capacity and osteogenic potential [83–86]. Adipocytes have demonstrated decreased insulin sensitivity, unregulated triglyceride storage, increased production of reactive oxygen species and pro-inflammatory cytokines, and decreased adiponectin secretion when cultured in high glucose conditions [87–89]. Finally, osteoblasts cultured in high glucose have shown reduced proliferative capacity, mineralization capabilities, collagen I synthesis, and expression of differentiation markers [90–93]. However, how these individual consequences impact cellular cross-talk between

all three cell types remains to be fully understood, though previous work has shown that intercellular communication is affected in the context of diabetes. For instance, murine osteoblasts in co-culture with bone marrow cells from diabetic mice undergo increased cell death as compared to those co-cultured with bone marrow cells from normal mice [283]. This indicates that MSCs derived from diabetic tissues may have an altered secretome, but how these changes influence interactions between MSCs and neighboring cell types in the bone marrow niche remains largely unexplored. Understanding how hyperglycemic conditions influence MSCs both directly and indirectly (through soluble signaling from neighboring osteoblasts and adipocytes) may provide insight into how the altered stem cell microenvironment contributes to tissue dysregulation, particularly in the development of diabetes-related osteoporosis.

To gain such biological insight, it is necessary to use an *in vitro* culture system that permits the co-culture of multiple cell types but still allows specific cell population analyses. As opposed to *in vivo* experiments, *in vitro* systems can be advantageous by eliminating the confounding factors present in animal models and by permitting use of human cells. In past *in vitro* studies, both 2D techniques, such as transwell-based systems and cell patterning [284,285], and 3D techniques, involving various biomaterial-based scaffolds [96,286], have provided useful information about cellular interactions. However, in many of these systems, both separation of unique cell populations for analysis and retrieval of live cells for further experimentation are difficult. Therefore, this study demonstrates the development and implementation of a 3D tri-culture platform that permits individual cell type analysis [32] and on-demand retrieval and further analysis of live MSCs post-culture. To achieve live cell retrieval, a matrix metalloprotease (MMP)-

degradable poly(ethylene-glycol) (PEG)-based material was included in the culture system. This material has been used previously to encapsulate MSCs with no decrease in cell viability [287–289]. With this culture system, we were able to co-culture MSCs, osteoblasts, and adipocytes in normal and high glucose conditions, and then analyze each cell type separately for gene expression, histological markers, and cell viability.

In many *in vitro* studies of intercellular cross-talk, only single outcome measures are reported, which often does not elucidate how genes, proteins, and other measure of cell response interact and contribute to an observed cell behavior [267]. In recent years, some of these shortcomings have been addressed by developing heat-maps of gene and protein arrays, modeling proposed signaling networks by integrating results from many different experiments, and constructing multivariate statistical models [32,274,290]. In particular, multivariate statistical analysis techniques can provide insight into the greatest sources of variance in complex biological systems and can elucidate how outcome measures correlate with different environmental and culture conditions [291]. We have previously used multivariate statistical techniques to evaluate gene expression data from simultaneous co-culture of three cell types, showing in a proof-of-concept experiment that these models can provide valuable biological insight in a multicellular *in vitro* system [32]. In this study, these techniques were further utilized to gain insights into how neighboring cell type and environment interact to influence MSC behavior and gene expression in an *in vitro* model of hyperglycemia. Specifically, we studied cellular response to elevated glucose levels in three different culture configurations: monoculture (one cell type), co-culture (two different cell types) and tri-culture (three different cell types) (Figure 3.1). Cellular response was analyzed by measuring gene expression levels,

viability, histological markers, and MSC colony-forming potential over a seven day time period using both univariate and multivariate analysis approaches.

3.2 Materials and Methods

3.2.1 Preliminary Cell Culture

All cell culture reagents were obtained from Mediatech unless otherwise specified. Primary human MSCs were obtained from Texas A&M Health Sciences Center and expanded in Minimal Essential Medium-Alpha (αMEM) with 16.5% fetal bovine serum (FBS; Hyclone), 1 g/L glucose, 2 mM L-glutamine, 1% amphotericin B, and 0.1% gentamicin and cultured at 37°C and 5% CO_2 in a humidified incubator. Primary human osteoblasts (Lonza) were expanded to 4 population doublings in OGM Osteoblast Growth Medium (Lonza) containing 10% FBS, ascorbic acid, 50 μg/mL gentamicin, and 37 ng/mL amphotericin B. Primary human subcutaneous pre-adipocytes (Lonza) were expanded to 1-2 population doublings according to the manufacturer's protocol in PGM-2 Basal Medium (Lonza) containing 10% FBS, 2 mM L-glutamine, 50 μg/mL gentamicin, and 37 ng/mL amphotericin B. Cultures at 80% confluence were differentiated into adipocytes for 9 days in Dulbecco's Modified Eagle Medium (DMEM) with 10% FBS, 1 g/L glucose, 60 μM indomethacin, 0.5 mM 3-isobutyl-1-methylxanthine, 0.5 μM dexamethasone, and 45 pM insulin.

3.2.2 Fabrication of Culture System

Cells were encapsulated in PEG-based materials (Sigma-Aldrich, unless otherwise noted). PEG-diacrylate (PEG-DA) (*Mn* = 8kDa) was synthesized by combining acryloyl chloride and PEG according to previous methods [148] (See Figure 3.1C for PEG-DA cross-linking schematic).

To promote cell adhesion and viability, PEG-based materials containing fibronectin-derived GRGDS (Bachem) and laminin-derived YIGSR (Anaspec) were synthesized from Acryl-PEG-succinimidyl valerate (SVA) (*Mn*=3.4kDa; Laysan Bio) according to previous methods [32,148] to obtain Acryl-PEG-RGDS and Acryl-PEG-YIGSR. To allow on-demand degradation of particular blocks in the culture system, a collagenase-degradable peptide sequence, GGGLGPAGGK (abbreviated LGPA), was bi-functionalized with Acryl-PEG-SVA (*Mn*=3.4kDa) according to previous methods [289,292] to obtain PEG-LGPA-DA polymer chains (See Figure 3.1D for PEG-LGPA-DA cross-linking and degradation schematic).

To fabricate cultures, cells were suspended in precursor hydrogel solutions at 15×10^6 cells/mL. Solutions were formulated with 10% w/w PEG-DA (osteoblasts and adipocytes) or PEG-LGPA-DA (MSCs) and 0.05% w/w D2959 photoinitiator (Ciba), with 1 mM Acryl-PEG-RGDS and Acryl-PEG-YIGSR for MSCs and adipocytes, respectively. Precursor hydrogel solutions were photopatterned into 1.5 × 1.5 × 1 mm laminated gel structures using a PDMS mold and UV light according to previous methods (Figure 3.1) [32]. An opaque photomask was used in subsequent steps to prevent any further UV light exposure and crosslinking. Each subsequent layer is laminated to the prior and constructs do not separate over the course of the experiment or experience changes in tensile properties, as demonstrated in prior work [32,287,293]. Laminated constructs were extracted from the device and sectioned with a scalpel perpendicular to the long axis of the laminate to yield up to eighteen 1.5 mm-wide mono-, co-, and tri-culture constructs (Figure 3.1).

3.2.3 Culture of Encapsulated Cells

Gel structures were cultured in individual wells of a 12 well plate in DMEM with 10% FBS, 5.5 mM glucose (100 mg/dL, similar concentration to normal fasting serum glucose level in humans), 2 mM L-glutamine, 70 µM L-ascorbate, 45 pM insulin (6.4 µU/mL, normal fasting serum insulin level), 1% amphotericin B, and 0.1% gentamicin. After 1 day, a subset of constructs was switched to 22.3 mM glucose (400 mg/dL, similar to hyperglycemic glucose level in poorly-controlled diabetic patients). All constructs were then cultured for a total of 7 days with an additional media change at Day 4 (Figure 3.1).

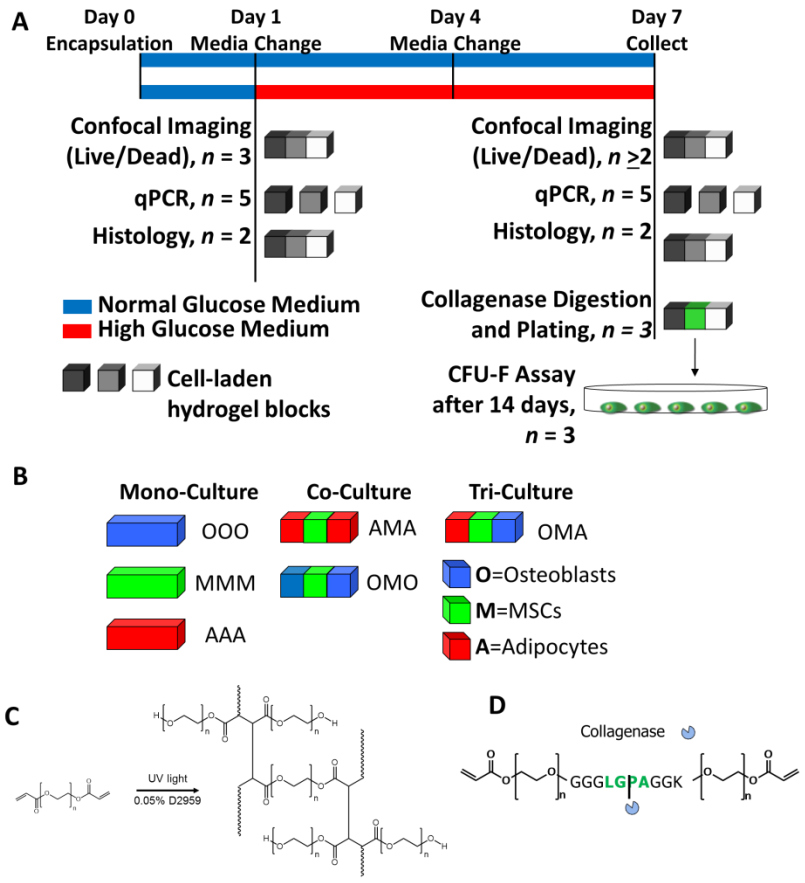

Figure 3.1. Six culture configurations were evaluated in this study. (A) Cells were cultured in mono-, co-, or tri-culture hydrogel constructs for up to 7 days and then analyzed as depicted above. After one day in culture, media was changed and half of the

constructs were switched to high glucose. Shades of gray and white blocks represent hydrogel blocks of different types of cells in either mono-, co-, or tri-culture. (B) Tri-culture configurations consisted of adipocytes, MSCs, and osteoblasts (designated OMA); co-culture configurations consisted of osteoblasts and MSCs or adipocytes and MSCs (designated OMO and AMA, respectively); and mono-culture configurations consisted of osteoblasts, MSCs or adipocytes (designated OOO, MMM, and AAA, respectively). (C) Schematic for PEG-DA cross-linked via photoinitiated free-radical polymerization. (D) Schematic of PEG-LGPA-DA cross-linking and degradation via collagenase.

3.2.4 Cell Viability and Image Analysis

Hydrogel constructs (n = 3 for all mono-culture, co-culture, and day 1 (D1) tri-cultures; n = 2 for day 7 (D7) tri-cultures) were analyzed on Days 1 and 7 culture using a LIVE/DEAD assay (Invitrogen). Constructs were rinsed in sterile phosphate buffer saline (PBS) at 37 °C for 30 minutes and then incubated in LIVE/DEAD dyes (1 µM calcein AM, 1 µM ethidium homodimer-1) for 45 minutes at 37 °C. Constructs were then rinsed with PBS for 15 minutes and imaged with confocal microscopy (10x objective, LSM 700; Zeiss). For each construct, 1 image stack was collected for each cell type present (dimensions: 693 × 693 µm; stack depth = 0 – 800 µm with 10-µm intervals). Image stacks were analyzed using ImageJ software (version 1.46a; NIH). Each stack was split into green (calcein) and red (EthD-1) channels. Every fifth image was analyzed for total number of live and dead cells. Particles of diameter greater than 94 μm^2 and 12 μm^2 were counted for the live and dead cell analysis, respectively, using the Particle Analysis macro. Subsequently, fraction viable cells (# live cells/# total cells counted) was calculated for each stack and normalized to Day 1 normal glucose conditions.

3.2.5 Colony Forming Unit-Fibroblasts (CFU-F) Analysis

To evaluate clonogenicity, at day 7, MSC-containing PEG-LGPA-DA hydrogel constructs (n = 3) were incubated in a 1,100 U/mL collagenase (Gibco) solution in MSC

expansion medium for 1 hour. Fractions of the media containing the recovered cells (100 µL for MMM, 200 µL for OMO and AMA, and 300 µL for OMA; volumes determined in order to seed approximately the same number of cells for each construct type) were plated into 15-cm tissue culture dishes (Corning) containing 20 mL of MSC expansion medium. Media was changed 1 day after seeding and cells were then fed every 3 days for 14 days of culture. Clonogenicity was evaluated by counting colonies $\geq$ 2 mm (stained with 3% crystal violet (Sigma-Aldrich), 100% methanol (BDH)) after 14 days.

3.2.6 Histological Analysis

For histological analysis, all culture configurations under both normal and high glucose conditions were infiltrated by graded concentrations of sucrose in PBS followed by graded concentrations of optimal cutting temperature compound (OCT; Sakura Finetek), frozen in liquid nitrogen, and stored at -80°C until sectioning. Embedded gel constructs were serially cryosectioned at a 20 µm thickness (Microm HM 560 Cryostat; Thermo Scientific) and mounted on Superfrost Plus slides (Fisher). Sections were stained either for lipids (10 µg Nile Red/mL in 1% acetone) or alkaline phosphatase (ALP) activity according to the manufacturer's protocol (Vector Red Alkaline Phosphatase Substrate Kit; Vector Labs). In both cases, sections were counterstained with Hoechst 33258 (0.25 mg/mL in PBS for 5 min; Molecular Probes). Sections were visualized with epifluorescence microscopy under FITC filters for Nile Red, Texas Red Filters for ALP, and DAPI filters for Hoechst.

3.2.7 mRNA Isolation and qPCR

Hydrogel constructs (n = 5) were rinsed in PBS and blocks containing individual cell populations were separated from each other using a scalpel for gene expression

analysis by qPCR after 1 and 7 days in mono-, co-, or tri-culture. Gel blocks containing the same cell type were pooled from 2 co-culture constructs or 3 tri-culture constructs of the same culture configuration and glucose condition to provide sufficient and equivalent amounts of mRNA for quantification. Pooled blocks were homogenized in microcentrifuge tubes with pellet grinders and mRNA was extracted using a QIAshredder tissue homogenizer and RNeasy kit with DNase I digestion (Qiagen). cDNA was generated using SuperScript III Reverse Transcriptase (Invitrogen) with Oligo(dT)15 primers and dNTPs (Promega). Gene expression was analyzed with quantitative PCR amplification performed on a StepOnePlus™ Real-Time PCR System (Applied Biosystems) in the presence of SYBR Green/ROX master mix (Applied Biosystems). In addition to endogenous controls (40S ribosomal protein S18 (*RPS18*) and beta-actin), gene expression was measured for genes indicating osteogenesis (runt-related transcription factor 2 (*RUNX2*), Osteocalcin (*OCN*), and Osteoprotegerin (*OPG*)); adipogenesis (peroxisome proliferator-activated receptor γ (*PPARγ2*), CCAAT/enhancer-binding protein beta (*CEBPB*), Leptin (*LEP*), and adiponectin (*ADIPOQ*)); and glucose-responsive transcription factors (activating transcription factor 2 (*ATF2*), forkhead box protein O1 (*FOX01*), c-jun (*JUN*), and nuclear factor kappa B (*NFKB1*)). Sequences for custom-designed primers (Invitrogen) can be found in Table 3.1.

Table 3.1 National Library of Medicine accession number and primer sequences for target genes in qPCR.

Target Gene	NML Accession #	Sequence (Forward, Reverse)
RUNX2	NM_001024630	TTTGCACTGGGTCATGTGTT
		TGGCTGCATTGAAAAGACTG
OCN	NM_199173	GTGCAGAGTCCAGCAAAGGT
		AGCAGAGCGACACCCTAGAC
OPG	NM_002546	CGGGAAAGAAAGTGGGAGCAGAAG
		CGTCTTTGAGTGCTTTAGTGCGTG

Table 3.1 Continued

PPARG2	NM_015869	TCCATGCTGTTATGGGTGAA
		GGGAGTGGTCTTCCATTACG
CEBPB	NM_005194	CGAGTCAGAGCCGCGCAC
		GCAGGGGGAGACATGCTGGG
LEP	NM_000230	ACCCTGTGCGGATTCTTGTGGCTTTGG
		GGCTCTGCCTACCCCTCTGCCCT
ADIPOQ	NM_001177800	ATCTGGTTGGGGTGGGCTCCTTAC
		GTTGACTCTCTCTGTGCCTCTGGTT
ATF2	NM_001880	GGTCCTTCCTCTCCCCAACCAGTA
		CTGTAGTGGATGTGGCTGGCTGT
JUN	NM_002228	GACAGACACAGCCAGCCAGCCAG
		GGACACTCCCGAAACACCAGCCC
FOXO1	NM_002015	GCTACCAATAACCCCAGCCCCAA
		AATGCCAGGTTGGTCTGTTCGCA
NFKB1	NM_003998	AGACAAAAACTGGGCTACTCTGGCG
		TGAGAGGTGGTCTTCACTGGGCT
RPS18	NM_022551	CGATGGGCGGCGGAAAATAGCCTTGC
		CAGTGGTCTTGGTGTGCTGGCCTCGG
ACTB	NM_001101	GCAGTCGGTTGGAGCGAGCATCCCC
		TCCCCTGTGTGGACTTGGGAGAGGAC

To analyze PCR amplification data, the raw fluorescence data was processed using LinRegPCR (v12.11; http://www.hartfaalcentrum.nl). Starting amplicon number (N_o) was calculated based on mean efficiencies (E) and cycle threshold (Ct) using the formula $N_o = N_t/E^{Ct}$, where N_t is the amplicon number at the cycle threshold. N_o for each target gene were normalized to a geometric mean of the starting amplicon numbers of the endogenous controls to obtain relative expression values.

3.2.8 Univariate Statistical Analysis of Cell Viability and Colony Formation

Viability and CFU-F results are depicted as mean ± standard deviation. Prior to statistical analysis, all data were transformed with a Box-Cox transformation. Where significant factors and interactions were identified by ANOVA, Tukey's post hoc test

(significance level $p < 0.05$) was used to generate pairwise comparisons between means of individual sample groups and determine statistically significant differences.

3.2.9 Multivariate Models of Gene Expression

Statistical modeling was performed using SIMCA-P+ software (version 12.0.1.0, Umetrics) on gene expression results. All Box-Cox-transformed data were mean-centered and scaled to unit variance prior to analysis as a means of normalization to allow all variables to be considered equally scaled in the principal components or latent variables [291]. For PCA, N x K X-matrices were generated of N culture condition observations and K time-variant gene expression responses. PCA was conducted to determine the source of maximum variation in the dataset, resulting in clusters of similar observations separated across one or more principal components. Based on clustering, partial least squares discriminate analysis (PLS-DA) was performed to find LV that served as discriminating factors to best separate observations [32,294]. For PLS-DA, N x M Y-matrices were generated of N culture condition observations and M responses, which were based on assigned classes (culture configuration or glucose level). To optimize model quality, pruning processes were performed to remove observations that lied outside of the 95% confidence interval and variables that were not influential in model generation. The overall quality of each model is summarized by two parameters: R^2X (PCA) or R^2Y (PLS-DA) provide a measure of the extent that the model explains the variation in data matrices and indicates a goodness of fit; and Q^2 provides a measure of the extent to which the variation of a future experimental data set may be predicted by the model and indicates a goodness of prediction [294]. For further model quality assessment, model validation based on permutation testing was performed in SIMCA-P.

In brief, this technique randomly shuffles the positions of variables in the Y-block and then fits a new PLS model to the permuted Y-block. Cross-validation methods are used to generate R^2Y and Q^2 values for new models. If the R^2Y and Q^2 values of the new models are lower than R^2Y and Q^2, the model is valid [295].

3.3 Results

3.3.1 Adipocyte Response to Culture Conditions and Glucose Levels

Adipocytes were cultured under normal and high glucose conditions in three different culture configurations: mono-culture with only adipocytes (AAA), co-culture with MSCs (AMA), or tri-culture with MSCs and osteoblasts (OMA), where the underlined letter represents the cell type being discussed from a particular culture configuration (Figure 3.1). Lipid deposition was observed using Nile Red staining at all time-points and experimental conditions (Figure 3.2A). Lipid deposition was constant throughout the duration of culture and no changes in lipid deposits were observed regardless of time, glucose level, or culture configuration (data not shown).

Expression levels for a variety of genes that act as markers of adipogenesis and energy metabolism (Table 3.1) were measured for each condition using qPCR. Using this data, Principal Component Analysis (PCA) was conducted to model adipocyte gene expression data that included all experimental conditions (Figure E.1A, Appendix E). Based on observed clustering patterns in PCA, Partial Least Squares Discriminate Analysis (PLS-DA) was used to build a model for adipocytes assigned to classes by culture configuration (Figure 3.2B). The PLS-DA model yielded two latent variables (LV) that discriminate adipocytes by culture configuration (R^2Y=0.93 and Q^2= 0.92). The first LV discriminates OMA (or osteoblast-containing cultures) from AAA and AMA (or

non-osteoblast-containing cultures). The second LV discriminates AMA from AAA. The weight plot showed significant correlation of osteocalcin (*OCN*), leptin (*LEP*), adiponectin (*ADIPOQ)*, and *ATF2* with OMA cultures; peroxisome proliferator-activated receptor γ (*PPARγ2*), *ADIPOQ*, and osteoprotegrin (*OPG*) with AMA cultures; and *JUN*, *NFKB1*, *CEBPB*, and *RUNX2* with AAA cultures. Then, the dataset was further divided and sub-models of gene expression data from AAA, AMA, and OMA cultures were used in PCA (Figure E.1B, Appendix E). In the case of the AAA culture configuration, observations clustered by glucose level and classes assigned by normal and high glucose levels were further discriminated using PLS-DA (Figure 3.2C; Figure E.1C, Appendix E).

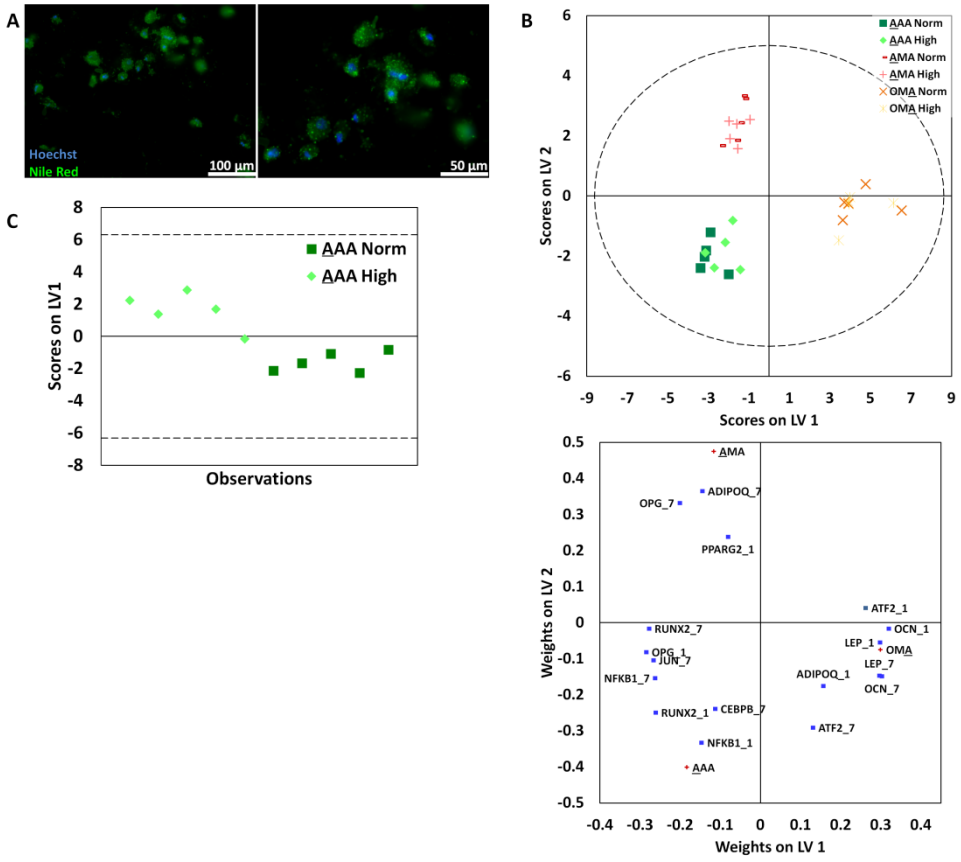

Figure 3.2. Adipocytes were assessed for response to culture conditions. (A) Representative images of adipocytes stained with Nile Red, specific for lipids (green) and

counterstained with Hoechst, specific for nuclei (blue). (B) PLS-DA was used to build models for adipocytes assigned to classes by culture configuration. Models yielded two latent variables that discriminated adipocytes by culture configuration (R^2Y=0.93 and Q^2= 0.92). (C) For AAA culture, classes based on normal and high glucose levels were discriminated using PLS-DA (AAA: R^2Y= 0.79 and Q^2= 0.70). The corresponding weight plot can be found in the supplementary information (Figure E.1C). In all models, dashed lines represent the 95% confidence limit of the distribution of weights.

Confocal microscopy was used to image hydrogel blocks of adipocytes stained with LIVE/DEAD reagents in each culture condition at each time point (representative images in Figure E.2A, Appendix E). Numbers of live and dead cells were quantified and the fraction of viable cells is reported normalized to day 1, normal glucose (Figure 3.3). Adipocytes maintained viability across the entire experiment, and no statistically significant differences were observed within each culture configuration.

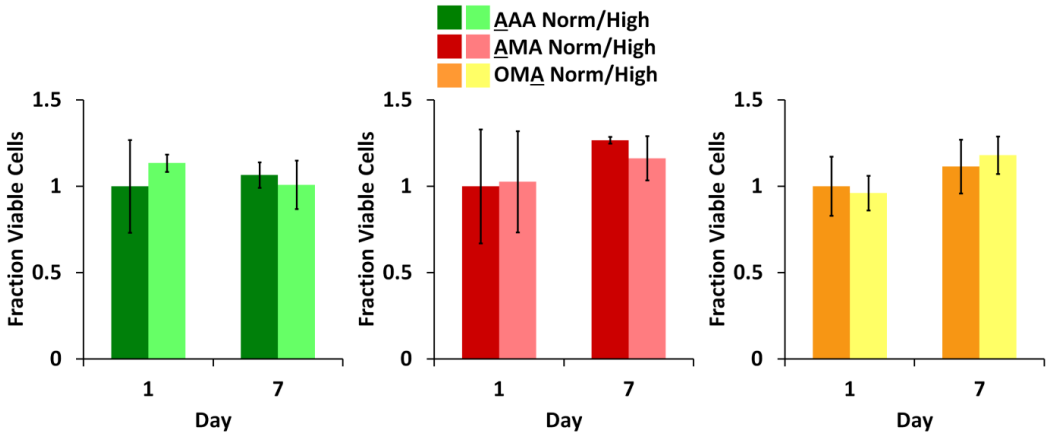

Figure 3.3. Viability of adipocytes was assessed in each culture configuration at normal and high glucose levels. Fraction viable cells (via LIVE/DEAD staining) for each culture condition is presented (n = 3 for AAA, AMA; n ≥2 for OMA; no statistically significant differences were seen, $p < 0.05$).

3.3.2 Osteoblast Response to Culture Conditions and Glucose Levels

Osteoblasts were cultured under normal and high glucose conditions in three different culture configurations: mono-culture (OOO), co-culture with MSCs (OMO), or tri-culture with MSCs and adipocytes (OMA) (Figure 3.1). Alkaline phosphatase (ALP)

activity was evaluated using ALP substrate stain in all experimental conditions across all time points. Similar levels of production were seen for normal and high glucose conditions (data not shown) and representative images from each culture configuration at both time points are presented (Figure 3.4A). Low production was seen throughout the duration of the culture and a transiently higher amount of ALP production was seen in osteoblasts from OMA cultures at day 1 (Figure 3.4A).

Expression levels for a variety of genes that act as markers of osteogenesis and energy metabolism (Table 3.1) were measured for each condition using qPCR. Using this data, PCA was conducted to model osteoblast gene expression data that included all experimental conditions (Figure 3.4B). The PCA yielded two principal components (R^2X= 0.81 and Q^2= 0.56). The first component indicates presence of random variance that can be attributed neither to culture configuration nor to glucose condition, possibly due to the genes measured in the experiment. However, the second component separates OMA cultures from OOO and OMO cultures. Further, three separate PCA models were built within each osteoblast culture configuration (Figure E.3A, Appendix E). In cases that the majority of observations clustered by glucose level in PCA (OOO and OMA cultures), classes based on normal and high glucose levels were further discriminated using PLS-DA (Figure 3.4C; Figure E.3B, Appendix E). Notably, a different set of genes served to separate glucose classes in OOO and OMA cultures configurations. PCA for osteoblasts in the OMO culture configuration indicated that primary variance in gene expression was not due to glucose level and did not warrant further discrimination using PLS-DA (Figure E.3A, Appendix E).

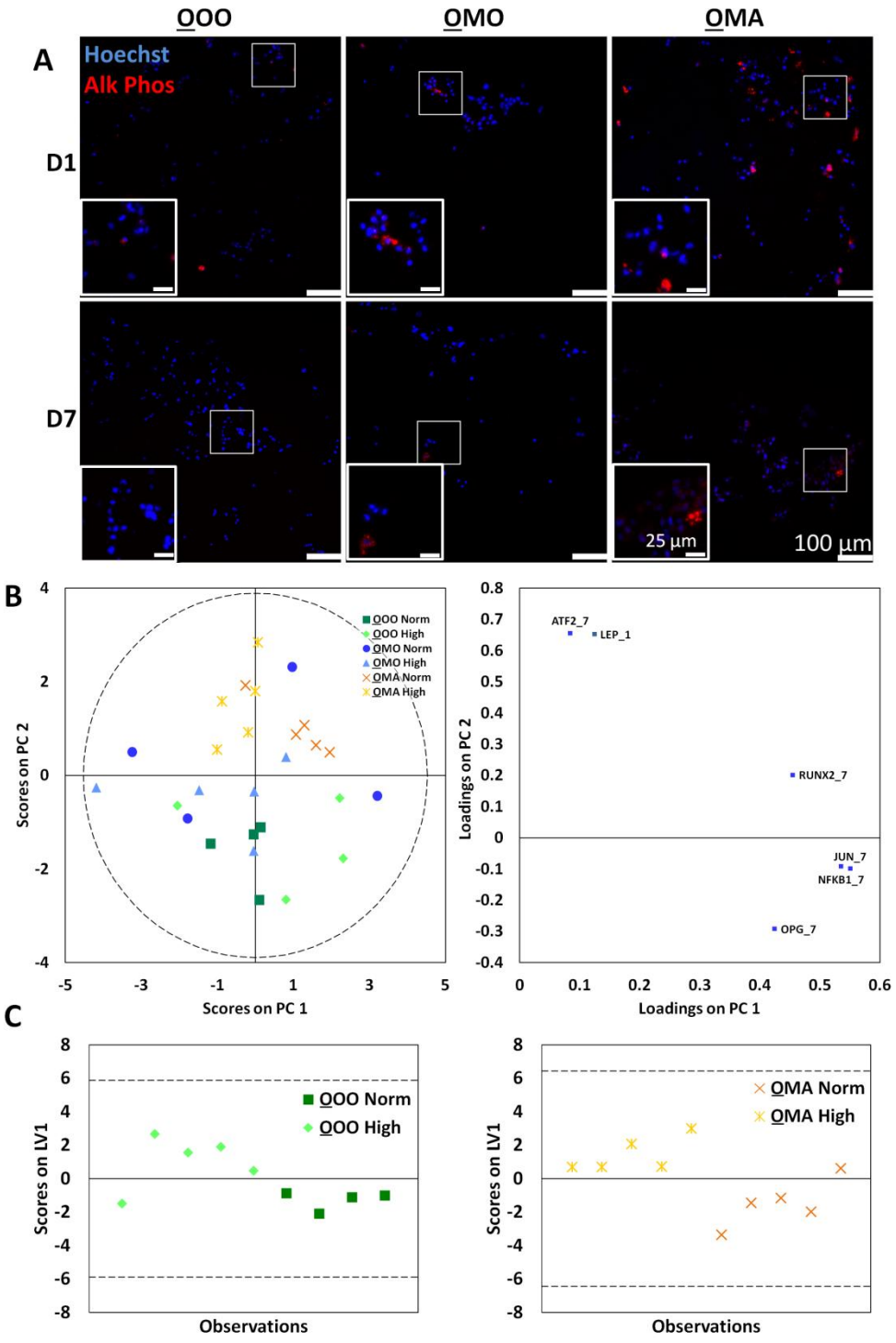

Figure 3.4. Osteoblasts were assessed for response to culture conditions. (A) Representative images of osteoblasts stained for ALP, a marker of osteogenic differentiation (red), and counterstained with Hoechst for nuclei (blue). Noticeably higher amount of ALP production was seen in osteoblasts from OMA cultures at day 1. (B) PCA was applied to the gene expression data of the global osteoblast population, yielding

two principal components (R^2X= 0.81 and Q^2= 0.56). (C) For OOO and OMA cultures, classes based on normal and high glucose levels were discriminated using PLS-DA (OOO: R^2Y= 0.5 and Q^2= 0.43; OMA: R^2Y=0.62 and Q^2= 0.55). The corresponding weight plots can be found in the supplementary information (Figure E.3B). In all models, dashed lines represent the 95% confidence limit of the distribution of scores.

Numbers of live and dead osteoblasts were quantified from confocal microscope images, as described above (Figure E.2B, Appendix E). Viability decreased for both OOO and OMA cultures in normal glucose at Day 7, while viability was maintained in the OMO cultures (Figure 3.5).

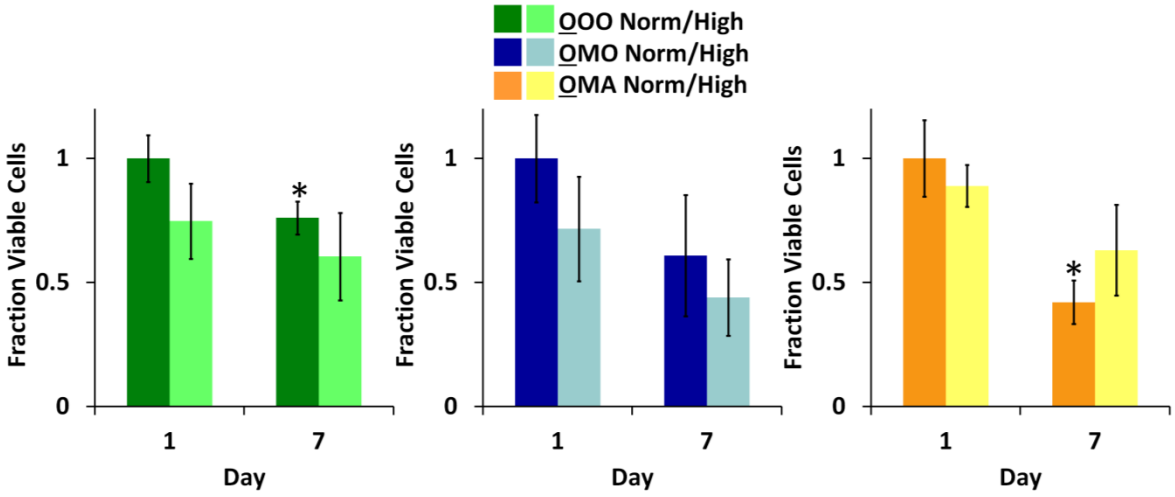

Figure 3.5. Osteoblast viability was measured in response to culture conditions. Fraction viable cells (via LIVE/DEAD staining) for each culture condition is presented (n = 3 for OOO, OMO; n ≥2 for OMA;* = Significantly different from same culture configuration and glucose condition on Day 1; $p < 0.05$).

3.3.3 MSC Response to Culture Conditions and Glucose Levels

MSCs were cultured under normal and high glucose conditions in four different culture configurations: mono-culture (MMM), co-culture with osteoblasts (OMO), co-culture with adipocytes (AMA), or tri-culture with osteoblasts and adipocytes (OMA) (Figure 3.1). Expression levels for a variety of genes that act as markers of osteogenesis, adipogenesis, and energy metabolism (Table 3.1) were measured for each condition using

qPCR. Using this data, PCA was conducted to build a model of MSC gene expression data that included all experimental conditions (Figure E.4, Appendix E). Based on observed clustering patterns, a PLS-DA model was built for MSCs assigned to classes by culture configuration (Figure 3.6). Models yielded three LV that discriminated MSCs by culture configuration (R^2Y=0.73 and Q^2= 0.63). The first LV discriminates MMM and AMA, the second discriminates MMM and OMA, and the third discriminates OMA and OMO. Then, four separate PCA models were built for each MSC culture configuration (Figure E.5, Appendix E). In the cases of OMO and AMA, observations clustered by glucose level in PCA and classes based on normal and high glucose levels were further discriminated using PLS-DA (Figure E.6, Appendix E). Similarly to osteoblast cultures that could be discriminated by glucose level, a different set of genes acted to separate MSCs by glucose level in OMO culture configurations as compared to AMA culture configurations.

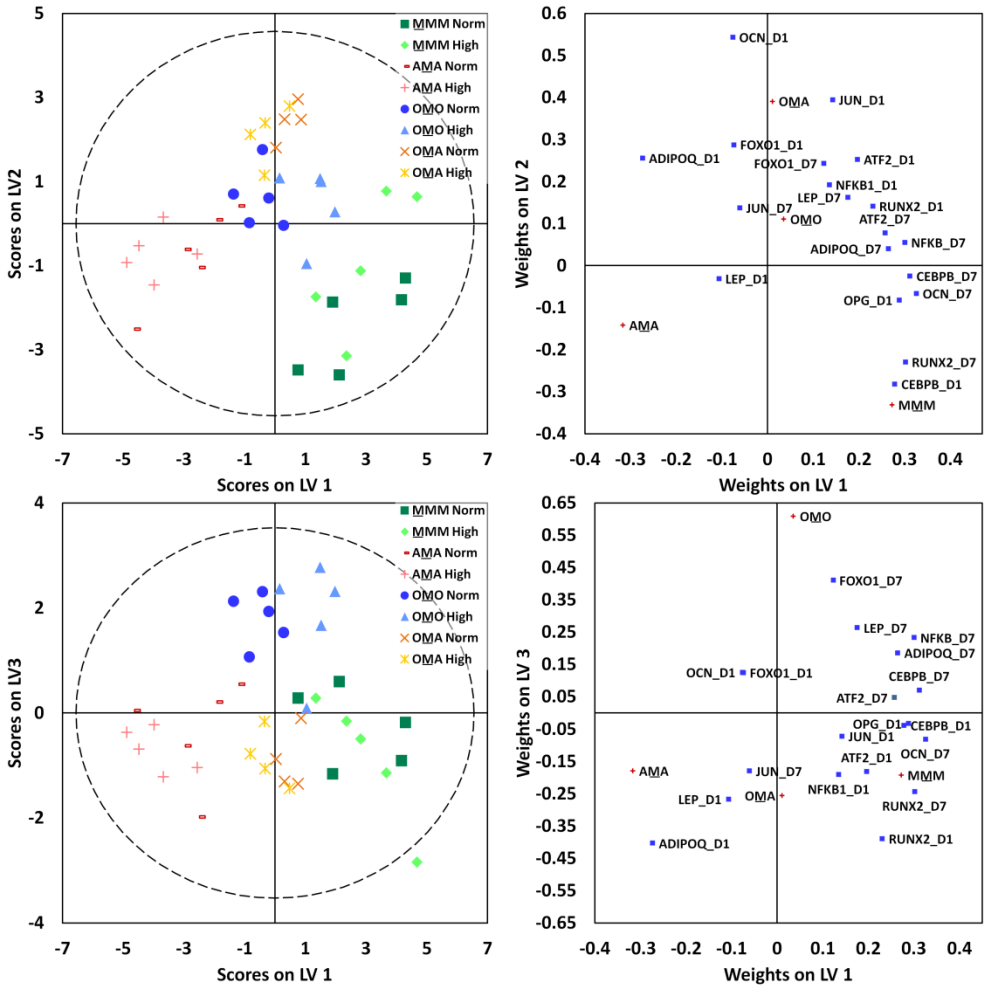

Figure 3.6. MSCs were assessed for gene expression changes response to culture conditions. PLS-DA models were constructed for MSCs assigned to classes by culture configuration. Models yielded three latent variables that discriminated MSCs by culture configuration (R^2Y=0.73 and Q^2= 0.63). In all models, dashed lines represent the 95% confidence limit of the distribution of weights.

After 7 days of culture in normal and high glucose conditions, the degradable MSC block in each culture configuration was exposed to collagenase and degraded. Live cells were recovered and colony forming ability was assessed after 14 days of growth (Figure 3.7A). Significantly fewer colonies were seen in MMM and OMO cultures in high glucose conditions as compared to normal glucose, but number of colonies were similar regardless of glucose level in in AMA and OMA cultures.

Numbers of live and dead MSCs were quantified from confocal microscope images, as described above (Figure E.2C, Appendix E). Decreases in viability were seen for MSCs in both high and normal glucose MMM cultures at Day 7 and also in normal glucose OMO cultures at Day 7 (Figure 3.7B).

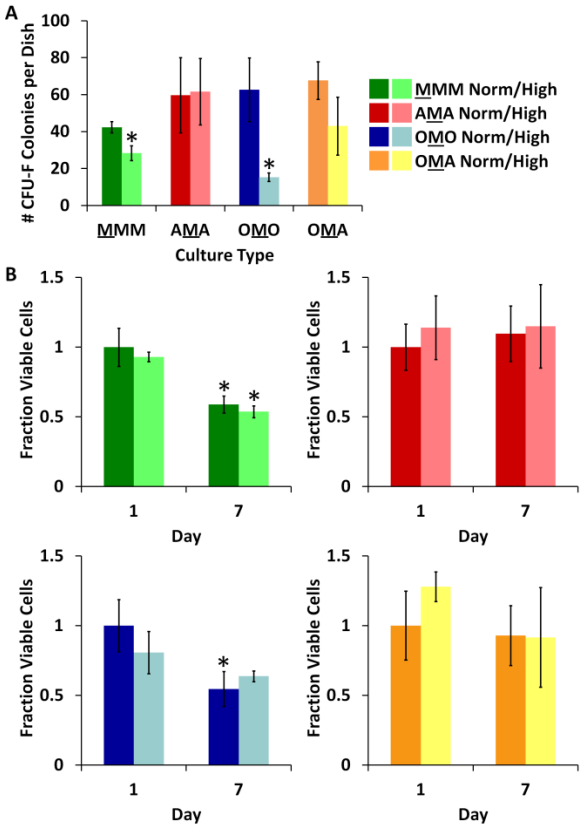

Figure 3.7. MSC clonogenicity was measured post-culture using colony forming assays (A) Number of colony-forming units greater than 2 mm in diameter per dish (n = 3) (* = Significantly different from same culture configuration; $p < 0.05$). (B) MSC viability was measured in response to culture conditions. Fraction viable cells (via LIVE/DEAD staining) for each culture condition is presented (n = 3 for MMM, OMO, AMA; n $\geq$2 for OMA; * = Significantly different from same culture configuration and glucose condition on Day 1; $p < 0.05$).

3.4 Discussion

As stem cell microenvironments have been observed to undergo changes that affect resident stem cells in disease states [281], the correlation between diabetes and

osteoporosis may be better explained by understanding the MSC response to the environmental changes inherent to diabetes. Thus, we were interested to characterize how MSCs are affected by soluble factors secreted by osteoblasts and adipocytes in hyperglycemic conditions. As experimental models available to date have not been satisfactory in addressing this technical need, we expanded upon a model system of the MSC microenvironment previously developed in our laboratory to include a degradable polymer for live-cell retrieval [32,287]. In this model system, we focused on decoupling the effects of paracrine signals from other types of signaling that may occur in the bone marrow niche. Within the bone marrow microenvironment, information is thought to be transmitted over relatively short length scales (on the order of hundreds of microns) given the well-defined, compact architecture [296,297], we believe the geometry of our tri-culture system sufficiently mimics this aspect of the structure of the bone marrow while allowing for separation of cell types post-culture. From this system, we analyzed gene expression, histological markers, cell viability, and MSC colony forming ability after 7 days of culture in normal or high glucose conditions.

3.4.1 Encapsulated Cells Maintain Viability and Phenotype

Previous experiments provided evidence that our culture platform was suitable for at least 18 days of culture [32]. In the experiments presented here, cell viability was generally maintained for the duration of the experiment in all cell types (Figure 3.3, 3.5, and 3.7B). However, osteoblasts in OOO and OMA culture configurations under normal glucose conditions exhibited significantly lower viability by day 7. The decreased viability observed in the mono- and tri-culture conditions remains unclear, but is possibly due to interactions with neighboring cell types. MSCs may have promoted osteoblast

viability in the co-culture, but these effects could have been interrupted by the presence of adipoctyes in the tri-culture. Clinically, osteoblast turnover is thought to occur on the order of days [298], suggesting that osteoblasts need constant replenishment from the stem cell compartment. While soluble signals from stem cells are present in this system, direct replenishment via differentiation is impossible. Thus, the maintenance of viability observed in OMO cultures might be a result of communication with MSCs that encouraged osteoblast survival. Further refinement of our culture platform could improve osteoblast viability by including more soluble signals known to contribute to normal osteoblast function *in vivo*.

Osteoblast production of ALP, a marker for osteogenic phenotype, persisted at generally low levels throughout the duration of culture time (Figure 3.4A). Similarly, adipocyte lipid deposition was evident in adipocytes throughout the duration of culture in all experimental conditions (Figure 3.2A). Taken together, the maintenance of viability and cell type-specific markers indicate that the culture system is a valid platform for analysis of interactions between these three cell types, even under hyperglycemic conditions.

3.4.2 Multivariate Models Allow Discrimination by Neighboring Cell Type and Glucose Level

Multivariate statistical modeling was used to better understand maximum sources of variance within the gene expression of each cell type as well as to inform future co-culture experimental design. In global multivariate models for all cell types, the maximum source of variance originated from differences in neighboring cell types, referred to as culture configuration (i.e. mono-, co-, or tri-culture), as determined by

clustering patterns and discrimination across principal components and latent variables (Figure 3.2B, 3.4B, and 3.6). In adipocyte global models, the first LV discriminated osteoblast containing cultures from non-osteoblast containing cultures. From this, we know that the presence of osteoblasts influences adipocyte behavior, an important consideration in designing future co-culture studies that aim to understand adipocyte behavior within the bone marrow microenvironment. Osteoblast models showed less distinct clustering patterns, possibly indicating a large amount of random variance in the system. Alternatively, these results may be indicative of osteoblast stability regardless of neighboring cell type. Overall, future co-culture experiments may need to analyze different genes or other output measures to gain a better understanding osteoblast behavior. Finally, MSC global models discriminated each culture type from the other except for MMM and OMO culture configurations. This suggests that interactions with adipocytes significantly influence MSCs, as was evident in other analyses and will be discussed further. As osteoblast presence did not seem to impact MSCs as strongly, at least based on gene expression data, future co-culture studies could aim to gain a deeper understanding of MSC and adipocyte communication and the mechanisms in which this communication influences MSC behavior.

Clustering by glucose level was not often observed in global models, indicating that neighboring cell types had a greater influence on gene expression than glucose conditions. However, this may have been partially due to the genes analyzed in this study, and by including more genes, discrimination by glucose in global models may have been possible. When sub-groups of the dataset were modeled to understand primary variance within each culture configuration, it was found that in several cases

discrimination by glucose level could be achieved (Figure 3.2C and 3.4C; Figure E.6, Appendix E). In other cases, it was more difficult to definitively determine if culture configurations could be separated by glucose level, and whether this is due to the choice of genes analyzed or the influence of the culture configuration on cellular response to glucose remains unclear. Overall, it was evident that the response of individual cell type to glucose level was unique to each culture configuration and thus interactions with neighboring cell types. This provides further incentive to probe cellular response to pathological conditions within a co-culture setting, as it better represents the simultaneous cell response to neighbors and environment that occurs *in vivo*.

The fact that correlations in the multivariate models were seen primarily based on type of neighboring cells strongly supports the idea that traditional monoculture platforms are not able to mimic/reproduce important features of systems-level cell-cell communication that occurs in disease states. Other indirect (no cell-cell contact) co-culture studies with bone marrow cells also report that cellular behavior changes when in communication with other orthopaedic-derived cells. Increased osteoblast death has been observed in response to diabetic bone marrow cells [283] and reduced MSC hypertrophy and mineralization was achieved when in co-culture with chondrocytes [299]. These studies and the work presented here provide strong motivation to include multiple cell types in *in vitro* studies of the bone marrow microenvironment in order to gain more relevant biological insights for diseases affecting the entire tissue. Thus, our culture platform provides a novel technology that is well-suited for future studies in which multiple co-cultured cell types responding both to each other and to environmental changes may be required to adequately recapitulate a complex *in vivo* disease state.

3.4.3 Adipocyte Co- and Tri-culture Conditions Correlate with Genes Related to Energy Metabolism and Adipogenesis

Multivariate models were also used to understand the correlations between gene expression and culture configuration. In the adipocyte-only model, markers of adipogenesis and energy metabolism (*OCN*, *LEP*, *ADIPOQ*, *PPARγ2*, *OPG*) showed statistically significant correlation with AMA and OMA cultures while markers of inflammation and oxidative stress (*JUN*, *NFKB1*, *CEBPB*) showed correlation with AAA cultures (Figure 3.2B). This suggests that presence of MSCs may promote adipocytes to up-regulate genes related to adipogenesis and energy metabolism. Interestingly, these differences in gene expression did not manifest in adipocyte viability data or levels of lipid deposition, as both were constant in all conditions (Figure 3.2A and 3.3). It is possible that adipocytes were robust to environmental changes, or that gene expression data provided an early view of adipocyte response to neighboring cells that may manifest in viability differences or changes in lipid at a later time. These results are consistent with experiments that have been done previously, in which adipocytes have been observed to secrete markers of inflammation and to undergo hypertrophy rather than apoptosis under hyperglycemic conditions [300]. Overall, these results indicate the presence of cross-talk between adipocytes and MSCs, which was further confirmed in additional studies discussed below.

3.4.4 MSCs Modulate Osteoblast Response to Glucose

Cell viability and MSC clonogenicity studies suggested that MSCs exert modulatory effects on osteoblasts at the expense of their own viability and clonogenicity, trends that were not seen when MSCs were co-cultured with adipocytes. MSCs in OMO

and MMM cultures demonstrated decreased viability and clonogenicity after 7 days of culture, while both viability and clonogenicity were maintained in AMA and OMA cultures (Figure 3.7). Similar to MSCs in OMO and MMM cultures, previous work has also shown reduction of MSC clonogenicity and viability under hyperglycemic conditions [86]. Osteoblast viability, on the other hand, was unlike that of MSCs, as only osteoblasts in the OMO cultures showed constant cell viability for the duration of culture (Figure 3.5), whereas MSCs from OMO cultures showed decreased viability over time in high glucose conditions (Figure 3.7B). These opposing trends were also seen in gene expression data, where MSCs from OMO cultures were seen to cluster by glucose level in the global multivariate model and culture configuration sub-model (Figure 3.6; Figure E.6, Appendix E) while osteoblasts from the OMO culture configuration could not be discriminated by glucose level (Figure E.3A, Appendix E). This complementing relationship may indicate that MSCs somehow act to modulate the response of osteoblasts to glucose in a way that changed their own behavior. As MSCs are known to secrete therapeutic soluble factors [301]. This work further suggests that the secretion of soluble factors in hyperglycemic conditions may have had positive effects on osteoblasts but was detrimental to some MSC functions. However, this does not appear to be a universal consequence of MSC co-cultured with differentiated cells, as these detrimental effects were not seen in MSCs cultured with adipocytes in any configuration, discussed below.

3.4.5 Adipocytes Promote MSC Viability and Clonogenicity and Early Osteoblast ALP Activity

Unlike MSCs in monoculture or co-culture with osteoblasts, MSCs in co-culture with adipocytes showed maintenance of viability and clonogenicity in high glucose conditions. Changes in adipocyte gene expression in the presence of MSCs also provides evidence that interactions between MSCs and adipocytes occurred, possibly due to an increase in expression of *LEP* and *ADPIQ* by adipocytes , which is known to act upon other cell types [300]. Furthermore, it appears that adipocytes also modulated osteoblast behavior, especially in regards to ALP production (Figure 3.4A). As ALP is a marker for osteogenesis, higher levels in osteoblasts co-cultured with adipocytes after one day may indicate that interactions with adipocytes promoted their activity, although high ALP staining was not observed by day 7 for any sample types. Thus, it appears that adipocytes may "buffer" MSCs from the reduction of clonogenicity and viability induced by hyperglycemic conditions. Analyzing these results alongside gene expression data, the ability of adipocytes to influence other cell types may correlate with upregulation of genes for adipogenesis and energy metabolism in adipocytes.

The idea that adipocytes may act to modulate MSC response to glucose has not, to our knowledge, been reported in other experiments. It is well known that adipocytes and osteoblasts co-exist in the bone marrow microenvironment, and that the ratio of adipocytes to osteoblasts increases with age [74,78]. It also has been observed that an increase of adipocytes in the marrow coincides with the onset of disease like osteoporosis and anorexia nervosa, but the direct impact of higher numbers of adipocytes on disease progression has yet to be determined [74,302]. It has been hypothesized that increased

marrow fat may be a compensatory mechanism in times of disease [302], or be a direct cause of reduced MSC osteoblastogenesis [302,303]. Our results suggest it is possible that, under hyperglycemic conditions, an increased number of adipocytes in the bone marrow may exert compensatory mechanisms to maintain MSC function and possibly delay the onset of osteoporosis. Thus, our system provides important insight into a complex biological system that has not been achieved through other mono- and co-culture experiments and highlights the interconnected nature of these three cell types in pathological conditions.

3.5 Conclusion

As a whole, the study presented illustrates a platform that facilitated elucidation of non-intuitive cellular behavior in a model of hyperglycemia. This tri-culture platform permitted the study of reciprocal cellular interactions, often impossible in other *in vitro* culture systems. Specifically, the tri-culture allows simultaneous analysis of cellular response to both pathological conditions and neighboring cell types. Also unique to our culture platform is the ability for on-demand retrieval of live cells, allowing for further analysis of individual cell response to their environment. In our model of the hyperglycemic bone marrow microenvironment, it was observed that neighboring cell type was the primary source of variance in our system and that disease-relevant environmental alterations can best be understood within the context of multi-cell systems. It was also found that while MSC clonogenicity and viability decreased when in culture with osteoblasts, both were maintained when in culture with adipocytes, regardless of the presence of osteoblasts. One possible explanation for this can be derived from adipocyte gene expression data, which indicates that cross-talk between adipocytes and MSCs

resulted in an altered reaction to high glucose levels, at least at early stages of hyperglycemia.

These results provide specific avenues of study that can follow. Further studies to understand mechanistic reasons for why MSC viability and colony forming ability is decreased in the presence of osteoblasts but not adipocytes could inform future therapies aimed to target diseases like osteoporosis. Also, as increased marrow adipocyte levels coincide with osteoporosis [74], it would be interesting to further investigate if the relative quantities of osteoblasts and adipocytes change MSC response to culture conditions. The culture system described here could be used to investigate these questions and to generate further hypotheses that could be studied *in vivo.* Overall, the technological innovations in our *in vitro* tri-culture platform permitted a deeper understating of cellular response to hyperglycemic conditions that may be used to direct future research into cell-based therapies for diabetes and its secondary pathologies.

After employing hydrogels to interrogate cell behavior, we were interested in using hydrogels to modulate cell behavior. However, to understand how our hydrogel-based materials affected cell behavior, a defined cell system was required. Thus, we transitioned away from the MSC, osteoblast, and adipocyte co-culture model and began using a well-defined model system of cellular differentiation to modulate cell behavior with heparin-based materials.

CHAPTER 4

HEPARIN MPS TO MODULATE CELL DIFFERENTIATION IN AN IN VITRO MODEL SYSTEM OF ENDOCHONDRAL OSSIFICATION

4.1 Introduction

Heparin is a highly sulfated GAG known to bind a variety of proteins involved in cellular differentiation, including BMPs, IHH, FGFs, Wnts, and TGFβs [25]. While heparin has often been used in controlled-delivery vehicles for enhanced protein affinity [53], recent studies have also shown its utility in sequestering cell-secreted protein for subsequent analysis or to modulate cell differentiation. For example, heparin cross-linked into hydrogels has been shown to enhance cardiac progenitor cell differentiation, osteogenesis, and chondrogenesis, and while the mechanism is still unknown, evidence points toward endogenous protein sequestration [38,40,41,198]. For example, in heparin hydrogels seeded with MSCs in co-culture with osteoblasts, enhanced markers for osteogenesis were observed in MSCs as heparin content increased, possibly due to increased growth factor sequestration [40]. In addition, hyaluronic acid and heparin-based hydrogels were degraded after acting as a scaffold for cardiac progenitor cells, and analysis of released proteins revealed higher concentrations of cell-secreted angiogenic factors in heparin-containing gels, which likely contributed to enhanced neovascular differentiation [41]. These studies indicate the ability of heparin to sequester endogenous protein to modulate differentiation, which could eliminate the need to deliver recombinant proteins in tissue regeneration applications [3]. Still, little is known about

the ability of heparin alone to modulate differentiation processes, especially in a temporally controlled manner. Thus, in this work, the ability of heparin to modulate differentiation in an *in vitro* model system of endochondral ossification was investigated.

Endochondral ossification is the process by which cartilage is converted into bone during skeletal development in vertebrates [23,106]. In this process, mesenchymal cells condense and differentiate into proliferative chondrocytes [23,106]. Eventually, these chondrocytes undergo hypertrophy and apoptosis, at which point they direct vascularization, mineralization, and osteoblast invasion of the tissue, converting the cartilage analgen into bone [23,106]. This process is tightly regulated by both systemic and local signaling by proteins such as FGFs, BMPs, TGFβs, IHH, PTHrP, Wnts, and IGFs [23,107,186]. In the growth plate, endochondral ossification continues through puberty and is required for normal bone elongation and growth [23,106]. Unfortunately, bone fractures that affect the growth plate can interrupt this process, and depending upon the severity of the injury, can result in limb length disparities, angular deformations in the bone, and possibly growth arrest in the limb [111,112]. Recently, tissue engineering strategies have been investigated to facilitate regeneration of the growth plate cartilage tissue using cell-seeded scaffolds, but only limited success has been observed [111,113–118]. Because heparin is known to bind a variety of proteins implicated in endochondral ossification, it is possible that heparin materials could be used to modulate the differentiation process through cell-secreted protein sequestration. In the future, such a technique could be employed to modulate the timing of endochondral ossification and possibly improve growth plate cartilage regeneration strategies.

The chondrogenic ATDC5 cell line was employed as a model cell system for these studies. Derived from the murine teratocarcinoma stem cell line AT805, ATDC5 cells are known to undergo the stages of endochondral ossification *in vitro* [304–307]. In the presence of insulin and often β-glycerophosphate and ascorbic acid, these cells show increases in gene expression for such as collagen II, aggrecan, BMPs, FGFs, IHH, and Pthr1; staining for GAGs, collagen II, and aggrecan in the cell matrix; and production of proteins such as BMP-2 and TGF-β1 within 10-20 days of monolayer culture [304,305,308–313]. Thus, in these studies the ATDC5 cell line was chosen to enable large-scale experiments to investigate the effect of heparin MPs on endochondral ossification in a reproducible manner.

Often, *in vitro* models of cellular differentiation are carried out in pellet culture [36]. Dense cell aggregates better mimic the *in vivo* cellular microenvironment of cartilage and bone tissue, as aggregates provide extensive opportunity for cell-cell and cell-matrix interactions [36,314]. One challenge to using cell aggregates is diffusion limitations of soluble factors through the dense cell matrix [315,316]. To overcome this challenge, protein loaded microparticles have recently been incorporated into cell aggregates to achieve more uniform protein delivery [256,258,260,261,263,264,317]. Using a similar argument, sequestration of cell-secreted proteins must occur uniformly throughout the aggregate. Therefore in these studies, heparin was incorporated into ATDC5 cell aggregates in microparticle format to ensure uniform sequestration of cell-secreted proteins. Besides being advantageous for incorporation into cell aggregates, MPs are also advantageous over bulk hydrogels due to their high surface area to volume ratio, which improves protein binding and release [211]. Previously, heparin MPs were

fabricated and shown to have a high binding capacity for BMP-2 [59], suggesting that heparin MPs will have the ability to sequester large quantities of protein in ATDC5 cell aggregate culture.

Herein, we present a model system using ATDC5 cells upon which to test the ability of heparin MPs to modulate cellular differentiation, specifically endochondral ossification, via sequestration of soluble factors. Heparin or PEG MPs, a low-binding material control, were incorporated into ATDC5 cell aggregates (spheroids) to evaluate the effect of heparin MPs on differentiation. Cell spheroids were cultured for 18 days and then assessed for viability, general morphology, GAG deposition, collagen deposition, and gene expression markers for chondrogenesis and hypertrophy. In addition, ATDC5 cells were cultured in monolayer transwell culture with heparin or PEG MPs to evaluate the mechanism of action behind heparin MP mediated changes in differentiation. Finally, growth factor sequestration studies were conducted to better understanding heparin MP protein binding. Overall, these studies indicate that heparin MPs can modulate cell differentiation, likely through the sequestration of soluble protein.

4.2 Materials and Methods

4.2.1 Material Synthesis

Heparin was functionalized with methacrylamide according to previous methods [40]. Briefly, the reaction was carried out in a phosphate buffer of pH 5 with 20 mg/mL heparin, 83 mM N-Hydroxysulfosuccinimide sodium salt (Sigma-Aldrich), 100 mM N-(3-aminopropyl) methacrylamide hydrochloride (Polysciences), and 78 mM (N-3-Dimethylaminopropyl)-N'-ethylcarbodiimide hydrochloride (EDC) (Sigma-Alrich) for 2

hours on ice. An additional round of EDC was added, resulting in a final molarity of 156 mM. After 4 more hours, solution was dialyzed for 2-3 days and lyophilized. PEG-diacrylate (PEG-DA) (MW=8 and 3.4 kDa) was synthesized by combining acryloyl chloride (Sigma-Aldrich) and PEG (Sigma-Aldrich) according to previous methods [148]. All polymers were stored at -20°C prior to use.

4.2.2 Microparticle Fabrication and Protein Pull-Down Studies

Heparin methacrylamide MPs were formed according to previous methods [59]. Briefly, an aqueous phase of 10% heparin methacrylamide (wt%), 18 mM ammonium persulfate (Sigma-Alrich), and 18 mM N,N,N′,N′-Tetramethylethylenediamine (Sigma) was emulsified against corn oil with 1.67% (v/v) Tween-20 (polysorbate 20; BDH) at a 1:120 ratio aqueous:oil phase. MPs were cross-linked under nitrogen purge at 60°C for 30 minutes (see Figure 4.1A for cross-linked structure), then washed with acetone and water. PEG MPs for spheroid studies and BMP-2 pull-down studies were fabricated via water-in-water emulsion between a 1:4 PEG-DA-rich phase (150 mg/mL 8 kDa PEG-DA, 2 mg/mL Poly-L-Lysine (PLL) (Sigma-Aldrich), 0.05% (w/v) Irgacure D2959 in PBS) to dextran phase (50% (w/v) 70 kDa dextran (Sigma-Alrich), 2 mg/mL (PLL) in PBS). Vortexing (30 seconds) was used to form an emulsion between the two phases and the resulting emulsion was ultrasonicated at 21 mW energy for 1 minute to reduce particle size. Then, the emulsion cross-linked under UV light at an intensity of 17 mW/m^2 and washed twice in PBS buffer pH 7.4 containing 1% Pluronic F127 (Sigma-Aldrich). PEG MPs for transwell and media sequestration studies were fabricated by homogenizing an aqueous phase containing 16 wt% PEG-DA (3.4 kDa), 0.05 wt% Irgacure 2959 Photoinitiator (Ciba), and 2 mg/mL poly-l-lysine (PLL, Sigma-Aldrich) against a mineral

oil phase (light, white; Ameresco) with 1.3% (v/v) Span-80 (sorbitan monooleate; TCI) at a 1:16.7 ratio aqueous:oil phase. MPs were then nitrogen purged for 1 minute, cross-linked under UV light (approximately 10.5 mW/cm^2) in a 35x10 mm petri dish for 10 minutes, and washed in water.

MPs were sized using phase microscopy images and ImageJ. For BMP-2 sequestration studies, 0.1 mg heparin and PEG MPs were incubated with 0.1 µg BMP-2 overnight in 0.5 mL 0.1% BSA in PBS. Concentration of BMP-2 was assessed by ELISA (R&D Systems). For cell studies, MPs were sterilized by incubating in 70% ethanol for 30 minutes followed by three 30 minute PBS washes.

4.2.3 ATDC5 Cell Culture, Spheroid Culture, and Transwell Culture

ATDC5 cells were expanded in maintenance media (DMEM/F-12 with L-glutamine (Life Technologies), 5% FBS (Atlanta biologics), 100 IU Penicillin (Mediatech), 100 ug/mL Streptomycin (Mediatech), 0.25ug/mL Amphotericin B1 (Mediatech), 30 nM Sodium Selenite (Sigma-Alrich), and 10 µg/mL transferrin (Life Technologies)) and experiments were conducted mineralization media (maintenance media plus 10 µg/mL insulin (Sigma-Alrich), 10 mM sodium β-glycerophosphate pentahydrate (Alfa Aesar), and 50 µg/mL L-ascorbic acid-2-phosphate sequimmagnesium salt hydrate (Sigma-Aldrich)). For spheroid studies, cells and MPs were combined at a 3:1 and 1:3 MP cell ratio and spheroids were formed via forced aggregation of the cell-MP solution into 400 µm agarose wells (Figure 4.2A). After about 18 hours, spheroids were removed from agarose wells with a wide-bore pipette tip and placed in non-stick dishes (6000 spheroids/plate; BD Biosciences, 10 cm diameter) on

rotary culture at 65 RPM. Media was changed every 3 days. For transwell studies, ATDC5 cells were plated at a 6500 cells/cm^2 in 12-well plates and cultured in maintenance media until confluent (3-5 days). Once confluent, media was changed to mineralization media and treatment groups in transwell inserts were added. For MP groups, a high or low (3.28 and 0.328 mg MPs, respectively) were added to the transwell insert. This mass was chosen to match, by mass, the high and low ratios used in the spheroid studies. Media was changed daily.

For spheroid studies, MP incorporation efficiency was determined incorporating MPs into ATDC5 spheroids at 1:3, 1:1, and 3:1 MP:cell ratios. After 6 hour, a portion of the spheroids was taken for counting, and the other portion was treated with 0.25% trypsin for 1 hour, followed by an overnight treatment with 5% sodium dodecyl sulfate (SDS) (Sigm-Aldrich). The number of MPs from dissociated spheroids were counted and incorporation efficiency was calculated by comparing MP number to number of spheroids and actual number of MPs expected (actual ratio/expected ratio). For each set of samples, incorporation efficiency was normalized to the 1:3 MP:Cell ratio.

4.2.4 qPCR and DNA Analysis

Spheroids were rinsed in PBS and subject to lysis buffer for an hour at 4°C before mRNA was extracted using a QIAshredder tissue homogenizer and RNeasy kit with DNase I digestion (Qiagen). For monolayer cells, cells were lifted with 0.05% trypsin and washed once in PBS, then incubated in lysis buffer for 15 minutes. cDNA was generated using SuperScript III Reverse Transcriptase (Invitrogen) with Oligo(dT)15 primers and dNTPs (Promega). Gene expression was analyzed using quantitative PCR amplification

performed on a StepOnePlus Real-Time PCR System (Applied Biosystems) in the presence of SYBR Green/ROX master mix (Applied Biosystems). Sequences for custom-designed primers (Invitrogen) are listed in Table 4.1.

Table 4.1. National Library of Medicine accession number and primer sequences (F=forward, R=reverse) for target genes used in qPCR.

Target Gene	NML Accession #	Sequence
RSP-18	NM_022551.2	F- CGATGGGCGGCGGAAAATAGCCTTTGC R- CAGTGGTCTTGGTGTGCTGGCCTCGG
Collagen II	NM_031163	F- ATGTATGGAAGCCCTCATCTTGC R- CAGCCTTCTCGTCATACCCTC
Aggrecan	NM_007424	F- TGGCTTCTGGAGACAGGACT R- GGGACATGGTTGTTTCTGCT
Collagen X	NM_009925	F- TGCCCGTGTCTGCTTTTACTGTCA R- TCAAATGGGATGGGGGCACCTACT

To analyze PCR amplification data, the raw fluorescence data were processed using LinRegPCR (v12.11; http://www.hartfaalcentrum.nl). The starting amplicon number (N_o) was calculated based on mean efficiencies (E) and cycle threshold (C_t) using the formula $N_o = N_t/E^{Ct}$,where N_t is the amplicon number at the cycle threshold. N_o for each target gene were normalized the starting amplicon numbers of the endogenous controls and then further normalized to no MP controls at each timepoint.

For DNA was extraction, cells were washed twice with PBS. DdH_2O was added to cells for 20 minutes and then cells were subjected to a freeze-thaw cycle. Cells were then scraped from the 96 well plate and cell lysate solution was transferred to 1.7 mL tube. Cell lysate was sonicated for 20 minutes, then subjected to another freeze-thaw cycle. This was repeated once, then samples were spun down and supernatant was used for analysis DNA content was assessed with the CyQUANT Assay (ThermoFisher Scientific).

4.2.5 Histological Analysis and Stain Extraction

For histological analysis of ATDC5 spheroids, spheroids were imbedded in histogel, sectioned at 10 μm sections and stained with Safranin-O or H&E according to standard protocols. Immunostaining for ECM deposition was performed using primary antibodies for collagen type II (Abcam). Antigen retrieval was performed by incubating in 20 μg/ml proteinase K (Sigma-Aldrich) for 10 minutes at 37°C, blocked with 1.5% goat serum (Fisher Scientific), and incubated with the primary antibodies at a 1:20 dilution overnight at 4°C. Secondary antibody binding with Alexa Fluor 488-conjugated goat polyclonal anti-mouse immunoglobulin G (IgG, Molecular Probes) was performed at room temperature for 1 hour. Samples were counterstained with Hoechst (Sigma-Aldrich) to visualize the nuclei.

For histological analysis of ATDC5 monolayer cells, cells were rinsed in ddH_2O and then fixed in 95% ice cold methanol for 30 minutes. Cells were stained with either 1% Alcian blue 8GX (Sigma-Aldrich) or 2% Alizarin red (Sigma-Aldrich) pH 4.2 in 0.1 M HCl for 1 hour. Cells were then rinsed with ddH_2O and imaged. Stain was extracted by incubating Alcian Blue stained cells with 6 M guanidine-HCl (Sigma-Aldrich) and Alizarin Red stained cells with 0.5M HCl and 5% SDS for 6 hours. Absorbance was measured at 630 and 405 nm for Alcian Blue and Alizarin Red extractions, respectively.

A LIVE/DEAD staining kit (Life Technologies) was used to assess cell viability via confocal microscopy. Stacks with slices every 2 μm were flattened using the Z-project function on Image-J.

4.2.6 Protein Analysis Experiments

For BMP-2 sequestration studies in conditioned media, 0.01, 0.2, and 1 mg of Heparin and PEG MPs were incubated in ATDC5 cell-conditioned media with 500 pg of BMP-2 overnight at 4°C on rotary. Supernatant was then analyzed using an ELISA (R&D Systems). For SDS-PAGE studies, heparin or PEG MPs were cultured in transwell with ATDC5 cells or media only, then isolated and washed once with PBS. MPs were combined with a loading buffer (63 mM Tris-HCl pH 6.8, 350 mM SDS, 6.84 M glycerol, 0.75 mM Bromophenol Blue, 1.78 M β-mercaptoethanol) at a 4:1 MP:buffer ratio, then heated to 90°C for 5 minutes. MPs and a protein ladder (BioRad) were loaded onto a 12% polyacrylamide gel (BioRad) and ran at 200 V for 30-60 minutes. The gel was stained with Silver Stain Plus (BioRad) according to the manufacturer's protocol.

4.2.7 Statistical Analysis

All results are depicted as mean $\pm$ standard deviation. ANOVA was used to identify significant factors and interactions, then Tukey's post hoc test (significance level $p \leq 0.05$) was used to generate pairwise comparisons between means of individual sample groups and determine statistically significant differences (Minitab 15 Statistical Software).

4.3 Results

4.3.1 Microparticle Fabrication, Characterization and Incorporation in Spheroids

Heparin-MAm and PEG-DA MPs had similar diameters, 5.0±3.1 and 4.9±3.9 μm, respectively (Figure 4.1B,C). In BMP-2 loading studies, heparin MPs loaded nearly

100% of the BMP-2 in solution, while PEG MPs loaded almost no BMP-2 (Figure 4.1D). These studies provided rationale for using the PEG MPs as a low-binding material control for the remainder of this work.

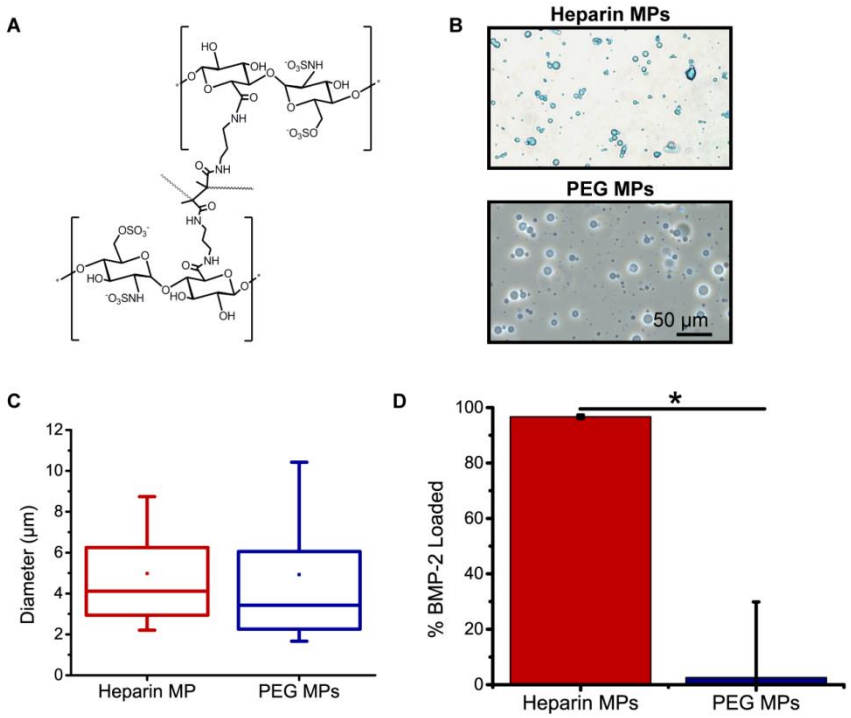

Figure 4.1. Similarly sized heparin and PEG MPs were fabricated. (A) Heparin MAm was cross-linked via free-radical initiated polymerization (B) Phase microscopy images of heparin (stained with alcian Blue) and PEG MPs. (C) Heparin MPs and PEG MPs had average diameters of 5.0±3.1 and 4.9±3.9 μm, respectively. (D) Percent BMP-2 loaded on heparin MPs vs. PEG MPs normalized to total BMP-2 in soluble control (*=significantly different than heparin MP group; $p<0.05$).

MPs could be incorporated into ATDC5 spheroids at several different ratios: 3:1, 1:1, and 1:3 MP:cell, as shown in sections of spheroids stained with Safranin-O and Fast Green (Figure 4.2B). Incorporation efficiency was similar for both heparin and PEG MPs, but decreased with increasing amounts of MPs (Figure 4.2C). The 3:1 MP:cell ratio

was used for the remainder of the studies, but when taking the incorporation efficiency into account, effectively becomes a 2:1 MP:cell ratio.

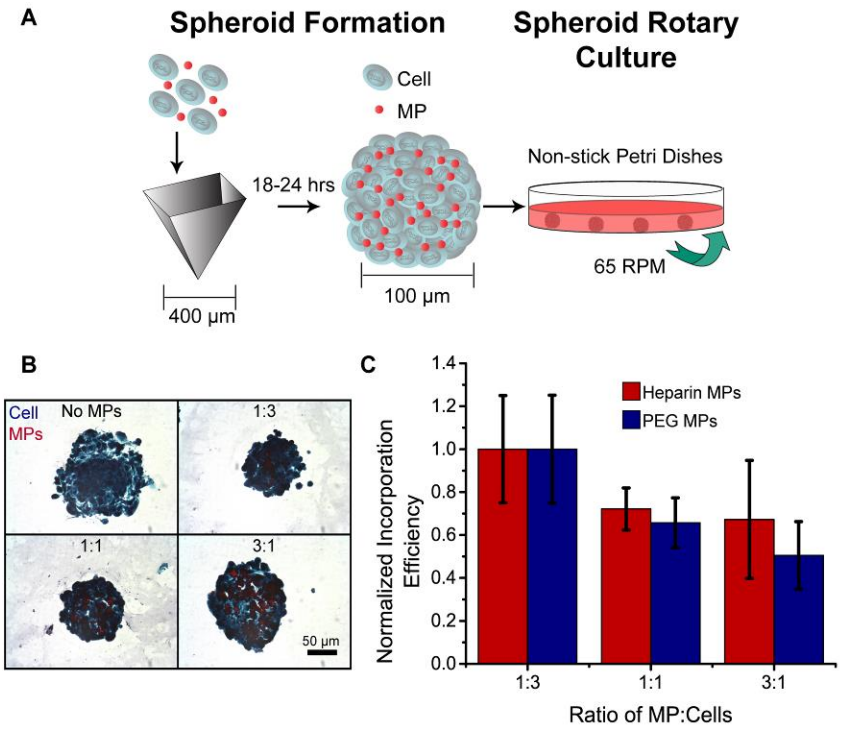

Figure 4.2. Heparin and PEG MPs can be incorporated into ATDC5 cell spheroids at similar efficiencies. (A) Heparin or PEG MPs are incorporated in spheroids via forced aggregation. (B) Heparin and PEG MPs (heparin MPs shown here in red, stained with Safranin-O) can be incorporated at a 1:3, 1:1, and 3:1 MP:cell ratio. (C) Heparin and PEG MPs can be incorporated into 700 cell ATDC5 spheroids with similar incorporation efficiency (no significant differences between heparin and PEG at each ratio, $p<0.05$).

4.3.2 Morphology and Viability of MP-Containing ATDC5 Spheroids

700 cell ATDC5 spheroids with high and low doses (3:1 and 1:3 MP:cell ratios, respectively) of heparin and PEG MPs were formed (Figure 4.3A). Spheroids were cultured for 18 days and timepoints were taken on days 1, 6, 12, and 18 to assess overall morphology, cell viability, GAG and collagen II deposition, and gene expression (Figure 4.3A). All spheroids were observed to grow over time and developed a dense cell border (Figure 4.3B). Heparin MPs stained a light purple with H&E staining, while PEG MPs

were dehydrated and either appeared as small purple spheres or were lost during histological processing, leaving behind holes in the matrix. No differences in spheroid viability were observed in any of the groups at day 18 (Figure 4.4).

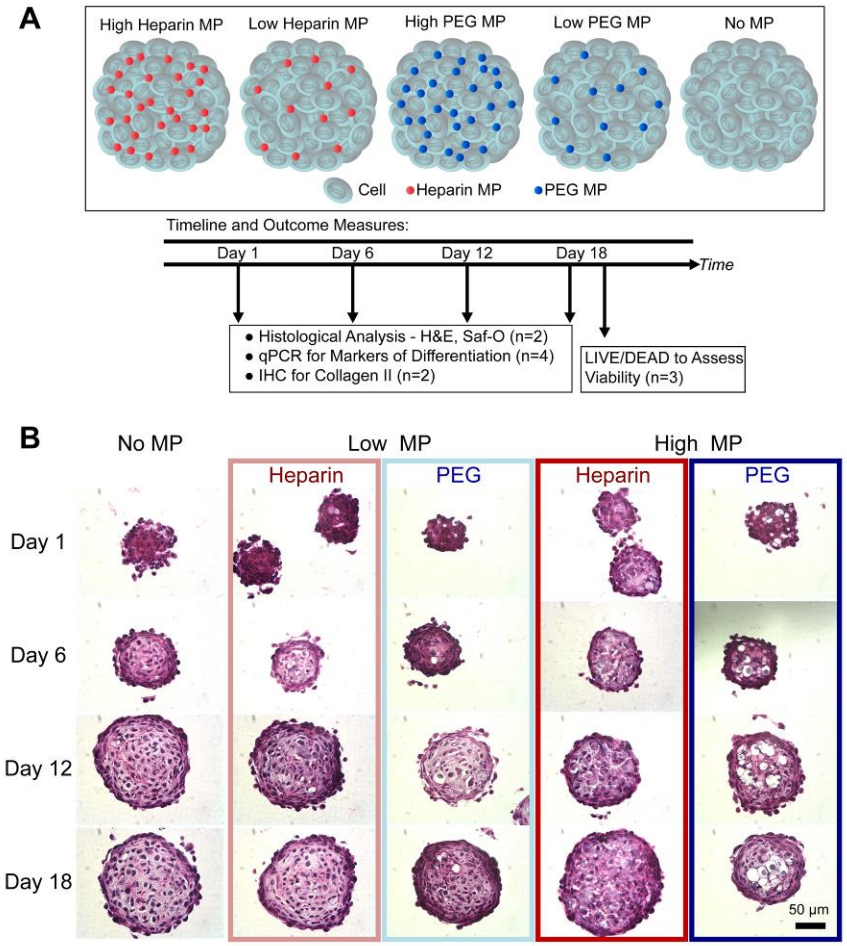

Figure 4.3. (A) Heparin and PEG MPs were incorporated at high and low ratios and cultured for 18 days on rotary culture. Gene expression and histological analyses were conducted at days 1, 6, 12, and 18, and viability analysis at day 18. (B) No MP control and heparin (reds) and PEG MP (blues) containing spheroids over the course of 18 days, stained with H&E. Groups are listed at the top of each set of images. PEG MPs appear as holes within the spheroid matrix due to histological processing.

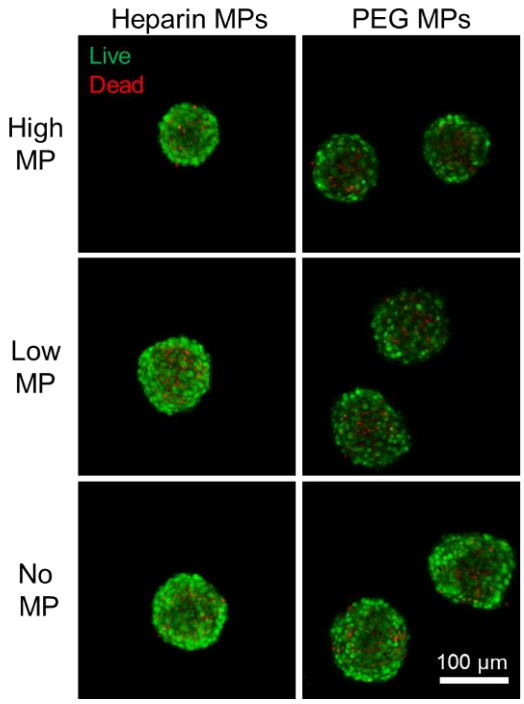

Figure 4.4. LIVE/DEAD staining for heparin MP and PEG MP groups at day 18. Confocal microscopy was used to image spheroids and stacks were z-projected after green (live) and red (dead) channels were merged.

4.3.3 Heparin MP-Mediated Modulation of ATDC5 Cell Spheroid Differentiation

Gene expression markers of chondrocytic differentiation were analyzed at days 1, 6, 12, and 18. Overall, it was observed that heparin MPs caused greater reductions in gene expression than PEG MPs (Figure 4.5). For *collagen II*, high heparin and PEG MP groups showed significantly lower gene expression than the cell control at day 6, but the magnitude was much greater for the heparin MP group (7.4±1.8- and 1.8±0.2-fold decreased for heparin and PEG, respectively). In addition, the low MP group was significantly decreased as compared to the cell control in the heparin group, while no differences were observed in the PEG group (Figure 4.5A). For *aggrecan*, the magnitude of gene expression decrease for heparin MPs as compared to PEG MPs was also much greater at day 6 (16.5±6.2- and 2.9±0.2-fold decrease for heparin and PEG, respectively). Furthermore, the decreased expression for *aggrecan* persisted through day 18 for the

heparin MP group, while only increases were observed in PEG MPs groups at later timepoints (Figure 4.5B). No differences in *collagen X* expression were observed for heparin MP groups, and PEG MP groups showed slight upregulation by days 12 and 18 (Figure 4.5C).

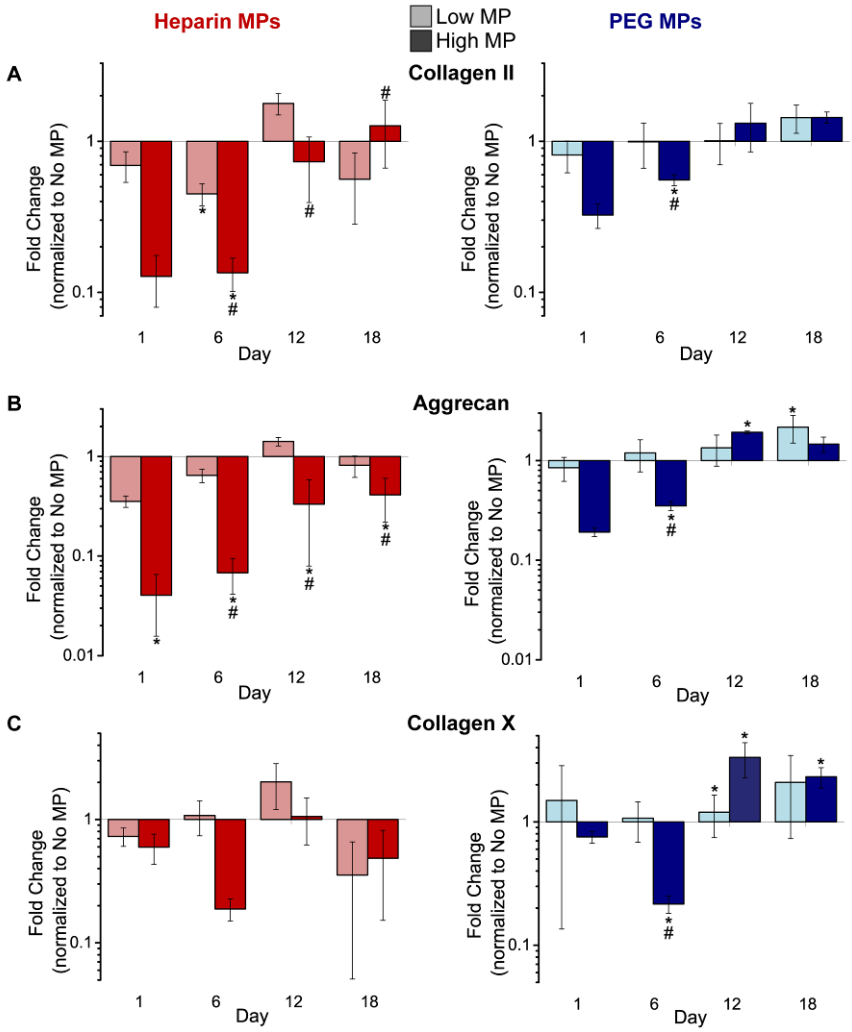

Figure 4.5. Chondrocytic gene expression for heparin and PEG MPs groups at high and low MP ratio for (A) *collagen II*, (B) *aggrecan*, and (C) *collagen X*. Fold change normalized to the no MP control is reported (*=significantly different than no MP on same TP; #=significantly different than low MP on same TP; $p<0.05$).

IHC for collagen II was assessed for heparin and PEG MP groups on days 12 and 18. At day 12, less staining for collagen II deposition was observed in the low and high

heparin MP groups as compared to the PEG MP groups (Figure 4.6A). By day 18, levels of staining appeared to be similar, though possibly still slightly lower in the high heparin MP group compared to all other groups (Figure 4.6B).

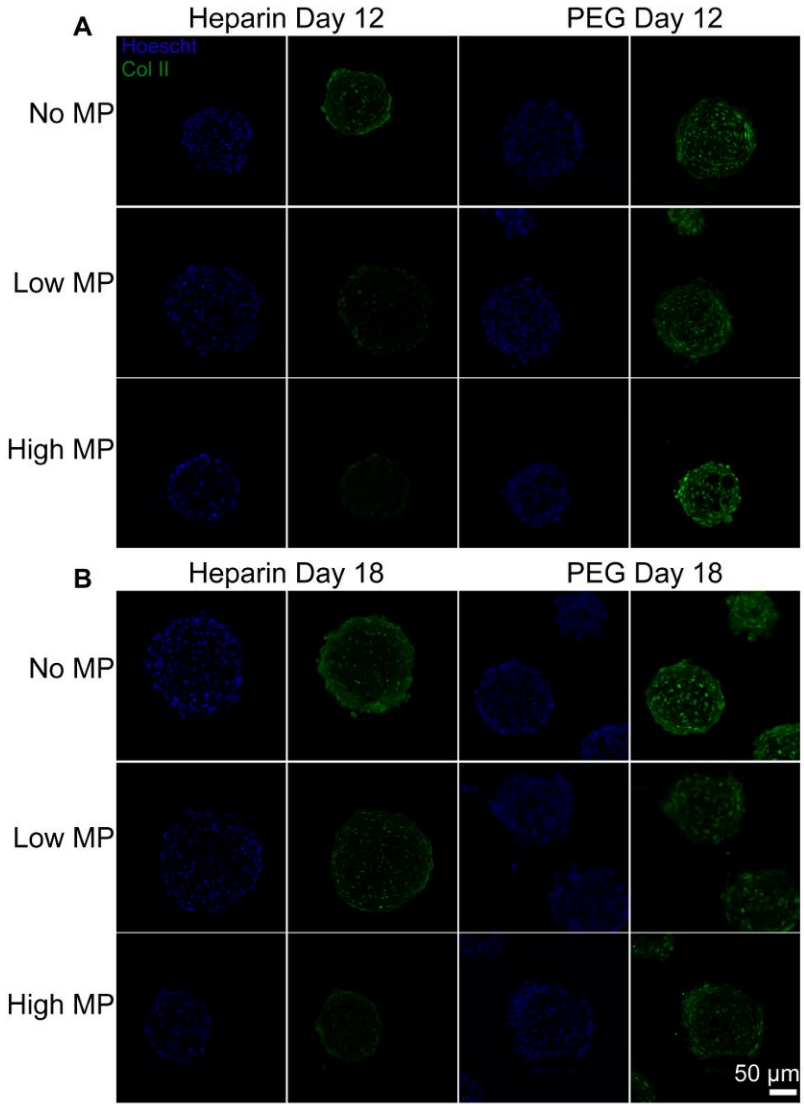

Figure 4.6. IHC for collagen II (green) at (A) day 12 and (B) day 18 for heparin and PEG groups with low and high MPs. Nuclei are shown in blue.

GAG deposition was assessed at days 1, 6, 12, and 18. Little staining for GAG deposition was observed at days 1 and 6 (data not shown), but substantial staining for GAG deposition was observed at days 12 and 18 in PEG and no MP groups (Figure 4.7).

In contrast, very little staining for GAG deposition was observed in heparin MP groups at both 12 and 18 days. High magnification images indicate staining for pericellular GAG deposition in all groups but the high heparin MP group (Figure 4.7, arrows in high mag images). As heparin MPs stain with safranin-O, they also appear stained red in the matrix (Figure 4.7, arrowheads in high mag images), but look distinctly different from the endogenous pericelluar GAG deposition.

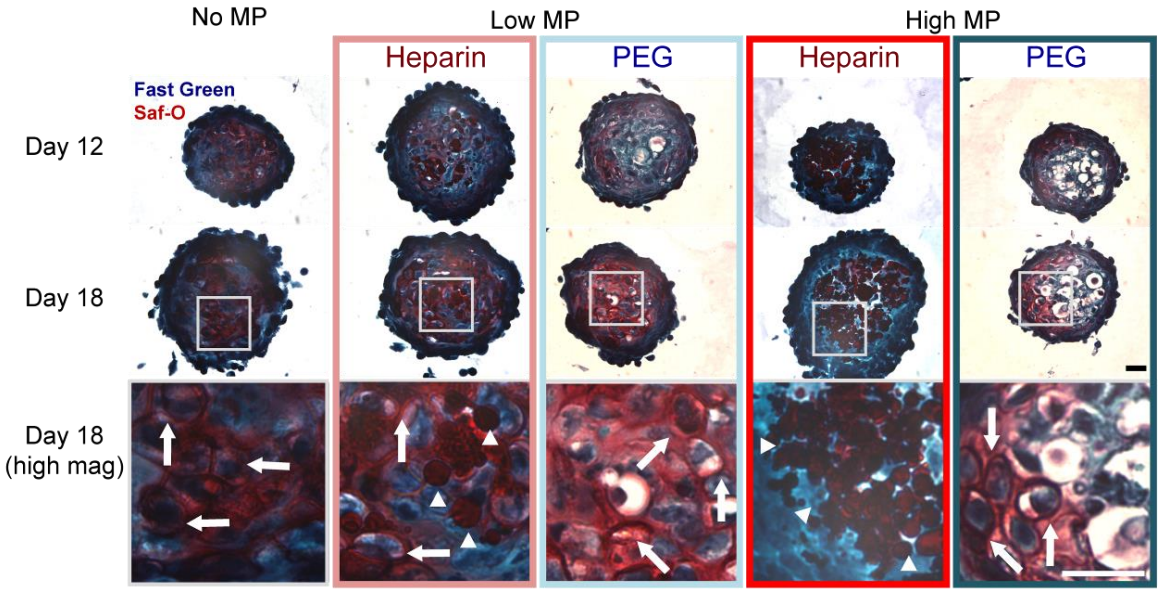

Figure 4.7. Safranin-O staining for GAG deposition (red) in heparin and PEG groups with low and high MPs. Heparin MPs appear dark red and PEG MPs appear clear or light purple. Inset boxes on day 18 are shown at high mag below original image. Staining for GAG deposited by cells appears pericellularly (arrows with tail) while GAG MPs appear round (arrows without tail) (scale bars = 50 μm).

4.3.4 Heparin MP-Mediated Modulation of ATDC5 Cells in Transwell Culture

ATDC5 cells were cultured in transwell with heparin and PEG MPs (low and high dose for heparin MPs, high dose only for PEG MPs), allowing for exchange of soluble factors but no physical contact between cells and MPs. Gene expression was measured at day 6 and 12 and GAG and mineral deposition was assessed at day 12 (Figure 4.8). At

day 6, significant down regulation was observed in the high heparin MP group for chondrocytic markers *collagen II* and *aggrecan* as compared to the low and no MP groups. In contrast, no differences were observed between PEG MP groups and the no MP control group at day 6. No differences in gene expression were observed between any groups at day 12 (Figure 4.8A). At day 12, cells were stained for GAG (alcian blue) and mineral deposition (alizarin red), and reduced staining was observed in the heparin MP groups compared to the PEG and no MP group. The stain was extracted and quantified, which confirmed that the heparin MP groups showed significantly less staining than the PEG MP and no MP control groups (Figure 4.8B and C).

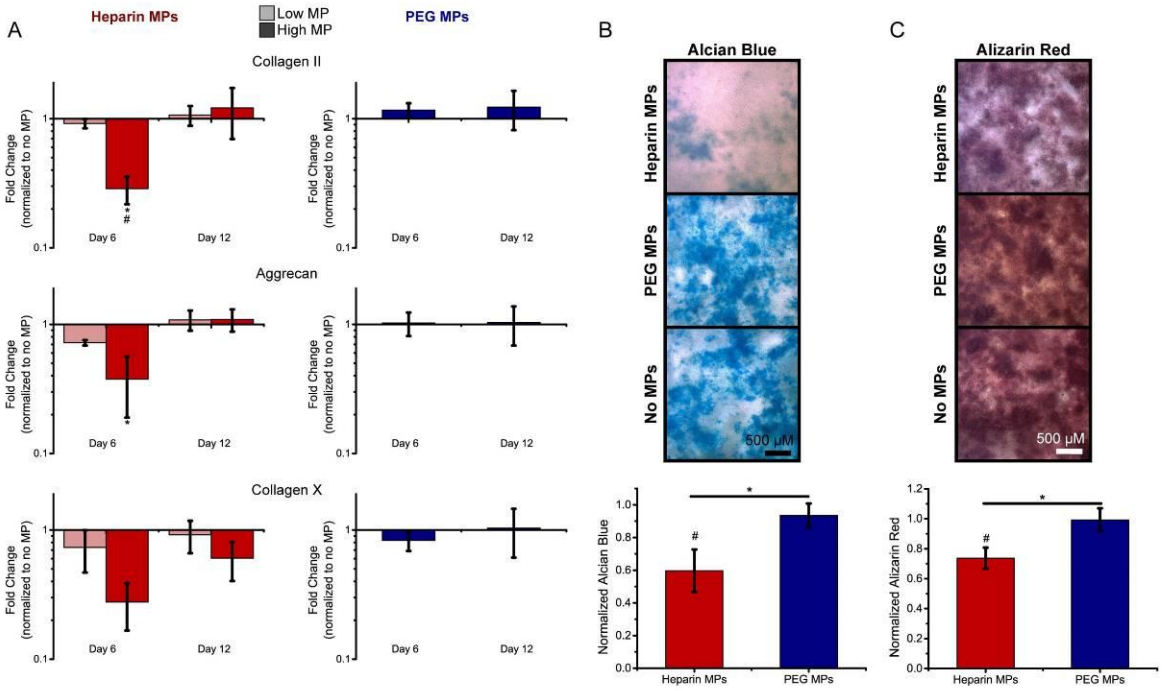

Figure 4.8 ATDC5 cells were cultured in transwell with heparin and PEG MPs. (A) Gene expression for chondrocytic markers *collagen II*, *aggrecan*, and *collagen X* at day 6 is reported as fold change normalized to the no MP group (*=significantly different than no MP group; $p<0.05$). (B) Representative images of GAG (alcian blue) and (C) mineral (alizarin red) deposition. Graphs show quantification of stain extraction (#=significantly different than cell only group; *=significantly different than indicated group, $p<0.05$).

Finally, DNA content was measured for both heparin and PEG MP groups to assess difference in cell number. Heparin MP groups showed significantly more DNA than the cell control group, while the PEG MP showed no significant differences (Figure 4.9).

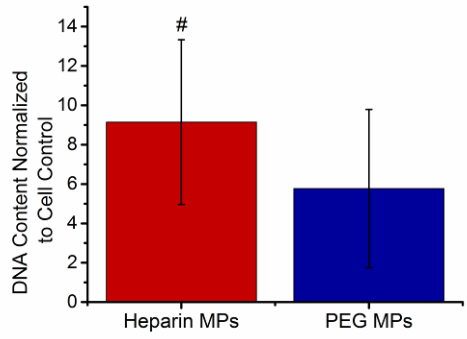

Figure 4.9 DNA content for heparin and PEG MP groups normalized to no cell control (#=significantly different than cell only group, $p<0.05$).

4.3.5 Protein Sequestration and Analysis

SDS-PAGE gels showed more proteins at greater intensity for heparin MPs as compared to PEG MPs incubated with ATDC5 cells for two and four days (Figure 4.10A). In addition, heparin MPs were able to sequester BMP-2 in conditioned media while PEG MPs did not sequester BMP-2 (Figure 4.10B). This held true for MPs/protein ratios at least as low as 500 pg BMP-2/0.01 mg MPs, or 0.05 µg BMP-2/mg MP. Finally, when run on SDS-PAGE, an additional band at approximately 16-17 kDa was observed for heparin MPs incubated with cells compared to those incubated in media only (Figure 4.10C).

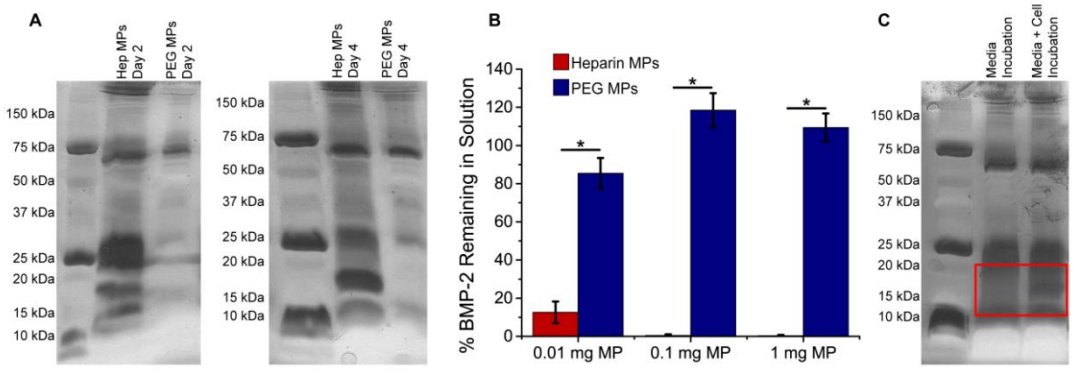

Figure 4.10. Analysis of heparin and PEG MP protein sequestration (A) SDS-PAGE for Heparin and PEG MPs in transwell with ATDC5 cells for 2 or 4 days. (B) Heparin and PEG MP sequestration of BMP-2 in ATDC5 conditioned media (*=significantly different than indicated group, $p \leq 0.05$). (C) SDS-PAGE for Heparin MPs incubated overnight in transwell with cells (right, "Media + Cell Incubation") or with media alone (left, "Media Incubation"). Red box indicates a band observed only in MPs incubated with cells, approximately 16-17 kDa.

4.4 Discussion

In these studies, heparin and PEG MPs were cultured with ATDC5 cells in spheroid and monolayer culture, and in both formats heparin MPs were able to delay or decrease differentiation, likely through soluble factor sequestration. Overall, the objective of this study was to modulate endochondral ossification through presentation of heparin materials, as heparin is known to bind an abundance of growth factors implicated in differentiation, including BMP-2, IHH, FGF-2, WNT, and TGF-β [25]. Thus, heparin MPs were incorporated into ATDC5 spheroids to evaluate their effect in a three-dimensional environment, which better mimics the cell-cell and cell-matrix interactions important for chondrocytic and osteogenic differentiation [36,314]. However, when integrated in spheroids, it is possible that these MPs would exert not only an effect on the concentration of growth factors in the matrix, but also on the number of cell-cell interactions that could form, which are often implicated in differentiation and cell

behavior [316]. To ensure that observed results were due to protein binding and not due to the physical presence of MPs in the matrix, PEG MPs were used as a low-binding material control [28,318–320]. Thus, heparin and PEG MPs of similar diameter were formed (Figure 4.1 B,C) and protein sequestration studies indicated that while heparin MPs loaded nearly 100% of BMP-2, PEG MPs loaded very little of this protein. Then, heparin and PEG MPs were incorporated into ATDC5 spheroids at several different ratios with varying efficiencies (Figure 4.2B, C). A final ratio of 3:1 MP:cell (2:1 MP:cell ratio if efficiency is accounted for) was selected as the high MP dose because previous results indicated that this ratio can present a large amount of material in the ECM without compromising spheroid formation [259]. A ten-fold lower ratio (1:3 MP:Cell) was chosen for the low MP ratio in these experiments to evaluate if the influence of heparin MPs was dose-dependent.

While there are many examples of successful incorporation of positively and negatively charged MPs into cell spheroids [232,233,259,263], we and others have been unable to incorporate unmodified PEG materials into dense cell aggregates [220]. Previously, the fibronectin cell-adhesive sequence RGD has been incorporated into PEG MPs to promote incorporation into spheroids [220], but MPs functionalized with the RGD peptide have been found to enhance chondrocytic differentiation when integrated into cell aggregates [220,254], which would be counterproductive in the PEG control group. It has been suggested that the negatively charged cell glycocalyx causes cells to be attracted to positive surfaces, and poly-l-lysine (PLL) has been used previously to promote cell binding on PEG-based surfaces [258]. Thus, in an effort to confer a slight positive charge on the MP surface and allow for incorporation into spheroids without

changing the low protein-binding properties of PEG, PLL was encapsulated into PEG MPs during MP fabrication. The addition of PLL allowed PEG MPs to be incorporated into the ATDC5 spheroids without affecting the low-binding capacity of PEG MPs (Figures 4.1C and 4.10A,B). More so, as PLL can be toxic at high levels [321], LIVE/DEAD staining indicated that the concentration of PLL used in the PEG MPs was not cytotoxic (Figure 4.4).

Heparin and PEG MPs were incorporated into ATDC5 spheroids for 18 days to assess the influence of heparin MPs on endochondral ossification, a time period found to be sufficient for ATDC5 cells to produce chondrocytic and osteogenic gene expression markers and matrix proteins when cultured in mineralization media [304,305,308–313]. General spheroid morphology was assessed over the course of culture, and spheroids were found to grow larger over time, consistent with the high proliferative capacity observed for ATDC5 cell *in vitro* culture in previous work [306,322], and to form a dense cell border on the spheroid surface (Figure 4.3B). Such dense cell borders have also been observed in spheroids composed of other cell types [220,233,259,323], and may be a result of cell reorganization due to nutrient availability or differentiation state. MPs remained in the matrix over the course of 18 days; however, due to sectioning and the solvents used in the staining process, PEG MPs often shrunk or fell out of the matrix during histological processing, leaving behind what appear as holes in the spheroid matrix (Figure 4.3B). Finally, no differences in LIVE/DEAD staining were observed among any of the culture conditions, indicating that viability was not negatively impacted by incorporation of MPs into ATDC5 cell aggregates (Figure 4.4). Thus, general

morphology and viability staining validated this platform for further evaluation of the influence of heparin MPs on endochondral ossification.

Cellular differentiation was delayed or reduced in groups with heparin MPs as compared to PEG MP and no MP control groups, as shown by gene expression and stains for matrix molecules. In the presence of a high dose of heparin MPs, gene expression for chondrocytic markers was downregulated as compared to no MP and PEG MP controls, indicating that heparin MPs delayed chondrocytic differentiation. As only subtle differences were observed for the low heparin MP group, the observed delay may have been dose-dependent. Interestingly, gene expression for the high heparin MP group was similar to that of the no MP control by later time points, suggesting that the effect of heparin MPs also might have been transient (Figure 4.5). Decreased staining for collagen II and GAG was observed in the high heparin MP group as compared to PEG MP and no MP control groups, confirming trends observed in gene expression data (Figures 4.6 and 4.7). Taken as a whole, these results indicate that heparin MPs transiently delay or reduce endochondral ossification in a dose-dependent manner.

To further confirm that changes in differentiation observed were due to the presence of heparin and not simply due to MPs in the aggregate matrix, heparin and PEG MPs were cultured in transwell culture with monolayer ATDC5 cells, allowing exchange of soluble factors between cells and MPs without physical contact. Similar to what was observed in spheroid culture, heparin MPs decreased/delayed chondrocytic differentiation in ATDC5 cell transwell culture, which also appeared to be dose-dependent and transient (Figure 4.8). DNA content analysis indicated that observed affects were not due to decreases in cell numbers in the heparin MP group, as DNA content was higher in this

group than cell controls (Figure 4.9). In addition, proteins bound by heparin and PEG MPs from days 2 and 4 in transwell culture were run on SDS-PAGE gels, and observed protein profiles showed that PEG MPs bound fewer proteins than heparin MPs days 2 and 4 (Figure 4.10A). Finally, gels also showed few differences between the protein profiles of the heparin MP groups at days 2 and 4 (Figure 4.10A). This may indicate that heparin MPs become saturated with protein quickly, and while exchange of protein may occur initially, eventually high affinity proteins may cover the MP, preventing further binding. The "saturation" of heparin MPs could possibly explain why a transient delay in differentiation is observed and why the response is dose-dependent. Overall, as heparin is known to be a potent binder of many growth factors involved in endochondral ossification [25,106], from these results it was hypothesized that sequestration of soluble factors was the mechanism behind heparin MP-mediated modulation in differentiation.

In ATDC5 cell culture, two types of proteins could potentially be sequestered by heparin MPs: 1) cell-secreted proteins and 2) proteins found in FBS, as ATDC5 cell culture is carried out in serum. ATDC5 cells produce a variety of heparin-binding growth factors that could affect differentiation, including IGF-2, TGFβ-2, WNT, BMP-2, IHH, FGF-9 and FGF-18 [25,308,309,324,325]. Furthermore, many heparin-binding proteins are also present in serum, including but not limited to fibronectin, fibrinogen, kininogen, plasminogen, vitronectin, haptglobin, and lipoproteins [326–332]. Serum can also contain heparin-binding growth factors, but generally at a very low concentrations compared to the high abundant proteins listed above [326,327]. Thus, to evaluate if heparin MPs could still bind small growth factors in the presence of cell-conditioned, serum-containing media, sequestration of BMP-2 that had been spiked into ATDC5 conditioned media was

assessed. Results indicate that heparin MPs can still bind BMP-2 in the presence of cell-conditioned media containing serum, while PEG MPs did not show any BMP-2 binding (Figure 4.10B). This suggests that heparin MPs have the potential to sequester cell-secreted protein in ATDC5 culture, and to further investigate this possibility, heparin MPs incubated in transwell with cells or in FBS-containing media alone were run on SDS-PAGE. Resulting protein profiles indicated that heparin MPs incubated with cells bound additional proteins in comparison to heparin MPs incubated in media alone (Figure 4.10C). These additional proteins had a MW of approximately 17 kDa, which suggests that these proteins could be one or more of several ATDC5 produced growth factors. Overall, these results indicate that heparin-mediated delays in differentiation were likely a result of the binding of both cell-secreted and serum proteins.

Future experiments could help elucidate the mechanisms behind observed changes in differentiation. To determine if saturation of heparin MPs is responsible for transient delays in differentiation, heparin MPs previously cultured with ATDC5 cells for 12 days could be incubated with a second population of ATDC5 cells. If MPs truly do become saturated, then no changes in differentiation would be observed in the second population. In addition, to determine if the response is dose-dependent on heparin and not the total amount of MPs, heparin MPs with varying amounts of heparin could be employed. Heparin MPs with different amounts of heparin have different protein binding capacities (see Chapter 6 and Figure 6.5B), allowing control of heparin dosage while maintaining equal MP number. Finally, to identify the protein(s) comprising the 17 kDa band observed for heparin MPs incubated with cells, mass spectrometry or western blots for proteins implicated in endochondral ossification, mentioned above, could be

performed. If particular proteins are able to be identified, these proteins could be dosed back into ATDC5 cell cultures containing heparin MPs. If normal differentiation was restored when the protein dose overwhelmed the binding capacity of heparin MPs, this would provide more evidence that this phenomenon is mediated by protein sequestration.

Employing heparin materials to delay differentiation has the potential to be beneficial for growth plate injury repair and several other applications. Currently, the gold standard for growth plate defect repair is to fill the defect with an inert substances, such as fat, muscle, bone wax, or silicone to prevent bony bridge formation [112]. These materials cannot stimulate regeneration of the damaged growth plate tissue, which has motivated the development of biomaterial-based strategies [112,113]. In general, therapeutic cell types such as MSCs or chondrocytes are seeded into hydrogel-based scaffolds and implanted into the defect. This technique has been met with varying levels of success, but directing regeneration of the tissue by native or delivered cells has not been achieved [111,113–118]. Thus, the use of heparin-based materials could be explored to modulate cellular differentiation through sequestration of cell-secreted proteins, possibly delaying or preventing undesirable ossification. Additionally, heparin-based materials could be useful in craniosynostosis, which involves premature fusion of cranial bones and can lead to craniofacial deformities and neurological complications if left untreated [207,208,333]. The current treatment involves surgery to separate and reshape fused cranial bones, but resynostosis, or refusing of the bones, is common due to high osteogenic potential in the tissue [207]. Biomaterial-based strategies to prevent resynostosis include delivery of antibodies against osteogenic proteins such as BMPs and TFGβs, but the short half-life of antibodies decreases the efficacy of these therapies

[209,210,334]. However, heparin materials, which unlike antibodies do not undergo rapid degradation *in vivo*, could be employed to sequester osteogenic proteins to prevent resynostosis. Finally, for *in vitro* differentiation of MSCs in chondrogenic applications, cells often undergo hypertrophic differentiation rather than maintaining a chondrocytic phenotype [37]. Current strategies to promote a chondrocytic phenotype revolve around achieving the proper milieu of growth factors, either by adding exogenous growth factors to the culture [37,129,130] or by relying on proteins secreted during MSC-chondrocyte co-culture [128,131–135]. It may be possible that application of heparin MPs would help prevent or delay hypertrophic differentiation through growth factor sequestration. Thus, the therapeutic potential of heparin-mediated delays in differentiation could be explored in variety of tissue engineering applications that require modulation of the differentiation timeline.

In these studies, heparin was selected due to its ability to bind many proteins involved in differentiation [25], enabling the material to make a significant impact on the cellular microenvironment. This could be beneficial over other systems that allow for specific sequestration of single proteins, as multiple growth factors are generally required for cellular differentiation and such systems tend to be expensive. In addition, as cell phenotype and consequential protein release profile evolve with time, a material with specific-sequestration abilities would only be relevant at certain stages during differentiation, while heparin could continue to bind an assortment of proteins throughout the entire course of differentiation. Still, sequestration of proteins in a non-discriminate manner is not always advantageous, as two heparin-binding growth factors might have opposing affects in a differentiation process, such as BMPs and FGFs in endochondral

ossification [23,106]. In such cases, single-protein affinity systems could be beneficial. Some of these systems, such as antibody-based sequestration platforms, have short half-lives [209,210]. Other systems have utilized peptide sequences that sequester specific proteins, such as VEGF, TNFα, and FGF [43,46,335], to increase the stability of the sequestering system. As analyses techniques for heparin-sequestered proteins improve, heparin MPs could be used as a "first pass" to understand how protein sequestration affects a system of interest, and analysis of sequestered protein could inform design of future, protein-specific sequestration systems to enhance control of differentiation. Thus, the ability of heparin to sequester a variety of growth factors involved in differentiation enables the employment of heparin MPs as tools to modulate cellular differentiation and investigate sequestered proteins.

4.5 Conclusion

In this work, heparin MPs delayed chondrocytic differentiation in the ATDC5 cell line in both spheroid and transwell culture as assessed by chondrocytic gene expression and matrix molecule deposition. In contrast, PEG MPs did not have a strong effect on differentiation, suggesting that protein sequestration was possibly responsible for the affects observed. SDS-PAGE supported this hypothesis, indicating that after culture with ATDC5 cells, more proteins were bound to heparin MPs than PEG MPs, and that heparin MPs may have been able to sequester cell-secreted proteins in the ~17 kDa size range. Overall, the studies presented here act as a proof-of-concept for GAG-based modulation of endogenous growth factors to control cell behavior. The ability harness the potential of endogenous growth factors within the cellular microenvironment is an emerging theme in the field of regenerative medicine, as it eliminates the need for exogenous protein, thus

reducing cost, requirements for FDA approval, and concerns about recombinant protein potency [3]. Thus, heparin materials have the potential to be used to sequester proteins toward the applications of modulating cell behavior, a valuable technique in tissue engineering and regenerative medicine.

Once we observed the ability of heparin MPs to modulate cellular differentiation, we set out to design heparin-based technologies that enabled enhanced temporal control over protein sequestration and subsequent re-presentation. In addition, we were interested in designing degradable heparin-based MPs to allow release and subsequent analysis of sequestered proteins. Thus, we developed core-shell heparin-PEG and degradable heparin-PEG-based MPs to achieve these goals.

CHAPTER 5

CORE-SHELL MICROPARTICLES FOR PROTEIN SEQUESTRATION AND CONTROLLED RELEASE OF A PROTEIN-LADEN CORE[5]

5.1 Introduction

Tissue regeneration is a complex process that involves intricate coordination of cellular events, many of which are modulated by proteins [3]. The concentration of these proteins, often growth factors or cytokines, must be spatially and temporally controlled to ensure proper tissue growth [175]. While biomaterial-based controlled delivery systems have traditionally been used to deliver single growth factors [10,42], tissue regeneration may require more complex temporal control over growth factor presentation and cell signaling [3]. Of particular interest, cell-secreted proteins have the potential to be captured and manipulated to enhance tissue regeneration and repair [3,336]. For example, a protein might be locally sequestered by a biomaterial and its effect thus amplified during tissue repair [40,43–45]; alternatively, an undesirable protein might be captured and eliminated from the cellular microenvironment [46]. Combining these two ideas, a protein undesirable at one point in time might be captured and temporarily eliminated from the microenvironment until it is released at a second point in time, when its expression is desirable for tissue regeneration [3]. Thus, development of dynamic

[5] Portion of this section were adapted T.E Rinker, B.D. Philbrick, and J.S. Temenoff, Core-Shell Microparticles for Protein Sequestration and Controlled Release of a Protein-Laden Core, in revision.

biomaterials that can sequester and temporarily isolate cell-secreted proteins prior to a triggered release may achieve the level of temporal control needed to more fully regulate tissue regeneration and repair.

Core-shell microparticle (MP) technologies are a particularly attractive technology for temporally modulating protein presentation in the cellular microenvironment [237,245]. Traditionally, core-shell MPs have either been used to prolong release and activity of cargo in an inner core by manipulating the degradation prolife of an outer shell [51,52] or to sequester and concentrate various biomarkers from bodily fluids, such as plasma or urine, for diagnostic tests [48–50]. To date, only a handful of core-shell MP systems have been used to deliver proteins [52,245–247]. In these studies, core-shell MPs were advantageous because either 1) burst release of the protein encapsulated in the core was significantly reduced due to the protective shell [52,245,247], or 2) the shell significantly prolonged protein bioactivity [246]. Similarly, only a few studies have shown the ability of core-shell MPs to sequester protein [48–50]. In contrast to core-shell MPs used for controlled release, core-shell MPs for biomarker sequestration are designed with an outer shell of small mesh size to exclude large proteins such as albumin, but to allow passage of smaller biomolecules, which remain trapped in the protein-binding core until retrieved for further analysis [48–50]. The two core-shell MP applications discussed above, protein delivery and biomarker sequestration, do not fully address the need for technologies able to sequester, isolate, and release cell-secreted proteins. However, taking inspiration from these technologies, it may be possible to create core-shell MPs not only to sequester proteins of interest, but also redeliver them at a user-defined time. Thus, in this work, we set out to develop a multifunctional heparin-

poly(ethylene-glycol) (PEG) core-shell MP that 1) preserves protein bioactivity, 2) delivers protein in a temporally controlled manner with minimal burst release and 3) sequesters and re-delivers protein on a user-defined timescale.

A non-degradable heparin MP was used as a protein-sequestering core due to its high affinity for growth factors and ability to preserve protein bioactivity. Heparin is a highly sulfated glycosaminoglycan, often used in tissue engineering scaffolds due to its ability to bind positively charged proteins [11,42,58,59,196,337]. Importantly, heparin can bind many growth factors involved in tissue formation, including bone morphogenetic protein-2 (BMP-2), Indian hedgehog (IHH), basic fibroblast growth factor (FGF-2), WNT, and transforming growth factor-β (TGF-β) [25]. Previous studies with these heparin MPs have shown high BMP-2 loading capacity and have suggested that BMP-2 is bioactive and can interact with cells while still bound to the MP [59]. Furthermore, heparin can protect proteins from denaturation, as it has been well documented that it protects FGF-2 from thermal and proteolytic degradation [338] and recently found that it can protect BMP-2 from degradation by heat and in aqueous solutions at physiological pH [58,339]. Thus, use of heparin MPs as a sequestering core could minimize burst release, present protein to cells only when the protein-loaded core is in contact with cells, and prevent protein denaturation.

PEG-diacryate (PEG-DA) was used for the degradable shell, as PEG can be chemically modified with a variety of functional groups and PEG hydrogels permit protein diffusion [27,28]. To achieve user-defined shell degradation, dithiothreitol (DTT) was integrated into the PEG-DA network, which enhances hydrolytic degradation of the polymer network [60]. Thus, use of a PEG-DA-based shell enables protein diffusion into

the heparin MP core, which then remains physically separated from cells until shell degradation.

In this work, we developed heparin-PEG core-shell MPs for potential applications in protein sequestration and subsequent re-delivery. A re-emulsification method was established to encapsulate pre-formed heparin MPs in a degradable PEG-based shell. Then, a proof-of-principle experiment was conducted to demonstrate that BMP-2-laden heparin MPs can be delivered in a temporally controlled manner to cells from core-shell MPs with a hydrolytically-degradable shell. Subsequently, it was shown that BMP-2 could be sequestered through the PEG-based shell onto the heparin core, and the BMP-2-laden heparin core could then be released to stimulate a cell response, thus demonstrating that the core-shell MPs provide enhanced temporal control over protein sequestration and release for potential applications in tissue regeneration and repair.

5.2. Materials and Methods

5.2.1 Polymer Synthesis

PEG-DA was synthesized according to previous methods [148]. Briefly, PEG (Sigma-Aldrich; Mn = 3.4 kDa) was reacted with acryoloyl chloride (Sigma-Aldrich) in 100% molar excess in methylene chloride (Fisher Scientific), with trimethylamine (Sigma-Aldrich) acting as a catalyst at a 1:1 molar ratio with PEG. The reaction was allowed to proceed under nitrogen purge overnight, at which point the aqueous and organic phases were separated and PEG was precipitated from the organic phase using diethyl ether (EDM Millipore) and dried. Heparin was functionalized with methacrylamide according to previous methods [40]. Briefly, the reaction was carried out in a phosphate buffer of pH 5 with 20 mg/mL heparin, 83 mM N-

hydroxysulfosuccinimide sodium salt (Sigma-Aldrich), 100 mM N-(3-aminopropyl) methacrylamide hydrochloride (Polysciences), and 78 mM (N-3-Dimethylaminopropyl)-N'-ethylcarbodiimide hydrochloride (EDC) (Sigma-Alrich) for 2 hours on ice. An additional round of EDC was added, resulting in a final molarity of 156 mM. After 4 more hours, solution was dialyzed for 2-3 days and lyophilized. All polymers were stored at -20°C prior to use. To fluorescently tag heparin, heparin methacrylamide was dissolved at 10 mg/mL in 0.1 M Na_2HPO_4, pH 6 and reacted with Alexa-Flour (AF) 633 Hydrazide (Invitrogen) at 5.7 μM concentration with 0.1 M EDC for 1 hour. The solution was dialyzed for 2 days and lyophilized. Proton NMR (^{1}H NMR) was used to determine the percent functionalization of heparin methacrylamide as previously described [59]. Briefly, Heparin was dissolved at 10 mg/mL in deuterated water and run on a Bruker Avance III 400 spectrometer. The percent of carboxyl groups substituted with methacrylamide groups was determined by comparing the integration regions of N-(3-aminopropyl) methacrylamide hydrochloride and unmodified heparin.

5.2.2 Microparticle Fabrication

For Heparin MP fabrication, Heparin methacrylamide MPs were formed according to previous methods [59]. Briefly, an aqueous phase of 10% heparin methacrylamide (wt%), 18 mM ammonium persulfate (Sigma-Alrich), and 18 mM N,N,N′,N′-Tetramethylethylenediamine (Sigma) were emulsified against corn oil with 1.67% (v/v) Tween-20 (polysorbate 20; BDH) at a 1:120 ratio aqueous:oil phase. MPs were cross-linked under nitrogen purge at 60°C for 30 minutes, then washed with acetone and water. Heparin MPs were filtered using a size extrusion device (Lipex Thermoline extruder, Northern Lipids) against a 12 μm nucleopore membrane to ensure MPs were all

less than12 μm in diameter. For AF633 tagged heparin MPs, the same procedure was followed but tagged heparin was included at 70 wt% total polymer content.

Core-shell MPs were formed by suspending pre-formed heparin MPs in a precursor aqueous phase containing 16 wt% PEG-DA, 0.05 wt% Irgacure 2959 Photoinitiator (Ciba), 2 mg/mL poly-L-lysine (PLL, Sigma-Aldrich), 45 mM DTT (degradable MPs only) and 0.33 mg/mL FITC-PEG-SH (1 kDa; NANOCS; for fluorescently tagged MPs only). For MPs with FITC-PEG or DTT, the aqueous phase was allowed to incubate for 1 hour at 37°C to allow for a click reaction to occur between the thiolated FITC molecule or DTT and the acrylate group on the PEG molecules. The aqueous phase was then emulsified with a homogenizer against a mineral oil phase (light, white; Ameresco) with 0.3-1.3% (v/v) Span-80 (sorbitan monooleate; TCI) at a 1:16.7 ratio aqueous:oil phase, nitrogen purged for 1 minute, then cross-linked under UV light (approximately 10.5 mW/cm^2) in a 35x10 mm petri dish for 10 minutes. Core-shell MPs were then washed with water and filtered using the size extrusion device against a 12 μm filter to remove any remaining free heparin MPs. PEG-based MPs were made in a similar fashion to the core-shell MPs, but without heparin MPs in the aqueous phase.

PEG-based MPs were made in a similar fashion to the core-shell MPs, but without heparin MPs in the aqueous phase. Dithiothreitol (DTT) was added to the aqueous phase at a 40 or 45 mM concentrations, corresponding to a PEG:DTT molar ratio of 1.42:1 or 1.21:1 , for the slow- and fast-degrading MPs, respectively. For sizing studies, 0.07, 1.3, and 2.0 wt% Span-80 was included in the oil phase.

5.2.3 Microparticle Characterization

To characterize core-shell MPs, fluorescent core-shell MPs were imaged via confocal microscopy. Heparin methacrylamide tagged with Alexa Flour (AF) 633 was used to fabricate the heparin MP core and FITC-PEG-SH was included in the aqueous PEG phase. Confocal microscopy (20x objective, LSM 700; Zeiss) was used to image stacks of MPs at 2 μm intervals. To immobilize MPs for imaging studies, core-shell MPs were suspended in a 10 wt% PEG-DA (8kDa) phase with 0.05% D2959 and cross-linked under UV light (approximately 10.5 mW/cm^2) in PTFE (Teflon) wells for 10 minutes to form MP-containing hydrogels discs of approximately 6 mm in diameter and 1 mm thick. This kept MPs from drifting while confocal stacks were being taken. Stacks were then z-projected and orthogonal views were used to confirm complete encapsulation of heparin MPs within the PEG-based shell.

To quantify number of heparin MPs/core-shell MP, ImageJ was used to z-project and split stacks into FITC (green, PEG-based shell) and AF633 (red, heparin core) channels. Then, each PEG-based shell was defined as a Regions of Interest (ROI) through thresholding and particle analysis of the FITC channel. Next, the number of heparin MPs in each ROI was counted using thresholding and particle analysis of the AF633 channel. Finally, number of heparin MPs per each core-shell MP was graphed against its cross-sectional area (CSA; μm^2). Linear correlations were obtained for masses of 0.1, 0.25, 0.5. 0.75, and 1 mg heparin MPs suspended in precursor PEG phase and each mass was tested in three separate MP batches (n=3 batches, 50-100 MPs analyzed/batch).

In all subsequent studies, a mass of 1 mg heparin MPs was used. For each batch of core-shell MPs used for protein pull-down studies and cell studies, core-shell MPs

were sized and a histogram of core-shell CSA was constructed with binning at every 40 μm^2. The average slope of the lines of the linear correlations obtained for a mass of 1 mg was then used to determine an average number of heparin MPs/core-shell MP based on average number of core-shell MPs per each bin. With this information, the correct number of core-shell MPs could be used to match the mass of heparin in the core-shell MPs to the mass of the heparin MP controls.

For core-shell and PEG-based MP degradation studies, MPs were counted with a hemocytometer and 1 million MPs/mL of PBS were incubated at 37°C on a shaker plate at 65 RPM (Barnstead Lab-Line, Multipurpose Rotor). 30 µL aliquots of MP solution was taken every 2-3 days and imaged using phase microscopy. Core-shell MPs were determined to be degraded when few (less than10 MPs) or no core-shell MPs were visible. Slow- and fast-degrading PEG-based MPs were treated in a similar fashion.

For PEG-based MP sizing studies, PEG-based MPs with 0.07, 1.3, and 2.0 wt% Span-80 were fabricated. MPs were sized by using ImageJ to manually measure MP diameter from phase microscopy images (n=3 MP batches for each Span-80 concentration; 150 MPs analyzed for each batch).

5.2.4 Protein Loading and Release

Degradable core-shell MPs and PEG-based MPs (45 mM DTT) were prepared. The mass of heparin MPs was 0.02 mg for both the degradable core-shell MPs and the heparin MPs. The number of degradable PEG-based MPs was matched to the number of degradable core-shell MPs. 90 ng of recombinant human BMP-2 or stromal cell-derived factor-α (SDF-1α) (R&D Systems) was loaded onto the MPs in a 0.1% bovine serum albumin (BSA) PBS solution in low-binding tubes, resulting in 4.5 µg protein/mg heparin

MP. MPs were incubated at 4°C on rotary for 2 or 24 hours, at which point they were centrifuged and the supernatant was analyzed using an enzyme-linked immunosorbent assay (ELISA; R&D Systems).

Two techniques were used for loading core-shell MPs. In the first technique, heparin MPs were loaded with protein prior to encapsulation into the PEG shell ("pre-fabrication load"; Figure 5.5A). In the second technique, core-shell MPs were formed and then loaded with protein ("post-fabrication load"; Figure 5.7A). Because small proteins are able to diffuse through PEG-DA networks [27], it was hypothesized that encapsulated heparin MPs would still be able to sequester protein, which was confirmed in pull-down studies. For "pre-fabrication load" studies, 1 mg heparin MPs were loaded at a concentration of 1.5 µg BMP-2/mg MP in a 0.1% BSA solution in low-binding tubes at 4°C on rotary overnight. MPs were centrifuged and supernatant was removed and analyzed using an ELISA (R&D Systems) to calculate total BMP-2 loaded. Then, loaded heparin MPs were used to form degradable and non-degradable core-shell MPs. Degradable core-shell MP, core-shell MP, and heparin MP groups all contained 0.02 mg heparin MPs and were incubated in a 0.1% BSA solution in PBS at 37°C for seven days on a shaker plate. At days 1, 4, and 7, MPs were centrifuged and supernatant was removed for analysis and replaced with fresh 0.1% BSA solution. Supernatant was analyzed using an ELISA (R&D Systems).

For "post-fabrication load" studies, degradable core-shell and PEG-based MPs were fabricated. Degradable core-shell MP contained 0.02 mg heparin MPs. The number of PEG-based MP and core-shell MPs were matched. All MPs were loaded at a concentration of 4.5 µg BMP-2/mg MP in a 0.1% BSA PBS solution in low-binding

tubes at 4°C on rotary overnight. MPs were centrifuged and supernatant was removed and analyzed using an ELISA (R&D Systems) to calculate total BMP-2 loaded. Supernatant was replaced with a fresh 0.1% BSA solution in PBS and MPs were incubated at 37°C for seven days on a shaker plate. At days 1, 4, and 7, MPs were centrifuged and supernatant was removed for analysis and replaced with a fresh 0.1% BSA solution. Supernatant was analyzed using an ELISA (R&D Systems).

5.2.5 ALP Activity Assays

The C2C12 cell line was used to evaluate the ability of core-shell MPs to delivery bioactive BMP-2 after shell degradation, as C2C12 cells produce ALP in response to BMP-2 [340]. C2C12 cells were cultured at 37°C, 5% CO_2 in DMEM with 4.5 g/L glucose, fetal bovine serum (FBS) (10% for growth media, 1% for assay media; Hyclone), 2 mM L-glutamine, 50 IU Penicillin and 50 μg/mL Streptomycin. For assays, cells were plated at 62,500 cells/cm^2 in 96 well plates and were incubated for 6 hours to allow adherence before the assay was started.

Microparticles were prepared for pre- or post-fabrication load experiments as described above and were sterilized by washing with 70% ethanol for 30 minutes, followed by 3 washes with PBS for 30 minutes each. For pre-fabrication studies, groups included pre-fabrication loaded and non-loaded degradable core-shell MPs, pre-fabrication loaded and non-loaded core-shell MPs, and a soluble BMP-2 and a no BMP-2 media control (Figure 5.5A). For post-fabrication studies, groups included post-fabrication loaded and non-loaded degradable core-shell microparticles, loaded and non-loaded degradable PEG-based MPs, and a soluble BMP-2 and no BMP-2 control (Figure 5.7A). All MPs were incubated for 2.5 days prior to being added to cells for pre-

degradation. This allowed MP shell degradation to occur during the three day cell assay (while degradation occurs throughout the entire time course, the majority of the PEG-based MP degradation occurred between days 3-6 for these MPs; Figure 5.1C). All core-shell and heparin MP groups had 0.02 mg of heparin and the degradable PEG-based control group had the same number of MPs as the core-shell group. Cells were cultured for 3 days and then media/MPs were removed.

After media and MP removal, cells were washed twice with PBS. DdH_2O was added to cells for 20 minutes and then cells subjected to a freeze-thaw cycle. Cells were then scraped from the 96-well plate and cell lysate solution was transferred to 1.7 mL tube. Cell lysate was sonicated for 20 minutes, then subjected to another freeze-thaw cycle. This was repeated once, then samples were centrifuged at 10,000 RCF for 5 minutes and supernatant was used for analysis. For ALP activity, 50 µL sample was combined with 50 µL 1.5M 2-amino-2-methyl-1-propanol (Sigma-Aldrich), 50 µL 10 mM magnesium chloride, and 50 µL 20 mM p-nitrophenol phosphate disodium salt hexahydrate (Sigma-Aldrich). For standards, *p*-nitrophenol (Sigma-Aldrich) was used. Samples were allowed to incubate for 2 hours and absorbance was read at 405 nm. DNA content was assessed with the CyQUANT Assay following the manufacturer's instructions and using bacteriophage λ DNA to create a standard curve (ThermoFisher Scientific). The assay was read at excitation/emission of 480/520.

5.2.6 Statistical Analysis

All results are depicted as mean ± standard deviation. Analysis of Variance (ANOVA) was used to identify significant factors and interactions, then Tukey's post hoc test (significance level $p \leq 0.05$) was used to generate pairwise comparisons between

means of individual sample groups and determine statistically significant differences (Minitab 15 Statistical Software).

5.3 Results

5.3.1 PEG Shell Fabrication and Characterization

At 0.7% Span-80, non- (no DTT), slow- (40 mM DTT), and fast- (45 mM DTT) degrading MPs had average diameters of 18.3±15.8, 70.0±49.0, and 44.6±36.1 µm, respectively, a range of about 52 µm. At 1.3 wt% Span-80, non-, slow-, and fast-degrading MPs had average diameters of 11.1±7.3, 31.5±28.1, and 15.3±12.7 µm, a range of 20 µm. At 2.0 wt% Span-80, non-, slow-, and fast-degrading MPs had average diameters of 9.2±4.8, 13.4±11.0, and 23.2±22.3 µm, a range of 14 µm (Figure 5.1A).

For degradation studies, DTT was incorporated into the network via Michael-Type addition to accelerate hydrolytic degradation (Figure 5.1B). Slow-degrading MPs were observed to degrade in about 23 days, while fast-degrading MPs degraded in about 8 days (Figure 5.1C). MPs were determined to have degraded if few (less than 10) or no MPs were visible via phase microscopy.

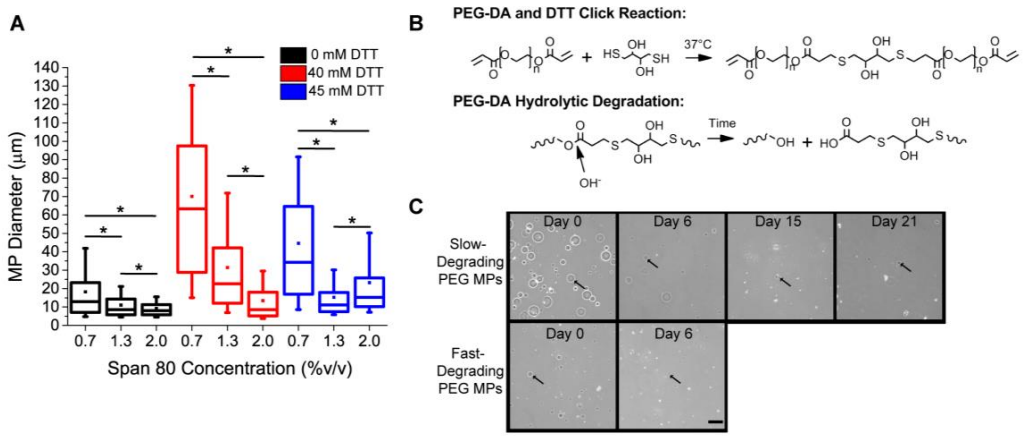

Figure 5.1. PEG-based MPs with tunable size and degradation profiles. (A) PEG-based MPs of 0mM, 40mM, and 45mM DTT concentrations were fabricated with varying Span-

80 surfactant concentrations (*=significantly different than other groups with same DTT concentration; $p<0.05$, n=3 batches of MPs). (B) Cross-linking schematic for PEG-DA and DTT. DTT clicks into the PEG-DA via Michael-Type addition at the acrylate bonds, and accelerates hydrolysis of the ester bond and thus degradation of the network. (C) Degradation time course for slow- and fast-degrading MPs (40 and 45 mM DTT, respectively). Slow-degrading MPs degraded by day 23 and fast-degrading MPs degraded by day 8. Arrows indicate MPs (n=3 batches of MPs, scale bar = 100 μm).

5.3.2 Core-Shell MP Fabrication and Characterization

Core-shell MPs were fabricated by suspending heparin MPs (15-27% methacrylamide functionalization) of known mass in a precursor aqueous PEG-DA phase that was emulsified against mineral oil and then cross-linked via free radical initiated polymerization (Figure 5.2A). The size of core-shell MPs could be controlled by varying the concentration of Span-80 in the oil phase (Figure 5.1A). Heparin MPs appeared encapsulated inside PEG-based shell in phase microscopy images (Figure 5.2B) and encapsulation was confirmed using orthogonal views of three-dimensional image stacks from confocal microscopy (Figure 5.2C).

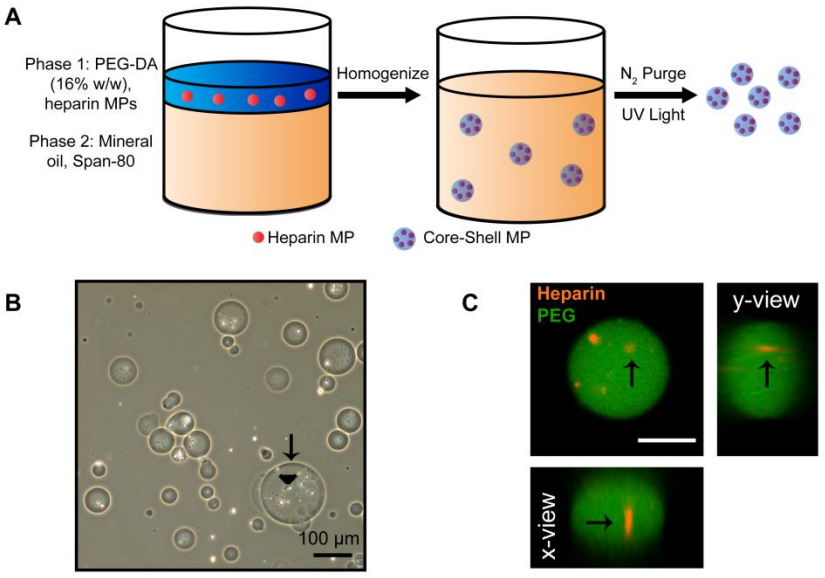

Figure 5.2. (A) Core-shell MPs were formed via a water-in-oil emulsion. (B) Phase images of core-shell MPs. Arrows and arrowheads indicate the PEG-based shell and

heparin core, respectively. (C) Orthogonal view from 3D confocal image stacks confirmed encapsulation of heparin core (red, arrow) into PEG-based shell (green) (scale bar = 25 μm).

As multiple heparin MPs are encapsulated in each PEG-based shell in this fabrication process, the number of heparin MPs per core-shell MP was determined in order to achieve known heparin dosages for subsequent cell studies. Using ImageJ, the number of heparin MPs per core-shell MP was determined and a linear correlation was found between the number of heparin MPs and the CSA of each core-shell MP (Figure 5.3A). As the CSA of the core-shell MP increased, the number of heparin MPs increased (Figure 5.3A and B). The ratio of the number of heparin MPs:core-shell CSA also increased as the mass of heparin MPs in the pre-cursor was increased, evidenced by the increasing slope in graphs of heparin MPs vs. core-shell CSA (Figure 5.3A). A second linear correlation was found between mass of heparin MPs in precursor PEG phase and the ratio of heparin MPs:core-shell CSA (Figure 5.3C). Thus, for similarly sized core-shell MPs, the number of heparin MPs increases as the mass of heparin MPs in the pre-cursor PEG phase increases (Figure 5.3C and D).

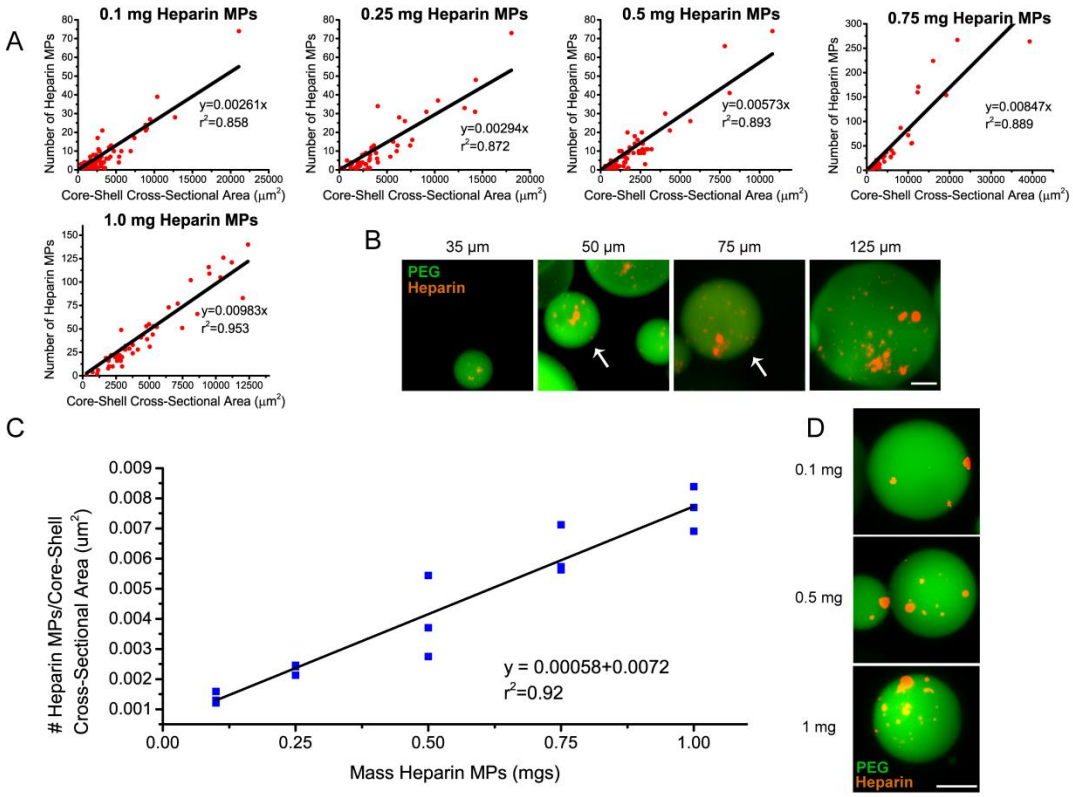

Figure 5.3. The heparin content in core-shell MP is correlated to MP size and mass of heparin MPs in the precursor PEG solution. (A) Number of heparin MPs correlated linearly with core-shell MP cross-sectional area for five masses of heparin tested. Note axes are different in 0.75 and 1 mg groups due to increases in MP size (n=3 batches of MPs for each mass). (B) Representative images of MPs fabricated with 1 mg of heparin ranging from 35-125 μm in diameter, noted above each image and pointed out by white arrows if more than one MP/image (PEG in green, heparin in red ; scale bar = 25 μm). (C) The ratio of heparin MPs/core-shell size increases as the mass of heparin MPs in precursor PEG phase is increased (n=3 batches of MPs for each mass). (D) Representative images of 0.1, 0.5, and 1 mg heparin MP encapsulated in PEG shell (scale bar = 25 μm).

5.3.3 Core-Shell MP Degradation

Hydrolytic degradation of PEG-DA MPs can be accelerated by adding DTT into the network, which enhances the susceptibility to hydrolysis of the ester bond [60]. By varying the concentration of DTT, degradation rate of PEG-based MPs could be temporally modulated, allowing a range of degradation time between 8 and 23 days (Figure 5.1C). For core-shell MPs, DTT was incorporated into the PEG-DA network at a

45 mM concentration (corresponding to a molar ratio of 1.21:1 PEG-DA:DTT) and the shell of the core-shell MPs were observed to degrade in approximately six days using phase microscopy. In addition, the non-degradable heparin MP core was released and present after shell degradation (Figure 5.4).

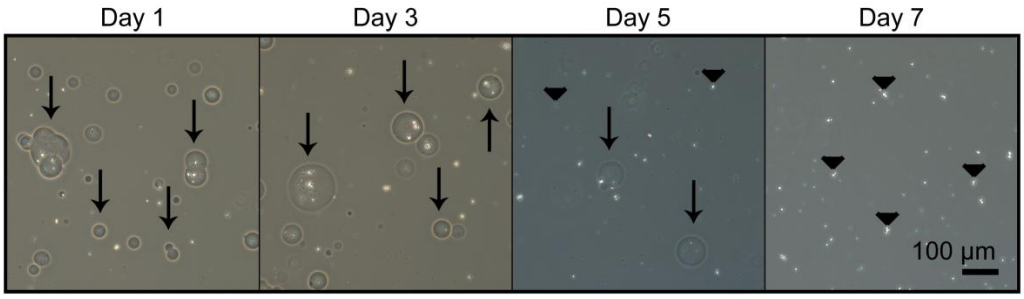

Figure 5.4. Degradation of PEG-based shell and release of heparin MP core from core-shell MPs. Core-shell MPs are present through day 5 (days 1-5, arrows), at which point they begin to degrade and release heparin MPs (days 5 and 7, arrowheads). Core-shell MPs are fully degraded by day 7.

5.3.4 Pre-Fabrication Load Bioactivity Studies

For pre-fabrication load studies, heparin MPs loaded 98.0±0.1 % of BMP-2. Degradable and non-degradable core-shell MPs were fabricated with loaded heparin MPs and release of BMP-2 was monitored over seven days. As BMP-2 binds tightly to heparin MPs, very little BMP-2 was released over the course of seven days (5.8±3.2%, 7.9±4.3%, and 2.5+1.7% for degradable core-shell, core-shell, and heparin MPs, respectively; Figure 5.5B). Degradable core-shell microparticles induced similar C2C12 ALP activity as the soluble control, while core-shell microparticles induced significantly lower activity after three days (85.4+19% vs. 9.0+4.8% of soluble control, respectively; Figure 5.5C). No signal was observed for groups without BMP-2, and an elevated DNA content was observed in all groups subjected to BMP-2 as compared to those without BMP-2. No trends in DNA content were observed between groups.

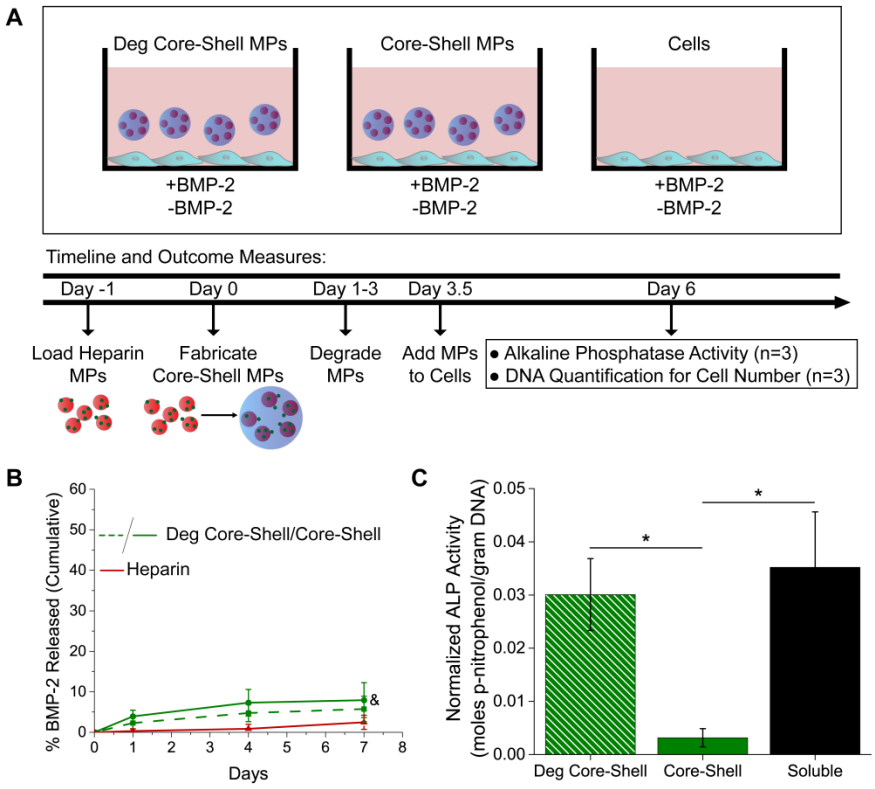

Figure 5.5. Degradable (Deg) core-shell MPs modulate loaded heparin MP delivery to cells. (A) Experimental set-up for pre-fabrication loaded core-shell MPs. (B) Cumulative percent released of loaded BMP-2 for deg core-shell, core-shell, and heparin MP groups (&=significantly different from heparin MP group, $p<0.05$, $n\geq3$). (C) Normalized ALP activity for deg core-shell, core-shell, and soluble BMP-2 groups (non-loaded groups showed no signal; *=significantly different from core-shell MP group, $p<0.05$, $n=4$).

5.3.5 Post-Fabrication Load Protein Sequestration Studies

When degradable core-shell MPs were loaded with BMP-2 and SDF-1α, sequestration of proteins was temporally delayed. At two hours, significantly more SDF-1α remained in solution after incubation with core-shell MPs than with heparin MPs (26.8±7.1% and 2.3±1.8%, respectively). However, by twenty-four hours similar amounts of protein were found for each group (6.0±0.7% and 1.2±0.4%, respectively; Figure 5.6A). BMP-2 behaved similarly, with significant differences in sequestration observed at 2 hours (47.8±2.4% and 15.2±4.6% remaining for core-shell and heparin

MPs, respectively) but similar levels of sequestration by twenty-four hours (10.7±1.4% and 9.0±1.2% remaining for core-shell MPs and heparin MPs, respectively; Figure 5.6B). In both cases, no protein sequestration was observed in the PEG-based shell group. All results are normalized to the soluble control group. These studies indicate that it is possible to sequester protein through the PEG-based shell of core-shell MPs, but that sequestration is temporally delayed. Thus, for all post-fabrication loading cell studies, a 24 hour loading time was used.

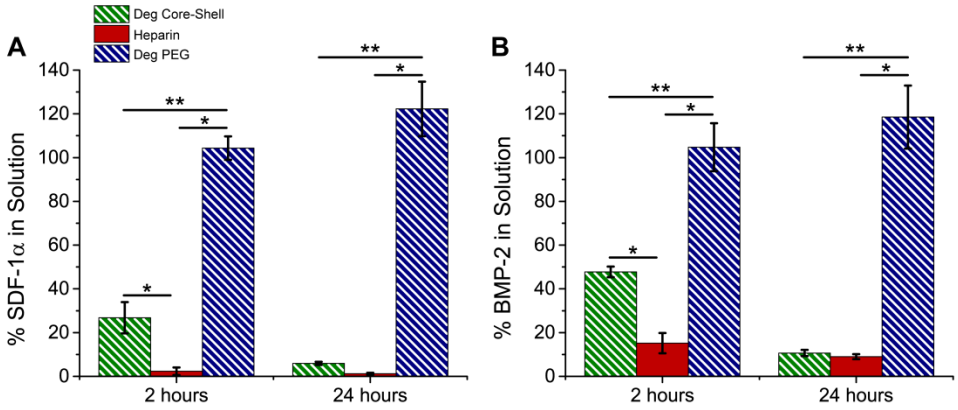

Figure 5.6. Core-shell MPs temporally modulate protein sequestration. Protein pull-down studies with growth factors (A) SDF-1α and (B) BMP-2. Graphs show percent of protein remaining in solution (i.e. percentage of protein not sequestered by MPs) normalized to soluble protein controls. (*=significantly different from heparin MP group, **=significantly different from degradable core-shell; $p<0.05$, $n\geq3$).

5.3.6 Post-Fabrication Load Bioactivity Studies

Loading studies indicated that degradable core-shell MPs loaded 93.5±1.0% of BMP-2 while degradable PEG MPs loaded only 11.5±14.6% as compared to the soluble control (Figure 5.7B). Core-shell MPs released only 2.7+1.6% of loaded BMP-2 over seven days (Figure 5.7C). Degradable core-shell MPs induced ~7-fold higher C2C12 ALP activity than the soluble control, while no detectable signal was observed for the

loaded degradable PEG-based MP group (Figure 5.7D). No signal was observed for groups without BMP-2.

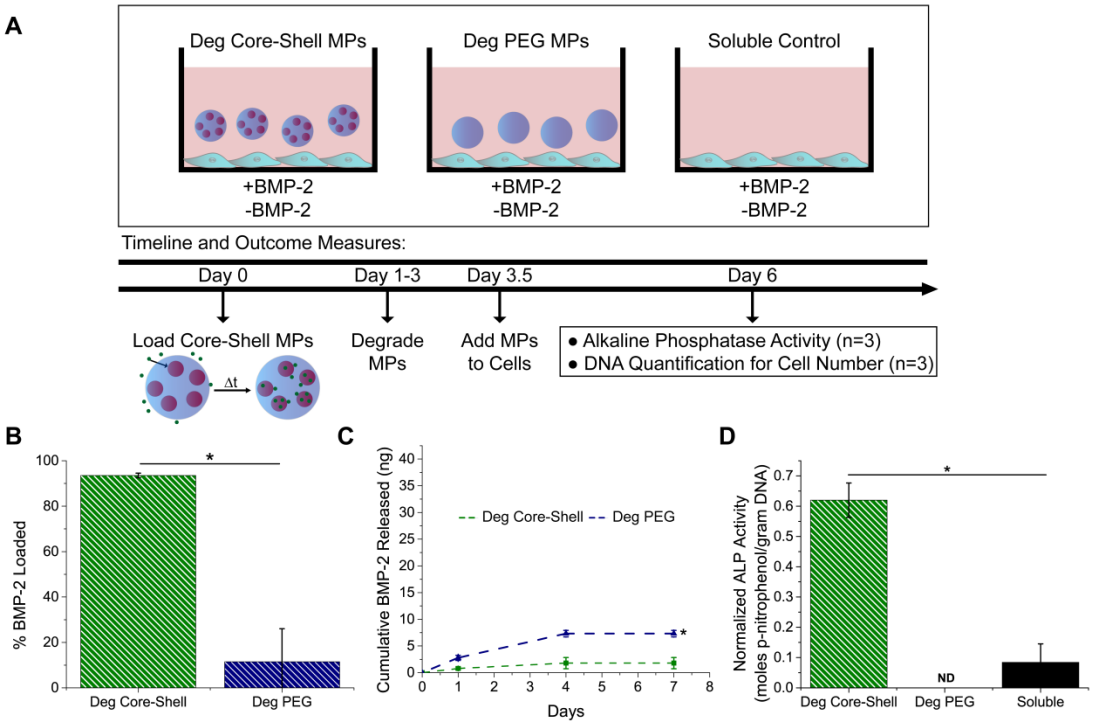

Figure 5.7. Post-fabrication loading allows for delivery of loaded heparin MPs. (A) Experimental set-up for post-fabrication loaded MPs. (B) Post-fabrication loading resulted in nearly 100% loading in deg core-shell MP group and less than 10% loading in deg PEG-based MP group. (C) Cumulative mass of BMP-2 released for deg core-shell and deg PEG-based MPs for seven days. (D) Normalized ALP activity for deg core-shell MP, deg PEG-based MP, and soluble groups. "ND" indicates not detectable (non-loaded groups showed no signal; *=significantly different from deg core-shell group; $p<0.05$, $n=4$).

5.4 Discussion

In these studies, core-shell MPs were designed to sequester, isolate and protect, and deliver protein on a user-defined timescale. First, a hydrolytically degradable PEG-based shell was required in order to release the protein-laden heparin core. Thus, DTT was incorporated into the PEG-DA aqueous phase via a click reaction, as DTT can

enhance the susceptibility of the resulting ester bond to hydrolytic degradation [60]. Slow- and fast-degrading MPs were formed by varying the concentration of DTT in the PEG-DA network. Because DTT links two PEG-DA chains via their acrylate groups, these acrylates are then no longer available for cross-linking in free radical initiated polymerization, which can result in longer chain lengths and thus larger mesh size (Figure 5.1B). This was likely the cause of larger MPs observed in previous work that utilized this technique, as it was shown that increasing the concentration of DTT resulted in increased MP size [221]. While those studies employed a water-in-water emulsion technique [221], a water-in-oil emulsion technique was used in these studies, as MP size could be modulated independently of DTT content by varying surfactant concentration (Figure 5.1A). First, for each type of MP (non-, slow-, and fast-degrading), increasing amounts of Span-80 resulted in a smaller MP diameter. Additionally, as Span-80 concentration was increased, the range in average MP diameter between the three types of MPs tightened. With the lowest amount of Span-80 (0.7% wt%), the diameter of non- and fast-degrading MPs was the most variable (a range of 52 μm) and showed similar trends to previous work [221], with increasing sizes observed with increasing DTT concentration. As Span-80 increased, however, MP size could be controlled with less dependence on DTT concentration, as diameter ranges dropped to 20 and 15 μm for higher concentrations of Span-80. These results indicated not only that Span-80 could be used to tune MP size within one DTT concentration, but also that concentration of Span-80 could be used to modulate MP size independently of DTT concentration (especially at higher wt%). Thus, non-, slow-, and fast-degrading PEG-based MPs of different sizes

could be formed by varying Span-80 concentrations, allowing size to be controlled independently of DTT concentration.

Degradation studies showed that slow- and fast-degrading MPs degraded at 8 and 23 days, respectively (Figure 5.1C). This indicates that by varying the DTT concentration in the MPs, the degradation rate could be varied, providing ample room for fine-tuning these concentrations to achieve MPs that degraded between 8-23 days or after 23 days. As DTT reacts with functional acrylate groups in the PEG-DA network, there is a limit to the amount of DTT, dependent upon the mass of PEG-DA, that can be incorporated into the PEG-DA network before MPs can no longer be formed (data not shown). In these studies, the fast-degrading PEG MPs contained the maximum amount of DTT that could be added to the network and still be crosslinked, indicating that the mass of PEG-DA would have to be adjusted in order to add more DTT and achieve faster degradation rates. However, within these limits, PEG-based MPs with tunable size and degradation profiles were developed, and the fast-degrading MPs with 2.0% Span-were used for the shell of core-shell MPs. Overall, a degradable PEG-based shell was designed to degrade over time in aqueous conditions, allowing shell degradation to occur after delivery to a biological system.

Previously, a variety of fabrication techniques have been employed to make core-shell MPs, including double-emulsion and layer-by-layer coating. While the double emulsion fabrication technique is a convenient, one-batch reaction, it requires two immiscible phases [238,239,242,341], restricting the chemical properties of the materials that can be used. Layer-by-layer coating can provide control over shell size, but requires layers to interact with each other through electrostatic interactions [246], again narrowing

material choice to those with positive or negative charges. Because the heparin-PEG core-shell MPs presented here required use of specific materials, each having a separate function, a fabrication technique that permitted greater flexibility in material choices was required. Thus, a re-emulsification technique was chosen [241] for core-shell MP fabrication to allow use of heparin and PEG-based materials. In this method, pre-formed heparin MPs were re-emulsified in a precursor PEG phase (Figure 5.2), a process mild enough to maintain protein bioactivity when protein was loaded onto heparin MPs pre-fabrication (loading of heparin MPs prior to re-emulsification; Figure 5.5C).

Core-shell MP characterization revealed that the number of heparin MPs was linearly correlated to the CSA of core-shell MPs, and that increasing the mass of heparin in the precursor PEG phase increased the number of heparin MPs encapsulated (Figure 5.3). Thus, although a heterogeneously-sized population of MPs was formed in each batch, the number of heparin MPs per core-shell MP was tunable and predictable. If more homogenously-sized MPs per batch are required for future experiments, this re-emulsion technique could be translated to a microfluidic device to increase core-shell MP size homogeneity [242], as a PEG-based MPs have previously been fabricated on microfluidic devices with a variety of cross-linking techniques [342–344].

Recently, it has been shown that hydrolytic degradation can be enhanced in PEG-DA hydrogels by integrating DTT into the polymeric network [60]. In this work, slow- and fast-degrading MPs were developed by varying the amount of DTT added to the aqueous PEG phase (Figure 5.1C). Previously, DTT has been incorporated into PEG-DA MPs using a water-in-water emulsion technique, but it was shown that increasing the concentration of DTT resulted in increased MP size, likely due to increased chain length

and consequently, a larger mesh size [221]. To overcome this limitation, a water-in-oil emulsion technique was used, as MP size could be modulated independently of DTT content by varying surfactant concentration (Figure 5.1A). Thus, tunable degradation and controllable size of the PEG-based MP shells was achieved, which was then applied to core-shell MPs to enable shell degradation in approximately six days (Figure 5.4).

In these experiments, core-shell MPs were loaded using two different techniques. In the first, a "pre-fabrication loading" technique (Figure 5.5A), heparin MPs were loaded with BMP-2 prior to encapsulation into the PEG-based shell. Using the pre-fabrication loading technique may be advantageous because the core-shell fabrication technique does not require use of solvents and heparin can protect proteins from denaturation [58,338,339], thus promoting maintenance of bioactivity of loaded proteins. Furthermore, pre-fabrication loading could allow for loading of proteins in both the heparin core and PEG-based shell in future experiments for dual-release applications. When core-shell MPs were pre-fabrication loaded with BMP-2, degradable and non-degradable core-shell MPs released very little protein over the course of seven days (5.8$\pm$3.2%, 7.9$\pm$4.3%, and 2.5+1.7% for degradable core-shell, core-shell, and heparin MPs, respectively; Figure 5.5B). These results are comparable to what has been seen in previous studies when heparin MPs loaded with 1000 ng BMP-2/mg heparin MPs showed less than 10% release of BMP-2 after 30 days [59].

Because so little protein is released from the core-shell MPs, only degradation of the PEG-based shell and release of the protein-laden heparin core would be able to initiate a response from C2C12 cells. This necessitates the ability of protein to interact with cell receptors while still bound to heparin. Here and in past studies [59], it was

evident that BMP-2 could interact with cells while bound to the heparin MPs (Figure 5.5C and 5.7D), possibly with greater efficiency, as ALP activity was higher in groups with BMP-2 loaded on core-shell MPs than soluble BMP-2 (Figure 5.7D). In addition, evidence from *in vivo* and *in vitro* studies indicates that many other proteins, such as IHH, FGF, and WNT can also interact with their cell surface receptor while bound to heparin or heparan sulfate, potentially with enhanced affinity [175,182], indicating that this core-shell technology is versatile and can be used for delivery of a variety of heparin-binding proteins.

Pre-fabrication loaded degradable core-shell MPs were able to initiate a cell response that was similar to the response initiated by the soluble control, unlike the non-degradable control group, which demonstrated limited cellular response (Figure 5.5C). This is distinctly different than many other delivery systems, which generally have an unavoidable burst release prior to more sustained delivery of protein [52,234,237]. Here, protein release from a loaded vehicle was prevented for over three days in the non-degradable group, strongly supporting the idea that in this system, the majority of protein presentation can only occur after shell degradation and release of the protein laden core. Additionally, when core-shell MPs were allowed only a two day pre-degradation period (rather than the three days allotted for the experiment above) prior to placement on cells, the response initiated by the degradable core-shell MPs was lower than the soluble control, indicating that the degradation state of the shell does temporally control cell response (Figure E.9).

By tuning the degradation rate of the PEG-based shell, it would be possible to further adjust the delay period between MP delivery and protein presentation, beneficial

for applications that require delivery of different proteins at different points in time. Specifically, optimization of cellular differentiation processes such as chondrogenesis for cartilage regeneration [37] or myogenesis for muscle regeneration [345] may benefit from such a technology that promotes complex temporal coordination of protein presentation. In addition, tissue repair processes such as wound healing and vascularization could benefit from release vehicles with tight temporal control over protein release [3].

For the second loading technique employed with these core-shell MPs, "post-fabrication loading," core-shell MPs were formed and then loaded with BMP-2 by diffusion through the outer shell (Figure 5.7A). First, protein sequestration studies were conducted to determine if protein diffusion through the PEG-based shell could occur, using two different model proteins, SDF-1α and BMP-2, chosen because they possess molecular weights (~7-16 kDa) that represent small to average size for many growth factors, including but not limited to BMP-2, IHH, FGF-2, and TGFβ-1 (molecular weights ranging from 12-20 kDa, R&D Systems website [346]). Interestingly, a slight temporal delay in sequestration of both proteins was observed in the core-shell MP groups as compared to the heparin MP control, indicating that the PEG-based shell delayed diffusion of these proteins. These findings are similar to previous studies that have shown that protein diffusion is slowed but not inhibited by a PEG-DA hydrogel network [27,347,348]. For example, one study found that myglobin (17 kDa, similar in size to the proteins used in this study) was able to diffuse through both 2 and 10 kDa PEG networks, but at a slower rate in the 2 kDa network [27]. (NB: Because PEG may protect protein from denaturation in aqueous solution [238], protein levels were observed to be

greater than 100% of soluble control (Figure 5.6)). Thus, for the rest of post-fabrication load studies, core-shell MPs were incubated with protein for 24 hours to ensure complete protein loading.

After loading with BMP-2, very little release was observed in post-fabrication loaded core-shell MPs over the course of 7 days (2.7+1.6% of loaded BMP-2), similar to what was seen in pre-fabrication loading release studies. In a proof-of-principle study, when incubated with C2C12 cells, post-fabrication loaded degradable core-shell MPs induced ~7-fold higher C2C12 ALP activity than the soluble control (Figure 5.7D), indicating that these MPs can effectively sequester and then re-present growth factors to cells. The degradable PEG-based MP control, in which no signal was detected, was used to ensure that cell response was not due to free BMP-2 caught in the PEG network during loading. Several studies have shown the potential for heparin-based materials to sequester endogenous proteins [40,44,45,349,350], but none of these have included a temporal control over re-presentation. Previously, core-shell MPs have been used to selectively sequester proteins through a size-exclusive shell to concentrate biomarkers [47–50], but few, if any, technologies can sequester, physically isolate, and then re-release protein to the external environment. As the core-shell MPs presented in this work has the potential to achieve this, it is possible that this technology can enhance temporal control over protein presentation in the cellular microenvironment for future tissue engineering applications.

The core-shell MPs in this work were designed to degrade in approximately 6 days, which is an appropriate timeframe for several different applications involving the ATDC5 cells used in Chapter 4. In both monolayer and spheroid culture, ATDC5 cells

began strongly expressing differentiation markers at days 4-12 [309] (Figures E.7 and 8). In order to sequester and re-deliver cell-secreted protein to ATDC5 cells, two different scenarios were envisioned. In the first, core-shell MPs would be incubated with ATDC5 cells for approximately three days (shell would be intact) to sequester cell-secreted proteins. The three day period would be chosen to achieve maximum binding of desired proteins, and days 6-9 would be used for initial tests as many proteins are likely released during this time to encourage cell differentiation based on increased gene expression levels. Then, intact and saturated core-shell MPs would be removed and placed on a second population of cells, either ATDC5 cells or another cell type, to enhance differentiation as the shell degraded between days 3-6 and released protein-laden heparin MPs. In the second scenario, core-shell MPs would be used to sequester protein from ATDC5 cells at early timepoints (for example, days 3-6) to effectively halt or restrict differentiation until shell degradation (days 6-9), at which point protein-laden heparin MPs would be re-delivered to accelerate or reinitiate differentiation. Thus, the ~6 day degradation timeframe was chosen specifically for ATDC5 cell differentiation, but could be modified for other applications (Figure 5.1).

In this system, degradable core-shell MPs enabled triggered or temporally off-set release of protein-laden heparin MPs through hydrolytic degradation. While a hydrolytically degradable system is advantageous because it permits a user-defined degradation rate and release of cargo that is initiated simply by the presence of water (and not an external stimuli), it is limited by its inability to respond to conditions in the cellular microenvironment or a user-defined stimuli. Other systems can overcome these limitations. For example, hydrogels can be engineered to degrade or deform via enzymes,

light exposure, change in pH, ultrasound exposure, temperature changes, or magnetic fields [351–354]. Materials that degrade due to enzymes, pH changes, or temperature changes can be useful due to their responsiveness to the cellular microenvironment. For example, as the concentration of a specific enzyme controls the release profile of encapsulated cargo in an enzymatically degradable hydrogel, release only occurs under particular conditions [353]. While beneficial for specific applications, these types of systems would not have widespread applicability. Ultrasound, light-mediated, and magnetic-mediated release are beneficial because they allow user-defined controlled release that can be varied in time and modified throughout the course of delivery. Ultrasound degradation usually functions by temporarily breaking reversible bonds; light-mediated degradation by directing UV, visible, or IR light in specific spatial locations on a hydrogel to break photolabile bonds; and magnetic-mediated release by applying a magnetic force to cause a deformation leading to increased water movement through the gel [351–354]. Negative aspects of these techniques are the requirements for light or magnetic field penetration (not always possible for *in vivo* applications), the need for specialized equipment, and the dependence of the system on an outside user. Still, in the future many of these techniques could be applied to enhance control over shell degradation in the core-shell MPs presented in this work.

5.5 Conclusions

In these experiments, heparin-PEG core-shell MPs were fabricated using a re-emulsification technique to encapsulate pre-formed heparin MPs within a degradable PEG-based shell, thus creating MPs with tunable amounts of encapsulated heparin. In pre-fabrication load studies with BMP-2, degradable core-shell MPs initiated enhanced

ALP activity as compared to non-degradable core-shell MPs, indicating these MPs can be used to temporally modulate protein presentation to cells. In addition, post-fabrication loading studies demonstrated that core-shell MPs were able to sequester BMP-2 through the PEG shell and then re-present that protein to cells to initiate enhanced ALP activity. Thus, the goals of developing a dynamic core-shell MP technology that preserved protein bioactivity, delivered cargo in a temporally controlled manner with no burst release, and sequestered and re-delivered proteins were achieved in this system. In the future, because the post-fabrication loading technique allows fully fabricated core-shell MPs to sequester protein, it could be extended to sequestration and release of cell-secreted proteins. Overall, the multifunctional core-shell technology presented here has the potential to temporally modulate the presentation of growth factors in the local cellular microenvironment and is therefore a unique tool to explore the emerging area of cell-secreted protein manipulation for enhancement of tissue regeneration.

CHAPTER 6

DEGRADABLE HEPARIN-PEG-BASED MPS FOR PROTEIN SEQUESTRATION AND RELEASE

6.1 Introduction

Heparin has frequently been integrated into controlled delivery bulk hydrogel systems due to its ability to attract and protect protein [9,174,338,339]. Integration of heparin into microparticle (MP)-based delivery systems could be particularly beneficial, as MPs are injectable and have a high surface area to volume ratio that can assist in efficient protein release [211], and several techniques have been explored. A common method includes layer-by-layer coating of heparin onto pre-formed MPs [222–225]. While this method has been used to deliver proteins like TGFβs and BMPs to successfully enhance cell differentiation [222–225], the layer-by-layer approach requires alternating layers of positively and negatively charged materials, which can limit the choices of materials used to fabricate MPs and thereby limit user-defined control over other MP properties, such as size and degradability. In addition, as electrostatic interactions are the only forces responsible for maintaining heparin in the delivery vehicle, premature release of heparin into the cellular microenvironment could occur. To combat these problems, heparin has been functionalized with methacrylamide and covalently cross-linked into MPs [59]. While these non-degradable MPs showed high loading efficiency of BMP-2, very little release (~10-15% of loaded BMP-2) was observed over the course of 30 days [59]. Thus, development of heparin-based MPs with controlled and tunable protein release remains a challenge.

Protein release can be more precisely tuned in degradable MPs, as degradation rate can be user-controlled, eliminating reliance solely on diffusion as the main mechanism of protein release [10]. In addition, degradable materials are preferable for *in vivo* applications, as they do not require surgical removal [10]. Recently, our lab developed heparin-PEG-based MPs using 4-arm PEG acrylate, thiolated heparin, and DTT [58]. The MPs were cross-linked via Michael Type addition, and DTT was included to enhance MP degradability by accelerating hydrolytic degradation of the ester bond in the acrylate group [58,60]. This method enabled MP degradation and a higher percent release of loaded BMP-2 as compared to what was observed previously for non-degradable, covalently cross-linked heparin MPs [58,59]. However, as these MPs were only cross-linked via Michael-Type addition of DTT and heparin, both of which accelerated MP degradation, an increase of heparin content increased degradation rate of the MPs [58].

Thus, this work presents an alternative strategy to fabricate degradable heparin-PEG-based MPs with enhanced control over degradation rate and incorporation of higher concentrations of heparin. Degradable MPs were fabricated by integrating DTT into a PEG-DA and heparin MAm network that was subsequently cross-linked via free-radical initiated polymerization. MPs were characterized to assess heparin content and degradation rate, and loading and release studies were conducted with histone, a positively charged protein. Finally, MPs were cultured with ATDC5 cells to investigate 1) sequestration and release of cell-secreted protein and 2) degradation of MPs within dense cell aggregates. Overall, these studies indicate that degradable heparin-PEG MPs

have the potential to be used for protein loading and release in tissue engineering applications.

6.2 Materials and Methods

6.2.1 Materials

Heparin MAm and 3.4 kDa PEG-DA were fabricated as described in Section 4.2.1.

6.2.2 MP Fabrication and Degradation Studies

For heparin-PEG-based MPs, an aqueous phase of PEG-DA was incubated with DTT (Sigma-Aldrich) in PBS for 30 minutes at 37°C to allow a click reaction between DTT and the acrylate groups on PEG-DA. Then, heparin was added to the aqueous phase for an additional 30 minute incubation. For MPs without heparin, called PEG-based MPs, PEG-DA and DTT were incubated for 1 hour. The amounts of heparin and PEG added for each MP formulation resulted in a total polymer content of 12 wt% and are listed in Table 6.1. DTT concentrations for each formulation are also listed in Table 6.1. After incubations, Irgacure 2959 Photoinitiator (Ciba) was added to the aqueous phase to achieve a final concentration of 0.05 wt%. The aqueous phase was then emulsified with a homogenizer against a mineral oil phase (light, white; Ameresco) with 0.3-1.3% (v/v) Span-80 (sorbitan monooleate; TCI) at a 1:16.7 ratio aqueous:oil phase, nitrogen purged for 1 minute, then cross-linked under UV light (approximately 10.5 mW/cm^2) in a 35x10 mm petri dish for 10 minutes. MPs were washed with water. 100% heparin MPs were prepared as described in Section 4.2.2.

Table 6.1. Amounts of heparin, PEG and DTT for each MP formulation.

Name of MP Formulation	% Heparin	Mass PEG-DA (mg)	Mass Heparin MAm (mg)	Concentration DTT (mM)
PEG-based MPs	0	42.4	0	32.5
10% Heparin MPs	10	38.1	4.2	30
20% Heparin MPs	20	33.9	8.5	27
30% Heparin MPs	30	29.7	12.7	23.5
40% Heparin MPs	40	25.4	17.0	20

For PEG-based MPs used for ATDC5 aggregate incorporation, MPs were formed as described in Section 5.2.2. MPs had 0 (non-degrading), 40 (slow-degrading) or 45 (fast-degrading) mM DTT.

For MP degradation studies in aqueous solutions, 0.1 mg/mL of MPs was incubated in 1 mL PBS unless another concentration is noted. MPs were incubated on rotary (65 RPM; Barnstead Lab-Line, Multipurpose Rotor) at 37°C. 30 µL aliquots of MP solution was taken every 2-3 days and imaged using phase microscopy. MPs were determined to be degraded when few (less than10 MPs) or no MPs were visible.

6.2.3 Alcian Blue Staining and Surfen Assay

PEG-based MPs and 10, 20, 30, and 40% heparin MPs were stained with 1% alcian blue 8GX (Sigma-Aldrich) in 0.1 M HCl for 30 minutes. Then, MPs were centrifuged at 10,000 RCF and stain was removed. MPs were resuspended in PBS, centrifuged again, and PBS was removed. This was repeated until the supernatant was clear. MPs were then imaged on phase microscopy.

For surfen studies, 0.025 mg/mL PEG-based MPs and 10, 20, 30, 40 and 100% heparin MPs were incubated with 10 µM surfen in PBS. 100 uL of the MP-surfen

solution was added to a 96 well plate, and an area-scan fluorescence reading was taken at excitation/emission 320/460 after 3 hours.

6.2.4 Histone Loading and Release Studies

10% heparin MPs were used for maximum loading studies. 0.1 mg MPs were incubated with 6, 8, 10, 15, 30, 60, 150, and 200 µg histone (Sigma-Aldrich) overnight on rotary at 4°C. MPs were then centrifuged and supernatant was analyzed using a Pierce BCA protein assay according to the manufacturer's instructions (ThermoFisher Scientific). BSA protein was used to construct the standard curve and absorbance was read at 562 nm. For loading and release studies, 0.1 mg PEG-based MPs and 10, 20, 30, and 40% heparin MPs were loaded with 20 µg of histone overnight on rotary at 4°C. MPs were then centrifuged at 10,000 RCF and supernatant was analyzed to determine loading efficiency. Fresh PBS was added to the MPs and MPs were incubated on a shaker plate (65 RPM; Barnstead Lab-Line, Multipurpose Rotor) at 37°C for 7 days, with timepoints taken at days 1, 4, and 7. For each timepoint, MPs were centrifuged, supernatant was collected for analysis, and fresh PBS was added to the MPs. Supernatant was analyzed using a Pierce Coomassie protein assay according to the manufaturer's protocol (ThermoFisher Scientific). A standard curve was constructed with histone and absorbance was read at 595 nm.

6.2.5 Transwell MP Studies

ATDC5 cells were expanded and prepared for transwell culture as described in Section 4.2.3. Mineralization media was used for all studies (composition described in Section 4.2.3). At day 6 in transwell culture, transwells with 0.1, 1, and 3 mg 10%

heparin or PEG-based MPs were added to either well plates with cells or well plates with media only. After an overnight incubation in a cell culture incubator (37°C, 5% CO_2), MPs were removed from the transwell inserts, transferred to low-binding microcentrifuge tubes, centrifuged at 10,000 RCF, and supernatant was removed. MPs were rinsed once with PBS, then incubated at 37°C on a shaker plate (65 RPM; Barnstead Lab-Line, Multipurpose Rotor) for 2 days. MPs were then centrifuged at 10,000 RCF, and supernatant was analyzed using a Coomassie Protein assay (see Section 6.2.4).

6.2.6 Incorporation of PEG-based MPs into ATDC5 Spheroids

ATDC5 cells were prepared for spheroid culture and MPs were incorporated into spheroids as described in Section 4.2.3. Non-, slow-, and fast-degrading PEG-based MPs were incorporated into ATDC spheroids at a 3:1 MP:cell ratio and cultured on rotary culture in mineralization media for 21 days. At days 1, 7, 14, and 21, spheroids were collected for histological analysis. Spheroids were sectioned, stained with H&E, and imaged as described in Section 4.2.5.

6.3 Results

6.3.1 Heparin Content in Heparin-PEG-based MPs

PEG-based MPs and 10, 20, 30, and 40% heparin MPs were fabricated (Figure 6.1).

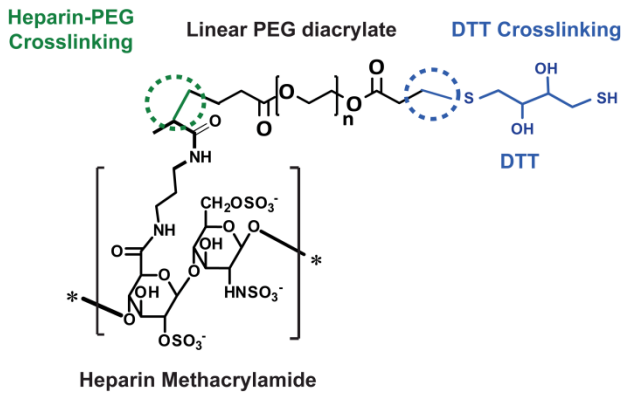

Figure 6.1. Cross-linking scheme for polymeric network in heparin-PEG-based MP fabrication. DTT is clicked into the PEG-DA network at the acrylate bond (blue circle), and heparin MAm and PEG-DA are cross-linked via free-radical initiated polymerization (green circle).

To validate that heparin had been cross-linked into the polymer network, MPs were stained with alcian blue, a stain specific for GAGs. All MPs fabricated with heparin stained blue, while PEG-based MPs did not (Figure 6.2A). Surfen, a small molecule that when bound to heparin emits a fluorescent signal [355] (see Appendix A), was incubated with PEG-based MPs and 10, 20, 30, 40, and 100% heparin MPs and fluorescence intensity increased as heparin content increased for 10, 20, and 30% heparin MPs, then plateaued for 40 and 100% heparin MPs. PEG MPs showed little fluorescent signal (Figure 6.2B).

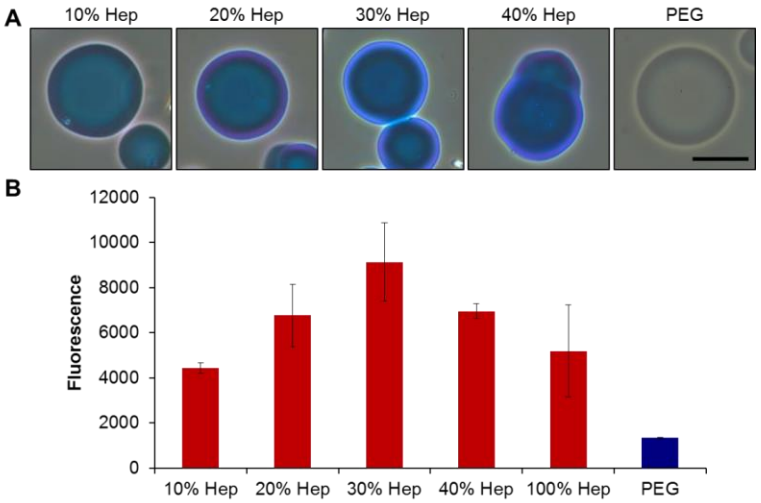

Figure 6.2. Heparin-PEG-based MPs can be fabricated with varying amounts of heparin. (A) 10, 20, 30, and 40% heparin MPs and PEG-based MPs (from left to right) were stained with Alcian Blue (scale bar = 50 µm). (B) Fluorescence intensity after incubation with surfen for MPs of varying amounts of heparin.

6.3.2 Degradation of Heparin-PEG-Based MPs

Heparin-PEG-based MPs were formed with the maximum amount of DTT that still permitted MP fabrication (Table 6.2). MPs degraded within 7-19 days,

Table 6.2. DTT concentration and degradation rate for varying heparin contents in heparin-PEG-based MPs.

% Heparin	Molar Ratio PEG:DTT	Degradation Time (days)
0	1.3	14-17
10	1.3	7-9
20	1.2	7-9
30	1.2	17-19
40	1.2	17-19

depending on the amount of heparin and DTT in the polymeric network (Table 6.1, Figure 6.3). 10% heparin MPs were incubated at 0.1, 1, and 3 mg/mL, and degradation

was dependent on initial MP concentration. MPs at 0.1 mg/mL degraded between 4-6 days, at 1 mg/mL between 11-14 days, and at 3 mg/mL between 14-17 days (Figure 6.4).

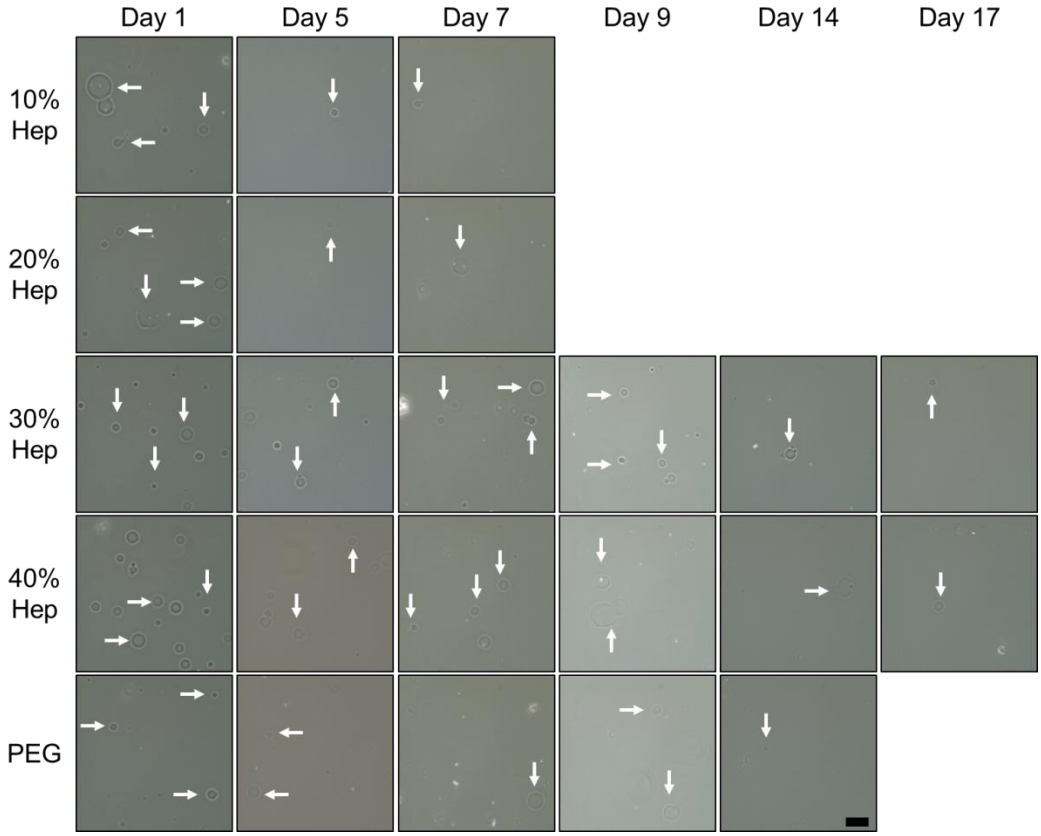

Figure 6.3. Degradation of PEG-based MPs and 10, 20, 30, and 40% heparin MPs. 10 and 20% heparin MPs degraded between days 7-9, 30-40% heparin MPs between days 17-19, and PEG-based MPs between days 14-17. White arrows point out MPs in each image. In images with many MPs, only a few are pointed out as examples (scale bar 100 µm).

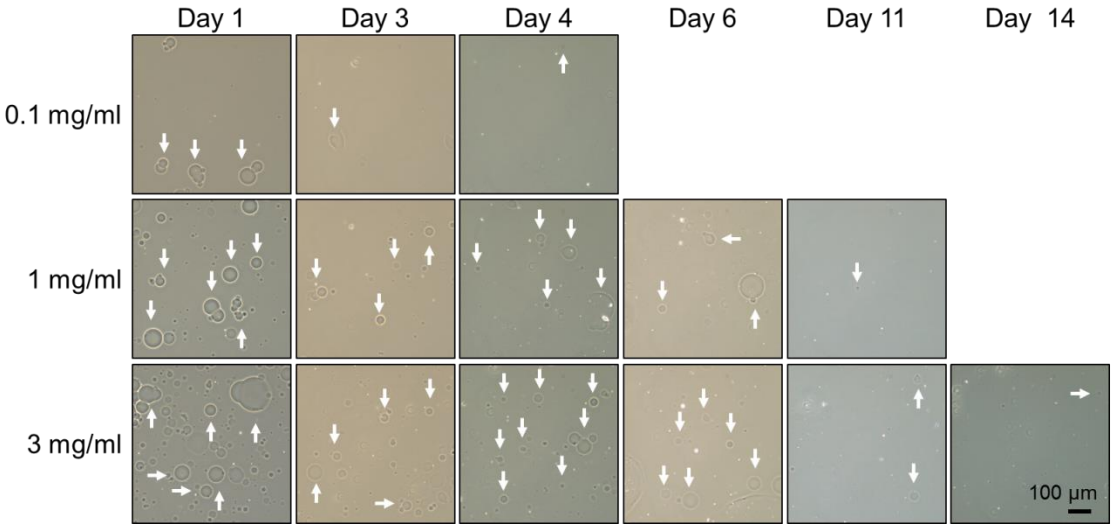

Figure 6.4. Degradation of 10% heparin MPs at 0.1, 1 or 3 mg MPs/mL initial concentration. MPs at 0.1 mg/mL degraded between 4-6 days, MPs at 1 mg/mL between 11-14 days, and MPs at 3 mg/mL between 14-17 days.

6.3.3 Loading and Release of Histone from Heparin-PEG-Based MPs

As 10% heparin MPs were loaded with increasing amounts of histone, a plateau was reached at 35 µg histone/0.1mg MP (Figure 6.5A). This corresponds to a max loading of 3500 µg histone/mg heparin. PEG-based MPs and 10, 20, 30, and 40% heparin MPs were loaded with histone at a 100 µg histone/0.1 mg MP ratio, or 10,000 µg histone/mg heparin. Less histone remained in solution, indicating that more histone was bound to MPs, as heparin content in the MP increased (Figure 6.5B).

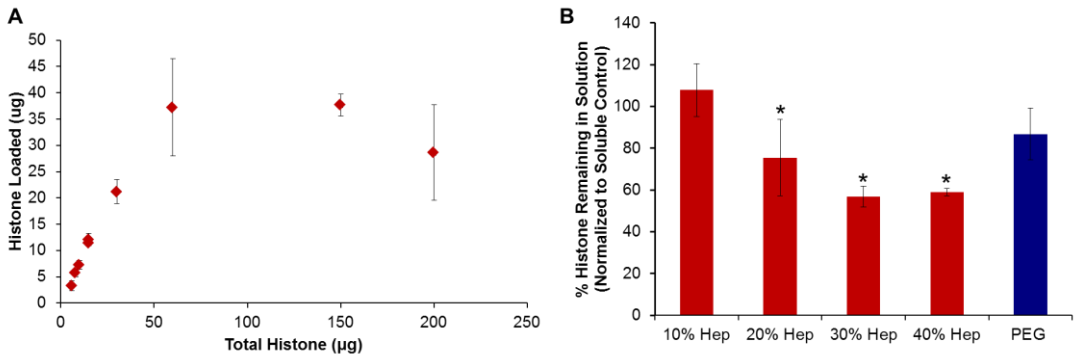

Figure 6.5. Heparin-PEG MP loading of histone. (A) 0.1 mg of 10% heparin MPs showed a max loading of 35 µg histone. (B) 10, 20, 30, and 40% heparin MPs show increasing

binding capacity as heparin content increases (*=significantly different than 10% heparin and PEG-based MP groups, $p<0.05$).

PEG-based MPs and 10, 20, 30, and 40% heparin MPs were loaded with 20 µg histone/0.1 mg MP and subsequent histone release was monitored for seven days. All MPs that contained heparin loaded about 80% of histone in solution, while PEG-based MPs only loaded about 10% (Figure 6.6A). All heparin containing MPs released protein over the course of seven days, and the majority of release occurred between days 1-3. By day 7, cumulative histone release was 33±1.2% for 10% heparin MPs, 26±3% for 20% heparin MPs, 8.1±3.4% for 30% heparin MPs, and 12±2% for 40% heparin MPs (Figure 6.6B).

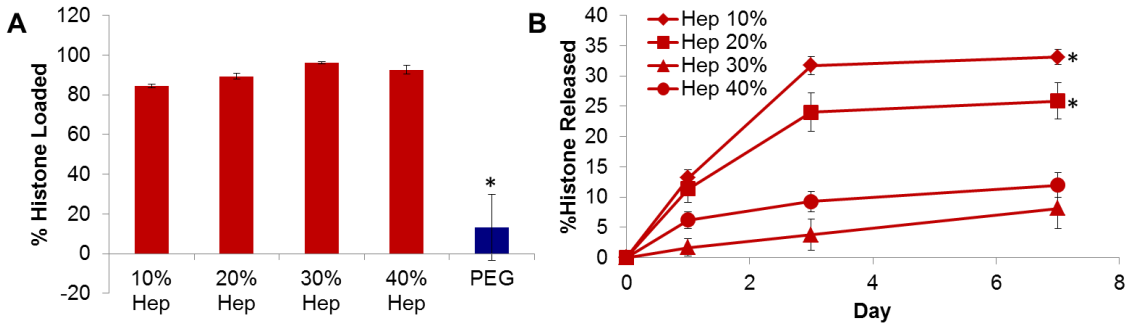

Figure 6.6. Heparin-PEG MP loading and release of histone. (A) Percentage of histone loaded onto 10, 20, 30, and 40% heparin MPs and PEG-based MPs, normalized to a soluble histone control. (B) Release of histone reported as the percentage of histone release relative to what was loaded over the course of seven days (*=significantly different from all other groups, $p<0.05$).

6.3.4 Sequestration and Release of Proteins in ATDC5 Transwell Studies

10% heparin MPs or PEG-based MPs incubated with ATDC5 cells or in media alone released protein in a mass-dependent manner. For 0.1 mg of MPs, about 3 mg protein was released, for 1 mg MPs, 5-8 mg of protein was released, and for 3 mg MPs, 8-10 mg of protein was released (Figure 6.7).

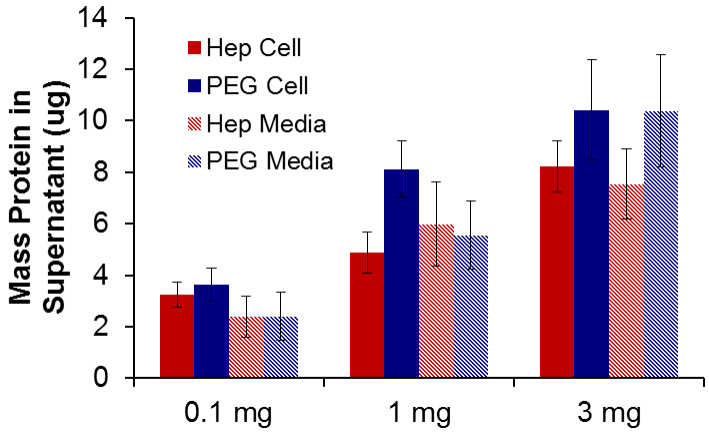

Figure 6.7. Total release of protein from varying masses of 10% Heparin and PEG-based MPs incubated with ATDC5 cells or in media alone after two days of MP incubation in PBS.

6.3.5 Incorporation of Degradable PEG-Based MPs into ATDC5 Spheroids

As a proof-of-principle study, fast- (45 mM DTT), slow- (40 mM DTT) and non- (0 mM DTT) degrading PEG-based MPs were incorporated into ATDC5 spheroids and degradation was monitored. During histological processing, PEG MPs fall out of the spheroid matrix and leave behind holes (arrows, Figure 6.8). From images, it was observed that fast-degrading MPs degraded in 1-7 days, slow-degrading MPs degraded in 7-14 days, and non-degrading MPs did not degrade throughout the course of culture (Figure 6.8).

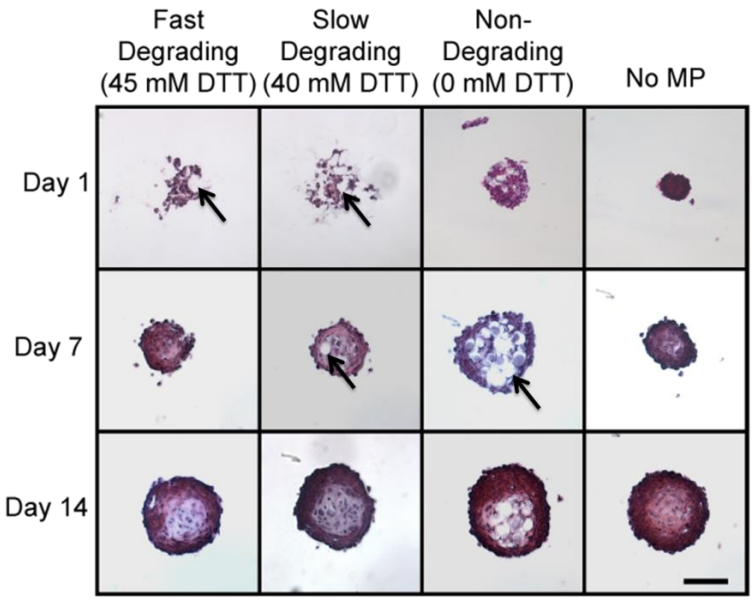

Figure 6.8. Degradation of PEG-based MPs in ATDC5 spheroids. Fast-degrading MPs (45 mM DTT) appeared to degrade between days 1-7and slow-degrading MPs (40 mM DTT) between days 7-14. Non-degrading MPs (0 mM DTT) did not appear to degrade. MPs appear as light purple spheres, or as holes in spheroid matrix due to removal during histological processing. Arrows point out holes left by MPs (scale bar 100 μm).

6.4 Discussion

Overall, these studies demonstrate the ability to fabricate degradable heparin-PEG MPs for protein loading and release, and provide examples of possible future applications in sequestering and releasing cell-secreted protein or delivering protein to cell aggregates. To characterize these MPs, alcian blue staining validated that heparin was successfully cross-linked into the polymeric network, and the staining appeared a deeper blue in heparin MPs with higher heparin content (Figure 6.2A). In addition, studies with surfen, previously shown to fluoresce upon binding to heparin (see Appendix A) [355], indicated that in solutions of equal masses of MPs, a higher fluorescence intensity was observed as the heparin content in MPs increased for 10, 20, and 30% heparin MPs. Then, fluorescence intensity appeared to plateau or even decrease slightly for 40 and 100% heparin MPs. While the reason for the plateau/decrease is unknown, it is possible that as

heparin content increased, steric hindrance between surfen molecules prevented further binding. To our knowledge, this and the data found in Appendix A are the first reports of utilizing surfen to assess heparin content in a hydrogel material.

To promote degradation of heparin-PEG-based MPs, DTT was incorporated into the polymeric network [60]. For all MPs, regardless of heparin content, the maximum molar ratio between PEG-DA and DTT that still allowed MP fabrication was between 1.2:1 and 1.3:1 moles PEG-DA:DTT. This was similar to previous work that found a maximum ratio of 1:25:1 PEG-DA:DTT in degradable MPs fabricated with 3.4 kDa PEG-DA [221]. As the heparin content in MPs was increased, the amount of PEG-DA was decreased to keep the total polymer content constant for each MP formulation, which also decreased the total amount of DTT that could be added. This particular limitation is inherent to this method of MP fabrication; thus, the degradation rates reported here are the maximum rates possible for each of MP formulations. With the maximum amount of DTT, MPs degraded between 1-2.5 weeks, with 10 and 20% heparin MPs degrading the fastest (7-9 days) and PEG-based MPs and 30 and 40% heparin MPs degrading slower (14-19 days) (Figure 6.4). This indicates that degradation rate was dependent on the total amount of DTT in the network, as 10 and 20% heparin MPs degraded before 30 and 40% heparin MPs, but also dependent on heparin content, as PEG-based MPs had higher DTT content than 10 and 20% heparin MPs but still degraded more slowly. This is similar to the previous set of studies that utilized heparin-PEG MPs, which showed that increasing heparin content increased degradation rate, possibly due to heparin's ability to attract more water into the network and accelerate hydrolysis of the ester linkages in the PEG-DA network [58,356]. Finally, it was observed that as MP concentration increased,

degradation rate decreased (Figure 6.4). This was likely due to decreased water availability in the more concentrated groups, as the MPs tend to pellet during incubation. These observations should be kept in mind for *in vivo* studies, and *in vitro* studies should aim to mimic the concentration that MPs would experience in future *in vivo* applications.

Histone was used as a model protein to evaluate the ability of heparin-PEG-based MPs to load and release protein. Histone is positively charged at physiological pH and similar in size to many growth factors (11-21 kDa). In studies to determine the maximum histone loading of 10% heparin MPs, a plateau region was found at about 35 µg histone/0.1 mg MPs, or 350 µg histone/mg MP (Figure 6.5A). On a per heparin basis, this corresponds to a max loading of 3500 µg histone/mg heparin. In previous studies with 100% non-degradable heparin MAm MPs, the maximum loading for BMP-2 was observed to be approximately 10 times lower than this, about 300 µg BMP-2/mg heparin [59]. This difference may be due to the different proteins used, as parts of the histone protein have a flexible structure [357] and may allow for more compact binding as compared to BMP-2. It also may be due to the relative concentration of heparin within the network. Recently, it has been suggested that the ECM can act as an "electrostatic bandpass", and it was shown that charged biomolecules are selectively filtered by ECM components like heparan sulfate [358]. In addition, a recent experiment with heparin hydrogels showed that as heparin content increased, depth of diffusion of histone into the gel decreased, indicating that heparin can affect diffusion of proteins through a hydrogel network [40]. Thus, the differences in loading capacity observed between the 10% heparin MPs in these studies and the 100% heparin MPs in previous studies [59] may be due to diffusion limitation imposed on the protein by higher heparin concentrations.

Finally, when loaded with a mass of protein that exceeded the loading capacity of 10% heparin MPs (100 µg histone/0.1 mg MPs), it was observed that 20, 30, and 40% heparin MPs bound more histone than 10% heparin MPs, as indicated by less histone remaining in the supernatant (Figure 6.5B). This suggests that increasing the heparin content in the heparin-PEG MPs can increase MP loading capacity to a certain point, but as no differences were observed between 20-40% heparin MPs, it is possible that diffusion limitations also arise in these MPs as heparin content is increased.

The rate of protein release from delivery systems is important to consider for tissue engineering applications [211]. Loading studies indicated that at a mass of protein below the maximum loading capacity of the MPs (20µg histone/0.1 mg MP), all MPs formulations loaded about 80% of histone in solution (Figure 6.6A). This is similar to what was observed in previous studies with heparin-PEG MPs, where similar amounts of BMP-2 were loaded into all MP formulations regardless of heparin content [58]. For 10 and 20% heparin MPs, the majority of histone release was observed between days 1-3, likely due to the faster degradation rate of these MPs. Release rate for 30 and 40% heparin MPs was more linear and had not yet plateaued by day 7, likely because either these MPs had not degraded at this timepoint or because the higher heparin content of these MPs trapped histone in the network, preventing release (Figure 6.6B). Overall, the maximum amount of histone released by any formulation was only about 30% of the total histone loaded, either indicating that histone was lost due to binding to plastic surfaces or that histone remained trapped in the MP network. Thus, these studies suggest that heparin content and degradation rate are likely both contributing factors to protein release rate,

and that these MPs can be tuned to achieve a desirable release profile as required for specific applications.

Previous work has highlighted the utility of employing heparin hydrogels to sequester cell-secreted protein to either modulate cell behavior or for analysis [40,41]. As heparin has a high affinity for proteins released by ATDC5 cells during differentiation [304,309,311,322,331], 10% heparin MPs were incubated with ATDC5 cells in a proof-of-principle study to demonstrate the ability of MPs to sequester and then release cell-secreted proteins for further analysis. MPs were incubated overnight with ATDC5 cells that had undergone six days of monolayer culture, as ATDC5 cells are seen to upregulate chondrocytic gene expression markers around this time, indicating that protein production may also be increased [309] (Appendix E.2). MPs were transferred to PBS to allow degradation and after 2 days, about 3-10 µg of protein was released, depending on the mass of MPs used (Figure 6.7). For each mass of MPs used, the same amount of protein was released from 10% heparin MPs and PEG-based MPs incubated with cells or in media alone. Thus, it was unclear if 1) protein sequestration was due to specific interactions with heparin and 2) the protein sequestered was secreted by cells or was from the FBS in the cell culture media. Studies discussed in prior chapters of this thesis indicate that heparin MPs bind more protein than PEG-based MPs and that heparin MPs incubated with cells bind additional proteins compared to those incubated in media alone (Chapter 4, Figure 4.10). This suggests that even if equal amounts of protein were sequestered in each group, the identity of those proteins may have been different.

To validate the hypothesis that released proteins in each MP groups were different, additional assays, such as ELISAs or mass spectrometry would need to be

conducted. Unfortunately, cell-secreted proteins would likely only be detectable if the amount of total protein released from MPs was at least 20 µg, based on assumptions described in Appendix F.1.The reasons for the low protein release observed in this study are unclear, but assuming each MP group bound the maximum amount of protein possible (Figure 6.5), 0.1, 1, and 3 mg MP groups should have theoretically loaded 35, 350, and 1050 µg protein, respectively. As only 2-10 µg protein was released, it is evident that the majority of the sequestered protein either was lost to plastic surfaces or remained bound to the heparin MPs. This may have been due to the short degradation time (2 days), chosen to maximize MP degradation and reduce the risk for protein denaturation. Thus, more work to optimize protein release needs to be conducted prior to further analyses are conducted to identify proteins.

Previously, MPs have been integrated into dense cell aggregates to achieve more uniform delivery of soluble biomolecules [253,255,256,258,260,261,263,264]. While biodegradable MPs have been incorporated into aggregates, including PLGA and CS MPs [253,255,264], modulating degradation rate of MPs within cell spheroids has yet to be achieved. Here, by tuning the concentration of DTT in the polymeric network, degradation of PEG-based MPs in cell aggregates was achieved in 7 days for fast-degrading MPs and 14 days for slow-degrading MPs (Figure 6.8). Degradation of MPs in spheroids could enhance release of biomolecules and could also be beneficial in cases where aggregates are injected *in vivo*. In the future, degradable heparin-PEG MPs could be integrated into spheroids to more finely tune protein release.

As mentioned, the fastest degradation rate for each MP formulation was used for these studies. Thus, if these degradation times are too long for a particular application, or

result in denaturation of sequestered proteins in studies aiming to capture and deliver cell-secreted proteins, other degradation techniques could be applied. First, as DTT accelerates the hydrolysis of the ester bond within the acrylate group of PEG-DA, employing 4- or 8-arm PEG-acrylate could enable more linkages between DTT and acrylate groups, increasing the number of sites susceptible to rapid degradation. In addition, incorporation of enzymatically degradable peptide sequences, such as MMP or plasmin-sensitive peptides [28,29], could aid in increasing degradation rate, as the concentration of the enzyme responsible for degradation could be controlled during *in vitro* experiments. For example, a recent study with PEG-DA MPs indicated that integration of a collagenase-sensitive sequence into the PEG network allowed degradation within 24 hours when MPs were incubated with collagenase [221]. Finally, degradability has been achieved in PEG materials via co-polymerization of degradable synthetic and natural polymers such as poly(lactic acid) [28,359], collagen [360], and hyaluronic acid [361]. While all of these options would require significant adjustment to the system described, they could be investigated in future work aiming to more tightly control degradation of PEG-based MPs.

6.5 Conclusion

Heparin-PEG MPs with tunable degradation rates and heparin content were developed. MP degradation occurred between 7-19 days and was dependent on the concentration of MPs in solution. In histone loading studies, it was observed that the maximum loading capacity of these MPs was about 3500 µg/mg heparin, and that increasing the amount of heparin increased loading capacity. MPs released histone over the course of seven days in a manner dependent likely on both degradation rate and heparin content. Finally, heparin-PEG-based MPs were used to sequester and release

proteins present in ATDC5 cell cultures and degradable PEG-based MPs were observed to degrade in ATDC5 cell aggregates between 7-14 days. Overall, these degradable heparin-PEG MPs have potential to modulate protein release for regenerative medicine applications.

CHAPTER 7

CONCLUSION AND FUTURE DIRECTIONS

7.1 Summary

In this work, biomaterial systems were engineered to enable analyses and modulation of dynamic cellular processes. Specifically, the changes in cell behavior in response to both external stimuli and cell-cell communication in disease states are difficult to capture in traditional cell culture systems. In addition, modulating cell phenotype as it changes in time during differentiation can be challenging with traditional methods, such as delivery of single growth factors. Thus, in this work, heparin and PEG-based biomaterial systems were designed to specifically account for dynamic cell behavior. For example, proof-of-concept studies with MSCs, adipocytes, and osteoblasts indicated that a PEG-based hydrogel system enabled cell cross-talk in hyperglycemic conditions. In addition, incorporation of heparin MPs in ATDC5 cell aggregates highlighted the utility of employing GAG-based materials to modulate cellular differentiation. With these results in mind, heparin-PEG core-shell MPs and hydrolytically degradable heparin-PEG MPs were developed to provide tighter temporal over heparin-mediated protein presentation in the cellular microenvironment for future applications. These technologies were addressed in detail in the four chapters presented in this thesis.

In Chapter 3, a PEG-based hydrogel system was used to co-culture MSCs, osteoblasts, and adipocytes in normal and high glucose conditions for seven days. Cell viability and gene expression for markers adipocyte/osteoblast differentiation and glucose-responsiveness were assessed for all three cell types, and clonogenicity was

assessed for MSCs. Overall, multivariate models indicated that the primary discrimination of gene expression dataset was dependent on neighboring cell type. Further discrimination by glucose level was dependent on culture configuration, suggesting that neighboring cells influenced cell response to glucose. Reduced clonogenicity and viability were observed in MSCs in mono-culture or in co-culture with osteoblasts, a trend not observed in MSCs cultured with adipocytes. In addition, adipogenic gene expression indicated that cross-talk between adipocytes and MSCs may have occurred. Taken together, these results indicate that cell cross-talk affected MSC, osteoblast, and adipocyte behavior, and highlights the importance of utilizing biomaterial based systems that permit culture and analysis of multiple cell types for *in vitro* disease models. In addition, this study showed the utility in hydrogel-based systems to interrogate dynamic cellular communication in response to external stimuli in an *in vitro* disease model.

In Chapter 4, heparin MPs were used to modulated differentiation in a model system with ATDC5 cells, known to under endochondral ossification *in vitro*. Heparin and PEG MPs were incorporated into ATDC5 spheroids and it was observed that in heparin MP groups, chondrocytic differentiation was decreased in a dose-dependent manner. This trend was also observed when monolayer ATDC5 cells were cultured in transwell with heparin and PEG MPs, indicating that this phenomenon was not dependent on physical contact with the MPs. Finally, to further elucidate mechanism behind observed decreases in differentiation, heparin MPs were run on SDS-PAGE, which indicated that heparin MPs cultured with cells sequestered protein in the 17 kDa range. As many growth factors implicated in endochondral ossification, such as IHH, BMPs,

and FGFs, fall in this range [346], it is possible that observed changes in differentiation were partially due to sequestration of cell-secreted growth factors. Overall, these studies indicate that heparin MPs can delay endochondral ossification, likely due to protein sequestration. Furthermore, they illustrate the ability of heparin materials to modulate the dynamic process of cell differentiation.

Having observed the effectiveness of heparin in modulating differentiation in ATDC5 cell studies, we aimed to develop heparin-based tools to achieve temporal modulation of protein sequestration and release. Thus, in Chapter 5 heparin-PEG core-shell MPs were developed for protein sequestration and temporally controlled release of a protein-laden core. Heparin-PEG core-shell MPs were fabricated using a re-emulsification technique to encapsulate pre-formed heparin MPs within a degradable PEG-based shell, thus creating MPs with tunable amounts of encapsulated heparin. In pre-fabrication load studies with BMP-2, degradable core-shell MPs initiated enhanced ALP activity as compared to non-degradable core-shell MPs, indicating these MPs can be used to temporally modulate protein presentation to cells. In addition, post-fabrication loading studies indicated that core-shell MPs were able to sequester BMP-2 through the PEG shell and then re-present that protein to cells to initiate enhanced ALP activity. Thus, this work developed a core-shell MP technology that utilized heparin to preserve protein bioactivity, delivered protein in a temporally controlled manner by employing a degradable PEG-based shell, and was able to sequester and re-deliver protein with no burst release. Overall, this technology has the potential to assist in further tuning dynamic cell behavior via protein sequestration and release.

Finally, in Chapter 6 heparin-PEG-based MPs with tunable hydrolytic degradation and heparin content were developed. Alcian blue staining and surfen binding studies validated that heparin was cross-linked into the MP network for 10, 20, 30, and 40 wt% heparin MPs. Degradation studies showed that MP degradation occurred in 1-2 weeks and was dependent DTT and heparin content in the MP as well as the concentration of MPs in solution. Loading studies with histone indicated that loading capacity increased for MPs with higher heparin content, as compared to 10% heparin MPs, and that histone was released from MPs in a manner dependent likely both on heparin content and degradation rate. Finally, MPs were used in proof-of-principle studies to show the feasibility of sequestration and release of cell-secreted proteins and degradation of MPs within ATDC5 cell aggregates. Overall, these studies characterized degradable heparin-PEG-based MPs and demonstrate their utility for protein loading and release as well as integration into cell aggregates for tissue engineering applications. Thus, in the future, these MPs can be used as tool to regulate and interrogate dynamic cell processes.

As a whole, this work demonstrates that dynamic cellular processes can be both studied and regulated using biomaterial-based approaches. In addition, heparin-based MP tools can aid in gaining enhanced temporal control over protein sequestration and release. Thus, these biomaterial based technologies have the potential to be used in a variety of tissue engineering applications.

7.2 Conclusions

The research presented in this dissertation highlights the utility of PEG- and heparin-based biomaterial technologies to better understand and control dynamic cell systems. Aspects of the *in vivo* microenvironment were captured by co-culturing cells in

an *in vitro* model system and by integrating heparin materials into culture systems and microparticle-based tools to modulate protein presentation. The results of this work suggest that 1) PEG-based platforms can enable complex analyses of cells in co-culture, 2) heparin materials can temporally modulate endochondral ossification, and 3) utilization of heparin in microparticle technologies can enable tighter temporal control over protein sequestration and release. Together, these results validate the use of biomaterials to study and modulate complex cellular behavior.

In Chapter 3, the utility of a laminated PEG-based hydrogel system to culture MSCs, osteoblasts, and adipocytes in mon-, co-, and tri-culture in normal and high glucose conditions for seven days was explored. PEG-based hydrogels were chosen because they have low capacity for protein binding, allow protein diffusion through the network , and can be chemically modified with peptide sequences to enhance cell attachment and matrix degradation [29,143,144]. Viability data and staining for adipocytic and osteoblastic markers (lipid deposition and ALP) indicated that the culture system was a valid platform for analysis of the three cell types. This validation was important, as both high glucose conditions and co-culture between these cell types has been shown to affect, sometimes negatively, cell viability and function [83–93,97–104]. In addition, this culture platform permitted MSCs retrieval from enzymatically degradable blocks for subsequent clonogenicity studies, and in the future could be employed for other functional post-co-culture cell analyses. Finally, gene expression for markers of osteogenesis/pro-bone formation, adipogenesis, pro-adipocyte function, energy metabolism, and glucose-responsiveness was assessed for all three cell types. In global multivariate model for each cell type, the primary source of variance was due to

neighboring cell type, indicating that cellular cross-talk occurred in this culture system. Discrimination by glucose level was only possible in some culture configurations, suggesting that neighboring cell type impacts cell response to glucose. These two observations support the use of the co-culture platform presented in this work, as traditional monoculture platforms cannot capture system-level cell communication that occurs in disease states.

Multivariate models permitted a deeper understanding of how cells were affected in co-culture settings. In the global PLS-DA gene expression model for adipocytes, the first latent variable separated osteoblast-containing (OMA) vs. non-osteoblast-containing (AMA, AAA) culture conditions, suggesting that osteoblasts, or the communication between osteoblasts and MSCs, had an impact on adipocytes. In addition, the adipocytes cultured with MSCs (AMA and OMA) showed correlation with markers of adipogenesis and energy metabolism, while those cultured without MSCs (AAA) correlated with markers of inflammation and oxidative stress, suggesting that MSCs promoted adipocytes to upregulate adipogenic and metabolic genes. MSC viability and clonogenicity was decreased in osteoblast-containing cultures (OMO), while osteoblast viability was highest in MSC-containing cultures (OMO), suggesting that MSCs exerted modulatory effects on osteoblasts at the expense of their own viability and clonogenicity. The positive influence of MSCs on both cell types may be due to their secretion of therapeutic soluble factors [78]. Finally, MSCs in co-culture with adipocytes (AMA and OMA) showed maintenance of viability and clonogenicity under high-glucose conditions, a trend not observed in other culture configuration (OMO and MMM). Overall, these results indicate that MSCs may exert compensatory effects on osteoblasts while adipocytes exert

compensatory effects on MSCs, and that adipocytes are affected by neighboring osteoblasts. More so, it illustrates the utility of advanced biomaterial-based cell culture platforms combined with multivariate modeling to interrogate dynamic cell systems implicated in disease.

In Chapter 4, we transitioned to utilizing heparin-based biomaterials to modulate another dynamic process: cell differentiation. In this set of studies, an *in vitro* model system of ATDC5 cell endochondral ossification with was used as a testbed for understanding how heparin MPs can modulate differentiation. As endochondral ossification is tight regulated by a variety of heparin-binding proteins, such as FGFs, BMPs, TGFβs, IHH, and Wnts [23,25,107,186], it is possible that heparin could sequester these proteins in a manner that modulates ATDC5 cell differentiation. Thus, heparin and PEG MPs, a low-binding material control [28], were integrated in ATDC5 cell aggregates (spheroids) at high and low doses and assessed for gene expression and matrix deposition markers of differentiation. It was observed that gene expression for *collagen II* and *aggrecan* were significantly downregulated in high heparin MP groups as compared to PEG and no MP groups, a trend that was confirmed by staining for GAG and collagen II matrix deposition. Overall, this suggests that heparin MPs can delay or reduce differentiation via protein sequestration, as this trend was not observed in PEG MP control groups.

To further assess if this phenomenon was actually due to heparin-mediated protein sequestration and not simply due to the presence of MPs in the spheroid matrix, heparin and PEG MPs were cultured with ATDC5 cells in monolayer transwell culture, allowing exchange of soluble factors without physical contact. Similar to trends observed

in spheroid culture, heparin MPs delayed or reduced differentiation as assessed by gene expression, staining for GAG and matrix mineralization, and quantification of extracted stains. Total DNA analysis confirmed that this phenomenon was not due to a decreased cell number in the heparin MP group. In addition, SDS-PAGE analysis of MPs incubated in transwell with cells suggested that heparin MPs bound more and different types of protein than PEG MPs. Finally, SDS-PAGE showed that while heparin MPs were able to bind proteins from the FBS-containing media, when incubated with cells, additional proteins of about 17 kDa were also sequestered. The identity of these protein remains unknown, but IHH, BMPs, TGFβs, and FGFs are likely candidates, as they all have MWs near 17 kDa. Taken together, these studies strongly support the hypothesis that the mechanism behind heparin MP-mediated changes in ATDC5 cell differentiation is soluble factor sequestration.

Several other studies have shown the ability of heparin materials to modulate cellular differentiation, likely through soluble factor sequestration [40,41]. This suggests that heparin-mediated sequestration of soluble factors is translatable to other cell systems. For example, heparin-based materials could be used to modulate endochondral ossification in injured growth plates, as current therapies under investigation cannot yet recapitulate native growth plate cartilage in animal models [111,113–118]. In addition, heparin materials could be used in place of antibodies to sequestered undesirable osteogenic factors in patients with craniosynostosis [209,210,334]. Finally, chondrocytic differentiation of MSCs requires tight control over chondrocytic factors [37], which could potentially be modulated by heparin materials. Overall, the studies presented in Chapter 4 highlight the ability of heparin-based biomaterials to modulate the dynamic process of

cellular differentiation, a characteristic of heparin materials that could be used in a variety of tissue repair processes.

Inspired by the potential for heparin MPs to modulate cellular processes via sequestration of growth factors, we developed a technology to temporally modulate this process in Chapter 5. In this work, heparin-PEG core-shell MPs were developed for protein sequestration and temporally modulated release of the protein-laden core. To fabricate these MPs, a re-emulsification technique was used to encapsulate previously formed heparin MPs with a PEG-DA shell. As this technique resulted in more than one heparin MP in each PEG shell, quantification methods were developed to show that heparin content in core-shell MPs was predictable and tunable, based on both the amount of heparin in the precursor polymer solution and the final core-shell MP cross-sectional area. Finally, the hydrolytically degradable PEG-based shell was able to degrade and release the heparin core in about 6-7 days by integrating DTT into the PEG-DA network. Thus, heparin-PEG core-shell MPs with predictable amounts of heparin and a degradable shell were formed.

Previous worked has indicated that BMP-2 bound to heparin MPs can enhance ALP activity in C2C12 cells [59]. Thus, in proof of concept studies, heparin MPs were pre-fabrication loaded (i.e. prior to core-shell MP fabrication) with BMP-2 and then encapsulated into degradable and non-degradable core shell MPs. Loading and release studies showed very little release (3-8% release) of BMP-2 over 7 days, indicating that observed cell response in subsequent cell studies would be due to release of the BMP-2 laden heparin core and not due to release of soluble BMP-2. When incubated with C2C12 cells, degradable core-shell MPs induced similar ALP activity as compared to the soluble

BMP-2 control, while cells cultured with non-degradable core-shell MPs showed significantly lower ALP activity. This indicates only degradable core-shell MPs were able to release the BMP-2-laden heparin core and initiate a cell response. Overall, these results show that core-shell heparin-PEG MPs could be used to gain tighter temporal control protein release, as well as reduce burst release, two sought-after characteristics in controlled release systems for tissue engineering applications [52,245,247].

In addition to pre-fabrication loading, core-shell MPs were post-fabrication loaded (i.e. loaded after core-shell MP fabrication) to evaluate the ability of proteins to diffuse through the PEG shell, be sequestered onto the heparin core, and then be released while bound to the heparin core to initiate a cell response. Loading studies indicated that degradable core-shell MPs were able to load almost 100% of the BMP-2 protein in solution, and release studies again showed very little protein release over 7 days (<3% release). When incubated with C2C12 cells, degradable core-shell MPs were able to initiate significantly higher ALP activity than the soluble control, again indicating release of the protein-laden heparin core to initiate a cell response. The ability to post-fabrication load these core-shell MPs could enable sequestration and temporally modulated re-delivery of cell-secreted proteins, a technique recently proposed as a means to more tightly control dynamic cellular processes [3]. For example, a protein that is undesirable at one point in time could be sequestered and effectively eliminated from the microenvironment until re-delivery at a point in time at which it is desirable again. Thus, studies conducted with the core-shell MPs developed in this work show their utility for use in future experiments to carefully tune protein presentation during differentiation or other cell processes.

Finally, in Chapter 6, degradable heparin-PEG based MPs were developed and investigated for future applications involving temporally controlled protein loading and release. Previously, control over heparin MP degradation has been a challenge due to cross-linking techniques [58,59]. Thus, in this work hydrolytically degradable heparin-PEG MPs of varying heparin content (10, 20, 30, and 40 wt% total polymer) were developed and characterized. Alcian blue staining and incubation with surfen indicated that heparin was successfully cross-linked into the network, and suggested that more heparin was cross-linked into the network as the amount of heparin in the precursor polymer solution was increased. DTT was integrated into the polymeric network, as it is known to enhance hydrolytic degradation PEG-DA materials [60]. MP degradation occurred between 1-2 weeks and was dependent both on DTT and heparin content in the MPs. Thus, degradable heparin-PEG-based MPs with tunable heparin content were developed.

To evaluate the ability of MPs to load protein, histone was used a model protein, as it is positively charged and similar in size to a variety of growth factors. The maximum loading capacity was evaluated to be about 3500 μg histone/mg heparin for 10% heparin MPs, which is about 10 times higher than what was previously observed for BMP-2 loading in 100% heparin MPs. This difference could be attributed to differences in protein binding for the two proteins, or to the ability of higher amounts of heparin to restrict diffusion of positively charged proteins into heparin-based hydrogels. Previously, it has been observed that heparan sulfate can act to selectively filter biomolecule passage through the ECM [358], and that as heparin content was increased in hydrogels, diffusion depth of histone was decreased [40]. The next set of studies supported the possibility that

increased amounts of heparin prevented protein diffusion, as the binding capacity of 20, 30, and 40% heparin MPs were not significantly different from each other, though they were significantly higher than 10% heparin MPs. Thus, protein loading capacity could be increased by increasing heparin content to a certain extent, at which point a plateau was reached. Finally, heparin MPs were able to release histone over the course of 7 days at a rate dependent likely both on degradation rate and heparin content. Thus, these heparin-PEG MPs can be tuned to achieve a degradation rate and protein release rate suitable for a given tissue engineering application.

Heparin-PEG MPs and PEG-based MPs were used in two proof-of-principle studies to demonstrate potential future applications for this technology. First, 10% heparin and PEG based MPs were incubated with ATDC5 cells, retrieved and degraded for two days. Analysis of supernatant indicated that no differences in protein release were observed between heparin and PEG groups, and that total protein released was lower than expected, indicating further optimization of the MPs is required before released cell-secreted proteins can be analyzed. Second, fast-, slow-, and non-degrading PEG-based MPs were incorporated into ATDC5 spheroids and monitored for degradation via histological processing. Fast- and slow-degrading MPs degraded in about 7 and 14 days, respectively, while non-degradable MPs did not degrade over the 14 day culture period. In the future, degradable heparin-PEG-based MPs loaded with protein could be incorporated into cell spheroids to affect cell differentiation via protein release. Thus, these studies demonstrate the utility of degradable heparin-PEG for future cell studies, either for isolation and concentration of cell-secreted proteins for analysis, or for protein delivery in dense cell aggregates. Overall, these MPs have the potential to modulate

dynamic cellular processes, such as differentiation, by temporally controlling protein delivery.

In these studies, two model systems were used to demonstrate the utility of biomaterial-based systems for analysis and regulation of cellular behavior. First, due to their implication in the diabetes and osteoporosis, MSCs, adipocytes, and osteoblasts were cultured on a co-culture platform that allowed cell-cross talk and subsequent analysis of each individual cell type, including live-cell retrieval of MSCs. Multivariate analyses indicated that cells were highly dependent on neighboring cell types in the culture configurations, validating the need for biomaterials to facilitate co-culture experiments. Second, ATDC5 cell endochondral ossification was used as a proof-of-principle model system to demonstrate the ability of heparin MPs to modulate cellular differentiation. These studies highlighted the ability of heparin to act on and modulate dynamic cell systems, likely through soluble factor sequestration, and motivated the development of two additional technologies to gain tighter control over heparin-mediated protein sequestration. Heparin-PEG core-shell MP and heparin-PEG MP technologies were developed and demonstrated to temporally control protein sequestration and release. Thus, overall this work demonstrates the utility of biomaterial-based technologies for studying cell behavior to gain further insight into various pathologies and cellular processes, and for modulating cellular differentiation for tissue regeneration and repair.

7.3 Future Directions

The results of this work highlight several technologies that are beneficial for understanding and controlling cellular behavior. The PEG-based co-culture system presented allowed analysis of complex interactions between MSCs, adipocytes, and

osteoblasts, and heparin MPs were able to modulate ATDC5 cell differentiation. Inspired by these experiments, heparin-based MP technologies were developed to further enable the use of heparin to modulate protein presentation in an effort to control cellular differentiation. However, another attractive aspect of these technologies is their flexibility and potential to be modified to meet different goals in tissue engineering and regenerative medicine. Thus, future work could extend and enhance these technologies for their use in a plethora of applications.

As the culture platform developed in Chapter 3 allows for post-culture retrieval of MSCs, several applications for released live cells could be explored. First, as it is hypothesized that increased marrow fat and decreased bone mineral density is due to dysregulated lineage allocation in MSCs [17], it would be interesting to conduct differentiation assays on MSCs retrieved from cultures with and without high glucose levels. If MSC osteoblastic differentiation was restricted in cultures with high glucose or if measures of osteoblastic function (such as matrix mineralization) were reduced, this would support the hypothesis that MSC differentiation is dysregulated in hyperglycemic conditions. Confirmation of this hypothesis could lead to development of drugs and therapies to counteract this dysregulation. Second, this platform and release of live cells could be extended to other applications in which cells could be "primed" within the hydrogel co-culture platform before use in other applications. For example, it has been observed that chondrocyte and MSC co-culture promotes the chondrocytic phenotype in MSCs [133–135]. This platform provides a 3D environment in which the two cell populations can be cultured, interact, and then be released for subsequent cartilage

therapy applications. Overall, the ability to retrieve live cells from a co-culture hydrogel system could be used in a variety of analysis and cell priming applications.

The co-culture platform presented in this work also allows for user-defined, dynamic changes to the culture system. For example, to better mimic the conditions observed in diabetes, additional adipocyte blocks could be laminated to the tri culture system over time. In the same vein, osteoblast blocks could be removed. We have shown in previous experiments that it is possible to laminate, separate, and then relaminate two cell-laden hydrogel blocks without loss of cell viability (Figure 7.1). Thus, it would be possible to 1) laminate additional adipocyte blocks onto the culture system and/or 2) remove osteoblast blocks through enzymatic degradation, both without loss of cell viability. This could be applied to other model systems in which cellular communication is transient or dynamic, such as communication between osteoblasts and chondrocytes during endochondral ossification [23] or signaling between inflammatory cells, osteoblasts, and chondrocytes in rheumatoid arthritis [362]. Overall, the co-culture platform can be tuned to mimic many cellular process that change in space and time.

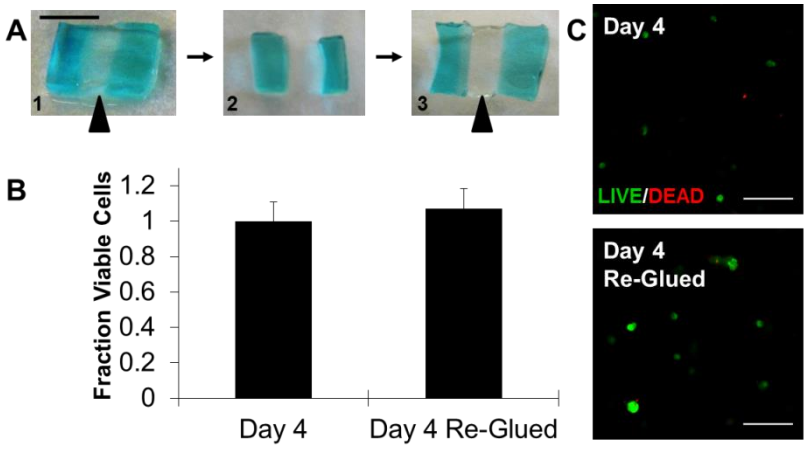

Figure 7.1 (A) 1.Fabrication, 2. separation via enzymatic degradation, and 3. re-lamination of hydrogel culture system, PEG-DA gels depicted with blue dye, Acrylate-

PEG-LGPA glue clear. All gels are acellular. Arrows indicate glue and scale bar = 0.5 mm. (B) Cell viability was calculated using LIVE/DEAD staining, confocal imaging, and ImageJ processing for hydrogels laminated, separated and relaminated (day 4 reglued) or control groups that were only originally laminated, all normalized to day 4 control group. No significant differences in viability were observed ($p<0.05$). (C) Representative images of LIVE/DEAD staining in each gel, scale bar = 100 μm.

The use of *in vitro* models for drug screening can be very beneficial, as human cells can be used and animal number is reduced [363]. In the co-culture model system presented in Chapter 3, it would be interesting to observe how cellular cross-talk is affected by drugs that aid in controlling diabetes, such as insulin. By extending the culture timeline and introducing insulin at various points in the experiment, it may be possible to gain an understanding of when and how insulin presentation can modulate communication between the three cell types. Eventually, this may lead to a better understanding of the clinical outcomes in patients with controlled and uncontrolled blood-glucose levels. Additionally, utilizing this system to develop and screen drugs or other therapeutic biomolecules to enable a return to normal differentiation potential in MSCs could allow reduction of diabetes-induced osteoporosis.

In Chapter 4, heparin MPs were shown to modulate endochondral ossification, likely through sequestration of soluble factors. While heparin MPs sequester positively charged protein in a rather non-discriminate manner, other affinity matrix systems have been developed to present peptide sequences that target and sequester specific proteins, such as VEGF, TNFα, and FGF [43,46,335], which would provide more predictable control over cellular processes. Specific sequestration would be beneficial in several of the applications mentioned in Chapter 4. For example, to modulate growth plate cartilage regeneration, it may not be beneficial to indiscriminately bind proteins, as heparin-binding proteins such as BMP-2 and IHH [25] enhance chondrocyte proliferation, which

is important for normal growth plate function [106]. However, the sequestration of heparin-binding proteins that suppress proliferation and promote hypertrophy, like FGFs and VEGF [25,106], could reduce the risk of bony bridge formation. This could also apply to therapies for articular cartilage regeneration and craniosynostosis. Thus, designing biomaterials that can specifically sequester proteins of interests could be beneficial as a means to more carefully modulate differentiation.

In addition to utilizing endogenous growth factors to manipulate differentiation, it is possible that heparin based materials could be used to sequester and thus concentrate proteins in the local cellular microenvironment for later analysis. Recently, it was shown that heparin-based materials could be used to identify proteins secreted by encapsulated cardiac progenitor cells, even when these growth factors were at a much lower concentration in the surrounding media [364]. Thus, by incubating heparin MPs with cells undergoing a process of interest, it would be possible to capture some of the proteins involved, which could enable a more mechanistic understanding of the process in question. One difficulty in analyzing heparin-bound proteins is removal of proteins from the MPs in a manner that allows subsequent analyses to be conducted. As proteins are electrostatically bound to heparin, disrupting these interactions with a concentrated salt solution enables protein release, but also interferes with subsequent assays, such as ELISAs. This technique is compatible with mass spectrometry, but low-abundant proteins are often masked by high-abundant proteins present in the serum in this analysis technique [328,365]. Combining this idea with the core-shell MP technology described in Chapter 5 could allow size exclusion by the PEG-based shell for additional filtration of proteins of interest, as discussed later on in this section. Separation of proteins from

heparin MPs using salt is also the first step for running SDS-PAGE, which when combined with western blots, could allow identification of proteins. However, western blots are very low throughput and require an idea of which proteins to assay for, resulting in a lot of guesswork. Finally, implementing degradable heparin-based MPs like those discussed in Chapter 6 could allow release of intact proteins, which could then be analyzed on protein arrays. Overall, use of heparin as a tool for concentrating proteins could enable identification of low abundant proteins such as biomarkers or growth factors that could potentially enable better treatments for disease or tissue regeneration.

The heparin-PEG core-shell MPs presented in Chapter 5 could be modified in several different ways that would provide innovative techniques to modulate protein in the cellular microenvironment. In the current design, degradation of the PEG-based shell is dependent on hydrolysis, which is controlled by the amount of DTT integrated into the PEG network. This preset degradation method is advantageous in well-defined systems, in which desirable timing for protein delivery is known, but possibly not as useful in poorly understood systems, as it does not allow degradation to be responsive to the local cellular microenvironment. Thus, as PEG can be chemically modified with enzymatically degradable peptide sequences, a shell designed to be degradable by a specific enzyme in the cellular microenvironment could better enable this core-shell MP system to respond to cellular behavior. Often, this technique has been employed to develop hydrogels responsive to enzymes implicated in inflammation, such as MMPs or human neutrophil elastase [366–368], or enzymes implication in cell migration, such as plasmin [369]. PEG materials can also be modified to be degradable in a pH-dependent manner [370], which could be beneficial in tissues with low pH, such as in tumors or inflammatory

environments [12,371]. While such a technique has yet to be developed, having a material whose degradation could be triggered by presence of a particular protein, not just an enzyme, would be particularly useful. This could be achieved by engineering a polymer linkage to break upon encountering said protein, possibly by inclusion of something that changed confirmation when it bound the protein (an inhibitor or peptide sequence) within the polymeric network. While the particular type of degradation would have to be selected for the application at hand, core-shell MPs with degradation responsive to cues in the cellular microenvironment could be highly beneficial.

Recently, ideas have circulated around utilization of biomaterials to modulate endogenous, cell-secreted proteins within the cellular microenvironment as a means to control dynamic cellular processes, in place of their traditional use in protein delivery or as cell scaffolds [3]. However, biomaterials that can engage with cellular microenvironment in a temporally controlled manner are only just emerging. Modifying the core-shell MPs presented in this work to prevent sequestration prior to shell degradation would result in a first of its kind technology for temporally controlled protein sequestration. As presented now, the core-shell MPs allow protein diffusion through the PEG-based shell, albeit at slightly slower rate. By decreasing the pore size in the shell, it would be possible to prevent protein diffusion into the core-shell MP prior to shell degradation. In effect, this would become a controlled delivery vehicle for sequestration agents (i.e. the heparin MP core). Then, the technology could be used to precisely time protein sequestration, beneficial in applications where timing of growth factor modulation is critical, such as cellular differentiation. One way to slow protein diffusion in PEG materials, especially of larger proteins, is to decrease the MW of the PEG

polymers [27,372]. If sufficiently small pore sizes to prevent protein diffusion cannot be achieved with PEG materials, other materials could be explored. For example, PLGA is a hydrophobic material with degradation kinetics that can be controlled by the MW of the polymer as well as the lactide:glycolide ratio [373,374]. On the microparticle size scale (<300 μm in diameter), network degradation occurs by bulk erosion due to hydrolysis of the ester linkage in the polymeric backbone [373,374]. However, unlike hydrophilic PEG materials, the hydrophobicity of PLGA only permits transport of small, hydrophobic molecules until aqueous pores have developed [373,374] . This characteristic may allow better control over protein diffusion in PLGA and other hydrophobic materials as compared to PEG. Thus, by modifying the shell of these core-shell MPs to prevent protein diffusion prior to degradation, it would be possible to develop a delivery vehicle that had controlled release of sequestration agents.

In addition, the shell of core-shell MPs could be tuned to exclude large proteins (>40 kDa) while allowing sequestration of smaller growth factors. This could be beneficial in any scenario that involves serum, as growth factors have to compete with large, heparin-binding serum proteins, such as fibrinogen or fibronectin [326–332], for binding sites on the heparin MP. However, if the pore size of the PEG shell was tuned to exclude large proteins, higher concentrations of growth factors could be bound. Studies utilizing PEG-based materials for cell encapsulation have indicated that PEGs of MWs ranging from 2-8 kDa could be used for this purpose [372], indicating that while the increases in chain length due to DTT in the network of the PEG-shell would still have to be accounted for, the core-shell MPs discussed in this work could be modified to exclude larger proteins. This could be beneficial for two different types of applications. First, if

these MPs were to be used to sequester endogenous protein *in vivo* (and even in most *in vitro* applications), serum proteins could interfere with their ability to affect differentiation by blocking sequestration of growth factors. Second, as discussed in a future direction for the heparin MPs in Chapter 4, using heparin MPs to identify proteins secreted during cell culture could of interest. However, as is the case with many experiments that attempt to identify low-abundance proteins from serum-containing solutions [328,365], a collaborating lab has found that serum proteins that bind to heparin MPs can mask the presence of low abundant proteins in mass spectrometry analysis. Thus, core-shell MPs with size-exclusive properties could act as a protein filter, sequestering and concentrating these proteins for future analysis. Recent studies have showed the utility in this by using core-shell MPs to selectively sequester biomarkers from blood and urine [48–50], but this technique has yet to be applied for analysis of growth factors. Overall, exclusion of large serum-bound proteins by the PEG-shell could allow core-shell MPs to bind growth factors at higher concentrations.

Currently, the core of the core-shell MPs presented is non-degradable. Because proteins can interact with cell receptors while bound to heparin [175,182], this is not necessarily problematic; however, it does impose spatial limitations on the system, as only cells in contact with heparin MPs will be affected by bound proteins. This problem could be remedied by making the heparin MP core degradable, so that sequestered proteins would eventually be released from the polymeric matrix into the cellular environment. Initiation of the heparin MP core degradation would ideally occur after shell degradation, so that proteins could be isolated from the cellular microenvironment on a timeline controlled solely by the degradation rate of the PEG shell. The heparin-PEG

MPs described in Chapter 6 show potential for this application, as higher heparin content MPs (30 and 40% heparin MPs) degrade on a longer timescale (17-19 days) than the PEG-based shell (6-7 days) and do not show high protein release during the initial 7 days of release after loading (<10% release). In addition, the environmentally triggered approaches described in the previous paragraph could also be used for the heparin core. Enzymatically triggered degradation could be particularly useful if the shell was able to exclude enzymes prior to its degradation. Finally, while a technique for this does not necessarily exist yet, if the degradation products of the PEG shell initiated degradation of the heparin core, the entire system could be responsive to cellular microenvironment, eliminating the requirement for preset degradation timelines. Overall, a degradable heparin core could aid in more uniform and effective release of sequestered protein in core-shell MPs.

Finally, it could be very interesting to include heparin materials within the co-culture platform discussed in Chapter 3. First, this could be done toward the goal of modulating cellular signaling. For example, in a co-culture system aiming to analyze cellular communication between osteoblasts and chondrocytes, integrating heparin into the chondrocyte hydrogel block may better mimic the ECM's natural ability to sequester and concentrate growth factors derived from other cell types. This could further our understanding of how GAGs are implicated in cellular signaling in a variety of other processes, such as maintenance of articular cartilage [108,375] or tumor development and maintenance [174]. In addition, integration of heparin into the co-culture platform could permit sequestration and subsequent retrieval of cell-secreted protein for analysis. In the study present in Chapter 3, this would be particularly beneficial, as secreted proteins

could provide another interesting variable to further strengthen multivariate models, and provide additional information upon which to build hypotheses and future experiments. As these hydrogels are PEG-based, a small amount of heparin could be integrated into enzymatically degradable gels, allowing degradation of gels and release of sequestered protein. Thus, integration of heparin into the co-culture system presented could aid in modulating protein-mediated cellular communication as well as permitting retrieval of cell-secreted proteins for further analysis.

These future possibilities only further highlight the power of the tunable biomaterial-based technologies presented in this work to modulate and study cellular processes. A variety of cell systems can be studied upon the co-culture platform presented, and some of the modifications presented would enable a deeper understanding of dynamic cell communication and behavior. In addition, heparin-based materials can be further engineered to actively engage with the cellular microenvironment, providing researchers even tighter control over and understanding of evolving cell processes like differentiation. Thus, this work lays a foundation for future technology development to interrogate and regulate dynamic cell behavior.

APPENDIX A

SURFEN INTERACTIONS WITH SOLUBLE HEPARIN AND HEPARIN MPS

A1. Introduction

Surfen (bis-2-methyl-4-amino-quinolyl-6- carbamide) is a small molecule that is known to bind heparin and other GAGs [355]. While the nature of the surfen-heparin interaction is not fully understood, recent work has uncovered that the dimeric aminoquinoline moiety is required for surfen to block heparin-protein interactions, indicating that the amine groups of surfen likely interact with positively charged sulfate groups to neutralize heparin [376]. Recently, surfen has been used to neutralize the affinity of heparin for growth factors. For example, surfen prevented heparin from activating antithromin and inhibited FGF-2 signaling in CHO cells, likely due to interactions with cell-surface heparin sulfate [355]. Furthermore, delivery of surfen resulted in ectopic cartilage formation in long bones, similar to results seen in mice deficient for a heparin sulfate-synthesizing enzyme, suggesting that surfen prevents heparin sulfate from functioning normally [187]. In addition, surfen was able to replace BMP-2 on heparin-functionalized agarose beads [187], suggesting it has a higher affinity to heparin than growth factors. Thus, we were interesting in using surfen to block heparin MPs, with the intent of neutralizing their protein-binding ability in order to act as a control in cell studies.

A2. Materials and Methods

A2.1 Materials

Surfen (Sigma-Alrich) was resuspended at 30 mM in dimethyl sulfoxide (DMSO) in a glass vial, as surfen binds to plastic [355], and stored at -20°C. Heparin MPs and AF633-tagged heparin MPs were prepared as described in Section 5.2.2. Histone was functionalized with FITC by reacting 4 mg/mL protein with 0.1 mg/mL FITC in DMSO and 150 M ammonium chloride in a bicarbonate buffer solution (pH 8.3) for 8 hours at 4°C. The product was then dialyzed and stored at -20°C.

A2.2 Incubating Heparin Materials with Surfen

Prior to incubations, all tubes were blocked using a 0.1% BSA solution for at least an hour. MPs and soluble heparin were added to a PBS solution and then surfen was added and quickly vortexed. A 10 µM surfen concentration was used for all incubations. All incubations were carried out at 37°C on a shaker plate.

A2.3 Surfen-Blocked Heparin MP Imaging and SDS-PAGE Studies

For surfen imaging studies, 10 µM surfen was added to AF633 heparin MPs at a 35 µg/mL concentration overnight at 37°C on a shaker plate. MPs were centrifuged and supernatant was removed, and MPs were washed once. 100 µg FITC-Histone/mg MP was then added in PBS and incubated overnight at 4°C on a rotary. MPs were then encapsulated in a PEG-DA hydrogel for imaging, as described (Section 5.2.3).

For surfen sodium dodecyl sulfate polyacrylamide gel electrophoresis (SDS-PAGE) studies, 10 µM surfen was added to heparin MPs at a 35 µg/mL concentration overnight at 37°C on a shaker plate. 2.4 µg BMP-2/mg heparin MPs was then added in a 0.1% BSA PBS solution and incubated overnight at 4°C on a rotary. MPs were then

rinsed once, loaded onto an agarose gel (0.21 mg MPs, corresponding to about 500 ng protein, in each well), and run against a protein ladder.

A3. Results and Discussion

A3.1 Surfen Dosage and Incubation Time

Previously, it has been observed that soluble heparin interacts with surfen in a dose-dependent manner [355]. Similar to previous results, we found that soluble heparin also interacts with surfen and plateaus around 10 µg/mL (Figure A.1A). In addition, we show that heparin MPs also interact with surfen in a dose-dependent manner (Figure A.1B), with a plateau around 100 µg/mL heparin MPs. Converting these numbers into molar ratios, soluble heparin and heparin MPs appeared saturated at 18:1 or 1.8:1 moles surfen to moles heparin ratio, respectively. The increase in molar ratio suggests that less surfen is required to fully block heparin MPs as compared to soluble heparin, which may indicate that there are fewer available surfen binding sites on heparin MPs as compared to soluble heparin. This could be due to the conformation or functionalization of heparin in MPs, discussed further below, and might also suggest that heparin MPs were unable to be fully blocked. To overcome this obstacle, we attempted to incubate surfen and MPs in a DMSO solution, but even lower fluorescent intensities were observed (data not shown), suggesting that it was energetically favorable for surfen to remain in solution rather than binding to heparin MPs. Overall, successfully blocking of heparin MPs with surfen proved challenging and should be further explored in the future. For example, dissolving surfen in a different organic solvent may enhance binding efficiency, or heparin-PEG MPs may have an increased mesh size that permits more surfen binding. If optimized,

surfen blocked heparin MPs could be an excellent tool for experimental control groups in subsequent studies.

Soluble heparin and MPs were incubated for up to 18 or 22 days, respectively. It was observed that surfen-soluble heparin interactions began to diminish around day 12 (Figure A.1A), possibly due to increasing amounts of surfen becoming stuck to the plastic tube or heparin degradation. In contrast, surfen remained bound to heparin MPs for at least 22 days (Figure A.1B), indicating that heparin MPs were better able to protect surfen from loss to the plastic tube or that heparin MPs were less likely to degrade. Overall, the stability of the surfen-heparin MP interaction indicates that surfen-blocked heparin MPs could be used for long experiments.

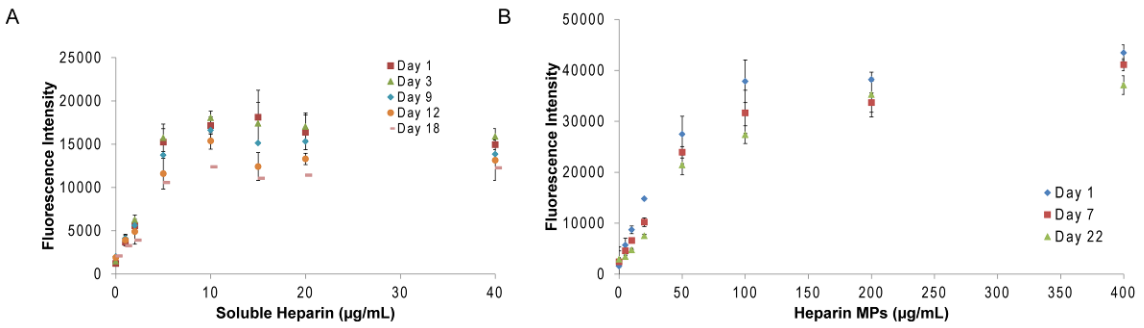

Figure A.1. Fluorescence intensity increases with mass of heparin in solution until a plateau is reached, indicating that surfen is able to bind to (A) heparin MPs and (B) soluble heparin until saturated.

A3.2 Protein Binding for Surfen-Blocked Heparin MPs

As evidenced by confocal microscopy, histone, a heparin-binding protein, was able to bind surfen-blocked heparin MPs (Figure A.2). From visual inspection, it did not appear that there was any decrease in the ability of surfen-blocked heparin MPs to bind histone as compared to unblocked MPs. Histone was found to appear rounded, possibly

because a rounded conformation was thermodynamically stable for the flexible histone protein, or possibly due to artifacts of imaging, as heparin MPs appear to have dark spots that do not emit a fluorescence signal. As these MPs are made with 70% AF633 heparin MAm, it is possible that the material is not distributed evenly throughout the MP during fabrication. Heparin MPs blocked with surfen appeared to have similar dark spots (data not shown).

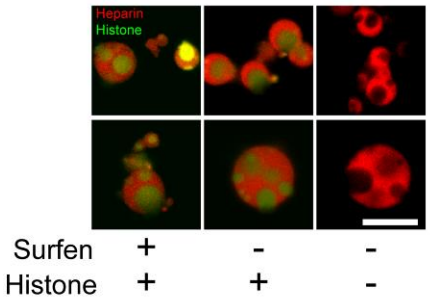

Figure A.2. Confocal microscopy images of surfen-blocked heparin MPs. Heparin MPs either blocked with surfen and incubated with histone, unblocked and incubated with histone, or unblocked without protein, as indicated by key below. Surfen does not prevent heparin MPs (red) from binding histone (green) (scale bar = 10μm).

To confirm the results obtained from confocal microscopy, surfen-blocked heparin MPs were incubated with BMP-2 and then run on a polyacrylamide gel. Previously, it has been observed that proteins bound to MPs will dissociate from the MPs when incubated with the surfactant SDS and subsequently run on the gel while the MPs remain stuck in the well, due to large size [377,378]. In this study, we hypothesized that surfen-blocked heparin MPs would not allow for BMP-2 binding, thus no BMP-2 band would be present on the gel for this group. In contrast to what we expected, we observed that even after being blocked by surfen, heparin MPs were able to bind BMP-2, evidenced by the BMP-2 band present in the surfen-blocked MP lane (Figure A.3). As the

intensity of the band is similar to the unblocked MP control, we concluded that surfen is unable to prevent heparin MP protein interactions.

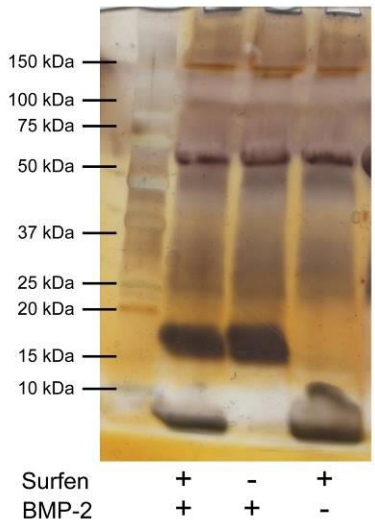

Figure A.3. Surfen-blocked heparin MPs run on SDS-PAGE. For both surfen-blocked and unblocked heparin MPs, BMP-2 was observed to run on the gel (dark band at 16 kDa, corresponding to the MW of BMP-2). For surfen containing samples, surfen can be seen as a bright bar below 10 kDa (surfen MW = 372.42 g/mol).

As mentioned above, it is possible that heparin MPs are not blocked as efficiently by surfen as soluble heparin, evidenced by the decrease in surfen required to reach the apparent max binding for surfen MPs (Figure A.1). Assuming that soluble heparin is 100% blocked by surfen upon reaching the plateau region, only 10% of the surfen-binding spots are taken on heparin MPs, which could lead to the protein binding we observed. More so, it has been observed that slight increases to the linker region between the two aminoquinoline dimers in surfen-like molecules enhances its effectiveness, up to a certain limit at which point the molecule becomes too hydrophobic [376]. This suggests a structure relationship between surfen and heparin, which might be interrupted when heparin is 1) functionalized and 2) cross-linked into MPs, thus reducing the effectiveness of surfen. Finally, previous work has not been able to confirm that surfen's mechanism of

action is solely to interact with heparin. While it is known to bind heparin avidly, it is also known to interact with other proteins and molecules [376], indicating that observed results may have been not only from surfen-heparin interactions, but potentially interactions with surfen and other proteins. We have observed that protein incubated with surfen is no longer detectable using ELISA, further suggesting that surfen effects protein. If surfen does affect protein, this would complicate the use of surfen-blocked heparin MPs as control groups. Thus, significantly more work would have to be done to efficiently block heparin MPs with surfen in order to use surfen-blocked heparin MPs as an experimental control group.

A4. Surfen Assay to Measure Heparin Concentration in Aqueous Solution

Although surfen did not function as we had hoped for our experiments, it was possible to use surfen to assay masses of soluble heparin in aqueous solution down to the µg level. Following is the protocol:

Surfen Assay Protocol
Surfen is a small molecule that binds to GAGs. It emits a weak fluorescent signal that increases when bound to GAGs, which is proportional to the amount of GAG bounds in the 0-10 µg/mL range. Surfen is not very soluble in water, and must be prepared in DMSO prior to addition to aqueous solution. Surfen concentration in aqueous solution should not exceed 10 µM. Because surfen binds avidly to plastic, glass or BSA-blocked tubes should be used for assay.

Supplies:

- Heparin
- BSA
- Surfen
- DMSO
- PBS

Material Prep:

- Surfen: dilute fresh surfen to a 30 mM concentration in DMSO in the glass vial it arrives in. Store at -20°C
- Tubes: Block tubes for at least 1 hour with 1% BSA in PBS. Removes solution prior to adding samples, no need to wash.

Assay:

1. Make heparin standard in PBS: make 1 mg/mL stock soln, 100x dilution for 10 ug/mL working solution

ug/mL	10 ug/mL	PBS
0	0	1000
1	100	900
2	200	800
4	400	600
6	600	400
8	800	200
10	1000	0

2. Prepare samples
3. Add surfen to each sample to achieve a final concentration of 10 uM surfen (ex: 0.33 uL surfen in 1 mL). Vortex immediately after adding.
4. Incubate for at least 3 hours at 37°C
5. Pipet 100 uL of each sample into a 96 well plate
6. Read at 320/460 fluorescence

A5. Conclusion

Surfen has previously been used to neutralize heparin-protein binding [187,355], likely due to electrostatic interactions between heparin's negatively charged sulfate groups and the amine groups on surfen's aminoquinoline groups [376]. For this reason, we were interested in using surfen-blocked heparin MPs as a control group in our spheroid and transwell studies (Chapter 4), as surfen blocked MPs would have the same mechanical properties as unblocked MPs but would not be able to bind protein. We show that surfen is able to saturate heparin at a 18:1 or 1.8:1 molar ratio for soluble heparin and heparin MPs, and that these interactions last for 12 to at least 22 days, respectively. Through two different studies, we show that surfen-blocked heparin MPs cannot prevent heparin-protein binding. This is likely due to an inefficient blocking protocol but may also be due to conformational changes in heparin when it is cross-linked into MPs. While unable to be used for blocking heparin MP-protein interactions, we were able to use surfen to assay masses of soluble heparin in aqueous solution down to the µg/mL level.

Overall, current strategies do no effectively block heparin MPs with surfen, and further investigation would need to be carried out to render this technique viable.

APPENDIX B

THE EFFECT OF HEPARIN CELL COATINGS ON ATDC5 SPHEROID DIFFERENTIATION

B1. Introduction

In the body, heparan sulfate (HS) is attached to membrane-bound (syndecans, glypicans, betaglycans) or ECM associated (perlecan, agrin, collagen XVIII) core proteins to form HS proteoglycans [174,175]. On the cell membrane, HS acts to facilitate ligand-receptor binding, and in the ECM, HS participates in the development of morphogen gradients and is thought to protect growth factors from degradation [174,175,177,178]. Thus, the function of HS differs based on its spatial location relative to the cell surface: HS can either localize protein near the cell surface and initiating signaling, or sequester it far from the cell surface and preventing signaling [174]. In this work, we asked if heparin localization relative to the cell surface would influence cell differentiation. We hypothesized that heparin cell coatings would enhance differentiation by concentrating growth factors near the cell surface, while heparin MPs would inhibit differentiation by sequestering growth factors away from the cell surface. As shown and discussed in Chapter 5, heparin MPs do delay differentiation in ATDC5 cells. Here, we show a similar study conducted with heparin cell coatings.

Recently, cell coatings have been investigated as a means to control the cellular microenvironment [379–381]. In general, they have potential applications in conferring biological function, masking cell-surface antigens to improve cell transplantation, promoting interactions between two cell populations with coatings that interact with each

other, and controlling stem cell lineage commitment [379]. Of all applications, the coating of islet cells to mask surface antigens and thus reduce the blood-mediated inflammatory reaction after transplantation has been the most widely investigated [380,382–385]. Given its activity as an anticoagulant in the coagulation cascade, coating islets with heparin has gained interest as a means to reduce coagulation and the inflammatory reaction [383,385]. Furthermore, researchers have shown that heparin coatings applied by covalent reactions on the cell-surface have not negatively impacted islet function [383,385], and have shown that heparin coatings can attract heparin-binding proteins like VEGF [384]. Our lab has shown that heparin coatings on MSCs do not reduce cell viability or reduce innate immunomodulatory properties, and additionally can interact with growth factors to modulate cell differentiation and proliferation [195,386]. Thus, in this study we used heparin cell coatings to better understand how heparin presented at the cell surface would affect ATDC5 chondrocytic differentiation.

B2. Materials and Methods

For soluble heparin studies, AF633 tagged heparin was mixed with single cells at a 5 mg/mL concentration prior to forming spheroids as described in Section 4.2.3. For heparin cell coating studies, heparin was biotinylated using EDC/HOBt chemistry as previously described [386,387]. Heparin cell coatings were applied by a layer-by-layer technique according to previous methods [386]. Cells were incubated in 4 mM EZ-Link Sulfo-NHS-LC-Biotin (Pierce) in PBS, then 0.5 mg/mL avidin (Invitrogen) in PBS, and finally 5 mg/mL biotin-conjugated heparin in PBS for 30 minutes each at 37°C [383]. Spheroids were formed with heparin coated cells as described. Cell viability was assessed with LIVE/DEAD staining via confocal microscopy. Stacks with slices every 2 μm were

flattened using the Z-project function on Image-J. Incorporation of heparin into the cell spheroid was assessed with confocal imaging of the AF633 heparin, and images from the center of the stack are presented. H&E and Safranin-O staining as well as qPCR were conducted and analyzed as described in Section 4.2.5.

B3. Results and Discussion

B3.1 Characterization of Heparin Coated ATDC5 Spheroids

Heparin can be incorporated into cell spheroids in several different ways. First, as shown in Chapter 4, heparin MPs can be incorporated into cell spheroids, which results in highly concentrated pockets of heparin throughout the cell matrix. To obtain a more homogenous distribution of heparin throughout the ECM, and to allow interactions at the cell surface, we investigated two techniques. First, we used a heparin cell coating method [386] to coat cells prior to spheroid formation. Second, we mixed soluble heparin with single cells during spheroid formation. For both techniques, we used fluorescently tagged heparin to visualize incorporation of 5 mg/mL heparin over the course of 14 days (Figure B.1). While both groups showed bright signal for heparin at day 1, we observed a rapid decrease in fluorescent intensity by day 7 in the soluble heparin group, while the signal persisted in the heparin coating group through day 14, though at diminished intensity (Figure B.1). These results indicate that soluble heparin either diffuses out of the cell spheroid or is degraded by heparanases over the culture period, and that covalently attaching heparin to the cell surface allows maintenance of heparin in the matrix over time. Thus, for future studies, we used heparin cell coatings to investigate the presentation of heparin at the cell surface.

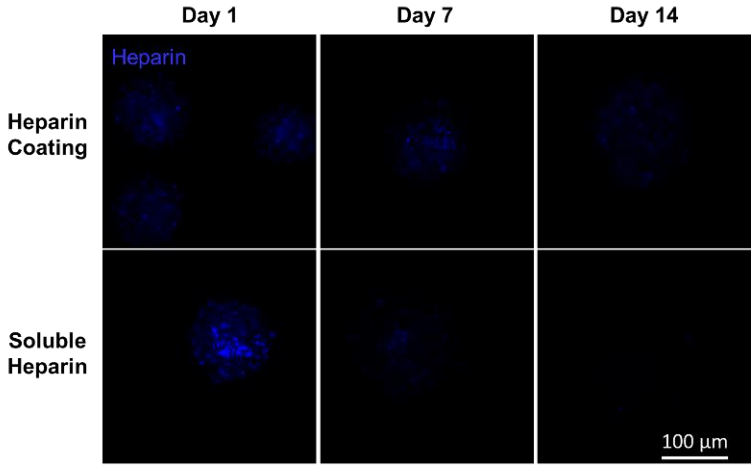

Figure B.1. Heparin (blue) was either incorporated into ATDC5 cell spheroids as a coating (top) or as soluble, unfunctionalized heparin (bottom). In coated groups, signal persisted through day 14, while in soluble groups, signal faded rapidly.

While previous results have indicated that MSCs show no decrease in viability when coated with heparin [386], we wanted to ensure that ATDC5 cells also remain viable after being coated with heparin. We found that heparin coated cell spheroids appeared viable after seven days of culture (Figure B.2). Thus, it is possible to use heparin cell coating techniques to investigate the influence of heparin located near the cell surface on cell differentiation.

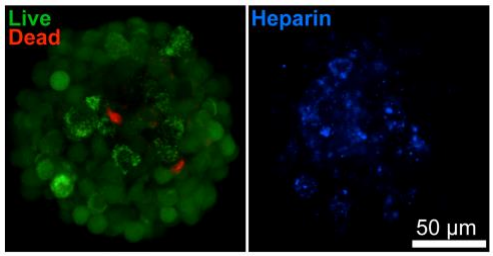

Figure B.2. Heparin coatings did not negatively impact ATDC5 cell spheroid viability after 7 days. Images courtesy of Jen Lei.

B3.2 Chondrocytic Differentiation of Heparin Coated ATDC5 Spheroids

To investigate the ability of heparin cell coatings to modulate chondrocytic differentiation, we cultured heparin coated cell spheroids for 18 days on rotary culture. We saw no differences in viability between the heparin coating group and the cell only group at day 18 (data not shown). H&E staining of spheroid sections showed no observable differences between the heparin coating group and the cell only control, and both groups increased in size over time and developed the thick border that we have found to be characteristic of ATDC5 cell spheroids (Figure B.3). Interestingly, in previous work from our lab, a rounded cell morphology was observed in heparin coated MSC aggregates, possibly because the coating influences cell packing within the aggregate [195]. The absence of this morphology in ATDC5 spheroids may be due to the rapid proliferation or matrix deposition of this cell line compared to MSCs.

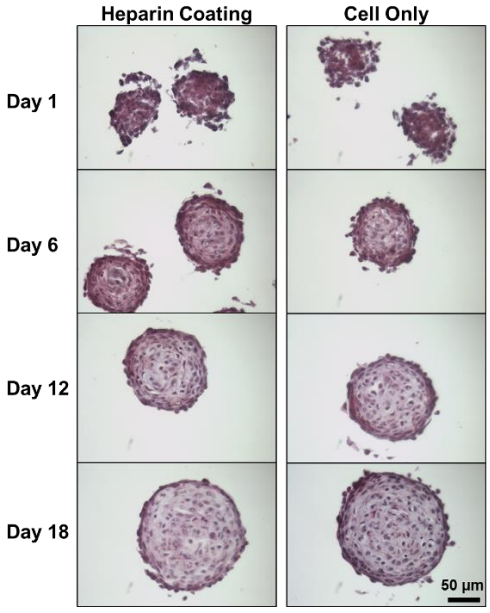

Figure B.3. H&E staining of ATDC5 spheroids with coating (left) and no coating (right) indicates no major morphological differences between groups over 18 days of culture.

To evaluate the influence of the heparin coating on differentiation, spheroids were stained with Safranin-O to assess GAG deposition. As they are composed of GAGs, heparin cell coatings could potentially be visible after staining, but were not be detected in day 1 staining (Figure B.4). This indicates that the heparin coating was at a concentration below the detection limit of the stain. At day 6, a transient increase in GAG deposition staining was observed in some of the heparin coated spheroid groups, unlike the cell only controls. However, by days 12 and 18, GAG deposition appeared similar in both groups and possibly increased in the cell only group as compared to the heparin cell coating group. Overall, it appeared the GAG deposition was not strongly affected by heparin cell coatings.

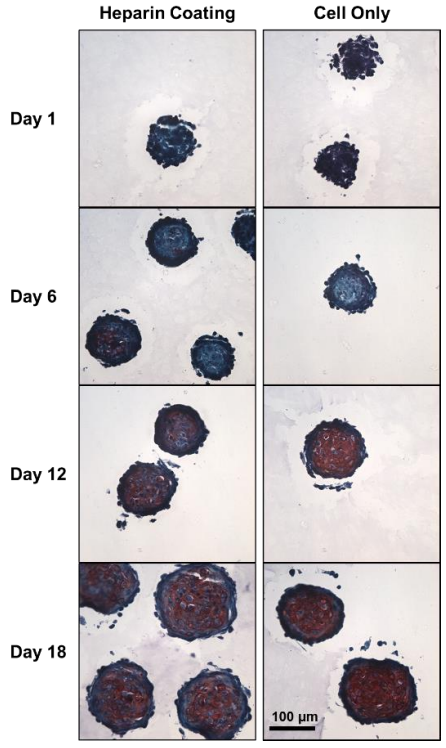

Figure B.4. Safranin-O staining of ATDC5 spheroids with coating (left) and no coating (right) indicates similar staining in all groups over time.

Gene expression was assessed for differentiation markers *collagen II*, *aggrecan*, and *collagen X*. Overall, it was observed that gene expression was similar between the two groups over the course of the experiments, with slight decreases in *aggrecan* at day 6 and *collagen X* at day 18 in the heparin cell coating group (Figure B.5). This combined with the GAG staining indicate that the heparin cell coating might induce a transient effect in ATDC5 cell differentiation, but generally did not affect differentiation.

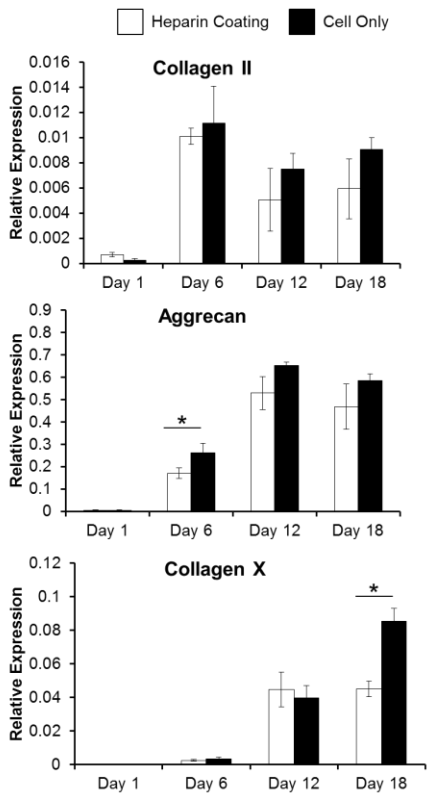

Figure B.5. Gene expression for ATDC5 spheroids with heparin coating (white) and cell only (black) for *collagen II*, *aggrecan*, and *collagen X* (*= significantly different than indicated group, $p<0.05$).

The lack of differences between the heparin coating and cell only groups may be explained by several different reasons. First, ATDC5 cells are known to proliferate rapidly, as evidenced by the increasing size of spheroids over the experimental time

course (Figure B.3), which would result in cells with reduced levels of the coating after cell division. In addition, ATDC5 cells lay down considerable amounts of GAG over time (Figure B.4), which would likely overpower the heparin cell coating except at very early timepoints. In the future, increasing the concentration of heparin coated to the cell surface could be investigated to initiate a stronger response.

In previous work, it has been observed that growth factor delivery to heparin-coated aggregates can modulate cell behavior. For example, we have seen that heparin coated MSC aggregates showed enhanced proliferation in the presence of FGF-2 [195]. Also, chondrocytic MSC differentiation was enhanced in TGFβ-1 containing media in heparin and desulfated heparin groups as compared to the cell only control [195]. Thus, both of these studies indicate that while heparin cell coatings alone do not affect differentiation, they may be able to manipulate heparin-binding growth factors in a way that modulates cell behavior. Overall, while these studies indicate that heparin cell coatings did not affect ATDC5 cells, future studies to investigate the effect of heparin presentation on growth factor delivery could be conducted with these coatings.

B4. Conclusion

These studies indicate that it is possible to coat ATDC5 cells with a heparin cell coating and maintain cell viability, and that the coating will remain in the spheroid for at least fourteen days. No changes in differentiation were observed in the heparin cell coating group, possibly because ATDC5 cells proliferate rapidly and deposit large amounts of endogenous GAG. Overall, future studies might investigate increasing the concentration of the heparin cell coating or use of the coating to modulate exogenous growth factors presentation to ATDC5 cells.

APPENDIX C

SPATIAL CONTROL OVER HEPARIN MPS IN ATDC5 SPHEROIDS

C1. Introduction

The field of tissue engineering strives to better mimic the structural complexity of native tissue in order to better mimic its function. A variety of approaches have been implemented to achieve these goals, including "top-down" and "bottom-up" engineering approaches. Top-down approaches include seeding cells into a pre-formed scaffold, in hopes that with the guidance of the scaffold's properties, the cells will rearrange and generate a tissue similar to one found in the body [388,389]. While useful at times, top-down approaches are limited by the requirement for a starting scaffold, which can reduce the number of cell-cell contacts and can provide potentially undesirable signals to the cells [390]. In bottom-up approaches, small tissue building blocks, or modules, are pieced together to make a larger tissue [388]. Modules can consist of materials laden with cells, cell sheets, or dense cell aggregates, called spheroids [388]. Spheroids are of particular interest, as these scaffold-free modules have abundant opportunity for cell-cell and cell-ECM contacts [388]. Still, spatially controlled differentiation within the spheroid can be difficult to achieve [250,263].

Recently, several studies have presented methods to achieve spatial patterning of cells and materials within cell spheroids. One study showed that microfluidic techniques could be used to generate "janus" spheroids, or spheroids with different cell types in each hemisphere [391]. Another study showed the ability to use magnetic particles to spatially orient and locate spheroids [250]. Finally, it was also shown that when BMP-4 loaded

microparticles were incorporated into only one hemisphere of an embryoid body, differentiation markers were confined to the cells in that hemisphere [263]. These studies indicate the potential to spatially modulate differentiation in cell aggregates, which would allow for further specification in modules used to build larger tissues.

As in one example mentioned above, integration of materials within cell aggregates has emerged as a method to direct cell differentiation [220,232,233,250,253,259,263]. This approach allows for homogenous delivery of biomolecules throughout the cell aggregate, which is not always possible when biomolecules are delivered to the external media due to diffusion limitations [263,315]. Thus, in these studies, we were interested in spatially modulating differentiation within the ATDC5 spheroids by localizing heparin MPs within one hemisphere of the spheroid. As described in Chapter 5, heparin MPs have been observed to delay or prevent differentiation when cultured throughout ATDC5 spheroids, indicating that they potentially could spatially modulate differentiation if localized into one hemisphere.

Thus, in this work, we developed spheroids with spatially localized MPs using a method involving pelleting of cells in agarose wells, similar to a method used in previous studies [263,389]. This method is advantageous, as it does not require the specialized equipment necessary for techniques such as microfluidics and photolithography [390]. By creating spheroids of cells that differentiate at different rates, it may be possible to develop gradients in differentiation, as observed in tissues like the growth plate [23]. These tissue modules could then be used as model systems to better understand tissue function, or eventually be translated into tissue replacements for a variety of applications.

C2. Materials and Methods

AF633 Heparin MPs were prepared as described in Section 5.2.2. ATDC5 were expanded in monolayer and cultured in spheroid culture as described Section 4.2.3, with

the following differences. Monolayer ATDC5 cells were stained with Cell Tracker Orange or Green (Invitrogen) according to the manufacturer's protocol, then lifted and pelleted in agarose wells to form 350 cell spheroids. One group of the green cells also contained AF633 tagged heparin MPs at a 6:1 MP:cell ratio. After 24 hours, orange spheroid groups were popped out of agarose wells using a wide bore pipette and added to the green MP containing and green cell only groups at a 2:1 orange spheroid:green spheroid ratio. Spheroids were incubated for an additional 24 hours to allow merging and then popped out and cultured in mineralization media on rotary culture.

C3. Results and Discussion

Several methods were attempted in order to make spatially organized spheroids. For one set of studies, 350 cell spheroids were formed for 6 hours and cell in suspension were added on top of spheroids. This method did not result in spatial separation of the two layers, likely due to mixing of cell in spheroids that were not fully formed. Thus, a 24 hour incubation to fully form spheroids was chosen. In addition, the ratios of spheroids on top and on bottom were varied and included 2:1, 1:1 and 1:2 ratios. A 2:1 ratio of spheroids on top compared to those on bottom resulted in the most efficient formation of spatially organized spheroids (only 2:1 data shown).

Immediately after formation, spatially organized spheroids showed separation of the two distinct cell populations: green stained cells with heparin MPs throughout the matrix and red/orange stained cells with no MPs (Figure C.1, Day 1). These results were encouraging, as they indicated that heparin MPs could be spatially confined to one hemisphere in cell spheroids. However, after six days in culture, cell populations and

MPs had mixed, resulting in spheroids with cells and MPs evenly spread throughout the matrix (Figure C.1, Day 6). As the goal for this work was to evaluate the possibility of spatially controlling differentiation, these results indicated that the ATDC5 cell line is not the optimal cell type for these studies.

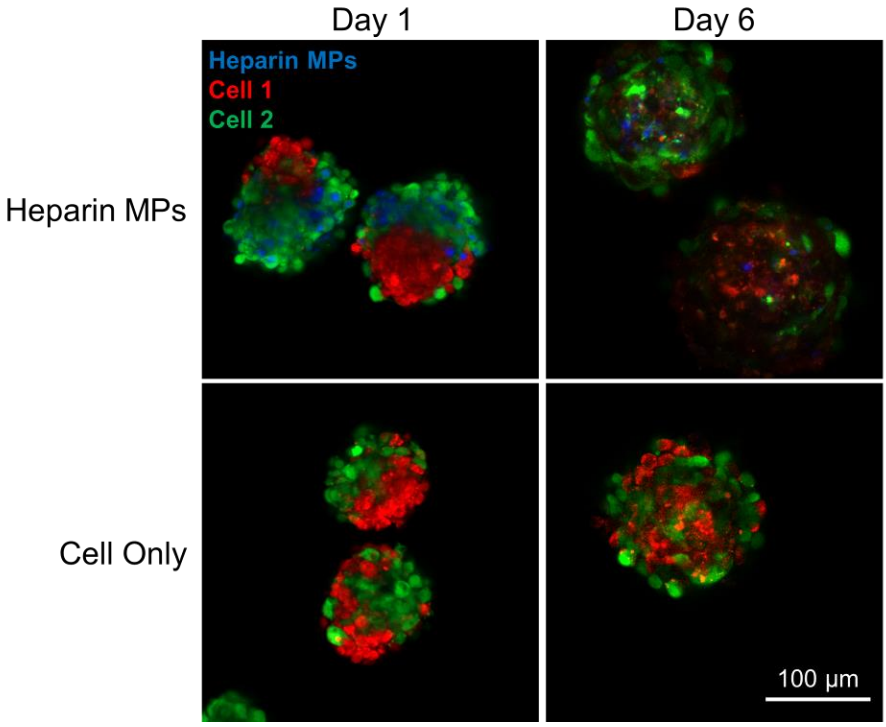

Figure C.1. Spatially organized cell spheroids at day 1 and day 6. Heparin MPs are shown in blue, cell population 1in red, and cell population 2 in green.

The ATDC5 cell line is a cancer cell line, which allows ATDC5 cells to grow quickly. They also deposit substantial amounts of ECM molecules such as GAG and collagen II [304,305,308–313], which likely results in cell re-arrangement. This indicates that spatial organization may not be possible in ATDC5 cell spheroids due to characteristics specific to its cell type. Thus, the application of this technique to other cell types that do not proliferate as quickly or lay down as much matrix may be a possible means to gain spatial control over cellular differentiation.

C4. Conclusion

A technique to spatially control cells within spheroids was developed by combining two populations of pre-formed spheroids. This technique resulted in spatial separation in ATDC5 cell spheroids at early timepoints and confinement of heparin MPs to one hemisphere of the spheroids. However, spatial separation was lost after six days in culture, likely due to the high rate of ATDC5 cell proliferation and matrix deposition. Overall, this technique allows for at least initial spatial separation and may be more applicable in other cell types with lower proliferative capacity.

APPENDIX D

HEPARIN MPS TO MODULATE OSTEOGENIC DIFFERENTIATION IN MC3T3 CELLS

D1. Introduction

Craniosynostosis involves the premature ossification of one or more cranial vault sutures [207,208]. Surgical intervention is currently the only treatment choice, and involves surgical removal of calvarial bones, which are then reshaped and reattached. Unfortunately, even after surgery, resynostosis can still occur due to abnormally high osteogenic potential [207]. Antibodies and other protein inhibitors against osteogenic proteins such as BMPs and TGFβs have been applied after surgery in animal models to prevent resynostosis, but have had only partial success [209,210,334], likely due to the short half-life of these molecules *in vivo.* Thus, we were interested in utilizing heparin MPs as a means to sequester osteogenic growth factors to prevent resynostosis. As a proof-of-principle study, the ability of heparin MPs to modulate the differentiation of MC3T3-E1 cells, a newborn mouse calvarial-osteoblast cell line known to undergo osteoblastic differentiation, was evaluated [392,393].

D.2 Materials and Methods

D.2.1 MC3T3 Cell Culture

MC3T3 cells were expanded in maintenance media (αMEM, 2 mM L-glutamine, 500 IU Penicillin, 500 µg/mL Streptomycin, and 10% FBS (Atlanta Biologics)) and experiments were conducted in differentiation media (maintenance media plus 10 mM

sodium β-glycerophosphate pentahydrate (Alfa Aesar) and 50 µg/ml L-ascorbic acid -2-phosphate sequimmagnesium salt hydrate (Sigma-Aldrich)). Cells were plated at 5000 cells/cm^2 in a 12-well plate and cultured in maintenance media until they reached confluence (3 days). Cells were then switched to differentiation media and treatment groups were added. Heparin MPs were added at 3.28 mg/transwell. Cells were fed every two days.

D.2.2 qPCR and Gene Expression Analysis

Analysis of gene expression was carried out using qPCR and normalized to the house-keeping gene *RSP-18*, as described in Section 4.2.4. Sequences for *RUNX2* and *Collagen I* are listed below:

Table D.1 National Library of Medicine accession number and primer sequences for target genes in qPCR

Target Gene	NML Accession #	Sequence
RUNX2	NM_009820	F-CTCACAAACAACCACAGAACCAC R-TGCAGCCTTAAATGACTCGGTTG
Collagen I	NM_007742.4	F- CTCCCAGAACATCACCTATCACT R-GGGAGGTCTTGGTGGTTTTGTATTC

D.2.3 ALP Activity and DNA Content

Cell lysis was carried out in a similar fashion to the process described in Section 4.2.4 except that cells were incubated in 0.1% Triton-X100. ALP activity was assessed as described in Section 5.2.5 and DNA content as described in Section 4.2.4.

D.2.4 Statistical Analysis

Statistical analysis was carried out as described in Section 4.2.7.

D.3 Results and Discussion

In order to determine if heparin MPs could potentially be used as a therapeutic materials for craniosynostosis, osteoblastic MC3T3 cells were cultured for fourteen days in transwell with heparin MPs. Gene expression for osteoblastic markers *Collagen I* and *RUNX2* were assessed and no differences in gene expression were observed at days 7 or 14 (Figure D.1). ALP expression was assessed and then normalized to DNA content at days 7 and 14, and was found to be increased in heparin MP groups compared to cell controls (Figure D.1). Overall, these results indicate that heparin MPs have little effect on MC3T3 cells, and as ALP activity is increased in heparin MP groups, it is possible that differentiation is actually accelerated in the presence of heparin MPs. Additional outcome measures, such as assessment of matrix mineralization and analyses at later time points, could provide more insight into how heparin MPs modulate MC3T3 cell differentiation. It is likely that heparin MPs affect different cell types in different ways, depending upon the growth factors present in the cellular microenvironment. Further analyses would need to be conducted to determine which proteins were bound by heparin MPs in MC3T3 cell culture as compared to ATDC5 cell culture, which could help elucidate reasons for differences observed. In addition, previous studies have indicated that the ability of heparan sulfate to enhance healing in a critical sized rat femur defect was dose dependent [197], suggesting that additional dosing studies may be required to achieve desired results. Overall, these results indicate that more studies need to be conducted to understand how heparin MPs can modulate other differentiation processes *in vitro*.

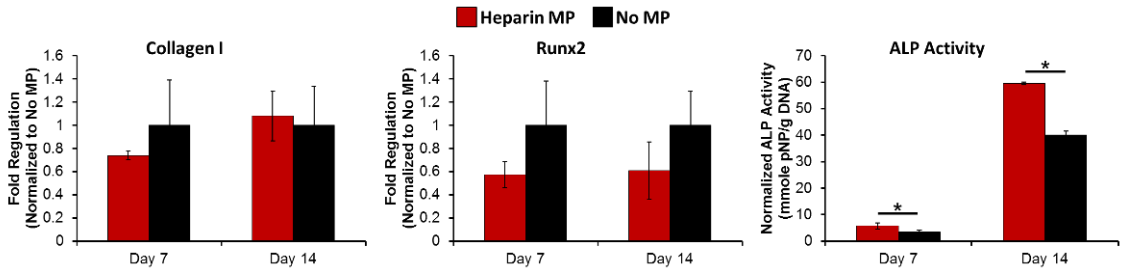

Figure D.1 Osteoblastic MC3T3 cells were cultured with or without heparin MPs in transwell for fourteen days and assessed for osteoblastic markers *collagen I* and *RUNX2*. ALP activity was measured and normalized to DNA content (*=significantly different than indicated group, $p \leq 0.05$).

APPENDIX E

SUPPLMENTARY FIGURES

E.1 Supplementary Figures for Chapter 3

All methods, results, and discussion for these figures are included in Chapter 3.

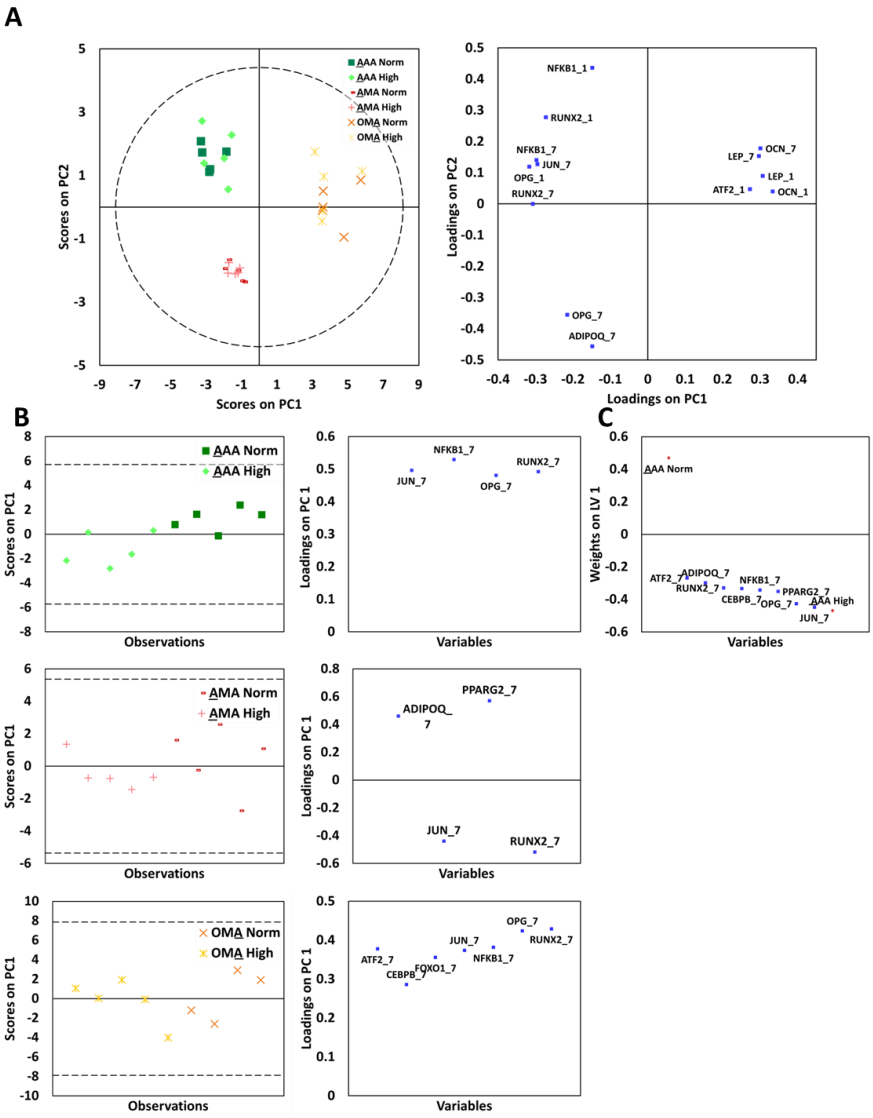

Figure E.1. Principal Component Analysis (PCA) was conducted to determine if difference in gene expression resulted in clustering of culture configuration or glucose levels prior to further assigning of classes for PLS-DA. (A) PCA for the entire adipocyte gene expression data set yielded two principal components that discriminated adipocytes by culture configuration (R^2X = 0.84, Q^2 = 0.74). (B) PCA score and loading plots for AAA (R^2X = 0.74, Q^2 = 0.45), AMA (R^2X = 0.65, Q^2 = 0.25), and OMA (R^2X = 0.74, Q^2

= 0.56) cultures yielded one PC. Observed clustering by glucose level warranted further investigated with PLS-DA for AAA. (C) PLS-DA weight plot for AAA model in Figure 3.2C.

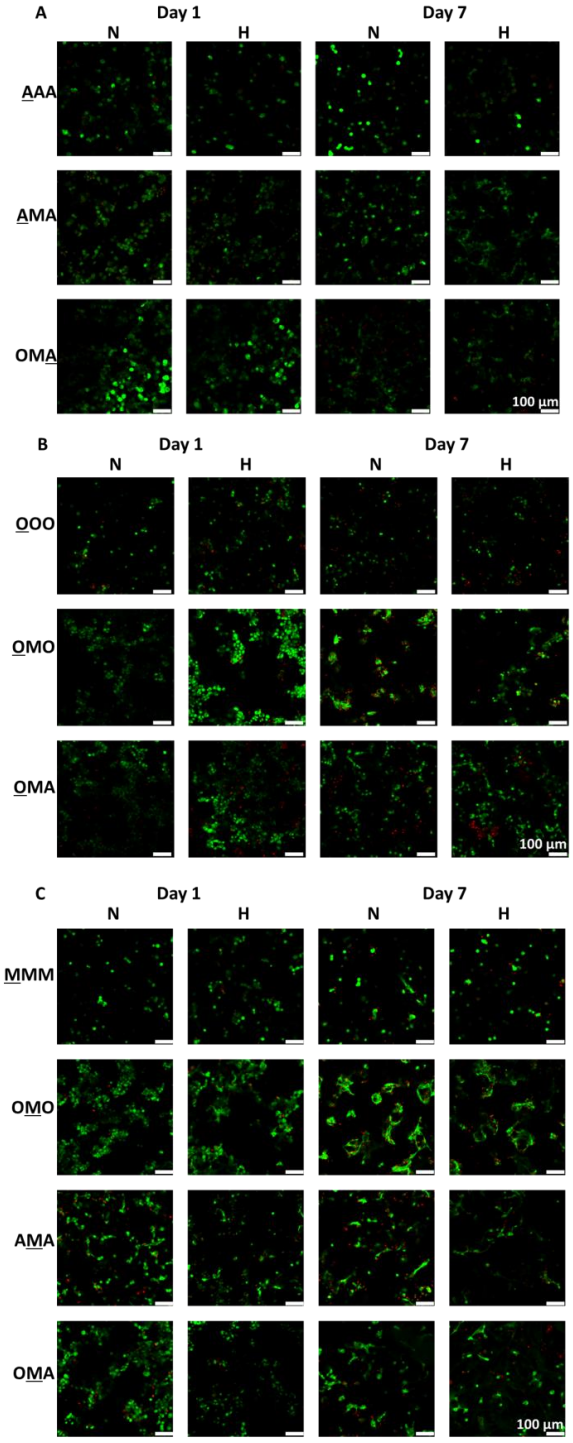

Figure E.2. Images were captured using confocal microscopy of calcein (green, live) and ethidium bromide (red, dead) staining in each experimental condition. Merged

representative images are presented here. Representative images of adipocytes (A), osteoblasts (B), and MSCs (C) on days 1 and 7 at normal and high glucose conditions in each culture configuration.

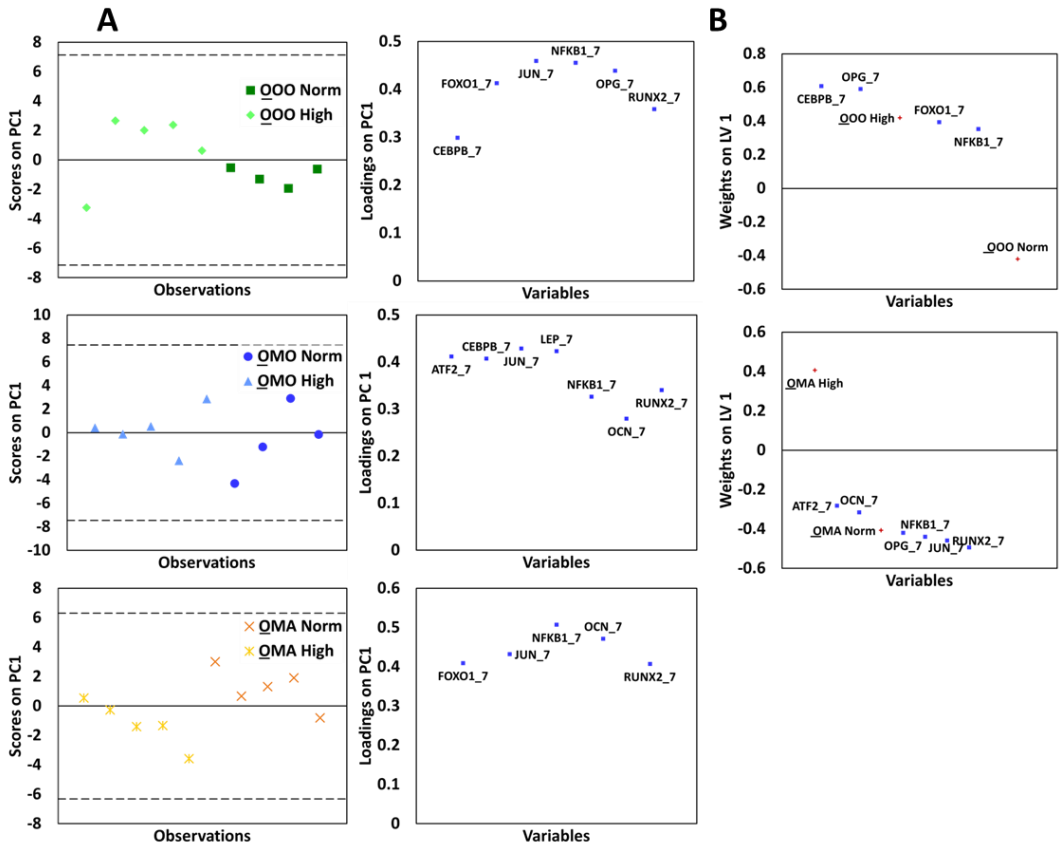

Figure E.3. PCA was conducted within culture configuration datasets to determine if difference in gene expression resulted in clustering glucose levels prior to further assigning of classes for PLS-DA. (A) PCA score and loading plots for OOO (R^2X = 0.71, Q^2 = 0.52), OMO (R^2X = 0.72, Q^2 = 0.51), and OMA (R^2X = 0.72, Q^2 = 0.41) cultures yielded one PC. Observed clustering by glucose level warranted further investigated with PLS-DA for OOO and OMA configuration for classes assigned according to glucose level. (B) PLS-DA weight plot for OOO and OMA models in Figure 3.4C.

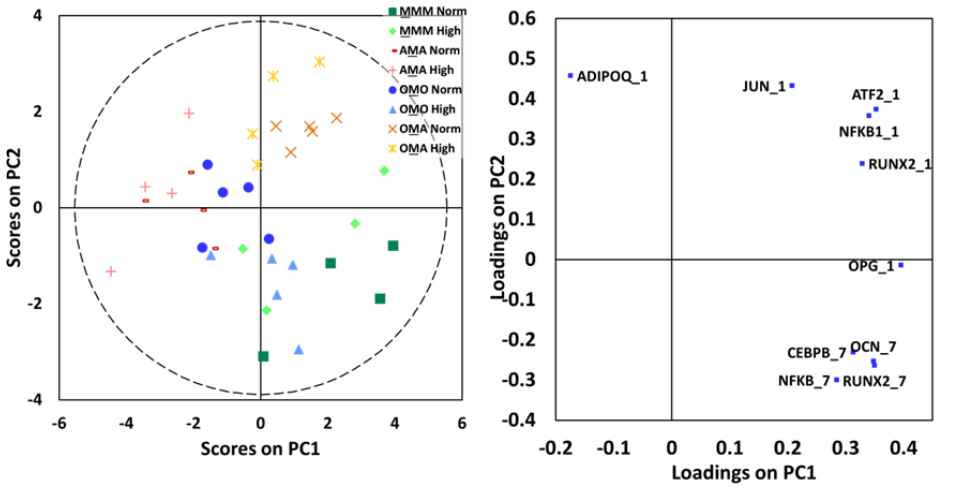

Figure E.4. PCA was conducted to determine if difference in gene expression resulted in clustering of culture configuration or glucose levels prior to further assigning of classes for PLS-DA. PCA for the entire MSC gene expression data set yielded two principal components and clustering by culture configuration (R^2X = 0.66, Q^2 = 0.36).

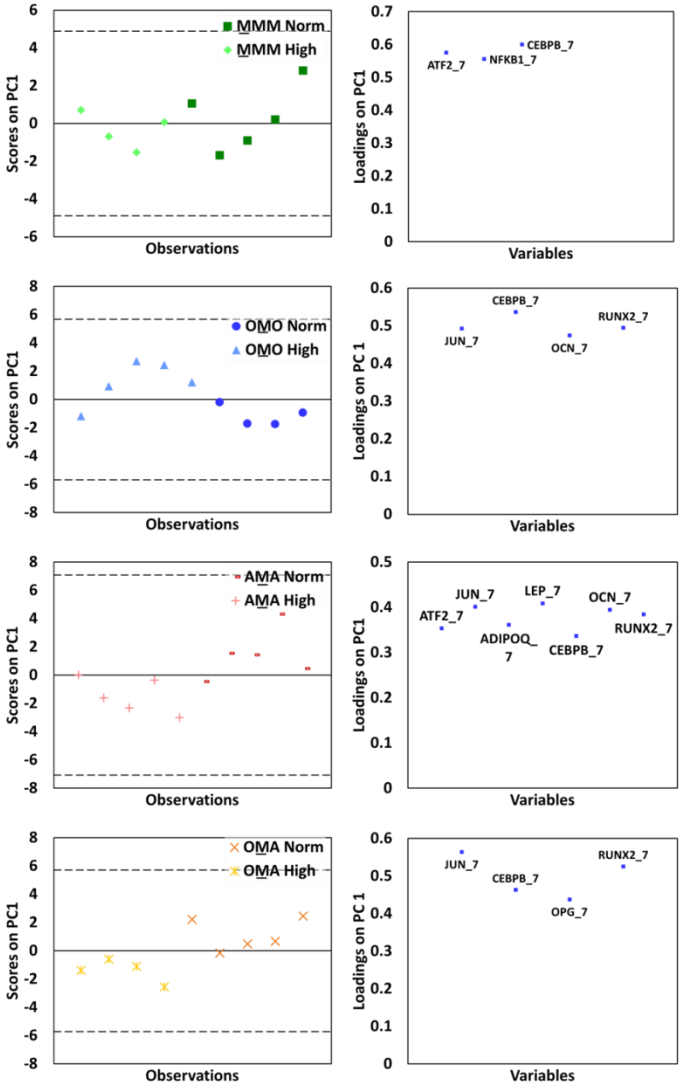

Figure E.5 PCA was conducted within culture configuration datasets to determine if difference in gene expression resulted in clustering glucose levels prior to further assigning of classes for PLS-DA. PCA score and loading plots for MMM (R^2X = 0.66, Q^2 = -0.1), OMO (R^2X = 0.73, Q^2 = 0.43), AMA (R^2X = 0.65, Q^2 = 0.42), and OMA (R^2X = 0.68, Q^2 = 0.02) cultures yielded one PC.

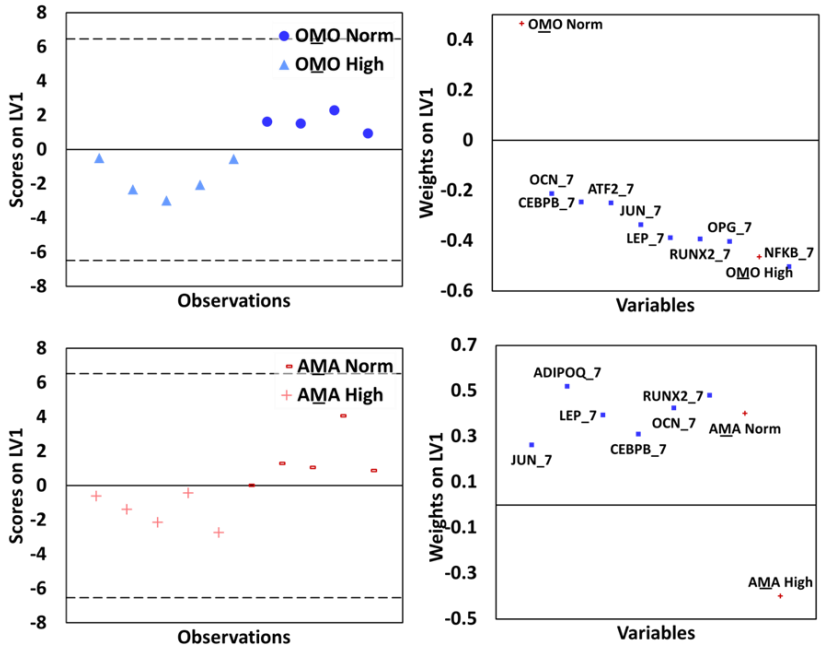

Figure E.6. Observed clustering by glucose level warranted further investigated with PLS-DA for OMO and AMA culture configurations with classes assigned according to glucose level. PLS-DA score and weight plot for OMO (R^2Y = 0.82, Q^2 = 0.73) and AMA (R^2Y = 0.62, Q^2 = 0.41).

E.2 Gene Expression Profiles for ATDC5 Cells in Monolayer and Spheroid Culture

E.2.1 Materials and Methods

ATDC5 cells were cultured in monolayer in 12 well plates for 22 days or in spheroids for 18 days in mineralization media. Further details can be found in Section 4.2.3. Analysis of gene expression was carried out using qPCR and normalized to the house-keeping gene *RSP-18*, as described in Section 4.2.4. Sequences for *aggrecan*, *collagen II*, and *collagen X* can be found in Section 4.2.4, and the sequence for *Ihh* is listed below:

Table E.1 National Library of Medicine accession number and primer sequences for target genes in qPCR in ATDC5 monolayer study

Target Gene	NML Accession #	Sequence
Ihh	NM_010544	F- CCCCGAACCTTCATCTTGGT R- GCCCCGAGAAACATTGGAGT

Statistical analysis is described in Section 4.2.7.

E.2.2 Results and Discussion

In monolayer culture, low levels of gene expression for all genes were observed at day 1, with increases at day 6 and a maximum expression level at day 12. For *Ihh* and *aggrecan*, decreases were observed by day 18, and for *collagen II* and *X*, by day 22 (Figure E.7). Overall, this upregulation between days 6-12 and gradual decrease of gene expression markers at longer times in culture is similar to what has been observed in past experiments [309].

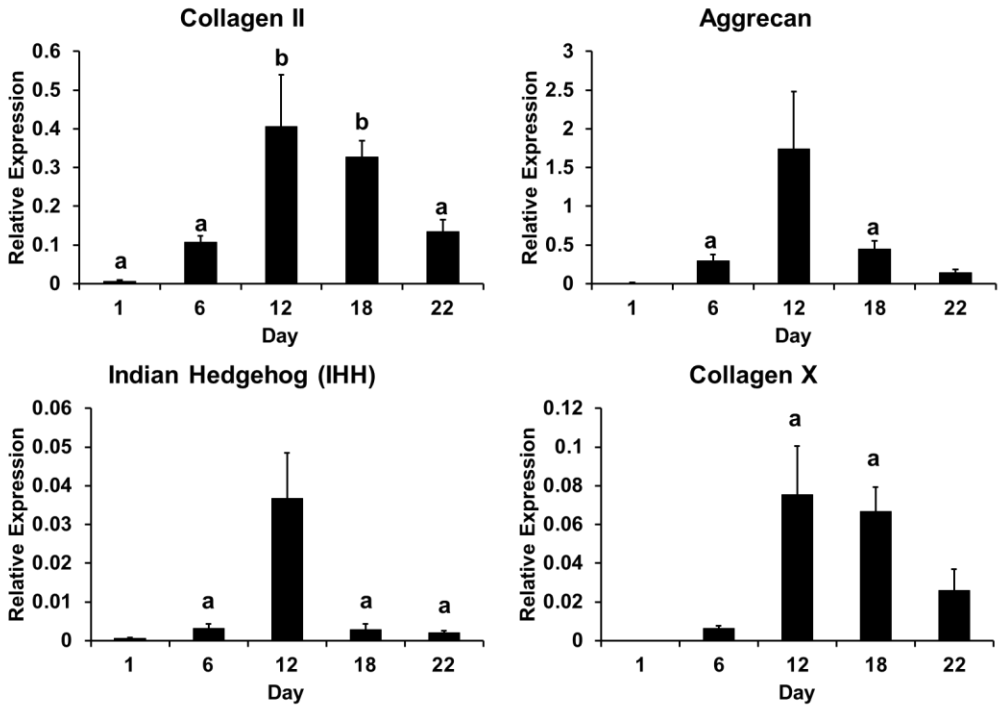

Figure E7. Gene expression of *collagen II*, *aggrecan*, *Ihh*, and *collagen X* for ATDC5 cells in monolayer culture for 22 days. Each gene is normalized to the *RSP-18*

housekeeping gene at each timepoint (a similar letter = not significantly different, $p<0.05$).

In spheroid culture, low levels of gene expression for all genes were observed at day 1, with increases at day 6 for *collagen II*, *aggrecan*, and *Ihh*, and increases at day 12 for *collagen X*. A maximum expression level for *collagen II* was observed at day 12, while *aggrecan*, *Ihh*, and *collagen X* continued increasing throughout the course of culture (Figure E.8). Overall, ATDC5 gene expression in spheroid culture was slightly delayed as compared to gene expression in monolayer culture, and is similar to what has been observed in ATDC5 aggregate culture in previous experiments [305].

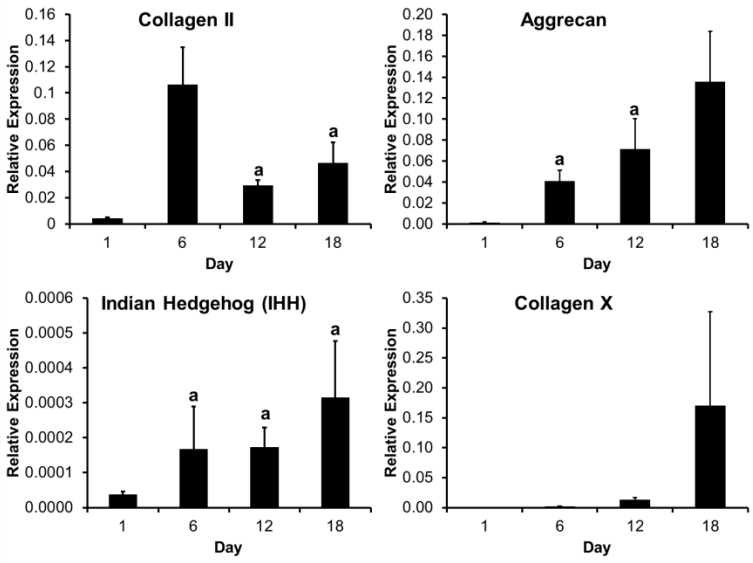

Figure E8. Gene expression of *coll II*, *aggrecan*, *Ihh*, and *collagen X* for ATDC5 cells in spheroid culture for 18 days. Each gene is normalized to the *RSP-18* housekeeping gene at each timepoint (a similar letter = not significantly different, $p<0.05$).

E.3 Additional Bioactivity Data for Pre-Loaded Core-Shell MPs

E.3.1 Materials and Methods

Microparticles were prepared and sterilized as described in Sections 5.2.4 and 5.2.5. MPs were incubated for 1.5 days prior to being added to cells for pre-degradation.

This allowed MP shell degradation to occur during the three day cell assay (while degradation occurs throughout the entire time course, the majority of the PEG-based MP degradation occurred between days 3-6 for these MPs; Figure 5.1C). All core-shell and heparin MP groups had 0.02 mg of heparin and the degradable PEG-based control group had the same number of MPs as the core-shell group. Cells were cultured for 3 days and then media/MPs were removed. C2C12 cell culture and ALP assay was conducted as described in Section 5.2.5.

E.3.2 Results and Discussion

Degradable core-shell and core shell microparticles induced a lower C2C12 ALP activity than the soluble control (27.6+14.6% and 12.9+1.6% of soluble control, respectively; Figure E9). No signal was observed for groups without BMP-2, and an elevated DNA content was observed in all groups subjected to BMP-2 as compared to those without BMP-2. No trends in DNA content were observed between groups.

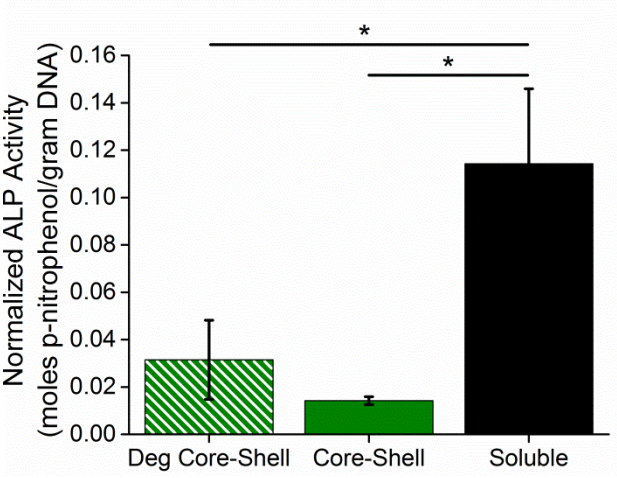

Figure E9. Degradable (Deg) core-shell MPs modulate loaded heparin MP delivery to cells. Normalized ALP activity for deg core-shell, core-shell, and soluble BMP-2 groups (non-loaded groups showed no signal; *=significantly different from soluble group, $p<0.05$, $n=4$).

Taken together with results presented in Chapter 5, these results suggest that degradable core-shell MPs have the potential to temporally modulate protein presentation to cells. While two days of pre-degradation did not result in sufficient degradation to initiate a cell response (suggesting that many heparin MPs were still encapsulated in PEG shells) (Figure E9), three days of pre-degradation was sufficient to initiate a cell response (suggesting that many heparin MPs had been released from PEG shells) (Figure 5.5). In the future, assays that can capture immediate changes in cell behavior in response to protein presentation could better highlight the potential of these MPs to temporally modulate protein presentation.

E.4 Soluble Heparin Release from Non-Degradable 100% Heparin MAm MPs

E.4.1 Materials and Methods

Heparin MAm MPs were formed and sterilized as described in Section 4.2.2. Heparin MPs were incubated in a PBS solution at a 0.2 mg/mL concentration at 37°C on a shaker plate. Supernatant was removed and saved for analysis at days 7, 14, and 21. Supernatant was replaced with fresh PBS at each timepoint. The surfen assay (described in Section A.4) was used to determine the total mass of soluble heparin released into the supernatant at each timepoint.

E.4.2 Results and Discussion

Over the course of 21 days, heparin MPs lost less than 3% of their total mass to heparin shedding. This indicates that for the non-degradable 100% heparin MPs used in this work, very little heparin was released throughout the experiments conducted. In cell

studies, daily media changes would have likely removed most of the released heparin, possibly before it could interact with cells. Thus, it is unlikely that soluble heparin released from 100% heparin MPs was a major contributor to resulting cell phenotype.

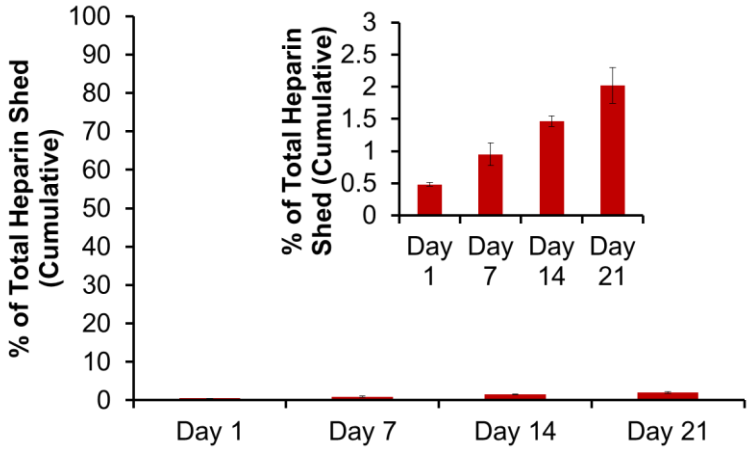

Figure E10. Percentage of total heparin in MPs shed over the course of 21 days. Less than 3% of total heparin in the heparin MPs was shed over the timecourse.

APPENDIX F

ADDITIONAL INFORMATION

F.1. Assumptions for Protein Release Requirements for Heparin-PEG MPs

The assumptions listed here describe why 20 µg of protein was used as a lower cut-off to determine if subsequent assays should be conducted on protein released from heparin-PEG MPs:

1. ELISA assays have the lowest detection limits of the assays considered (pg/mL as compared to ng/mL for western blots and ng-µg/mL for mass spectrometry).

2. Based on the number of ATDC5 cells plated in these experiments, the doubling time of these cells, and previous reports of protein secreted on a per cell and time basis, an estimated 10 ng of protein could be released by ATDC5 cells in a 24 hour period [311–313].

3. Based on the concentration of FBS in the media used for these experiments and previous reports about concentration of protein in FBS [327], about 5000 µg protein from FBS would be in each cell culture well.

4. Assuming that about 40% of the protein in serum is heparin-binding (based on break-down of serum components and which of those are known to bind heparin [175,180,326,327,330,332]), about 2000 µg of serum proteins could be bound by heparin MPs.

5. Estimating that 10 ng of protein is secreted by cells and all of this protein can bind to heparin MPs, then 0.0005% of the protein bound to heparin MPs would be cell-secreted vs. from the serum:

$$\frac{\mathbf{0.01}\ \mu \boldsymbol{g\ cell\ secreted\ proteins}}{\mathbf{2000}\ \mu \boldsymbol{g\ serum\ proteins}} = \mathbf{0.000005}, \boldsymbol{or}\ \mathbf{0.0005}\%$$

6. To enter a range detectable by ELISA (~100 pg/mL) an absolute minimum of 20 µg of total protein is required:

$$\mathbf{0.000005}(\boldsymbol{x\ concentration}) = \mathbf{100}\frac{\boldsymbol{pg}}{\boldsymbol{mL}}, \boldsymbol{x} = \mathbf{20}\ \frac{\mu \boldsymbol{g}}{\boldsymbol{mL}}$$

7. This estimate is the best-case scenario estimate for detection by ELISA. 100-1000s of µg would be required for western blots or mass spectrometry.

F.2 Methods for Relamination Study (Figure 7.1)

PEG-diacrylate (PEG-DA, M_n = 8kDa), and PEG-RGD (M_n = 3.4kDa) were synthesized as described in Section 3.2.2. The collagenase-sensitive glue was synthesized by reacting peptides (GGGLGPAGGK) with acrl-PEG-succinimidyl valerate (Acrl-PEG-SVA; M_n ~3.4 kDa) as described in Section 3.2.2. Tri-laminates were prepared from PEG-DA and PEG-RGD (cell-seeded gels only) solutions with 50 x 10^6 cells/mL human MSCs, passage 3. Using serial photolithography, a collagenase-sensitive glue was patterned between two cell-laden PEG-DA layers. After 1 day, laminates were degraded (collagenase, 1100 U/mL), immediately soaked in fresh media for 1 hour, and re-laminated with collagenase-sensitive glue. Cell viability at 1 day after initial fabrication

and 3 days after re-lamination (n=3) was observed using LIVE/DEAD stain. Viability was quantified using ImageJ and stats were run as described Sections 3.2.4 and 3.2.8.

REFERENCES

[1] D. Seliktar, Designing Cell-Compatible Hydrogels for Biomedical Applications, Science (80-.). 336 (2012) 1124–1128. doi:10.1126/science.1214804.

[2] M.W. Tibbitt, K.S. Anseth, Hydrogels as extracellular matrix mimics for 3D cell culture, Biotechnol. Bioeng. 103 (2009) 655–663. doi:10.1002/bit.22361.

[3] J.A. Burdick, W.L. Murphy, Moving from static to dynamic complexity in hydrogel design, Nat. Commun. 3 (2012) 1269. doi:10.1038/ncomms2271.

[4] J.W. Haycock, 3D Cell Culture: A Review of Current Approaches and Techniques, in: J.W. Haycock (Ed.), 3D Cell Cult. Methods Protoc. Methods Mol. Biol., Humana Press, Totowa, NJ, 2011: p. Chapter 1. doi:10.1007/978-1-60761-984-0.

[5] A. Astashkina, B. Mann, D.W. Grainger, A critical evaluation of in vitro cell culture models for high-throughput drug screening and toxicity., Pharmacol. Ther. 134 (2012) 82–106. doi:10.1016/j.pharmthera.2012.01.001.

[6] N. Huebsch, P.R. Arany, A.S. Mao, D. Shvartsman, O.A. Ali, S.A. Bencherif, J. Rivera-feliciano, D.J. Mooney, Harnessing Traction-Mediated Manipulation of the Cell-Matrix Interface to Control Stem Cell Fate, Nat. Mater. 9 (2010) 518–526. doi:10.1038/nmat2732.Harnessing.

[7] A. Nyga, U. Cheema, M. Loizidou, 3D tumour models: Novel in vitro approaches to cancer studies, J. Cell Commun. Signal. 5 (2011) 239–248. doi:10.1007/s12079-011-0132-4.

[8] L.G. Griffith, M.A. Swartz, Capturing complex 3D tissue physiology in vitro., Nat. Rev. Mol. Cell Biol. 7 (2006) 211–24. doi:10.1038/nrm1858.

[9] S.E. Sakiyama-Elbert, Incorporation of heparin into biomaterials., Acta Biomater. 10 (2014) 1581–7. doi:10.1016/j.actbio.2013.08.045.

[10] K.Y. Lee, S.H. Yuk, Polymeric protein delivery systems, Prog. Polym. Sci. 32 (2007) 669–697. doi:10.1016/j.progpolymsci.2007.04.001.

[11] C.-C. Lin, A.T. Metters, Hydrogels in controlled release formulations: network design and mathematical modeling., Adv. Drug Deliv. Rev. 58 (2006) 1379–408. doi:10.1016/j.addr.2006.09.004.

[12] Y. Qiu, K. Park, Environment-sensitive hydrogels for drug delivery, Adv. Drug Deliv. Rev. 53 (2001) 321–339. doi:10.1016/S0169-409X(01)00203-4.

[13] C.J. Kirkpatrick, S. Fuchs, R.E. Unger, Co-culture systems for vascularization--learning from nature., Adv. Drug Deliv. Rev. 63 (2011) 291–9. doi:10.1016/j.addr.2011.01.009.

[14] D. Jing, A.V. Fonseca, N. Alakel, F.A. Fierro, K. Muller, M. Bornhauser, G. Ehninger, D. Corbeil, R. Ordemann, Hematopoietic stem cells in co-culture with mesenchymal stromal cells -modeling the niche compartments in vitro, Haematologica. 95 (2010) 542–550. doi:10.3324/haematol.2009.010736.

[15] R.N.B. Bhandari, L.A. Riccalton, A.L. Lewis, J.R. Fry, A.H. Hammond, S.J.B. Tendler, K.M. Shakesheff, Liver Tissue Engineering: A Role for Co-culture Systems in Modifying Hepatocyte Function and Viability, Tissue Eng. 7 (2001) 345–357. doi:10.1089/10763270152044206.

[16] G. Chan, D.J. Mooney, New materials for tissue engineering: towards greater control over the biological response., Trends Biotechnol. 26 (2008) 382–92. doi:10.1016/j.tibtech.2008.03.011.

[17] K.J. Suchacki, W.P. Cawthorn, C.J. Rosen, Bone marrow adipose tissue: formation, function and regulation., Curr. Opin. Pharmacol. 28 (2016) 50–56. doi:10.1016/j.coph.2016.03.001.
[18] C.J. Rosen, C. Ackert-Bicknell, J.P. Rodriguez, A.M. Pino, Marrow Fat and the Bone Microenvironment: Developmental, Functional, and Pathological Implications Clifford, Crit Rev Eukaryot Gene Expr. 19 (2009) 109–124. http://linkinghub.elsevier.com/retrieve/pii/S088915910800264X.
[19] K. Wongdee, N. Charoenphandhu, Osteoporosis in diabetes mellitus: Possible cellular and molecular mechanisms., World J. Diabetes. 2 (2011) 41–8. doi:10.4239/wjd.v2.i3.41.
[20] S. Kurra, E. Siris, Diabetes and bone health: the relationship between diabetes and osteoporosis-associated fractures., Diabetes. Metab. Res. Rev. 27 (2011) 430–5. doi:10.1002/dmrr.1197.
[21] D. Merlotti, L. Gennari, F. Dotta, D. Lauro, R. Nuti, Mechanisms of impaired bone strength in type 1 and 2 diabetes., Nutr. Metab. Cardiovasc. Dis. 20 (2010) 683–90. doi:10.1016/j.numecd.2010.07.008.
[22] S. Muruganandan, a a Roman, C.J. Sinal, Adipocyte differentiation of bone marrow-derived mesenchymal stem cells: cross talk with the osteoblastogenic program., Cell. Mol. Life Sci. 66 (2009) 236–53. doi:10.1007/s00018-008-8429-z.
[23] H.M. Kronenberg, Developmental regulation of the growth plate., Nature. 423 (2003) 332–6. doi:10.1038/nature01657.
[24] C. Brochhausen, M. Lehmann, S. Halstenberg, A. Meurer, G. Klaus, C.J. Kirkpatrick, Signalling molecules and growth factors for tissue engineering of cartilage-what can we learn from the growth plate?, J. Tissue Eng. Regen. Med. 3 (2009) 416–29. doi:10.1002/term.192.
[25] P.C. Billings, M. Pacifici, Interactions of signaling proteins, growth factors and other proteins with heparan sulfate: mechanisms and mysteries, Connect. Tissue Res. 56 (2015) 272–280. doi:10.3109/03008207.2015.1045066.
[26] T. Miller, M.C. Goude, T.C. McDevitt, J.S. Temenoff, Molecular engineering of glycosaminoglycan chemistry for biomolecule delivery., Acta Biomater. 10 (2014) 1705–19. doi:10.1016/j.actbio.2013.09.039.
[27] L.M. Weber, C.G. Lopez, K.S. Anseth, Effects of PEG hydrogel crosslinking density on protein diffusion and encapsulated islet survival and function, J. Biomed. Mater. Res. Part A. 90A (2009) 720–729. doi:10.1002/jbm.a.32134.
[28] J.L. Ifkovits, J. a Burdick, Review: photopolymerizable and degradable biomaterials for tissue engineering applications., Tissue Eng. 13 (2007) 2369–2385. doi:10.1089/ten.2007.0093.
[29] P. Bajaj, R.M. Schweller, A. Khademhosseini, J.L. West, R. Bashir, 3D Biofabrication Strategies for Tissue Engineering and Regenerative Medicine., Annu. Rev. Biomed. Eng. 16 (2014) 247–76. doi:10.1146/annurev-bioeng-071813-105155.
[30] J.J. Bara, R.G. Richards, M. Alini, M.J. Stoddart, Concise review: bone marrow-derived mesenchymal stem cells change phenotype following in vitro culture: implications for basic research and the clinic., Stem Cells. 32 (2014) 1713–23. doi:10.1002/stem.1649.
[31] N. Di Maggio, E. Piccinini, M. Jaworski, A. Trumpp, D.J. Wendt, I. Martin,

Toward modeling the bone marrow niche using scaffold-based 3D culture systems., Biomaterials. 32 (2011) 321–9. doi:10.1016/j.biomaterials.2010.09.041.
[32] T.M. Hammoudi, C.A. Rivet, M.L. Kemp, H. Lu, J.S. Temenoff, Three-dimensional in vitro tri-culture platform to investigate effects of crosstalk between mesenchymal stem cells, osteoblasts, and adipocytes., Tissue Eng. Part A. 18 (2012) 1686–97. doi:10.1089/ten.TEA.2011.0691.
[33] T.M. Hammoudi, H. Lu, J.S. Temenoff, Long-Term Spatially Defined Coculture Within Three-Dimensional Photopatterned Hydrogels, Tissue Eng. Part C Methods. 16 (2010) 1621–1628. doi:10.1089/ten.tec.2010.0146.
[34] C.J. Rosen, M.L. Bouxsein, Mechanisms of disease: is osteoporosis the obesity of bone?, Nat. Clin. Pract. Rheumatol. 2 (2006) 35–43. doi:10.1038/ncprheum0070.
[35] N. Urao, M. Ushio-Fukai, Redox regulation of stem/progenitor cells and bone marrow niche, Free Radic. Biol. Med. 54 (2013) 26–39. doi:10.1016/j.freeradbiomed.2012.10.532.
[36] F. Tortelli, R. Cancedda, Three-dimensional cultures of osteogenic and chondrogenic cells: A tissue engineering approach to mimic bone and cartilage in vitro, Eur. Cells Mater. 17 (2009) 1–14. doi:19579210.
[37] R.A. Somoza, J.F. Welter, D. Correa, A.I. Caplan, Chondrogenic Differentiation of Mesenchymal Stem Cells: Challenges and Unfulfilled Expectations, Tissue Eng. Part B Rev. 20 (2014) 596–608. doi:10.1089/ten.teb.2013.0771.
[38] R. Jin, L.S. Moreira Teixeira, P.J. Dijkstra, C.A. Van Blitterswijk, M. Karperien, J. Feijen, Chondrogenesis in injectable enzymatically crosslinked heparin/dextran hydrogels, J. Control. Release. 152 (2011) 186–195. doi:10.1016/j.jconrel.2011.01.031.
[39] M. Kim, S.E. Kim, S.S. Kang, Y.H. Kim, G. Tae, The use of de-differentiated chondrocytes delivered by a heparin-based hydrogel to regenerate cartilage in partial-thickness defects., Biomaterials. 32 (2011) 7883–96. doi:10.1016/j.biomaterials.2011.07.015.
[40] S.P. Seto, M.E. Casas, J.S. Temenoff, Differentiation of mesenchymal stem cells in heparin-containing hydrogels via coculture with osteoblasts., Cell Tissue Res. 347 (2012) 589–601. doi:10.1007/s00441-011-1265-8.
[41] A.K. Jha, K.M. Tharp, J. Ye, J.L. Santiago-Ortiz, W.M. Jackson, A. Stahl, D. V. Schaffer, Y. Yeghiazarians, K.E. Healy, Enhanced survival and engraftment of transplanted stem cells using growth factor sequestering hydrogels, Biomaterials. 47 (2015) 1–12. doi:10.1016/j.biomaterials.2014.12.043.
[42] E.S. Place, N.D. Evans, M.M. Stevens, Complexity in biomaterials for tissue engineering., Nat. Mater. 8 (2009) 457–70. doi:10.1038/nmat2441.
[43] N.A. Impellitteri, M.W. Toepke, S.K. Lan Levengood, W.L. Murphy, Specific VEGF sequestering and release using peptide-functionalized hydrogel microspheres., Biomaterials. 33 (2012) 3475–84. doi:10.1016/j.biomaterials.2012.01.032.
[44] R.N. Shah, N. a Shah, M.M. Del Rosario Lim, C. Hsieh, G. Nuber, S.I. Stupp, Supramolecular design of self-assembling nanofibers for cartilage regeneration., Proc. Natl. Acad. Sci. U. S. A. 107 (2010) 3293–8. doi:10.1073/pnas.0906501107.
[45] D.S.W. Benoit, A.R. Durney, K.S. Anseth, The effect of heparin-functionalized PEG hydrogels on three-dimensional human mesenchymal stem cell osteogenic

differentiation., Biomaterials. 28 (2007) 66–77. doi:10.1016/j.biomaterials.2006.08.033.
[46] C.-C. Lin, A.T. Metters, K.S. Anseth, Functional PEG-peptide hydrogels to modulate local inflammation induced by the pro-inflammatory cytokine TNFalpha., Biomaterials. 30 (2009) 4907–14. doi:10.1016/j.biomaterials.2009.05.083.
[47] T. Basinska, Hydrophilic core-shell microspheres: a suitable support for controlled attachment of proteins and biomedical diagnostics., Macromol. Biosci. 5 (2005) 1145–68. doi:10.1002/mabi.200500138.
[48] C. Longo, G. Gambara, V. Espina, A. Luchini, B. Bishop, A.S. Patanarut, E.F. Petricoin, F. Beretti, B. Ferrari, E. Garaci, A. De Pol, G. Pellacani, L. a Liotta, A novel biomarker harvesting nanotechnology identifies Bak as a candidate melanoma biomarker in serum., Exp. Dermatol. 20 (2011) 29–34. doi:10.1111/j.1600-0625.2010.01187.x.
[49] C. Longo, A. Patanarut, T. George, B. Bishop, W. Zhou, C. Fredolini, M.M. Ross, V. Espina, G. Pellacani, E.F. Petricoin, L. a Liotta, A. Luchini, Core-shell hydrogel particles harvest, concentrate and preserve labile low abundance biomarkers., PLoS One. 4 (2009) e4763. doi:10.1371/journal.pone.0004763.
[50] D. Tamburro, C. Fredolini, V. Espina, T. a Douglas, A. Ranganathan, L. Ilag, W. Zhou, P. Russo, B.H. Espina, G. Muto, E.F. Petricoin, L. a Liotta, A. Luchini, Multifunctional core-shell nanoparticles: discovery of previously invisible biomarkers., J. Am. Chem. Soc. 133 (2011) 19178–88. doi:10.1021/ja207515j.
[51] Y. Wen, M.R. Gallego, L.F. Nielsen, L. Jorgensen, E.H. Møller, H.M. Nielsen, Design and characterization of core-shell mPEG-PLGA composite microparticles for development of cell-scaffold constructs., Eur. J. Pharm. Biopharm. 85 (2013) 87–98. doi:10.1016/j.ejpb.2013.03.027.
[52] J. Wu, T. Kong, K.W.K. Yeung, H.C. Shum, K.M.C. Cheung, L. Wang, M.K.T. To, Fabrication and characterization of monodisperse PLGA-alginate core-shell microspheres with monodisperse size and homogeneous shells for controlled drug release., Acta Biomater. 9 (2013) 7410–9. doi:10.1016/j.actbio.2013.03.022.
[53] S.E. Sakiyama-Elbert, Incorporation of heparin into biomaterials., Acta Biomater. 10 (2014) 1581–7. doi:10.1016/j.actbio.2013.08.045.
[54] B. Rai, V. Nurcombe, S.M. Cool, Heparan sulfate-based treatments for regenerative medicine., Crit. Rev. Eukaryot. Gene Expr. 21 (2011) 1–12. http://www.ncbi.nlm.nih.gov/pubmed/21967329.
[55] M. Kim, J.Y. Lee, C.N. Jones, A. Revzin, G. Tae, Heparin-based hydrogel as a matrix for encapsulation and cultivation of primary hepatocytes., Biomaterials. 31 (2010) 3596–603. doi:10.1016/j.biomaterials.2010.01.068.
[56] A. Zieris, S. Prokoph, K.R. Levental, P.B. Welzel, M. Grimmer, U. Freudenberg, C. Werner, FGF-2 and VEGF functionalization of starPEG-heparin hydrogels to modulate biomolecular and physical cues of angiogenesis., Biomaterials. 31 (2010) 7985–94. doi:10.1016/j.biomaterials.2010.07.021.
[57] S. Nakamura, Y. Kanatani, S. Kishimoto, S. Nakamura, C. Ohno, T. Horio, F. Masanori, H. Hattori, Y. Tanaka, T. Kiyosawa, T. Maehara, M. Ishihara, Controlled release of FGF-2 using fragmin/protamine microparticles and effect on neovascularization., J. Biomed. Mater. Res. A. 91 (2009) 814–23.

doi:10.1002/jbm.a.32265.
[58] L.E. Tellier, T. Miller, T.C. McDevitt, J.S. Temenoff, Hydrolysis and sulfation pattern effects on release of bioactive bone morphogenetic protein-2 from heparin-based microparticles, J. Mater. Chem. B. 3 (2015) 8001–8009. doi:10.1039/C5TB00933B.
[59] M.H. Hettiaratchi, T. Miller, J.S. Temenoff, R.E. Guldberg, T.C. McDevitt, Heparin microparticle effects on presentation and bioactivity of bone morphogenetic protein-2, Biomaterials. 35 (2014) 7228–7238. doi:10.1016/j.biomaterials.2014.05.011.
[60] P. van de Wetering, A.T. Metters, R.G. Schoenmakers, J. a Hubbell, Poly(ethylene glycol) hydrogels formed by conjugate addition with controllable swelling, degradation, and release of pharmaceutically active proteins., J. Control. Release. 102 (2005) 619–27. doi:10.1016/j.jconrel.2004.10.029.
[61] P. Bianco, "Mesenchymal" Stem Cells, Annu. Rev. Cell Dev. Biol. 30 (2014) 677–704. doi:10.1146/annurev-cellbio-100913-013132.
[62] P. Bianco, X. Cao, P.S. Frenette, J.J. Mao, P.G. Robey, P.J. Simmons, C.-Y. Wang, The meaning, the sense and the significance: translating the science of mesenchymal stem cells into medicine., Nat. Med. 19 (2013) 35–42. doi:10.1038/nm.3028.
[63] B. Sacchetti, A. Funari, C. Remoli, G. Giannicola, G. Kogler, S. Liedtke, G. Cossu, M. Serafini, M. Sampaolesi, E. Tagliafico, E. Tenedini, I. Saggio, P.G. Robey, M. Riminucci, P. Bianco, No identical "mesenchymal stem cells" at different times and sites: Human committed progenitors of distinct origin and differentiation potential are incorporated as adventitial cells in microvessels, Stem Cell Reports. 6 (2016) 897–913. doi:10.1016/j.stemcr.2016.05.011.
[64] I.R. Murray, C.C. West, W.R. Hardy, A.W. James, T.S. Park, A. Nguyen, T. Tawonsawatruk, L. Lazzari, C. Soo, B. Péault, Natural history of mesenchymal stem cells, from vessel walls to culture vessels, Cell. Mol. Life Sci. 71 (2014) 1353–1374. doi:10.1007/s00018-013-1462-6.
[65] P.S. Frenette, S. Pinho, D. Lucas, C. Scheiermann, Mesenchymal Stem Cell: Keystone of the Hematopoietic Stem Cell Niche and a Stepping-Stone for Regenerative Medicine, Annu. Rev. Immunol. 31 (2013) 285–316. doi:10.1146/annurev-immunol-032712-095919.
[66] M.B. Murphy, K. Moncivais, A.I. Caplan, Mesenchymal stem cells: environmentally responsive therapeutics for regenerative medicine., Exp. Mol. Med. 45 (2013) e54. doi:10.1038/emm.2013.94.
[67] N. Di Maggio, E. Piccinini, M. Jaworski, A. Trumpp, D.J. Wendt, I. Martin, Toward modeling the bone marrow niche using scaffold-based 3D culture systems, Biomaterials. 32 (2011) 321–329. doi:10.1016/j.biomaterials.2010.09.041.
[68] A. Ehninger, A. Trumpp, The bone marrow stem cell niche grows up: mesenchymal stem cells and macrophages move in., J. Exp. Med. 208 (2011) 421–8. doi:10.1084/jem.20110132.
[69] G.P. Fadini, F. Ferraro, F. Quaini, T. Asahara, P. Madeddu, Concise review: diabetes, the bone marrow niche, and impaired vascular regeneration., Stem Cells Transl. Med. 3 (2014) 949–57. doi:10.5966/sctm.2014-0052.
[70] J.P. Rodriguez, P. Astudillo, S. Rios, A.M. Pino, Involvement of Adipogenic

Potential of Human Bone Marrow Mesenchymal Stem Cells (MSCs) in Osteoporsosis, Curr. Stem Cell Res. Ther. 3 (2008).
[71] A.P. Rolo, C.M. Palmeira, Diabetes and mitochondrial function: role of hyperglycemia and oxidative stress., Toxicol. Appl. Pharmacol. 212 (2006) 167–78. doi:10.1016/j.taap.2006.01.003.
[72] P. Jackuliak, J. Payer, Osteoporosis, Fractures, and Diabetes, Int. J. Endocrinol. 2014 (2014) 1–10. doi:10.1155/2014/820615.
[73] B. Ponugoti, G. Dong, D.T. Graves, Role of forkhead transcription factors in diabetes-induced oxidative stress, Exp. Diabetes Res. 2012 (2012). doi:10.1155/2012/939751.
[74] F.J.A. de Paula, M.C. Horowitz, C.J. Rosen, Novel insights into the relationship between diabetes and osteoporosis., Diabetes. Metab. Res. Rev. 26 (2010) 622–30. doi:10.1002/dmrr.1135.
[75] N. Harvey, E. Dennison, C. Cooper, Osteoporosis: impact on health and economics., Nat. Rev. Rheumatol. 6 (2010) 99–105. doi:10.1038/nrrheum.2009.260.
[76] M.J. Devlin, C.J. Rosen, The bone-fat interface: Basic and clinical implications of marrow adiposity, Lancet Diabetes Endocrinol. 3 (2015) 141–147. doi:10.1016/S2213-8587(14)70007-5.
[77] V. V. Shanbhogue, D.M. Mitchell, C.J. Rosen, M.L. Bouxsein, Type 2 diabetes and the skeleton: New insights into sweet bones, Lancet Diabetes Endocrinol. 4 (2016) 159–173. doi:10.1016/S2213-8587(15)00283-1.
[78] P.K. Fazeli, M.C. Horowitz, O. a MacDougald, E.L. Scheller, M.S. Rodeheffer, C.J. Rosen, A. Klibanski, Marrow fat and bone--new perspectives., J. Clin. Endocrinol. Metab. 98 (2013) 935–45. doi:10.1210/jc.2012-3634.
[79] R. Sealand, C. Razavi, R.A. Adler, Diabetes Mellitus and Osteoporosis, Curr. Diab. Rep. 13 (2013) 411–418. doi:10.1007/s11892-013-0376-x.
[80] F. Long, Building strong bones: molecular regulation of the osteoblast lineage., Nat. Rev. Mol. Cell Biol. 13 (2012) 27–38. doi:10.1038/nrm3254.
[81] M. Kawai, F.J.A. de Paula, C.J. Rosen, New insights into osteoporosis: The bone-fat connection, J. Intern. Med. 272 (2012) 317–329. doi:10.1111/j.1365-2796.2012.02564.x.
[82] L. Tian, X. Yu, Lipid metabolism disorders and bone dysfunction-interrelated and mutually regulated (Review), Mol. Med. Rep. 12 (2015) 783–794. doi:10.3892/mmr.2015.3472.
[83] C. Cramer, E. Freisinger, R.K. Jones, D.P. Slakey, C.L. Dupin, E.R. Newsome, E.U. Alt, R. Izadpanah, Persistent high glucose concentrations alter the regenerative potential of mesenchymal stem cells., Stem Cells Dev. 19 (2010) 1875–84. doi:10.1089/scd.2010.0009.
[84] V. Gopalakrishnan, R.C. Vignesh, J. Arunakaran, M.M. Aruldhas, N. Srinivasan, Effects of glucose and its modulation by insulin and estradiol on BMSC differentiation into osteoblastic lineages., Biochem. Cell Biol. 84 (2006) 93–101. doi:10.1139/o05-163.
[85] Y.-M. Li, T. Schilling, P. Benisch, S. Zeck, J. Meissner-Weigl, D. Schneider, C. Limbert, J. Seufert, M. Kassem, N. Schütze, F. Jakob, R. Ebert, Effects of high glucose on mesenchymal stem cell proliferation and differentiation., Biochem.

Biophys. Res. Commun. 363 (2007) 209–15. doi:10.1016/j.bbrc.2007.08.161.
[86] A. Stolzing, N. Coleman, A. Scutt, Glucose-induced replicative senescence in mesenchymal stem cells., Rejuvenation Res. 9 (2006) 31–5. doi:10.1089/rej.2006.9.31.
[87] Y. Lin, A.H. Berg, P. Iyengar, T.K.T. Lam, A. Giacca, T.P. Combs, M.W. Rajala, X. Du, B. Rollman, W. Li, M. Hawkins, N. Barzilai, C.J. Rhodes, I.G. Fantus, M. Brownlee, P.E. Scherer, The hyperglycemia-induced inflammatory response in adipocytes: the role of reactive oxygen species., J. Biol. Chem. 280 (2005) 4617–26. doi:10.1074/jbc.M411863200.
[88] J. Sun, Y. Xu, Z. Dai, Y. Sun, Intermittent high glucose stimulate MCP-l, IL-18, and PAI-1, but inhibit adiponectin expression and secretion in adipocytes dependent of ROS., Cell Biochem. Biophys. 55 (2009) 173–80. doi:10.1007/s12013-009-9066-3.
[89] A. Gagnon, A. Sorisky, The effect of glucose concentration on insulin-induced 3T3-L1 adipose cell differentiation., Obes. Res. 6 (1998) 157–63. http://www.ncbi.nlm.nih.gov/pubmed/9545023.
[90] S. Botolin, L.R. McCabe, Chronic hyperglycemia modulates osteoblast gene expression through osmotic and non-osmotic pathways., J. Cell. Biochem. 99 (2006) 411–24. doi:10.1002/jcb.20842.
[91] a García-Hernández, H. Arzate, I. Gil-Chavarría, R. Rojo, L. Moreno-Fierros, High glucose concentrations alter the biomineralization process in human osteoblastic cells., Bone. 50 (2012) 276–88. doi:10.1016/j.bone.2011.10.032.
[92] M. Inaba, Y. Nishizawa, a. Shioi, H. Morii, Importance of sustained high glucose condition in the development of diabetic osteopenia: Possible involvement of the polyol pathway, Osteoporos. Int. 7 (1997) 209–212. doi:10.1007/BF03194374.
[93] M. Zayzafoon, C. Stell, R. Irwin, L.R. Mccabe, Extracellular Glucose Influences Osteoblast Differentiation and c–Jun Expression, J. Cell. Biochem. 79 (2000) 301–310. doi:10.1002/1097-4644(20001101)79:2<301::AID-JCB130>3.0.CO;2-0.
[94] K.L. Moffat, I.-N.E. Wang, S.A. Rodeo, H.H. Lu, Orthopaedic Interface Tissue Engineering for the Biological Fixation of Soft Tissue Grafts, Clin. Sport. Med. 28 (2009) 157–176. doi:10.1016/j.csm.2008.08.006.Orthopaedic.
[95] A.G. Mikos, S.W. Herring, P. Ochareon, J. Elisseeff, H.H. Lu, R. Kandel, F.J. Schoen, M. Toner, D. Mooney, A. Atala, M.E. Van Dyke, D. Kaplan, G. Vunjak-Novakovic, Engineering complex tissues, Tissue Eng. 12 (2006) 3307–39. doi:10.1089/ten.2006.12.3307.
[96] J. Lee, M.J. Cuddihy, N. a Kotov, Three-dimensional cell culture matrices: state of the art., Tissue Eng. Part B. Rev. 14 (2008) 61–86. doi:10.1089/teb.2007.0150.
[97] H. Zhou, W. Mak, Y. Zheng, C.R. Dunstan, M.J. Seibel, Osteoblasts directly control lineage commitment of mesenchymal progenitor cells through Wnt signaling., J. Biol. Chem. 283 (2008) 1936–45. doi:10.1074/jbc.M702687200.
[98] Y. Wang, V. Volloch, M.A. Pindrus, D.J. Blasioli, J. Chen, D.L. Kaplan, Murine osteoblasts regulate mesenchymal stem cells via WNT and cadherin pathways: mechanism depends on cell-cell contact mode., J. Tissue Eng. Regen. Med. 1 (2007) 39–50. doi:10.1002/term.6.
[99] M. Ilmer, M. Karow, C. Geissler, M. Jochum, P. Neth, Human osteoblast-derived factors induce early osteogenic markers in human mesenchymal stem cells., Tissue

Eng. Part A. 15 (2009) 2397–409. doi:10.1089/ten.tea.2008.0427.
[100] M.T. Tsai, D.J. Lin, S. Huang, H.T. Lin, W.H. Chang, Osteogenic differentiation is synergistically influenced by osteoinductive treatment and direct cell-cell contact between murine osteoblasts and mesenchymal stem cells, Int. Orthop. 36 (2012) 199–205. doi:10.1007/s00264-011-1259-x.
[101] E.. Birmingham, G.. L.. Niebur, P.. E.. McHugh, G. Shaw, F.P. Barry, L.M. McNamara, Osteogenic differentiation of mesenchymal stem cells is regulated by osteocyte and osteoblast cells in a simplified bone niche, Eur. Cells Mater. 23 (2012) 13–27.
[102] A.. Maurin, P.. Chavassieux, L. Frappart, P.. Delmas, C.. Serre, P.. Meunier, Influence of mature adipocytes on osteoblast proliferation in human primary cocultures, Bone. 26 (2000) 485–489. doi:10.1016/S8756-3282(00)00252-0.
[103] A. Clabaut, S. Delplace, C. Chauveau, P. Hardouin, O. Broux, Human osteoblasts derived from mesenchymal stem cells express adipogenic markers upon coculture with bone marrow adipocytes., Differentiation. 80 (2010) 40–5. doi:10.1016/j.diff.2010.04.004.
[104] X. Dong, L. Bi, S. He, G. Meng, B. Wei, S. Jia, J. Liu, FFAs-ROS-ERK/P38 pathway plays a key role in adipocyte lipotoxicity on osteoblasts in co-culture, Biochimie. 101 (2014) 123–131. doi:10.1016/j.biochi.2014.01.002.
[105] M.B. Goldring, Chondrogenesis, chondrocyte differentiation, and articular cartilage metabolism in health and osteoarthritis., Ther. Adv. Musculoskelet. Dis. 4 (2012) 269–85. doi:10.1177/1759720X12448454.
[106] E.J. Mackie, L. Tatarczuch, M. Mirams, The skeleton: a multi-functional complex organ: the growth plate chondrocyte and endochondral ossification., J. Endocrinol. 211 (2011) 109–21. doi:10.1530/JOE-11-0048.
[107] T. Michigami, Regulatory mechanisms for the development of growth plate cartilage., Cell. Mol. Life Sci. (2013). doi:10.1007/s00018-013-1346-9.
[108] K. Jochmann, V. Bachvarova, A. Vortkamp, Heparan sulfate as a regulator of endochondral ossification and osteochondroma development., Matrix Biol. 34 (2014) 55–63. doi:10.1016/j.matbio.2013.11.003.
[109] B.C.J. van der Eerden, M. Karperien, J.M. Wit, Systemic and local regulation of the growth plate., Endocr. Rev. 24 (2003) 782–801. doi:10.1210/er.2002-0033.
[110] S. Provot, E. Schipani, Molecular mechanisms of endochondral bone development., Biochem. Biophys. Res. Commun. 328 (2005) 658–65. doi:10.1016/j.bbrc.2004.11.068.
[111] S.K.C. Sundararaj, R.D. Cieply, G. Gupta, T.A. Milbrandt, D.A. Puleo, Treatment of growth plate injury using IGF-I-loaded PLGA scaffolds., J. Tissue Eng. Regen. Med. (2012). doi:10.1002/term.1670.
[112] R. Chung, B.K. Foster, C.J. Xian, Preclinical studies on mesenchymal stem cell-based therapy for growth plate cartilage injury repair., Stem Cells Int. 2011 (2011) 570125. doi:10.4061/2011/570125.
[113] R.C. McCarty, C.J. Xian, S. Gronthos, A.C.W. Zannettino, B.K. Foster, Application of autologous bone marrow derived mesenchymal stem cells to an ovine model of growth plate cartilage injury., Open Orthop. J. 4 (2010) 204–10. doi:10.2174/1874325001004010204.
[114] M. Tobita, M. Ochi, Y. Uchio, R. Mori, J. Iwasa, K. Katsube, T. Motomura,

Treatment of growth plate injury with autogenous chondrocytes: a study in rabbits., Acta Orthop. Scand. 73 (2002) 352–8. doi:10.1080/000164702320155383.
[115] F. Chen, J.H.P. Hui, W.K. Chan, E.H. Lee, Cultured mesenchymal stem cell transfers in the treatment of partial growth arrest., J. Pediatr. Orthop. 23 (2003) 425–9. http://www.ncbi.nlm.nih.gov/pubmed/12826936.
[116] R.M. Coleman, Z. Schwartz, B.D. Boyan, R.E. Guldberg, The therapeutic effect of bone marrow-derived stem cell implantation after epiphyseal plate injury is abrogated by chondrogenic predifferentiation., Tissue Eng. Part A. 19 (2013) 475–83. doi:10.1089/ten.TEA.2012.0125.
[117] L. Planka, P. Gal, H. Kecova, J. Klima, J. Hlucilova, E. Filova, E. Amler, P. Krupa, L. Kren, R. Srnec, L. Urbanova, J. Lorenzova, A. Necas, Allogeneic and autogenous transplantations of MSCs in treatment of the physeal bone bridge in rabbits., BMC Biotechnol. 8 (2008) 70. doi:10.1186/1472-6750-8-70.
[118] L. Plánka, a Necas, R. Srnec, P. Rauser, D. Starý, J. Jancár, E. Amler, E. Filová, J. Hlucilová, L. Kren, P. Gál, Use of allogenic stem cells for the prevention of bone bridge formation in miniature pigs., Physiol. Res. 58 (2009) 885–93. http://www.ncbi.nlm.nih.gov/pubmed/19093735.
[119] M. Ulrich-Vinther, M.D. Maloney, E.M. Schwarz, R. Rosier, R.J. O'Keefe, Articular cartilage biology., J. Am. Acad. Orthop. Surg. 11 (2003) 421–430.
[120] A.R. Poole, T. Kojima, T. Yasuda, F. Mwale, M. Kobayashi, S. Laverty, Composition and structure of articular cartilage: a template for tissue repair., Clin. Orthop. Relat. Res. 1 (2001) S26–S33. doi:11603710.
[121] M. Pacifici, E. Koyama, M. Iwamoto, Mechanisms of synovial joint and articular cartilage formation: recent advances, but many lingering mysteries., Birth Defects Res. C. Embryo Today. 75 (2005) 237–48. doi:10.1002/bdrc.20050.
[122] R.S. Decker, E. Koyama, M. Pacifici, Genesis and morphogenesis of limb synovial joints and articular cartilage., Matrix Biol. (2014). doi:10.1016/j.matbio.2014.08.006.
[123] M. Pacifici, E. Koyama, M. Iwamoto, C. Gentili, Development of articular cartilage: what do we know about it and how may it occur?, Connect. Tissue Res. 41 (2000) 175–84. http://www.ncbi.nlm.nih.gov/pubmed/11264867.
[124] C. Chung, J.A. Burdick, Engineering cartilage tissue, Adv. Drug Deliv. Rev. 60 (2008) 243–262. doi:10.1016/j.addr.2007.08.027.
[125] K.M. Hubka, R.L. Dahlin, V. V Meretoja, F.K. Kasper, A.G. Mikos, Enhancing Chondrogenic Phenotype for Cartilage Tissue Engineering: Monoculture and Coculture of Articular Chondrocytes and Mesenchymal Stem Cells, Tissue Eng. Part B Rev. 20 (2014) 641–654. doi:10.1089/ten.teb.2014.0034.
[126] T.A.E. Ahmed, M.T. Hincke, Strategies for articular cartilage lesion repair and functional restoration., Tissue Eng. Part B. Rev. 16 (2010) 305–29. doi:10.1089/ten.TEB.2009.0590.
[127] E.B. Hunziker, Articular cartilage repair: basic science and clinical progress. A review of the current status and prospects., Osteoarthritis Cartilage. 10 (2002) 432–63. doi:10.1053/joca.2002.0801.
[128] C. Acharya, A. Adesida, P. Zajac, M. Mumme, J. Riesle, I. Martin, A. Barbero, Enhanced chondrocyte proliferation and mesenchymal stromal cells

chondrogenesis in coculture pellets mediate improved cartilage formation., J. Cell. Physiol. 227 (2012) 88–97. doi:10.1002/jcp.22706.
[129] A.M. Handorf, W.-J. Li, Induction of mesenchymal stem cell chondrogenesis through sequential administration of growth factors within specific temporal windows., J. Cell. Physiol. 229 (2014) 162–71. doi:10.1002/jcp.24428.
[130] S. Weiss, T. Hennig, R. Bock, E. Steck, W. Richter, Impact of growth factors and PTHrP on early and late chondrogenic differentiation of human mesenchymal stem cells., J. Cell. Physiol. 223 (2010) 84–93. doi:10.1002/jcp.22013.
[131] J. Fischer, a Dickhut, M. Rickert, W. Richter, Human articular chondrocytes secrete parathyroid hormone-related protein and inhibit hypertrophy of mesenchymal stem cells in coculture during chondrogenesis., Arthritis Rheum. 62 (2010) 2696–706. doi:10.1002/art.27565.
[132] N. Ahmed, R. Dreier, A. Göpferich, J. Grifka, S. Grässel, Soluble Signalling Factors Derived from Differentiated Cartilage Tissue Affect Chondrogenic Differentiation of Rat Adult Marrow Stromal Cells, Cell. Physiol. Biochem. 20 (2007).
[133] V. V Meretoja, R.L. Dahlin, S. Wright, F.K. Kasper, A.G. Mikos, The effect of hypoxia on the chondrogenic differentiation of co-cultured articular chondrocytes and mesenchymal stem cells in scaffolds., Biomaterials. 34 (2013) 4266–73. doi:10.1016/j.biomaterials.2013.02.064.
[134] M.A. Sabatino, R. Santoro, S. Gueven, C. Jaquiery, D.J. Wendt, I. Martin, M. Moretti, A. Barbero, Cartilage graft engineering by co-culturing primary human articular chondrocytes with human bone marrow stromal cells., J. Tissue Eng. Regen. Med. (2012). doi:10.1002/term.1661.
[135] L. Bian, D.Y. Zhai, R.L. Mauck, J.A. Burdick, Coculture of human mesenchymal stem cells and articular chondrocytes reduces hypertrophy and enhances functional properties of engineered cartilage., Tissue Eng. Part A. 17 (2011) 1137–45. doi:10.1089/ten.TEA.2010.0531.
[136] V. Vickerman, J. Blundo, S. Chung, R.D. Kamm, Design, Fabrication and Implementation of a Novel Multi Parameter Control Microfluidic Platform for Three-Dimensional Cell Culture and Real-Time Imaging, Lab Chip. 8 (2008) 1468–1477. doi:10.1039/b802395f.Design.
[137] E. Cukierman, R. Pankov, K.M. Yamada, Cell interactions with three-dimensional matrices., Curr. Opin. Cell Biol. 14 (2002) 633–9. http://www.ncbi.nlm.nih.gov/pubmed/12231360.
[138] A. Abbott, Biology's new dimension, Nature. 424 (2003) 870–872.
[139] C.P. Huang, J. Lu, H. Seon, A.P. Lee, L. a Flanagan, H.-Y. Kim, A.J. Putnam, N.L. Jeon, Engineering microscale cellular niches for three-dimensional multicellular co-cultures., Lab Chip. 9 (2009) 1740–8. doi:10.1039/b818401a.
[140] J.L. Drury, D.J. Mooney, Hydrogels for tissue engineering: scaffold design variables and applications, Biomaterials. 24 (2003) 4337–4351. doi:10.1016/S0142-9612(03)00340-5.
[141] M.P. Lutolf, Biomaterials: Spotlight on hydrogels., Nat. Mater. 8 (2009) 451–3. doi:10.1038/nmat2458.
[142] S. Khetan, J.A. Burdick, Patterning network structure to spatially control cellular remodeling and stem cell fate within 3-dimensional hydrogels, Biomaterials. 31

(2010) 8228–8234. doi:10.1016/j.biomaterials.2010.07.035.
[143] S. a Fisher, R.Y. Tam, M.S. Shoichet, Tissue mimetics: engineered hydrogel matrices provide biomimetic environments for cell growth., Tissue Eng. Part A. 20 (2014) 895–8. doi:10.1089/ten.tea.2013.0765.
[144] J. a Burdick, A. Khademhosseini, R. Langer, Photopolymerization Process, Langmuir. 20 (2004) 8–11. doi:10.1021/la049298n.
[145] L. Wang, Y. Li, G. Huang, X. Zhang, B. Pingguan-Murphy, B. Gao, T.J. Lu, F. Xu, Hydrogel-based methods for engineering cellular microenvironment with spatiotemporal gradients., Crit. Rev. Biotechnol. 00 (2015) 1–13. doi:10.3109/07388551.2014.993588.
[146] J.C. Culver, J.C. Hoffmann, R.A. Poché, J.H. Slater, J.L. West, M.E. Dickinson, Three-Dimensional Biomimetic Patterning in Hydrogels to Guide Cellular Organization, Adv. Mater. 24 (2012) 2344–2348. doi:10.1002/adma.201200395.
[147] M.S. Hahn, J.S. Miller, J.L. West, Three-dimensional biochemical and biomechanical patterning of hydrogels for guiding cell behavior, Adv. Mater. 18 (2006) 2679–2684. doi:10.1002/adma.200600647.
[148] M.S. Hahn, L.J. Taite, J.J. Moon, M.C. Rowland, K.A. Ruffino, J.L. West, Photolithographic patterning of polyethylene glycol hydrogels., Biomaterials. 27 (2006) 2519–24. doi:10.1016/j.biomaterials.2005.11.045.
[149] S.H. Lee, J.J. Moon, J.L. West, Three-dimensional micropatterning of bioactive hydrogels via two-photon laser scanning photolithography for guided 3D cell migration, Biomaterials. 29 (2008) 2962–2968. doi:10.1016/j.biomaterials.2008.04.004.
[150] C.A. DeForest, B.D. Polizzotti, K.S. Anseth, Sequential click reactions for synthesizing and patterning three-dimensional cell microenvironments, Nat Mater. 8 (2009) 659–664. doi:10.1038/nmat2473.
[151] K.H. Benam, S. Dauth, B. Hassell, A. Herland, A. Jain, K.-J. Jang, K. Karalis, H.J. Kim, L. MacQueen, R. Mahmoodian, S. Musah, Y.-S. Torisawa, A.D. van der Meer, R. Villenave, M. Yadid, K.K. Parker, D.E. Ingber, Engineered In Vitro Disease Models., Annu. Rev. Pathol. 10 (2015) 195–262. doi:10.1146/annurev-pathol-012414-040418.
[152] M.R. Nelson, K. Roy, Bone-marrow mimicking biomaterial niches for studying hematopoietic stem and progenitor cells, J. Mater. Chem. B. 4 (2016) 3490–3503. doi:10.1039/C5TB02644J.
[153] A.P.D.N. De Barros, C.M. Takiya, L.R. Garzoni, M.L. Leal-Ferreira, H.S. Dutra, L.B. Chiarini, M.N. Meirelles, R. Borojevic, M.I.D. Rossi, Osteoblasts and bone marrow mesenchymal stromal cells control hematopoietic stem cell migration and proliferation in 3D in vitro model, PLoS One. 5 (2010). doi:10.1371/journal.pone.0009093.
[154] A. Braccini, D. Wendt, C. Jaquiery, M. Jakob, M. Heberer, L. Kenins, A. Wodnar-Filipowicz, R. Quarto, I. Martin, Three-Dimensional Perfusion Culture of Human Bone Marrow Cells and Generation of Osteoinductive Grafts, Stem Cells. 23 (2005) 1066–1072. doi:10.1634/stemcells.2005-0002.
[155] F.A. Saleh, M. Whyte, P.G. Genever, Effects of endothelial cells on human mesenchymal stem cell activity in a three-dimensional in vitro model., Eur. Cell. Mater. 22 (2011) 242–57; discussion 257.

http://www.ncbi.nlm.nih.gov/pubmed/22012735.
[156] S. Carrancio, B. Blanco, C. Romo, S. Muntion, N. Lopez-Holgado, J.F. Blanco, J.G. Briñon, J.F.S. Miguel, F.M. Sanchez-Guijo, M.C. del Cañizo, Bone marrow mesenchymal stem cells for improving hematopoietic function: An in vitro and in vivo model. Part 2: Effect on bone marrow microenvironment, PLoS One. 6 (2011). doi:10.1371/journal.pone.0026241.
[157] L. Hou, T. Liu, J. Tan, W. Meng, L. Deng, H. Yu, X. Zou, Y. Wang, Long-term culture of leukemic bone marrow primary cells in biomimetic osteoblast niche, Int. J. Hematol. 90 (2009) 281–291. doi:10.1007/s12185-009-0392-4.
[158] Y. Torisawa, C.S. Spina, T. Mammoto, A. Mammoto, J.C. Weaver, T. Tat, J.J. Collins, D.E. Ingber, Bone marrow-on-a-chip replicates hematopoietic niche physiology in vitro., Nat. Methods. 11 (2014) 663–9. doi:10.1038/nmeth.2938.
[159] R.A.A. Muzzarelli, F. Greco, A. Busilacchi, V. Sollazzo, A. Gigante, Chitosan, hyaluronan and chondroitin sulfate in tissue engineering for cartilage regeneration: A review, Carbohydr. Polym. 89 (2012) 723–739. doi:10.1016/j.carbpol.2012.04.057.
[160] Y.L. Chen, H.P. Lee, H.Y. Chan, L.Y. Sung, H.C. Chen, Y.C. Hu, Composite chondroitin-6-sulfate/dermatan sulfate/chitosan scaffolds for cartilage tissue engineering, Biomaterials. 28 (2007) 2294–2305. doi:10.1016/j.biomaterials.2007.01.027.
[161] C. Vinatier, D. Mrugala, C. Jorgensen, J. Guicheux, D. Noël, Cartilage engineering: a crucial combination of cells, biomaterials and biofactors, Trends Biotechnol. 27 (2009) 307–314. doi:10.1016/j.tibtech.2009.02.005.
[162] I.L. Kim, R.L. Mauck, J.A. Burdick, Hydrogel design for cartilage tissue engineering: A case study with hyaluronic acid, Biomaterials. 32 (2011) 8771–8782. doi:10.1016/j.biomaterials.2011.08.073.
[163] L. Bian, C. Hou, E. Tous, R. Rai, R.L. Mauck, J.A. Burdick, The influence of hyaluronic acid hydrogel crosslinking density and macromolecular diffusivity on human MSC chondrogenesis and hypertrophy, Biomaterials. 34 (2013) 413–421. doi:10.1016/j.biomaterials.2012.09.052.
[164] W.S. Toh, T.C. Lim, M. Kurisawa, M. Spector, Modulation of mesenchymal stem cell chondrogenesis in a tunable hyaluronic acid hydrogel microenvironment, Biomaterials. 33 (2012) 3835–3845. doi:10.1016/j.biomaterials.2012.01.065.
[165] J.M. Kemppainen, S.J. Hollister, Differential effects of designed scaffold permeability on chondrogenesis by chondrocytes and bone marrow stromal cells, Biomaterials. 31 (2010) 279–287. doi:10.1016/j.biomaterials.2009.09.041.
[166] J.T. Connelly, A.J. Garc??a, M.E. Levenston, Inhibition of in vitro chondrogenesis in RGD-modified three-dimensional alginate gels, Biomaterials. 28 (2007) 1071–1083. doi:10.1016/j.biomaterials.2006.10.006.
[167] P.W. Kopesky, E.J. Vanderploeg, J.S. Sandy, B. Kurz, A.J. Grodzinsky, Self-Assembling Peptide Hydrogels Modulate In Vitro Chondrogenesis of Bovine Bone Marrow Stromal Cells, Tissue Eng. Part A. 16 (2010) 465–477. doi:10.1089/ten.tea.2009.0158.
[168] Z. Lu, B.Z. Doulabi, C. Huang, R. a Bank, M.N. Helder, Collagen type II enhances chondrogenesis in adipose tissue-derived stem cells by affecting cell shape., Tissue Eng. Part A. 16 (2010) 81–90. doi:10.1089/ten.TEA.2009.0222.

[169] T. Re'em, Y. Kaminer-Israeli, E. Ruvinov, S. Cohen, Chondrogenesis of hMSC in affinity-bound TGF-beta scaffolds, Biomaterials. 33 (2012) 751–761. doi:10.1016/j.biomaterials.2011.10.007.
[170] J.L. Puetzer, J.N. Petitte, E.G. Loboa, Comparative review of growth factors for induction of three-dimensional in vitro chondrogenesis in human mesenchymal stem cells isolated from bone marrow and adipose tissue., Tissue Eng. Part B. Rev. 16 (2010) 435–44. doi:10.1089/ten.TEB.2009.0705.
[171] N.S. Hwang, S. Varghese, C. Puleo, Z. Zhang, J. Elisseeff, Morphogenetic signals from chondrocytes promote chondrogenic and osteogenic differentiation of mesenchymal stem cells., J. Cell. Physiol. 212 (2007) 281–4. doi:10.1002/jcp.21052.
[172] M.E. Cooke, a a Allon, T. Cheng, a C. Kuo, H.T. Kim, T.P. Vail, R.S. Marcucio, R. a Schneider, J.C. Lotz, T. Alliston, Structured three-dimensional co-culture of mesenchymal stem cells with chondrocytes promotes chondrogenic differentiation without hypertrophy., Osteoarthritis Cartilage. 19 (2011) 1210–8. doi:10.1016/j.joca.2011.07.005.
[173] L. Wu, J.C.H. Leijten, N. Georgi, J.N. Post, C.A. van Blitterswijk, M. Karperien, Trophic effects of mesenchymal stem cells increase chondrocyte proliferation and matrix formation., Tissue Eng. Part A. 17 (2011) 1425–36. doi:10.1089/ten.TEA.2010.0517.
[174] J.R. Bishop, M. Schuksz, J.D. Esko, Heparan sulphate proteoglycans fine-tune mammalian physiology., Nature. 446 (2007) 1030–7. doi:10.1038/nature05817.
[175] U. Lindahl, J. Li, Chapter 3 Interactions Between Heparan Sulfate and Proteins—Design and Functional Implications, in: Int. Rev. Cell Mol. Biol., 1st ed., Elsevier Inc., 2009: pp. 105–159. doi:10.1016/S1937-6448(09)76003-4.
[176] B. Gorsi, S.E. Stringer, Tinkering with heparan sulfate sulfation to steer development., Trends Cell Biol. 17 (2007) 173–7. doi:10.1016/j.tcb.2007.02.006.
[177] J. Turnbull, A. Powell, S. Guimond, Heparan sulfate: decoding a dynamic multifunctional cell regulator., Trends Cell Biol. 11 (2001) 75–82. http://www.ncbi.nlm.nih.gov/pubmed/11166215.
[178] U. Häcker, K. Nybakken, N. Perrimon, Heparan sulphate proteoglycans: the sweet side of development., Nat. Rev. Mol. Cell Biol. 6 (2005) 530–41. doi:10.1038/nrm1681.
[179] R. Lever, C.P. Page, Novel drug development opportunities for heparin., Nat. Rev. Drug Discov. 1 (2002) 140–8. doi:10.1038/nrd724.
[180] F. Peysselon, S. Ricard-Blum, Heparin–protein interactions: From affinity and kinetics to biological roles. Application to an interaction network regulating angiogenesis, Matrix Biol. 35 (2014) 73–81. doi:10.1016/j.matbio.2013.11.001.
[181] C.C. Rider, Heparin/heparan sulphate binding in the TGF-beta cytokine superfamily., Biochem. Soc. Trans. 34 (2006) 458–60. doi:10.1042/BST0340458.
[182] X. Lin, Functions of heparan sulfate proteoglycans in cell signaling during development., Development. 131 (2004) 6009–21. doi:10.1242/dev.01522.
[183] J. Whitelock, J. Melrose, Heparan sulfate proteoglycans in healthy and diseased systems., Wiley Interdiscip. Rev. Syst. Biol. Med. 3 (2011) 739–51. doi:10.1002/wsbm.149.
[184] S.M.-L. Smith, L.A. West, P. Govindraj, X. Zhang, D.M. Ornitz, J.R. Hassell,

Heparan and chondroitin sulfate on growth plate perlecan mediate binding and delivery of FGF-2 to FGF receptors., Matrix Biol. 26 (2007) 175–84. doi:10.1016/j.matbio.2006.10.012.
[185] C. Settembre, E. Arteaga-Solis, M.D. McKee, R. de Pablo, Q. Al Awqati, A. Ballabio, G. Karsenty, Proteoglycan desulfation determines the efficiency of chondrocyte autophagy and the extent of FGF signaling during endochondral ossification., Genes Dev. 22 (2008) 2645–50. doi:10.1101/gad.1711308.
[186] L. Koziel, M. Kunath, O.G. Kelly, A. Vortkamp, Ext1-dependent heparan sulfate regulates the range of Ihh signaling during endochondral ossification., Dev. Cell. 6 (2004) 801–13. doi:10.1016/j.devcel.2004.05.009.
[187] J. Huegel, C. Mundy, F. Sgariglia, P. Nygren, P.C. Billings, Y. Yamaguchi, E. Koyama, M. Pacifici, Perichondrium phenotype and border function are regulated by Ext1 and heparan sulfate in developing long bones: a mechanism likely deranged in Hereditary Multiple Exostoses., Dev. Biol. 377 (2013) 100–12. doi:10.1016/j.ydbio.2013.02.008.
[188] M.S. Shim, C.S. Kim, Y.-C. Ahn, Z. Chen, Y.J. Kwon, Combined multimodal optical imaging and targeted gene silencing using stimuli-transforming nanotheragnostics., J. Am. Chem. Soc. 132 (2010) 8316–24. doi:10.1021/ja100580y.
[189] H. Cao, S.Y. Xu, EDC/NHS-crosslinked type II collagen-chondroitin sulfate scaffold: Characterization and in vitro evaluation, J. Mater. Sci. Mater. Med. 19 (2008) 567–575. doi:10.1007/s10856-007-3281-5.
[190] K.Y. Chang, L.W. Cheng, G.H. Ho, Y.P. Huang, Y. Der Lee, Fabrication and characterization of poly(γ-glutamic acid)-graft-chondroitin sulfate/polycaprolactone porous scaffolds for cartilage tissue engineering, Acta Biomater. 5 (2009) 1937–1947. doi:10.1016/j.actbio.2009.02.002.
[191] C.S. Ko, J.P. Huang, C.W. Huang, I.M. Chu, Type II collagen-chondroitin sulfate-hyaluronan scaffold cross-linked by genipin for cartilage tissue engineering, J. Biosci. Bioeng. 107 (2009) 177–182. doi:10.1016/j.jbiosc.2008.09.020.
[192] K.Y. Chang, L.H. Hung, I.M. Chu, C.S. Ko, Y. Der Lee, The application of type II collagen and chondroitin sulfate grafted PCL porous scaffold in cartilage tissue engineering, J. Biomed. Mater. Res. - Part A. 92 (2010) 712–723. doi:10.1002/jbm.a.32198.
[193] P.A. Levett, F.P.W. Melchels, K. Schrobback, D.W. Hutmacher, J. Malda, T.J. Klein, A biomimetic extracellular matrix for cartilage tissue engineering centered on photocurable gelatin, hyaluronic acid and chondroitin sulfate, Acta Biomater. 10 (2014) 214–223. doi:10.1016/j.actbio.2013.10.005.
[194] S. Varghese, N.S. Hwang, A.C. Canver, P. Theprungsirikul, D.W. Lin, J. Elisseeff, Chondroitin sulfate based niches for chondrogenic differentiation of mesenchymal stem cells., Matrix Biol. 27 (2008) 12–21. doi:10.1016/j.matbio.2007.07.002.
[195] J. Lei, E. Trevino, J. Temenoff, Cell number and chondrogenesis in human mesenchymal stem cell aggregates is affected by the sulfation level of heparin used as a cell coating, J. Biomed. Mater. Res. Part A. 104 (2016) 1817–1829. doi:10.1002/jbm.a.35713.
[196] Y. Liang, K.L. Kiick, Heparin-functionalized polymeric biomaterials in tissue engineering and drug delivery applications, Acta Biomater. 10 (2014) 1588–1600.

doi:10.1016/j.actbio.2013.07.031.
[197] R.A. Jackson, M.M. McDonald, V. Nurcombe, D.G. Little, S.M. Cool, The use of heparan sulfate to augment fracture repair in a rat fracture model, J. Orthop. Res. 24 (2006) 636–644. doi:10.1002/jor.20103.
[198] M.A. Woodruff, S.N. Rath, E. Susanto, L.M. Haupt, D.W. Hutmacher, V. Nurcombe, S.M. Cool, Sustained release and osteogenic potential of heparan sulfate-doped fibrin glue scaffolds within a rat cranial model, J. Mol. Histol. 38 (2007) 425–433. doi:10.1007/s10735-007-9137-y.
[199] M. Fujita, M. Ishihara, M. Shimizu, K. Obara, S. Nakamura, Y. Kanatani, Y. Morimoto, B. Takase, T. Matsui, M. Kikuchi, T. Maehara, Therapeutic angiogenesis induced by controlled release of fibroblast growth factor-2 from injectable chitosan/non-anticoagulant heparin hydrogel in a rat hindlimb ischemia model, Wound Repair Regen. 15 (2007) 58–65. doi:10.1111/j.1524-475X.2006.00185.x.
[200] O. Jeon, C. Powell, L.D. Solorio, M.D. Krebs, E. Alsberg, Affinity-based growth factor delivery using biodegradable, photocrosslinked heparin-alginate hydrogels, J. Control. Release. 154 (2011) 258–266. doi:10.1016/j.jconrel.2011.06.027.
[201] J. Lee, W. Il Choi, G. Tae, Y.H. Kim, S.S. Kang, S.E. Kim, S.-H. Kim, Y. Jung, S.H. Kim, Enhanced regeneration of the ligament–bone interface using a poly(l-lactide–co-ε-caprolactone) scaffold with local delivery of cells/BMP-2 using a heparin-based hydrogel, Acta Biomater. 7 (2011) 244–257. doi:10.1016/j.actbio.2010.08.017.
[202] A. Nilasaroya, L.A. Poole-Warren, J.M. Whitelock, P. Jo Martens, Structural and functional characterisation of poly(vinyl alcohol) and heparin hydrogels, Biomaterials. 29 (2008) 4658–4664. doi:10.1016/j.biomaterials.2008.08.011.
[203] J.S. Park, D.G. Woo, H.N. Yang, H.J. Lim, H.-M. Chung, K.-H. Park, Heparin-bound transforming growth factor-beta3 enhances neocartilage formation by rabbit mesenchymal stem cells., Transplantation. 85 (2008) 589–596. doi:10.1097/TP.0b013e3181639b3a.
[204] A. Watarai, L. Schirmer, S. Thönes, U. Freudenberg, C. Werner, J.C. Simon, U. Anderegg, TGFβ functionalized starPEG-heparin hydrogels modulate human dermal fibroblast growth and differentiation, Acta Biomater. 25 (2015) 65–75. doi:10.1016/j.actbio.2015.07.036.
[205] G. Bhakta, B. Rai, Z.X.H. Lim, J.H. Hui, G.S. Stein, A.J. van Wijnen, V. Nurcombe, G.D. Prestwich, S.M. Cool, Hyaluronic acid-based hydrogels functionalized with heparin that support controlled release of bioactive BMP-2, Biomaterials. 33 (2012) 6113–6122. doi:10.1016/j.biomaterials.2012.05.030.
[206] D.D.R. Sebinger, A. Ofenbauer, P. Gruber, S. Malik, C. Werner, ECM modulated early kidney development in embryonic organ culture., Biomaterials. 34 (2013) 6670–82. doi:10.1016/j.biomaterials.2013.05.031.
[207] E.K. Moioli, P. a Clark, D.R. Sumner, J.J. Mao, Autologous stem cell regeneration in craniosynostosis., Bone. 42 (2008) 332–40. doi:10.1016/j.bone.2007.10.004.
[208] G.M. Morriss-Kay, A.O.M. Wilkie, Growth of the normal skull vault and its alteration in craniosynostosis: insights from human genetics and experimental studies., J. Anat. 207 (2005) 637–53. doi:10.1111/j.1469-7580.2005.00475.x.
[209] M.P. Mooney, H.W. Losken, A.M. Moursi, J. Bradley, K. Azari, T.O. Acarturk,

G.M. Cooper, B. Thompson, L. a Opperman, M.I. Siegel, Anti-TGF-beta2 antibody therapy inhibits postoperative resynostosis in craniosynostotic rabbits., Plast. Reconstr. Surg. 119 (2007) 1200–12; discussion 1213–5. doi:10.1097/01.prs.0000258403.49584.ec.

[210] A.M. Moursi, P.L. Winnard, D. Fryer, M.P. Mooney, Delivery of transforming growth factor-beta2-perturbing antibody in a collagen vehicle inhibits cranial suture fusion in calvarial organ culture., Cleft Palate. Craniofac. J. 40 (2003) 225–32. doi:10.1597/1545-1569(2003)040<0225:DOTGFA>2.0.CO;2.

[211] M. Ye, S. Kim, K. Park, Issues in long-term protein delivery using biodegradable microparticles, J. Control. Release. 146 (2010) 241–260. doi:10.1016/j.jconrel.2010.05.011.

[212] A. Vila, H. Gill, O. McCallion, M.J. Alonso, Transport of PLA-PEG particles across the nasal mucosa: Effect of particle size and PEG coating density, J. Control. Release. 98 (2004) 231–244. doi:10.1016/j.jconrel.2004.04.026.

[213] L.J. White, G.T.S. Kirby, H.C. Cox, R. Qodratnama, O. Qutachi, F.R.A.J. Rose, K.M. Shakesheff, Accelerating protein release from microparticles for regenerative medicine applications, Mater. Sci. Eng. C. 33 (2013) 2578–2583. doi:10.1016/j.msec.2013.02.020.

[214] G. Ruan, S.S. Feng, Preparation and characterization of poly(lactic acid)-poly(ethylene glycol)-poly(lactic acid) (PLA-PEG-PLA) microspheres for controlled release of paclitaxel, Biomaterials. 24 (2003) 5037–5044. doi:10.1016/S0142-9612(03)00419-8.

[215] X. Zhu, L. Lu, B.L. Currier, A.J. Windebank, M.J. Yaszemski, Controlled release of NFkappaB decoy oligonucleotides from biodegradable polymer microparticles., Biomaterials. 23 (2002) 2683–92. http://www.ncbi.nlm.nih.gov/pubmed/12059017.

[216] L. Lu, G.N. Stamatas, a G. Mikos, Controlled release of transforming growth factor beta1 from biodegradable polymer microparticles., J. Biomed. Mater. Res. 50 (2000) 440–451. doi:10.1002/(SICI)1097-4636(20000605)50:3<440::AID-JBM19>3.0.CO;2-G [pii].

[217] N. Motlekar, M.A. Khan, B.B.C. Youan, Preparation and characterization of genistein containing poly(ethylene glycol) microparticles, J. Appl. Polym. Sci. 101 (2006) 2070–2078. doi:10.1002/app.23827.

[218] E. Secret, K.E. Crannell, S.J. Kelly, M. Villancio-Wolter, J.S. Andrew, Matrix metalloproteinase-sensitive hydrogel microparticles for pulmonary drug delivery of small molecule drugs or proteins, J. Mater. Chem. B. 3 (2015) 5629–5634. doi:10.1039/C5TB00443H.

[219] T. Miao, K.S. Rao, J.L. Spees, R.A. Oldinski, Osteogenic differentiation of human mesenchymal stem cells through alginate-graft-poly(ethylene glycol) microsphere-mediated intracellular growth factor delivery, J. Control. Release. 192 (2014) 57–66. doi:10.1016/j.jconrel.2014.06.029.

[220] S. Ravindran, J.L. Roam, P.K. Nguyen, T.M. Hering, D.L. Elbert, A. McAlinden, Changes of chondrocyte expression profiles in human MSC aggregates in the presence of PEG microspheres and TGF-β3., Biomaterials. 32 (2011) 8436–45. doi:10.1016/j.biomaterials.2011.07.056.

[221] M. Parlato, A. Johnson, G. a. Hudalla, W.L. Murphy, Adaptable Poly(ethylene

glycol) Microspheres Capable of Mixed-mode Degradation, Acta Biomater. 9 (2013) 9270–80. doi:10.1016/j.actbio.2013.08.011.
[222] L.J. De Cock, O. De Wever, S. Van Vlierberghe, E. Vanderleyden, P. Dubruel, F. De Vos, C. Vervaet, J.P. Remon, B.G. De Geest, Engineered (hep/pARG)2 polyelectrolyte capsules for sustained release of bioactive TGF-β1, Soft Matter. 8 (2012) 1146. doi:10.1039/c1sm06618h.
[223] S. Abbah, W.M.R. Lam, T. Hu, J. Goh, H. Wong, Sequestration of rhBMP-2 into self-assembled polyelectrolyte complexes promotes anatomic localization of new bone in a porcine model of spinal reconstructive surgery., Tissue Eng. Part A. 20 (2014) 1679–88. doi:10.1089/ten.TEA.2013.0593.
[224] A.K. Jha, W. Yang, C.B. Kirn-Safran, M.C. Farach-Carson, X. Jia, Perlecan domain I-conjugated, hyaluronic acid-based hydrogel particles for enhanced chondrogenic differentiation via BMP-2 release., Biomaterials. 30 (2009) 6964–75. doi:10.1016/j.biomaterials.2009.09.009.
[225] X. Xu, A.K. Jha, R.L. Duncan, X. Jia, Heparin-decorated, hyaluronic acid-based hydrogel particles for the controlled release of bone morphogenetic protein 2., Acta Biomater. 7 (2011) 3050–9. doi:10.1016/j.actbio.2011.04.018.
[226] K.E. Brown, K. Leong, C.H. Huang, R. Dalal, G.D. Green, H.B. Haimes, P.A. Jimenez, J. Bathon, Gelatin/chondroitin 6-sulfate microspheres for the delivery of therapeutic proteins to the joint, Arthritis Rheum. 41 (1998) 2185–2195. doi:10.1002/1529-0131(199812)41:12<2185::AID-ART13>3.0.CO;2-C.
[227] E.S. Lee, K.H. Park, D. Kang, I.S. Park, H.Y. Min, D.H. Lee, S. Kim, J.H. Kim, K. Na, Protein complexed with chondroitin sulfate in poly(lactide-co-glycolide) microspheres, Biomaterials. 28 (2007) 2754–2762. doi:10.1016/j.biomaterials.2007.01.049.
[228] K. Maculotti, E.M. Tira, M. Sonaggere, P. Perugini, B. Conti, T. Modena, F. Pavanetto, In vitro evaluation of chondroitin sulphate-chitosan microspheres as carrier for the delivery of proteins., J. Microencapsul. 26 (2009) 535–43. doi:10.1080/02652040802485725.
[229] S.W. Tsai, C.C. Chen, H.M. Liou, F.Y. Hsu, Preparation and characterization of microspheres comprised of collagen, chondroitin sulfate, and apatite as carriers for the osteoblast-like cell MG63, J. Biomed. Mater. Res. - Part A. 93 (2010) 115–122. doi:10.1002/jbm.a.32502.
[230] L. Huang, W. Sui, Y. Wang, Q. Jiao, Preparation of chitosan/chondroitin sulfate complex microcapsules and application in controlled release of 5-fluorouracil, Carbohydr. Polym. 80 (2010) 168–173. doi:10.1016/j.carbpol.2009.11.007.
[231] W. Park, K. Na, Dermatan sulfate as a stabilizer for protein stability in poly(lactide-co-glycolide) depot, Biotechnol. Bioprocess Eng. 14 (2009) 668–674. doi:10.1007/s12257-009-0058-3.
[232] J.J. Lim, T.M. Hammoudi, A.M. Bratt-Leal, S.K. Hamilton, K.L. Kepple, N.C. Bloodworth, T.C. McDevitt, J.S. Temenoff, Development of nano- and microscale chondroitin sulfate particles for controlled growth factor delivery., Acta Biomater. 7 (2011) 986–95. doi:10.1016/j.actbio.2010.10.009.
[233] M.C. Goude, T.C. McDevitt, J.S. Temenoff, Chondroitin Sulfate Microparticles Modulate Transforming Growth Factor-β 1 -Induced Chondrogenesis of Human Mesenchymal Stem, Cells Tissues Organs. (2014) 1–14. doi:10.1159/000365966.

[234] M.P.A. Lim, W.L. Lee, E. Widjaja, S.C.J. Loo, One-step fabrication of core–shell structured alginate–PLGA/PLLA microparticles as a novel drug delivery system for water soluble drugs, Biomater. Sci. 1 (2013) 486. doi:10.1039/c3bm00175j.
[235] P. Agarwal, S. Zhao, P. Bielecki, W. Rao, J. Choi, Y. Zhao, J. Yu, W. Zhang, X. He, One-Step Microfluidic Generation of Pre-Hatching Embryo-Like Core-Shell Microcapsules for Miniaturized 3D Culture of Pluripotent Stem Cells, Lab Chip. (2013). doi:10.1039/c3lc50678a.
[236] V.R. Babu, M. Sairam, K.M. Hosamani, T.M. Aminabhavi, Development of 5-fluorouracil loaded poly(acrylamide-co-methylmethacrylate) novel core-shell microspheres: in vitro release studies., Int. J. Pharm. 325 (2006) 55–62. doi:10.1016/j.ijpharm.2006.06.020.
[237] H. Wu, C. Liao, Q. Jiao, Z. Wang, W. Cheng, Y. Wan, Fabrication of core–shell microspheres using alginate and chitosan–polycaprolactone for controlled release of vascular endothelial growth factor, React. Funct. Polym. 72 (2012) 427–437. doi:10.1016/j.reactfunctpolym.2012.04.007.
[238] K.K. Kim, D.W. Pack, Microspheres for Drug Delivery, in: M. Ferrari (Ed.), BioMEMS Biomed. Nanotechnol., Springer US, Boston, MA, 2006: pp. 19–50. doi:10.1007/978-0-387-25842-3_2.
[239] S. Mitragotri, J. Lahann, Physical approaches to biomaterial design, Nat. Mater. 8 (2009) 15–23. doi:10.1038/nmat2344.
[240] Y. Zhang, H.F. Chan, K.W. Leong, Advanced materials and processing for drug delivery: the past and the future., Adv. Drug Deliv. Rev. 65 (2013) 104–20. doi:10.1016/j.addr.2012.10.003.
[241] A. Göpferich, M. Alonso, R. Langer, Development and characterization of microencapsulated microspheres, Pharm. Res. 11 (1994).
[242] D. Dendukuri, P.S. Doyle, The Synthesis and Assembly of Polymeric Microparticles Using Microfluidics, Adv. Mater. 21 (2009) 4071–4086. doi:10.1002/adma.200803386.
[243] W.J. Duncanson, T. Lin, A.R. Abate, S. Seiffert, R.K. Shah, D. a Weitz, Microfluidic synthesis of advanced microparticles for encapsulation and controlled release., Lab Chip. 12 (2012) 2135–45. doi:10.1039/c2lc21164e.
[244] E. Tumarkin, E. Kumacheva, Microfluidic generation of microgels from synthetic and natural polymers., Chem. Soc. Rev. 38 (2009) 2161–8. doi:10.1039/b809915b.
[245] D.H. Choi, C.H. Park, I.H. Kim, H.J. Chun, K. Park, D.K. Han, Fabrication of core-shell microcapsules using PLGA and alginate for dual growth factor delivery system., J. Control. Release. 147 (2010) 193–201. doi:10.1016/j.jconrel.2010.07.103.
[246] Z. She, C. Wang, J. Li, G.B. Sukhorukov, M.N. Antipina, Encapsulation of basic fibroblast growth factor by polyelectrolyte multilayer microcapsules and its controlled release for enhancing cell proliferation., Biomacromolecules. 13 (2012) 2174–80. doi:10.1021/bm3005879.
[247] D.H. Choi, R. Subbiah, I.H. Kim, D.K. Han, K. Park, Dual growth factor delivery using biocompatible core-shell microcapsules for angiogenesis., Small. 9 (2013) 3468–76. doi:10.1002/smll.201300427.
[248] P.R. Baraniak, M.T. Cooke, R. Saeed, M. a. Kinney, K.M. Fridley, T.C. McDevitt, Stiffening of human mesenchymal stem cell spheroid microenvironments induced

by incorporation of gelatin microparticles, J. Mech. Behav. Biomed. Mater. 11 (2012) 63–71. doi:10.1016/j.jmbbm.2012.02.018.
[249] L.D. Solorio, E.L. Vieregge, C.D. Dhami, E. Alsberg, High-density cell systems incorporating polymer microspheres as microenvironmental regulators in engineered cartilage tissues., Tissue Eng. Part B. Rev. 19 (2013) 209–20. doi:10.1089/ten.TEB.2012.0252.
[250] A.M. Bratt-Leal, K.L. Kepple, R.L. Carpenedo, M.T. Cooke, T.C. McDevitt, Magnetic manipulation and spatial patterning of multi-cellular stem cell aggregates, Integr. Biol. 3 (2011) 1224. doi:10.1039/c1ib00064k.
[251] S.K. Sahoo, A.K. Panda, V. Labhasetwar, Characterization of Porous PLGA / PLA Microparticles as a Scaffold for Three Dimensional Growth of Breast Cancer Cells, Growth (Lakeland). (2005) 1132–1139.
[252] K. Hayashi, Y. Tabata, Preparation of stem cell aggregates with gelatin microspheres to enhance biological functions, Acta Biomater. 7 (2011) 2797–2803. doi:10.1016/j.actbio.2011.04.013.
[253] R.L. Carpenedo, A.M. Bratt-Leal, R. a Marklein, S. a Seaman, N.J. Bowen, J.F. McDonald, T.C. McDevitt, Homogeneous and organized differentiation within embryoid bodies induced by microsphere-mediated delivery of small molecules., Biomaterials. 30 (2009) 2507–15. doi:10.1016/j.biomaterials.2009.01.007.
[254] E. Woo, H. Park, K.Y. Lee, Shear Reversible Cell/Microsphere Aggregate as an Injectable for Tissue Regeneration., Macromol. Biosci. (2014) 1–9. doi:10.1002/mabi.201300365.
[255] R.L. Carpenedo, S.A. Seaman, T.C. McDevitt, Microsphere size effects on embryoid body incorporation and embryonic stem cell differentiation, J. Biomed. Mater. Res. - Part A. 94 (2010) 466–475. doi:10.1002/jbm.a.32710.
[256] L.D. Solorio, A.S. Fu, R. Hernández-Irizarry, E. Alsberg, Chondrogenic differentiation of human mesenchymal stem cell aggregates via controlled release of TGF-β1 from incorporated polymer microspheres, J. Biomed. Mater. Res. Part A. 9999A (2009) NA–NA. doi:10.1002/jbm.a.32440.
[257] H.J. Chung, T.G. Park, Injectable cellular aggregates prepared from biodegradable porous microspheres for adipose tissue engineering., Tissue Eng. Part A. 15 (2009) 1391–1400. doi:10.1089/ten.tea.2008.0344.
[258] M.J. Mahoney, W.M. Saltzman, Transplantation of brain cells assembled around a programmable synthetic microenvironment., Nat. Biotechnol. 19 (2001) 934–9. doi:10.1038/nbt1001-934.
[259] A.M. Bratt-Leal, R.L. Carpenedo, M.D. Ungrin, P.W. Zandstra, T.C. McDevitt, Incorporation of biomaterials in multicellular aggregates modulates pluripotent stem cell differentiation., Biomaterials. 32 (2011) 48–56. doi:10.1016/j.biomaterials.2010.08.113.
[260] Y. Han, Y. Wei, S. Wang, Y. Song, Cartilage regeneration using adipose-derived stem cells and the controlled-released hybrid microspheres, Jt. Bone Spine. 77 (2010) 27–31. doi:10.1016/j.jbspin.2009.05.013.
[261] L.D. Solorio, C.D. Dhami, P.N. Dang, E.L. Vieregge, E. Alsberg, Spatiotemporal regulation of chondrogenic differentiation with controlled delivery of transforming growth factor-β1 from gelatin microspheres in mesenchymal stem cell aggregates., Stem Cells Transl. Med. 1 (2012) 632–639. doi:10.5966/sctm.2012-0039.

[262] S. Goetghebeur, W.S. Hu, Cultivation of anchorage-dependent animal cells in microsphere-induced aggregate culture, Appl. Microbiol. Biotechnol. 34 (1991) 735–741. doi:10.1007/BF00169343.
[263] A.M. Bratt-Leal, A.H. Nguyen, K. a Hammersmith, A. Singh, T.C. McDevitt, A microparticle approach to morphogen delivery within pluripotent stem cell aggregates, Biomaterials. 34 (2013) 7227–7235. doi:10.1016/j.biomaterials.2013.05.079.
[264] M. Goude, T. McDevitt, J. Temenoff, Chondroitin sulfate microparticles modulate TGF-beta 1- induced chondrogenesis of human mesenchymal stem cell spheroids, Cells Tissues Organs. In Press (2014).
[265] A.M. Wheelock, C.E. Wheelock, Trials and tribulations of 'omics data analysis: assessing quality of SIMCA-based multivariate models using examples from pulmonary medicine., Mol. Biosyst. 9 (2013) 2589–2596. doi:10.1039/c3mb70194h.
[266] K.A. Janes, M.B. Yaffe, Data-driven modelling of signal-transduction networks, Nat. Rev. Mol. Cell Biol. 7 (2006) 820–828. doi:10.1038/nrm2041.
[267] B.D. Cosgrove, L.G. Griffith, D. a. Lauffenburger, Fusing Tissue Engineering and Systems Biology Toward Fulfilling Their Promise, Cell. Mol. Bioeng. 1 (2008) 33–41. doi:10.1007/s12195-008-0007-9.
[268] J. Quackenbush, COMPUTATIONAL GENETICS: COMPUTATIONAL ANALYSIS OF MICROARRAY DATA, Nat. Rev. Genet. 2 (2001) 418–427. doi:10.1038/35076576.
[269] J.G. Albeck, G. MacBeath, F.M. White, P.K. Sorger, D. a Lauffenburger, S. Gaudet, Collecting and organizing systematic sets of protein data., Nat. Rev. Mol. Cell Biol. 7 (2006) 803–812. doi:10.1038/nrm2042.
[270] K.Y. Yeung, W.L. Ruzzo, Principal component analysis for clustering gene expression data, Bioinformatics. 17 (2001) 763–774. doi:10.1093/bioinformatics/bti465.Differential.
[271] B.D. Cosgrove, L.G. Alexopoulos, T. Hang, B.S. Hendriks, P.K. Sorger, L.G. Griffith, D.A. Lauffenburger, Cytokine-Associated Drug Toxicity in Human Hepatocytes Is Associated with Signaling Network Dysregulation, Mol. Biosyst. 6 (2010) 1195–1206. doi:10.1039/b926287c.
[272] K.S. Lau, A.M. Juchheim, K.R. Cavaliere, S.R. Philips, D. a Lauffenburger, K.M. Haigis, In vivo systems analysis identifies spatial and temporal aspects of the modulation of TNF-α-induced apoptosis and proliferation by MAPKs., Sci. Signal. 4 (2011) ra16. doi:10.1126/scisignal.2001338.
[273] K. Miller-Jensen, K. a Janes, J.S. Brugge, D. a Lauffenburger, Common effector processing mediates cell-specific responses to stimuli., Nature. 448 (2007) 604–608. doi:10.1038/nature06001.
[274] C. a Rivet, A.S. Hill, H. Lu, M.L. Kemp, Predicting cytotoxic T-cell age from multivariate analysis of static and dynamic biomarkers., Mol. Cell. Proteomics. 10 (2011) M110.003921. doi:10.1074/mcp.M110.003921.
[275] M.A. Kinney, R. Saeed, T.C. McDevitt, Mesenchymal morphogenesis of embryonic stem cells dynamically modulates the biophysical microtissue niche., Sci. Rep. 4 (2014) 4290. doi:10.1038/srep04290.
[276] M.O. Platt, C.L. Wilder, A. Wells, L.G. Griffith, D.A. Lauffenburger,

Multipathway kinase signatures of multipotent stromal cells are predictive for osteogenic differentiation: Tissue-specific stem cells, Stem Cells. 27 (2009) 2804–2814. doi:10.1002/stem.215.
[277] G. Mazziotti, J. Bilezikian, E. Canalis, D. Cocchi, a Giustina, New understanding and treatments for osteoporosis., Endocrine. 41 (2012) 58–69. doi:10.1007/s12020-011-9570-2.
[278] A. Giaccari, G. Sorice, G. Muscogiuri, Glucose toxicity: the leading actor in the pathogenesis and clinical history of type 2 diabetes - mechanisms and potentials for treatment., Nutr. Metab. Cardiovasc. Dis. 19 (2009) 365–77. doi:10.1016/j.numecd.2009.03.018.
[279] D.L. Jones, A.J. Wagers, No place like home: anatomy and function of the stem cell niche., Nat. Rev. Mol. Cell Biol. 9 (2008) 11–21. doi:10.1038/nrm2319.
[280] J.J. Minguell, A. Erices, P. Conget, P.A.C. Onget, Mesenchymal Stem Cells, Exp. Biol. Med. 226 (2001) 507–520. http://www.ncbi.nlm.nih.gov/pubmed/22156044 (accessed March 29, 2013).
[281] N.Z. Kuhn, R.S. Tuan, Regulation of stemness and stem cell niche of mesenchymal stem cells: implications in tumorigenesis and metastasis., J. Cell. Physiol. 222 (2010) 268–77. doi:10.1002/jcp.21940.
[282] S. Lecourt, V. Vanneaux, A. Cras, D. Freida, D. Heraoui, L. Herbi, C. Caillaud, C. Chomienne, J.-P. Marolleau, N. Belmatoug, J. Larghero, Bone marrow microenvironment in an in vitro model of Gaucher disease: consequences of glucocerebrosidase deficiency., Stem Cells Dev. 21 (2012) 239–48. doi:10.1089/scd.2011.0365.
[283] L.M. Coe, R. Irwin, D. Lippner, L.R. McCabe, The bone marrow microenvironment contributes to type I diabetes induced osteoblast death., J. Cell. Physiol. 226 (2011) 477–83. doi:10.1002/jcp.22357.
[284] R. Nakaoka, S.X. Hsiong, D.J. Mooney, Regulation of Chondrocyte Differentiation Level via Co-culture with Osteoblasts, Tissue Eng. 12 (2006) 2425–2433.
[285] Y. Tsuda, A. Kikuchi, M. Yamato, G. Chen, T. Okano, Heterotypic cell interactions on a dually patterned surface., Biochem. Biophys. Res. Commun. 348 (2006) 937–44. doi:10.1016/j.bbrc.2006.07.138.
[286] L. Leng, A. McAllister, B. Zhang, M. Radisic, A. Günther, Mosaic hydrogels: one-step formation of multiscale soft materials., Adv. Mater. 24 (2012) 3650–8. doi:10.1002/adma.201201442.
[287] S.K. Hamilton, N.C. Bloodworth, C.S. Massad, T.M. Hammoudi, S. Suri, P.J. Yang, H. Lu, J.S. Temenoff, Development of 3D hydrogel culture systems with on-demand cell separation, Biotechnol. J. 8 (2013) 485–495. doi:10.1002/biot.201200200.
[288] J. Patterson, J. a Hubbell, Enhanced proteolytic degradation of molecularly engineered PEG hydrogels in response to MMP-1 and MMP-2., Biomaterials. 31 (2010) 7836–45. doi:10.1016/j.biomaterials.2010.06.061.
[289] P.J. Yang, M.E. Levenston, J.S. Temenoff, Modulation of mesenchymal stem cell shape in enzyme-sensitive hydrogels is decoupled from upregulation of fibroblast markers under cyclic tension., Tissue Eng. Part A. 18 (2012) 2365–75. doi:10.1089/ten.TEA.2011.0727.

[290] D.C. Kirouac, C. Ito, E. Csaszar, A. Roch, M. Yu, E. a Sykes, G.D. Bader, P.W. Zandstra, Dynamic interaction networks in a hierarchically organized tissue., Mol. Syst. Biol. 6 (2010) 417. doi:10.1038/msb.2010.71.
[291] S. Gaudet, K.A. Janes, J.G. Albeck, E.A. Pace, D.A. Lauffenburger, P.K. Sorger, A compendium of signals and responses triggered by prodeath and prosurvival cytokines., Mol. Cell. Proteomics. 4 (2005) 1569–90. doi:10.1074/mcp.M500158-MCP200.
[292] J.J. Moon, J.E. Saik, R.A. Poche, J.E. Leslie-barbick, A.A. Smith, M.E. Dickinson, J.L. West, R. a Poché, S.-H. Lee, Biomimetic hydrogels with pro-angiogenic properties., Biomaterials. 31 (2010) 3840–7. doi:10.1016/j.biomaterials.2010.01.104.
[293] J.S. Temenoff, K.A. Athanasiou, R.G. Lebaron, A.G. Mikos, Effect of poly(ethylene glycol) molecular weight on tensile and swelling properties of oligo(poly(ethylene glycol) fumarate) hydrogels for cartilage tissue engineering, J. Biomed. Mater. Res. 59 (2002) 429–437. doi:10.1002/jbm.1259.
[294] L. Eriksson, E. Johansson, N. Kettaneh-Wold, J. Trygg, C. Wikstrom, S. Wold, Multi- and Megavariate Data Analysis Part I: Basic Principles and Applications, 2nd ed., Umetrics AB, Umea, Sweden, 2006.
[295] L. Eriksson, E. Johansson, N. Kettaneh-Wold, J. Trygg, C. Wikstrom, S. Wold, Multi- and Megavariate Data Analysis Part II: Advanced Applications and Method Extensions, 2nd ed., Umetrics, Umea, Sweden, 2006.
[296] S. Wasnik, A. Tiwari, M. a Kirkland, G. Pande, Osteohematopoietic stem cell niches in bone marrow., 1st ed., Elsevier Inc., 2012. doi:10.1016/B978-0-12-394309-5.00003-1.
[297] G.S. Travlos, Normal structure, function, and histology of the bone marrow., Toxicol. Pathol. 34 (2006) 548–65. doi:10.1080/01926230600939856.
[298] S.C. Manolagas, Birth and death of bone cells: basic regulatory mechanisms and implications for the pathogenesis and treatment of osteoporosis., Endocr. Rev. 21 (2000) 115–37. http://www.ncbi.nlm.nih.gov/pubmed/10782361.
[299] E.J. Sheehy, T. Vinardell, C.T. Buckley, D.J. Kelly, Engineering osteochondral constructs through spatial regulation of endochondral ossification., Acta Biomater. 9 (2013) 5484–92. doi:10.1016/j.actbio.2012.11.008.
[300] K. Cusi, The role of adipose tissue and lipotoxicity in the pathogenesis of type 2 diabetes., Curr. Diab. Rep. 10 (2010) 306–15. doi:10.1007/s11892-010-0122-6.
[301] A.I. Caplan, Adult Mesenchymal Stem Cells for Tissue Engineering Versus Regenerative Medicine, J. Cell. Physiol. (2007) 341–347. doi:10.1002/JCP.
[302] M. a Bredella, P.K. Fazeli, K.K. Miller, M. Misra, M. Torriani, B.J. Thomas, R.H. Ghomi, C.J. Rosen, A. Klibanski, Increased bone marrow fat in anorexia nervosa., J. Clin. Endocrinol. Metab. 94 (2009) 2129–36. doi:10.1210/jc.2008-2532.
[303] J.F. Griffith, D.K.W. Yeung, H.T. Ma, J.C.S. Leung, T.C.Y. Kwok, P.C. Leung, Bone marrow fat content in the elderly: a reversal of sex difference seen in younger subjects., J. Magn. Reson. Imaging. 36 (2012) 225–30. doi:10.1002/jmri.23619.
[304] P.T. Newton, K. a Staines, L. Spevak, a L. Boskey, C.C. Teixeira, V.E. Macrae, a E. Canfield, C. Farquharson, Chondrogenic ATDC5 cells: an optimised model for rapid and physiological matrix mineralisation., Int. J. Mol. Med. 30 (2012) 1187–

93. doi:10.3892/ijmm.2012.1114.
[305] H.E. Weiss, S.J. Roberts, J. Schrooten, F.P. Luyten, A semi-autonomous model of endochondral ossification for developmental tissue engineering., Tissue Eng. Part A. 18 (2012) 1334–43. doi:10.1089/ten.TEA.2011.0602.
[306] T. Atsumi, Y. Miwa, K. Kimata, Y. Ikawa, A chondrogenic cell line derived from a differentiating culture of AT805 teratocarcinoma cells., Cell Differ. Dev. 30 (1990) 109–16. http://www.ncbi.nlm.nih.gov/pubmed/2201423.
[307] C. Shukunami, K. Ishizeki, T. Atsumi, Y. Ohta, F. Suzuki, Y. Hiraki, Cellular Hypertrophy and Calcification of Embryonal Carcinoma-Derived Chondrogenic Cell Line ATDC5 In Vitro, J. Bone Miner. Res. 12 (1997) 1174–1188.
[308] T.D. Challa, Y. Rais, E.M. Ornan, Effect of adiponectin on ATDC5 proliferation, differentiation and signaling pathways., Mol. Cell. Endocrinol. 323 (2010) 282–91. doi:10.1016/j.mce.2010.03.025.
[309] L. Chen, T. Fink, X.-Y. Zhang, P. Ebbesen, V. Zachar, Quantitative transcriptional profiling of ATDC5 mouse progenitor cells during chondrogenesis., Differentiation. 73 (2005) 350–63. doi:10.1111/j.1432-0436.2005.00038.x.
[310] R.S. Tare, D. Howard, J.C. Pound, H.I. Roach, R.O.C. Oreffo, Tissue engineering strategies for cartilage generation--micromass and three dimensional cultures using human chondrocytes and a continuous cell line., Biochem. Biophys. Res. Commun. 333 (2005) 609–21. doi:10.1016/j.bbrc.2005.05.117.
[311] H.J. Kwon, Y. Han, Dual Monitoring of Secretion and ATP Levels during Chondrogenesis Using Perfusion Culture-Combined Bioluminescence Monitoring System, Biomed Res. Int. 2015 (2015) 1–6. doi:10.1155/2015/219068.
[312] D. Wübbenhorst, K. Dumler, B. Wagner, G. Wexel, A. Imhoff, B. Gansbacher, S. Vogt, M. Anton, Tetracycline-regulated bone morphogenetic protein 2 gene expression in lentivirally transduced primary rabbit chondrocytes for treatment of cartilage defects, Arthritis Rheum. 62 (2010) 2037–2046. doi:10.1002/art.27461.
[313] J.L. Allen, M.E. Cooke, T. Alliston, ECM stiffness primes the TGF pathway to promote chondrocyte differentiation, Mol. Biol. Cell. 23 (2012) 3731–3742. doi:10.1091/mbc.E12-03-0172.
[314] A.M. DeLise, L. Fischer, R.S. Tuan, Cellular interactions and signaling in cartilage development, Osteoarthr. Cartil. 8 (2000) 309–334. doi:10.1053/joca.1999.0306.
[315] M.A. Kinney, C.Y. Sargent, T.C. McDevitt, The Multiparametric Effects of Hydrodynamic Environments on Stem Cell Culture, Tissue Eng. Part B Rev. 17 (2011) 249–262. doi:10.1089/ten.teb.2011.0040.
[316] R.-Z. Lin, R.-Z. Lin, H.-Y. Chang, Recent advances in three-dimensional multicellular spheroid culture for biomedical research., Biotechnol. J. 3 (2008) 1172–84. doi:10.1002/biot.200700228.
[317] H. Fan, C. Zhang, J. Li, L. Bi, L. Qin, H. Wu, Y. Hu, Gelatin microspheres containing TGF-beta3 enhance the chondrogenesis of mesenchymal stem cells in modified pellet culture., Biomacromolecules. 9 (2008) 927–34. doi:10.1021/bm7013203.
[318] P. Krsko, M. Libera, Biointeractive hydrogels, Mater. Today. 8 (2005) 36–44. doi:10.1016/S1369-7021(05)71223-2.
[319] C.R. Nuttelman, M.C. Tripodi, K.S. Anseth, Synthetic hydrogel niches that promote hMSC viability., Matrix Biol. 24 (2005) 208–18.

doi:10.1016/j.matbio.2005.03.004.
[320] J.J. Rice, M.M. Martino, L. De Laporte, F. Tortelli, P.S. Briquez, J. a Hubbell, Engineering the regenerative microenvironment with biomaterials., Adv. Healthc. Mater. 2 (2013) 57–71. doi:10.1002/adhm.201200197.
[321] H. Lu, L. Guo, N. Kawazoe, T. Tateishi, G. Chen, Effects of poly(L-lysine), poly(acrylic acid) and poly(ethylene glycol) on the adhesion, proliferation and chondrogenic differentiation of human mesenchymal stem cells., J. Biomater. Sci. Polym. Ed. 20 (2009) 577–89. doi:10.1163/156856209X426402.
[322] Y. Yao, Y. Wang, ATDC5: An excellent in vitro model cell line for skeletal development, J. Cell. Biochem. 114 (2013) 1223–1229. doi:10.1002/jcb.24467.
[323] J. a Zimmermann, T.C. Mcdevitt, Pre-conditioning mesenchymal stromal cell spheroids for immunomodulatory paracrine factor secretion, Cytotherapy. 16 (2014) 331–345. doi:10.1016/j.jcyt.2013.09.004.
[324] E.G. Loboa, D. Ph, Osteogenic Differentiation of Human Mesenchymal Stem Cells on Bone Morphogenetic Protein (BMP-2) mRNA Expression, Tissue Eng. 12 (2006).
[325] K. Mitani, N. Haruyama, J. Hatakeyama, K. Igarashi, Amelogenin splice isoforms stimulate chondrogenic differentiation of ATDC5 cells., Oral Dis. (2012) 1–5. doi:10.1111/j.1601-0825.2012.01967.x.
[326] H.J. Issaq, Z. Xiao, T.D. Veenstra, Serum and plasma proteomics, Chem. Rev. 107 (2007) 3601–3620. doi:10.1021/cr068287r.
[327] X. Zheng, H. Baker, W.S. Hancock, F. Fawaz, M. McCaman, E. Pungor, Proteomic analysis for the assessment of different lots of fetal bovine serum as a raw material for cell culture. Part IV. Application of proteomics to the manufacture of biological drugs, Biotechnol. Prog. 22 (2006) 1294–1300. doi:10.1021/bp060121o.
[328] W.-J. Qian, D.T. Kaleta, B.O. Petritis, H. Jiang, T. Liu, X. Zhang, H.M. Mottaz, S.M. Varnum, D.G. Camp, L. Huang, X. Fang, W.-W. Zhang, R.D. Smith, Enhanced detection of low abundance human plasma proteins using a tandem IgY12-SuperMix immunoaffinity separation strategy., Mol. Cell. Proteomics. 7 (2008) 1963–73. doi:10.1074/mcp.M800008-MCP200.
[329] I. Capila, R.J. Linhardt, Heparin-Protein Interactions, Angew. Chemie Int. Ed. 41 (2002) 390–412. doi:10.1002/1521-3773(20020201)41:3<390::AID-ANIE390>3.0.CO;2-B.
[330] J.C. Fredenburgh, B. a. Leslie, A.R. Stafford, T. Lim, H.H. Chan, J.I. Weitz, Zn2+ Mediates High Affinity Binding of Heparin to the C Domain of Fibrinogen, J. Biol. Chem. 288 (2013) 29394–29402. doi:10.1074/jbc.M113.469916.
[331] F. Peysselon, S. Ricard-Blum, Heparin-protein interactions: from affinity and kinetics to biological roles. Application to an interaction network regulating angiogenesis., Matrix Biol. 35 (2014) 73–81. doi:10.1016/j.matbio.2013.11.001.
[332] P. Andrade-Gordon, S. Strickland, Interaction of heparin with plasminogen activators and plasminogen: effects on the activation of plasminogen., Biochemistry. 25 (1986) 4033–4040. doi:10.1074/jbc.M110.108720.
[333] C.D. Hermann, S.L. Hyzy, M. Walker, J.K. Williams, B.D. Boyan, Z. Schwartz, Craniosynostosis and Resynostosis : Models , Imaging , and Dental Implications, (2016). doi:10.1177/0022034516643315.

[334] K. Shen, S.M. Krakora, M. Cunningham, M. Singh, X. Wang, F.Z. Hu, J.C. Post, G.D. Ehrlich, Medical treatment of craniosynostosis: recombinant Noggin inhibits coronal suture closure in the rat craniosynostosis model., Orthod. Craniofac. Res. 12 (2009) 254–62. doi:10.1111/j.1601-6343.2009.01460.x.
[335] C.-C. Lin, K.S. Anseth, Controlling Affinity Binding with Peptide-Functionalized Poly(ethylene glycol) Hydrogels., Adv. Funct. Mater. 19 (2009) 2325. doi:10.1002/adfm.200900107.
[336] M. a Kinney, T.C. McDevitt, Emerging strategies for spatiotemporal control of stem cell fate and morphogenesis., Trends Biotechnol. 31 (2013) 78–84. doi:10.1016/j.tibtech.2012.11.001.
[337] U. Freudenberg, A. Zieris, K. Chwalek, M. V. Tsurkan, M.F. Maitz, P. Atallah, K.R. Levental, S. a. Eming, C. Werner, Heparin desulfation modulates VEGF release and angiogenesis in diabetic wounds, J. Control. Release. 220 (2015) 79–88. doi:10.1016/j.jconrel.2015.10.028.
[338] M. Kan, F. Wang, J. Xu, J.W. Crabb, J. Hou, W.L. Mckeehan, An Essential Heparin-Binding Domain in the Fibroblast Growth Factor Receptor Kinase, Science (80-.). 259 (1993) 1918–1291.
[339] S.P. Seto, T. Miller, J.S. Temenoff, Effect of selective heparin desulfation on preservation of bone morphogenetic protein-2 bioactivity after thermal stress., Bioconjug. Chem. 26 (2015) 286–93. doi:10.1021/bc500565x.
[340] T. Katagiri, A. Yamaguchi, M. Komaki, E. Abe, N. Takahashi, T. Ikeda, V. Rosen, J.M. Wozney, A. Fujisawa-sehara, T. Suda, Bone Morphogenic Protein-2 Converts the Differentiation Pathway of C2C12 Myoblasts into the Osteoblast Lineage, J. Cell Biol. 127 (1994) 1755–1766.
[341] C. Cha, J.H. Jeong, H. Kong, Poly(ethylene glycol)-poly(lactic-co-glycolic acid) core–shell microspheres with enhanced controllability of drug encapsulation and release rate, J. Biomater. Sci. Polym. Ed. 26 (2015) 828–840. doi:10.1080/09205063.2015.1058575.
[342] C. Siltanen, M. Yaghoobi, A. Haque, J. You, J. Lowen, M. Soleimani, A. Revzin, Microfluidic fabrication of bioactive microgels for rapid formation and enhanced differentiation of stem cell spheroids, Acta Biomater. 34 (2016) 1–8. doi:10.1016/j.actbio.2016.01.012.
[343] L. Deveza, J. Ashoken, G. Castaneda, X. Tong, M. Keeney, L.-H. Han, F. Yang, Microfluidic Synthesis of Biodegradable Polyethylene-Glycol Microspheres for Controlled Delivery of Proteins and DNA Nanoparticles, ACS Biomater. Sci. Eng. 1 (2015) 157–165. doi:10.1021/ab500051v.
[344] D.M. Headen, G. Aubry, H. Lu, A.J. García, Microfluidic-based generation of size-controlled, biofunctionalized synthetic polymer microgels for cell encapsulation., Adv. Mater. 26 (2014) 3003–8. doi:10.1002/adma.201304880.
[345] R.W. Ten Broek, S. Grefte, J.W. Von Den Hoff, Regulatory factors and cell populations involved in skeletal muscle regeneration, J. Cell. Physiol. 224 (2010) 7–16. doi:10.1002/jcp.22127.
[346] R&DSystemsIncorporated, R&D Systems, (2016). https://www.rndsystems.com/ (accessed October 8, 2016).
[347] C.L. Bell, N. a. Peppas, Water, solute and protein diffusion in physiologically responsive hydrogels of poly(methacrylic acid-g-ethylene glycol), Biomaterials. 17

(1996) 1203–1218. doi:10.1016/0142-9612(96)84941-6.
[348] N. a. Peppas, Y. Huang, M. Torres-Lugo, J.H. Ward, J. Zhang, Physicochemical Foundations and Structural Design of Hydrogels in Medicine and Biology, Annu. Rev. Biomed. Eng. 2 (2000) 9–29. doi:10.1146/annurev.bioeng.2.1.9.
[349] M.C. Cushing, J.-T. Liao, M.P. Jaeggli, K.S. Anseth, Material-based regulation of the myofibroblast phenotype., Biomaterials. 28 (2007) 3378–87. doi:10.1016/j.biomaterials.2007.04.005.
[350] M.H. Hettiaratchi, R.E. Guldberg, T.C. McDevitt, Biomaterial Strategies for Controlling Stem Cell Fate Via Morphogen Sequestration, J. Mater. Chem. B. 4 (2016) 3464–3481. doi:10.1039/C5TB02575C.
[351] N. Huebsch, C.J. Kearney, X. Zhao, J. Kim, C.A. Cezar, Z. Suo, D.J. Mooney, Ultrasound-triggered disruption and self-healing of reversibly cross-linked hydrogels for drug delivery and enhanced chemotherapy, Proc. Natl. Acad. Sci. (2014). doi:10.1073/pnas.1405469111.
[352] X. Zhao, J. Kim, C. a Cezar, N. Huebsch, K. Lee, K. Bouhadir, D.J. Mooney, C. Link, X. Zhao, J. Kim, C. a Cezar, N. Huebsch, K. Lee, Active scaffolds for on-demand drug and cell delivery., Proc. Natl. Acad. Sci. U. S. A. 108 (2011) 67–72. doi:10.1073/pnas.1007862108.
[353] P.M. Kharkar, K.L. Kiick, A.M. Kloxin, Designing degradable hydrogels for orthogonal control of cell microenvironments, Chem. Soc. Rev. 42 (2013) 7335–7372. doi:10.1039/C3CS60040H.
[354] Rein V. Ulijn, Nurguse Bibi, Vineetha Jayawarna, Paul D. Thornton, Simon J. Todd, Robert J. Mart, Andrew M. Smith, J.E. Gough, Bioresponsive hydrogels, Mater. Today. 10 (2007) 40–48. doi:10.1016/S1369-7021(07)70049-4.
[355] M. Schuksz, M.M. Fuster, J.R. Brown, B.E. Crawford, D.P. Ditto, R. Lawrence, C. a Glass, L. Wang, Y. Tor, J.D. Esko, Surfen, a small molecule antagonist of heparan sulfate., Proc. Natl. Acad. Sci. U. S. A. 105 (2008) 13075–80. doi:10.1073/pnas.0805862105.
[356] E.S. Place, J.H. George, C.K. Williams, M.M. Stevens, Synthetic polymer scaffolds for tissue engineering., Chem. Soc. Rev. 38 (2009) 1139–51. doi:10.1039/b811392k.
[357] T. Jenuwein, Allis, Translating the Histone Code, Science (80-.). 293 (2001) 1074–1080. doi:10.1126/science.1063127.
[358] O. Lieleg, R.M. Baumgärtel, A.R. Bausch, Selective filtering of particles by the extracellular matrix: An electrostatic bandpass, Biophys. J. 97 (2009) 1569–1577. doi:10.1016/j.bpj.2009.07.009.
[359] H. Tan, K.G. Marra, Injectable, biodegradable hydrogels for tissue engineering applications, Materials (Basel). 3 (2010) 1746–1767. doi:10.3390/ma3031746.
[360] T.D. Sargeant, A.P. Desai, S. Banerjee, A. Agawu, J.B. Stopek, An in situ forming collagen-PEG hydrogel for tissue regeneration, Acta Biomater. 8 (2012) 124–132. doi:10.1016/j.actbio.2011.07.028.
[361] J.A. Wieland, T.L. Houchin-Ray, L.D. Shea, Non-viral vector delivery from PEG-hyaluronic acid hydrogels, J. Control. Release. 120 (2007) 233–241. doi:10.1016/j.jconrel.2007.04.015.
[362] S.R. Goldring, Pathogenesis of bone and cartilage destruction in rheumatoid arthritis., Rheumatology (Oxford). 42 Suppl 2 (2003) ii11–6.

doi:10.1093/rheumatology/keg327.
[363] M.J. Taylor, S. Tanna, T. Sahota, In vivo study of a polymeric glucose-sensitive insulin delivery system using a rat model., J. Pharm. Sci. 99 (2010) 4215–4227. doi:10.1002/jps.
[364] A.K. Jha, K.M. Tharp, J. Ye, J.L. Santiago-Ortiz, W.M. Jackson, A. Stahl, D. V. Schaffer, Y. Yeghiazarians, K.E. Healy, Enhanced survival and engraftment of transplanted stem cells using growth factor sequestering hydrogels, Biomaterials. 47 (2015) 1–12. doi:10.1016/j.biomaterials.2014.12.043.
[365] J.N. Adkins, Toward a Human Blood Serum Proteome: Analysis By Multidimensional Separation Coupled With Mass Spectrometry, Mol. Cell. Proteomics. 1 (2002) 947–955. doi:10.1074/mcp.M200066-MCP200.
[366] B.P. Purcell, D. Lobb, M.B. Charati, S.M. Dorsey, R.J. Wade, K.N. Zellars, H. Doviak, S. Pettaway, C.B. Logdon, J.A. Shuman, P.D. Freels, J.H. Gorman Iii, R.C. Gorman, F.G. Spinale, J.A. Burdick, Injectable and bioresponsive hydrogels for on-demand matrix metalloproteinase inhibition., Nat. Mater. 13 (2014) 653–61. doi:10.1038/nmat3922.
[367] B. V. Sridhar, J.L. Brock, J.S. Silver, J.L. Leight, M.A. Randolph, K.S. Anseth, Development of a cellularly degradable PEG hydrogel to promote articular cartilage extracellular matrix deposition, Adv. Healthc. Mater. 4 (2015) 702–713. doi:10.1002/adhm.201400695.
[368] A.A. Aimetti, A.J. Machen, K.S. Anseth, Poly(ethylene glycol) hydrogels formed by thiol-ene photopolymerization for enzyme-responsive protein delivery, Biomaterials. 30 (2009) 6048–6054. doi:10.1016/j.biomaterials.2009.07.043.
[369] J.L. Roam, Y. Yan, P.K. Nguyen, I.S. Kinstlinger, M.K. Leuchter, D.A. Hunter, M.D. Wood, D.L. Elbert, A modular, plasmin-sensitive, clickable poly(ethylene glycol)-heparin-laminin microsphere system for establishing growth factor gradients in nerve guidance conduits, Biomaterials. 72 (2015) 112–124. doi:10.1016/j.biomaterials.2015.08.054.
[370] L. Zhang, Y.-I. Jeong, S. Zheng, S. Il Jang, H. Suh, D.H. Kang, I. Kim, Biocompatible and pH-sensitive PEG hydrogels with degradable phosphoester and phosphoamide linkers end-capped with amine for controlled drug delivery, Polym. Chem. 4 (2013) 1084. doi:10.1039/c2py20755a.
[371] N. Murthy, Y.X. Thng, S. Schuck, M.C. Xu, J.M.J. Fr??chet, A novel strategy for encapsulation and release of proteins: Hydrogels and microgels with acid-labile acetal cross-linkers, J. Am. Chem. Soc. 124 (2002) 12398–12399. doi:10.1021/ja026925r.
[372] J.J. Schmidt, J. Rowley, H.J. Kong, Hydrogels used for cell-based drug delivery., J. Biomed. Mater. Res. A. 87 (2008) 1113–22. doi:10.1002/jbm.a.32287.
[373] R. Qodratnama, L.P. Serino, H.C. Cox, O. Qutachi, L.J. White, Formulations for modulation of protein release from large-size PLGA microparticles for tissue engineering, Mater. Sci. Eng. C. 47 (2015) 230–236. doi:10.1016/j.msec.2014.11.003.
[374] A.N. Ford Versypt, D.W. Pack, R.D. Braatz, Mathematical modeling of drug delivery from autocatalytically degradable PLGA microspheres - A review, J. Control. Release. 165 (2013) 29–37. doi:10.1016/j.jconrel.2012.10.015.
[375] C.W. Archer, E.H. Morrison, M.T. Bayliss, M.W. Ferguson, The development of

articular cartilage: II. The spatial and temporal patterns of glycosaminoglycans and small leucine-rich proteoglycans., J. Anat. 189 (Pt 1 (1996) 23–35. http://www.pubmedcentral.nih.gov/articlerender.fcgi?artid=1167824&tool=pmcentrez&rendertype=abstract.

[376] R.J. Weiss, P.L.S.M. Gordts, D. Le, D. Xu, J.D. Esko, Y. Tor, Small molecule antagonists of cell-surface heparan sulfate and heparin–protein interactions, Chem. Sci. 6 (2015) 5984–5993. doi:10.1039/C5SC01208B.

[377] M. Lundqvist, J. Stigler, G. Elia, I. Lynch, T. Cedervall, K.A. Dawson, Nanoparticle size and surface properties determine the protein corona with possible implications for biological impacts., Proc. Natl. Acad. Sci. U. S. A. 105 (2008) 14265–70. doi:10.1073/pnas.0805135105.

[378] D.G. Belair, W.L. Murphy, Specific VEGF sequestering to biomaterials: influence of serum stability., Acta Biomater. 9 (2013) 8823–31. doi:10.1016/j.actbio.2013.06.033.

[379] Y. Teramura, H. Iwata, Cell surface modification with polymers for biomedical studies, Soft Matter. 6 (2010) 1081. doi:10.1039/b913621e.

[380] S. Schneider, P.J. Feilen, V. Slotty, D. Kampfner, S. Preuss, S. Berger, J. Beyer, R. Pommersheim, Multilayer capsules: a promising microencapsulation system for transplantation of pancreatic islets., Biomaterials. 22 (2001) 1961–70. http://www.ncbi.nlm.nih.gov/pubmed/11426874.

[381] A.J. Swiston, C. Cheng, S.H. Um, D.J. Irvine, R.E. Cohen, M.F. Rubner, Surface functionalization of living cells with multilayer patches., Nano Lett. 8 (2008) 4446–53. doi:10.1021/nl802404h.

[382] J.T. Wilson, C. a Haller, Z. Qu, W. Cui, M.K. Urlam, E.L. Chaikof, Biomolecular surface engineering of pancreatic islets with thrombomodulin., Acta Biomater. 6 (2010) 1895–903. doi:10.1016/j.actbio.2010.01.027.

[383] S. Cabric, J. Sanchez, T. Lundgren, A. Foss, M. Felldin, R. Källen, K. Salmela, A. Tibell, G. Tufveson, R. Larsson, O. Korsgren, B. Nilsson, Islet surface heparinization prevents the instant blood-mediated inflammatory reaction in islet transplantation., Diabetes. 56 (2007) 2008–15. doi:10.2337/db07-0358.

[384] S. Cabric, J. Sanchez, U. Johansson, R. Larsson, B. Nilsson, O. Korsgren, P.U. Magnusson, Anchoring of vascular endothelial growth factor to surface-immobilized heparin on pancreatic islets: implications for stimulating islet angiogenesis., Tissue Eng. Part A. 16 (2010) 961–70. doi:10.1089/ten.tea.2009.0429.

[385] Y. Teramura, H. Iwata, Islets surface modification prevents blood-mediated inflammatory responses., Bioconjug. Chem. 19 (2008) 1389–95. doi:10.1021/bc800064t.

[386] J. Lei, L.T. McLane, J.E. Curtis, J.S. Temenoff, Characterization of a multilayer heparin coating for biomolecule presentation to human mesenchymal stem cell spheroids, Biomater. Sci. 2 (2014) 666. doi:10.1039/c3bm60271k.

[387] E.S. Trindade, C. Oliver, M.C. Jamur, H. a O. Rocha, C.R.C. Franco, R.I. Bouças, T.R. Jarrouge, M. a S. Pinhal, I.L.S. Tersariol, T.C. Gouvêa, C.P. Dietrich, H.B. Nader, The binding of heparin to the extracellular matrix of endothelial cells up-regulates the synthesis of an antithrombotic heparan sulfate proteoglycan., J. Cell. Physiol. 217 (2008) 328–37. doi:10.1002/jcp.21504.

[388] J.W. Nichol, A. Khademhosseini, Modular Tissue Engineering: Engineering Biological Tissues from the Bottom Up., Soft Matter. 5 (2009) 1312–1319. doi:10.1039/b814285h.
[389] D.L. Elbert, Bottom-up tissue engineering, Curr. Opin. Biotechnol. 22 (2011) 674–680. doi:10.1016/j.copbio.2011.04.001.
[390] Y. Du, E. Lo, S. Ali, A. Khademhosseini, Directed assembly of cell-laden microgels for fabrication of 3D tissue constructs, Proc. Natl. Acad. Sci. 105 (2008) 9522–9527. doi:10.1073/pnas.0801866105.
[391] Y. Torisawa, B. Mosadegh, G.D. Luker, M. Morell, K.S. O'Shea, S. Takayama, Microfluidic hydrodynamic cellular patterning for systematic formation of co-culture spheroids., Integr. Biol. (Camb). 1 (2009) 649–54. doi:10.1039/b915965g.
[392] H. Kodama, Y. Amagai, H. Sudo, S. Kasai, S. Yamamoto, Establishment of a Clonal Osteogenic Cell Line from Newborn Mouse Calvaria, Japanese J. Oral Biol. 23 (1981) 899–901. https://www.jstage.jst.go.jp/article/joralbiosci1965/23/4/23_4_899/_article.
[393] H. Sudo, H.A. Kodama, Y. Amagai, S. Yamamoto, S. Kasai, In vitro differentiation and calcification in a new clonal osteogenic cell line derived from newborn mouse calvaria, J. Cell Biol. 96 (1983) 191–198. doi:10.1083/jcb.96.1.191.